

1-26-2017

Changing the Pathobiological Paradigm in Myelodysplastic Syndromes: The NLRP3 Inflammasome Drives the MDS Phenotype

Ashley Basiorka

University of South Florida, aabasiorka@gmail.com

Follow this and additional works at: <http://scholarcommons.usf.edu/etd>



Part of the [Molecular Biology Commons](#)

Scholar Commons Citation

Basiorka, Ashley, "Changing the Pathobiological Paradigm in Myelodysplastic Syndromes: The NLRP3 Inflammasome Drives the MDS Phenotype" (2017). *Graduate Theses and Dissertations*.
<http://scholarcommons.usf.edu/etd/6613>

This Dissertation is brought to you for free and open access by the Graduate School at Scholar Commons. It has been accepted for inclusion in Graduate Theses and Dissertations by an authorized administrator of Scholar Commons. For more information, please contact scholarcommons@usf.edu.

Changing the Pathobiological Paradigm in Myelodysplastic Syndromes: The NLRP3
Inflammasome Drives the MDS Phenotype

by

Ashley Ann Basiorka

A dissertation submitted in partial fulfillment
of the requirements for the degree of
Doctor of Philosophy
Department of Cell Biology, Microbiology, and Molecular Biology
College of Arts and Sciences
University of South Florida

Major Professor: Alan List, M.D.
Sheng Wei, M.D.
PK Epling-Burnette, PharmD., Ph.D.
Javier Pinilla-Ibarz, M.D., Ph.D.

Date of Approval:
January 24, 2017

Keywords: pyroptosis, caspase-1, S100A9, NADPH oxidase, β -catenin

Copyright © 2017, Ashley Ann Basiorka

DEDICATION

This dissertation is written with dedication to my incredible family, who matters most to me above all else. I recognize how fortunate and blessed I am to have each of you in my life. Your unwavering support has made it possible for me to be here, pursuing my greatest dreams and aspirations.

First and foremost, this work is dedicated to my father, whose diagnosis of acute lymphoblastic leukemia set a nine-year-old girl on a tireless mission to make advances in hematology oncology. I am who I am because of you. I cannot erase the past, and I know those memories are ingrained in you as they are in me. I do, however, hope you take pride in this work, and that it may serve as a positive consequence of an extraordinarily trying time. Thank you for never giving up and for never losing hope.

Next, I wholeheartedly dedicate this work to my mother. I will never be able to properly express just how fortunate I am to be your daughter. Never forget how incredible you are. You have worn many hats over the years, and I thank you for being my biggest fan through it all, from my fleeting interests to my greatest passions. You are my foundation, and I thank you for molding me into the person I am today. I hope to always make you proud.

To Eric, the greatest brother a girl could hope to have. How lucky I am to call you my best friend. Thank you for always making me laugh, even when it hasn't been easy on us. I promise to always be the "best little sister that [you] never wanted." In chasing

your aspirations with an unrelenting force, you have taught me how to dream. I find your ardency to be contagious, and I thank you for being my inspiration. Thank you for always having my back no matter what. It will always be us against the world.

Ta praca jest także dedykowana do mojej ukochanej Babcia. Babciu, dziękuję ci serdecznie za wszystkie Twoje modlitwy w mojej intencji, które zawsze mi pomagały. Dziękuję za ciepło, troskę, miłość i dobroć jaką mi zawsze dałaś. Nauczyłaś mi jak być dobrym człowiekiem. Wpołaś we mnie wszystkie tradycje rodzinne. Babciu za twoją dobroć i miłość składam wyrazy szacunku i podziękowania. Bądź zawsze uśmiechnięta i nie zapomnij jak bardzo Cię Kocham!

I thank my godmother, Grace, for knowing me better than I know myself. Thank you for always being honest and direct, for your constant encouragement, and most importantly, for teaching me your strength and independence. I would be lost without you.

To Christopher, I thank you for being the parts of me that are lacking and so much more than just that. You are engrained in every part of my being and I know that I am my best and truest self because of you. Thank you for supporting me in every facet and for being my optimism, motivation and strength when I've needed it the most. May our memories remind us of where we've been, may the future belong to our dreams and aspirations, and may the present be a time we can finally share together.

Last, but certainly not least, thank you to the remainder of my family and to my closest friends. Each of you has played an instrumental role in my progress, and I cannot thank you enough for being alongside me every step of the way.

ACKNOWLEDGMENTS

First and foremost, I want to begin by acknowledging my mentor, Dr. Alan List. It has truly been the privilege of a lifetime working for you. Thank you for taking a chance on me, and allowing me to work in your laboratory as an undergraduate student when I had no formal research experience. In doing so, you provided me the opportunity to become so completely enthralled and passionate about research, which has brought me to where I am today. I am very fortunate to have worked on your team, and to have had the opportunity to learn from someone as inspirational and outstanding as yourself. Thank you for believing in me and helping me grow as a scientist. Most importantly, I thank you for giving me the chance to make contributions to malignant hematology, a field of research that means so much to me personally. A lifetime of thanks seems insufficient to account for the influence you have had on me and my career. Thank you for being such an extraordinary mentor.

To my committee members, Dr. Sheng Wei, Dr. PK Epling-Burnette, and Dr. Javier Pinilla-Ibarz, I thank you for all of your guidance and support, and for being alongside me during this process. Dr. Wei, thank you for making sure I'm always smiling and for sharing your life lessons with me. You have been a constant source of support, and I appreciate it immensely. You will always be my favorite countryman. I thank Dr. Epling-Burnette and Dr. Pinilla-Ibarz for epitomizing what it means to be great translational scientists. Your unique insights and ideas highlight the forward-thinking I

hope to have as an investigator. I wish to also extend my sincerest appreciation to Dr. Daniel Starczynowski, a distinguished investigator whom I have the privilege of having as my outside chairman. I have the upmost respect for you and your work. You are a talented and accomplished translational investigator, and it is really an honor to have you take part in my defense.

I would like to recognize the members of the List laboratory, all of my colleagues and collaborators, my committee members' labs, and the core facilities located here at Moffitt Cancer Center, especially the Flow Cytometry and Microscopy core facility staff. Thank you for sharing your wisdom, for offering advice and direction, and for ultimately making me a better scientist. I would like to thank Dr. Erika Eksioglu and Dr. Xianghong Chen for diligently trying to make me love animal work and for always being friendly and welcoming faces across the bridge. Erika, you have been a true friend. Thank you for always looking out for me, and for all the great memories. Dr. Eric Padron, I thank you for being a Food Network channel-worthy baking critic, but more importantly for sharing your ideas with me and challenging me to think about my work from different perspectives. I know that both my baking and my science have improved because of you. I am honored to have worked closely with Dr. David Sallman, The Guardian of The Guardian. Thank you for sharing your humor and for keeping science fun. You have always had a positive outlook for me and I've appreciated the support. I would like to thank Dr. John Cleveland for the time he has generously provided to critique and guide my work. You are an impressive investigator and it has been a real honor to have you familiar with and invested in my research.

Moreover, I want to extend my appreciation to the members of the List laboratory, both past and present, who helped shape my learning and progress as both a student and a researcher. Dr. Lubomir Sokol, thank you for sharing your brilliance with me. If I have even half of your intelligence and wisdom one day, I know I'll make for a great scientist. I feel very fortunate to have had the opportunity to work with you and learn from you. Dr. Kathy McGraw, I thank you for being patient with me over the years in answering all of my questions and curiosities. I would like to thank Brittany Irvine for appreciating my quirkiness, sharing my love of happy dances and random self-composed songs, and for diversifying my antibody repertoire with constant immune attacks. I will undoubtedly miss you! Amy McLemore, I thank you for the support you've shown me these last few months. It has been fun "science-ing" with you. To Dianne Sullivan, Guinevere Hart, and Krystal Ring, I cannot thank you enough for your behind the scenes help and support. You each go beyond your responsibilities to support me, and it has not gone unappreciated or unnoticed.

Lastly, I extend my thanks to those individuals who I have not named but have contributed to my success. Whether it was through assisting on an experiment, offering knowledge or technical expertise, or even as simple as sharing a smile or greeting in passing, I thank you for helping make my time at USF/Moffitt as memorable and extraordinary as it has been.

TABLE OF CONTENTS

List of Tables	v
List of Figures	vi
Abstract	x
Chapter 1: Background.....	1
Myelodysplastic Syndromes (MDS).....	1
MDS Overview	1
Etiology of MDS	2
MDS Classification	3
MDS Prognostication	6
MDS Treatment.....	10
Treatment of lower-risk patients	11
Treatment of higher-risk patients	13
Molecular and Cytogenetic Alterations	15
Aberrant Immune Activation in MDS.....	19
Autoimmune Disease and Infection	19
Cytokine, Chemokine and Growth Factor Profile	19
Overview of TLR Signaling	20
TLR Signaling Dysregulation in MDS.....	22
Bone Marrow Microenvironment Abnormalities	25
Overview of Hematopoiesis	27
Lymphoid Cell Lineage Involvement	29
The Role of Myeloid-Derived Suppressor Cells (MDSC) and S100A9	32
The 5q- Syndrome	35
Overview	35
Treatment of Del(5q) MDS.....	37
Pathobiology of the 5q- Syndrome.....	38
Ribosomal protein S14 (RPS14)	38
Casein kinase 1A1 (CSNK1A1)	40
TLR4-TRAF6-NF- κ B-dependent signaling axis.....	41
Diaphanous related formin 1 (DIAPH1).....	43
Programmed Cell Death	43
Caspases	43
Apoptosis	45
Autophagy.....	48
Historic View of Cell Death in MDS.....	50
Pyroptotic Cell Death	52

History and Hallmarks of Pyroptosis	52
NLR Proteins	56
Inflammasome Complexes and Canonical Activation and Signaling	57
Non-Canonical Inflammasome Signaling	63
The NLRP3 Inflammasome	65
NLRP3 Agonists.....	65
NLRP3 Inflammasome Activation: Signal 1	67
NLRP3 Inflammasome Activation: Signal 2	68
Endogenous Regulation of the NLRP3 Inflammasome	71
Evidence of Pyroptosis in the MDS Literature	73
β -Catenin	74
Canonical Wnt/ β -Catenin Signaling	74
Activation of β -Catenin is Regulated by Oxidative Stress.....	77
Chapter 2: The NLRP3 Inflammasome Functions as a Driver of the Myelodysplastic Syndromes Phenotype	79
Introduction	79
Results.....	81
MDS HSPC manifest inflammasome activation and pyroptosis	81
The alarmin S100A9 initiates pyroptosis.....	88
Inflammasome-activated cation channels increase the size of MDS progenitors	90
Inhibition of pyroptosis promotes effective hematopoiesis in MDS.....	92
S100A9 is sufficient to provoke HSPC pyroptosis <i>in vivo</i>	93
S100A9 and MDS somatic gene mutations trigger pyroptosis and β -catenin activation via ROS.....	99
MDS HSPC are primed for NLRP3 inflammasome activation	108
MDS MSC and stromal-derived lineages undergo pyroptosis	110
Discussion	114
Methods	120
MDS patient specimens	120
Mice	122
Reagents and cells	122
Immunofluorescence confocal microscopy	122
Flow cytometry analyses.....	123
Lentiviral infection of primary mononuclear cells	125
Enzyme-linked immunosorbent assays (ELISA).....	128
Intracellular S100A9 flow cytometry.....	128
Pore formation assay	128
Real-time quantitative PCR.....	129
Colony formation assays.....	129
ROS detection.....	130
ICTA mouse treatment studies	130
SRSF2 transfection of HEK293T cells	130
Immunoblotting	130
Immunoprecipitation.....	131

ASC crosslinking	131
Next-generation sequencing and mutation identification	132
POP-1 overexpression	132
Statistical analyses	134
 Chapter 3: Pyroptosis of Erythroid Progenitors Accounts for the Erythroid Defect	
Characteristic of the 5q- Syndrome	135
Introduction	135
Results	137
<i>Rps14</i> haploinsufficiency induces NLRP3 inflammasome activation in erythroid progenitors but not HSPC	137
<i>Rps14</i> haploinsufficient erythroid precursors predominantly undergo pyroptosis	140
ROS and β -catenin activation are significantly increased in <i>Rps14</i> haploinsufficient erythroid progenitors	142
Concurrent loss of <i>mDia1</i> and <i>miR-146a</i> results in pyroptotic cell death of erythroid precursors	143
ROS and β -catenin activation are significantly increased in <i>mDia1/miR-146a</i> double knockout mice	147
NLRP3 inflammasome inhibition restores effective erythropoiesis in del(5q) MDS	148
Discussion	150
Methods	154
MDS patient specimens	154
Mice	154
Reagents and cells	154
Immunofluorescence confocal microscopy	154
Cell death flow cytometry assay	155
ROS detection	155
ASC oligomerization	156
Colony formation assays	156
Statistical analyses	156
 Chapter 4: NLRP3 Inflammasome-Derived ASC Specks are a Diagnostic Biomarker for Myelodysplastic Syndromes (MDS)	
Introduction	157
Results	158
ASC specks are significantly increased in MDS	158
The percentage of PB plasma-derived ASC specks is a diagnostic biomarker for MDS	162
Specks may serve as a biomarker index of ineffective hematopoiesis	166
Discussion	168
Methods	172
Patient specimens	172
Reagents and cells	173

ASC speck staining	173
Immunofluorescence confocal microscopy	173
Enzyme-linked immunosorbent assay (ELISA).....	174
Statistical analyses	174
Chapter 5: Discussion	176
Implications	176
MDS-Specific Implications	176
Implications Related to Other Inflammatory Conditions and Diseases of Major Health Concern	178
Inflammasomopathies	179
Type 2 diabetes mellitus	182
Cardiovascular disease	184
Multiple sclerosis	185
Alzheimer’s disease	186
Parkinson’s disease	187
Gout and pseudogout.....	188
Fibrosing disorders.....	189
Ischemia-reperfusion injury	192
Future Directions	193
NLRP1 Inflammasome Activation	193
ER Stress/Inflammasome Signaling Axis.....	198
5’ Adenosine Monophosphate (AMP)- Activated Protein Kinase	199
Conclusion	202
References	204
Appendix 1.....	239
Copyright Permission.....	239

LIST OF TABLES

Table 1. Overview of the FAB and WHO classification systems for MDS.....	7
Table 2. IPSS and IPSS-R scoring systems for MDS risk stratification	9
Table 3. Standard and investigational therapeutic approaches for the treatment of MDS	12
Table 4. Primer sequences used for real-time quantitative PCR	129
Table 5. Clinical and genotypic characteristics of sequenced patients	133
Table 6. Mean percentage of PB plasma-derived ASC speck values across sample cohorts	164

LIST OF FIGURES

Figure 1. Temporal order and frequency of recurrent somatic gene mutations in MDS	17
Figure 2. Overview of MyD88-dependent and TRIF-dependent TLR signaling pathways	23
Figure 3. Hierarchy of the mesenchymal lineage	26
Figure 4. Overview of hematopoiesis	30
Figure 5. General mechanisms of hematopoietic inhibition by MDSC and the role of the MDSC/S100A9 axis in MDS	36
Figure 6. Classification of human caspases	46
Figure 7. Simplistic overview of the intrinsic and extrinsic apoptotic pathways	47
Figure 8. Autophagy and mitophagy maintain cellular homeostasis through catabolism	49
Figure 9. The hallmarks of pyroptosis	53
Figure 10. Domain organization of the nucleotide-binding oligomerization domain (NOD)-like receptors (NLRs)	58
Figure 11. Activation of pro-caspase-1 by inflammasome complexes requires ASC-dependent or ASC-independent nucleation and polymerization.....	62
Figure 12. The non-canonical inflammasome signaling pathway	66
Figure 13. Canonical Wnt/ β -catenin signaling depicted in the context of pathway inactivation and activation	76
Figure 14. Oxidative stress positively regulates β -catenin activation and signaling	78
Figure 15. Fulminant pyroptosis is manifest in HSPC and progeny in MDS	82

Figure 16. NLRP3 inflammasome assembly may be MDS-specific	85
Figure 17. Caspase-1 activation significantly correlates with the extent of pyroptosis detected in MDS BM-MNC.....	87
Figure 18. S100A9 initiates pyroptosis in MDS	89
Figure 19. MDS precursors evidence cell swelling, a pyroptotic hallmark.....	91
Figure 20. Inhibition of pyroptosis abrogates MDS HSPC death and augments colony forming capacity.....	94
Figure 21. Pyroptosis is the principal mechanism of HSPC death in S100A9 transgenic mice	96
Figure 22. ICTA inhibits inflammasome activation	98
Figure 23. S100A9 induces ROS through NADPH oxidase to activate β -catenin.....	100
Figure 24. <i>U2AF1</i> mutations manifest in MDS provoke pyroptosis and induce NOX-dependent activation of β -catenin	102
Figure 25. <i>SF3B1</i> K700E induces pyroptosis and supports self-renewal through β -catenin activation	105
Figure 26. <i>SRSF2</i> mutations induce pyroptosis and support self-renewal through β -catenin.....	107
Figure 27. <i>Asx1</i> and <i>Tet2</i> deletions are sufficient to induce pyroptosis and drive self-renewal through β -catenin activation.....	109
Figure 28. Somatic gene mutations and mutation variant allele fraction correlate with the extent of pyroptosis in MDS	111
Figure 29. Inflammasome activation occurs via up-regulation of TXNIP and down-regulation of POP-1	113
Figure 30. Pyroptosis is manifest in MSC and stromal-derived lineages in MDS	115
Figure 31. An S100A9/pyroptosis circuit provokes phenotypes manifest in MDS	121
Figure 32. Flow cytometry gating strategies for evaluating the extent of pyroptosis versus apoptosis in normal/MDS specimens and WT/S100A9Tg mice	126

Figure 33. <i>Rps14</i> haploinsufficiency induces NLRP3 inflammasome activation in erythroid progenitors but not HSPC.....	138
Figure 34. <i>Rps14</i> haploinsufficient erythroid progenitors predominantly undergo pyroptotic cell death	141
Figure 35. ROS and β -catenin activation are markedly increased in erythroid progenitors in the context of <i>Rps14</i> haploinsufficiency	144
Figure 36. Concurrent loss of <i>mDia1</i> and <i>miR-146a</i> results in pyroptotic cell death of erythroid progenitors	146
Figure 37. ROS and β -catenin activation are significantly increased with dual loss of <i>mDia1</i> and <i>miR-146a</i>	148
Figure 38. NLRP3 inflammasome inhibition restores effective erythropoiesis in patients with del(5q) MDS	149
Figure 39. The percentage of plasma ASC specks increases with protein concentration.....	159
Figure 40. ASC specks are significantly increased in MDS and may have prognostic value	161
Figure 41. The percentage of glucose-adjusted, PB plasma-derived ASC specks is specific for MDS.....	165
Figure 42. PB plasma-derived ASC specks are a response biomarker to lenalidomide treatment.....	167
Figure 43. PB plasma-derived ASC specks are a response biomarker to lenalidomide treatment in two independent data sets	169
Figure 44. PB plasma-derived ASC specks remain unchanged after response to ESA or HMA therapy	170
Figure 45. NLRP3 inflammasome activation is a pathobiological driver of many inflammatory conditions and diseases of major health concern.....	180
Figure 46. NLRP1 inflammasome formation and activation is significantly increased in MDS BM-MNC	195
Figure 47. S100A9 induces NLRP1 inflammasome formation in U937 cells and normal BM-MNC.....	196

Figure 48. ER stress triggers NLRP3 activation, leading to mitochondrial dysfunction and activation of the NLRP3 inflammasome complex.....200

ABSTRACT

Note: Portions of this abstract have been previously published in the journal *Blood*, Basiorka et al. *Blood*. 2016 Oct 13, and has been reproduced in this manuscript with permission from the publisher.

Myelodysplastic syndromes (MDS) are genetically diverse hematopoietic stem cell malignancies that share a common phenotype of cytological dysplasia, ineffective hematopoiesis and aberrant myeloid lineage maturation. Apoptotic cell death potentiated by inflammatory cytokines has been considered a fundamental feature of MDS for over two decades. However, this non-inflammatory form of cell death cannot account for the inflammatory nature of these disorders. We report that a hallmark of lower-risk (LR) MDS is activation of the NLRP3 inflammasome, which drives clonal expansion and pyroptosis, a caspase-1-dependent programmed cell death induced by danger-associated molecular pattern (DAMP) signals. Independent of genotype, MDS hematopoietic stem and progenitor cells (HSPC) overexpress pyroptosis-related transcripts, inflammasome proteins and manifest activated NLRP3 inflammasome complexes that direct caspase-1 activation, IL-1 β and IL-18 maturation and pyroptotic cell death. Using the S100A9 transgenic (S100A9Tg) mouse model that phenocopies human MDS, we demonstrated that forced expression of S100A9 was sufficient to drive pyroptosis *in vivo*, implicating pyroptosis as the principal mechanism of HSPC cell death in S100A9Tg mice. The lytic cell death releases intracellular contents that include alarmins and catalytically active ASC specks, which can propagate bystander

inflammation. Notably, MDS mesenchymal stromal cells (MSC) and stromal-derived lineages were found to predominantly undergo pyroptosis, with marked activation of caspase-1 and NLRP3 inflammasome complexes. These findings may account for the clusters of both HSPC and stromal cell death previously described in the bone marrows of patients with MDS.

Mechanistically, pyroptosis is triggered by the alarmin S100A9 that is found in excess in MDS HSPC and bone marrow (BM) plasma. Further, both somatic gene mutations and S100A9-induced signaling activate NADPH oxidase (NOX), generating reactive oxygen species (ROS) that initiate cation influx, cell swelling and β -catenin activation. Accordingly, ROS and active β -catenin were significantly increased in MDS BM mononuclear cells (BM-MNC) and S100A9Tg mice compared to normal controls, as well as in human cell lines harboring gene mutations and in murine models of gene mutation knock-in or gene loss. ROS and β -catenin nuclear translocation were significantly reduced by NLRP3 or NOX inhibition, indicating that S100A9 and somatic gene mutations prime cells to undergo NOX1/4-dependent NLRP3 inflammasome assembly, pyroptosis and β -catenin activation. Together, these data explain the concurrent proliferation and inflammatory cell death characteristic of LR-MDS.

Given that loss of a gene-rich area in del(5q) disease results in derepression of innate immune signaling, we hypothesized that this genetic deficit would trigger assembly of the NLRP3 inflammasome complex, akin to the pathobiological mechanism characteristic of non-del(5q) MDS. To this end, we utilized two distinct murine models of del(5q) disease, namely in the context of *Rps14* haploinsufficiency and concurrent loss of *mDia1* and *microRNA (miR)-146a*. In both models, pyroptosis was not evident in the

HSPC compartment; however, early erythroid progenitors displayed high fractions of pyroptotic cells. This was associated with significant increases in caspase-1 and NLRP3 inflammasome activation, ROS and nuclear localization of β -catenin, which was extinguished by inflammasome or NOX complex inhibition. These data suggest that early activation of the inflammasome drives cell death and prevents terminal maturation of erythroid precursors, accounting for the progressive anemia characteristic of del(5q) disease, whereby hematopoietic defects are primarily restricted to the erythroid compartment. Importantly, these data implicate a similar pathobiological mechanism in del(5q) MDS as is observed in non-del(5q) patients.

The identification of the NLRP3 inflammasome as a pathobiological driver of the LR non-del(5q) and del(5q) MDS phenotype allows for novel therapeutic agent development. Notably, knockdown of NLRP3 or caspase-1, neutralization of S100A9, and pharmacologic inhibition of NLRP3 or NOX suppresses pyroptosis, ROS generation and nuclear β -catenin in MDS, and are sufficient to restore effective hematopoiesis. In del(5q) murine models, inhibition of the NLRP3 inflammasome significantly improved erythroid colony forming capacity by a mechanism distinct from that of lenalidomide, highlighting the translational potential for targeting this innate immune complex in this subset of MDS. Thus, alarmins and founder gene mutations in MDS license a common redox-sensitive inflammasome circuit, which suggests new avenues for therapeutic intervention.

Furthermore, aggregated clusters of the NLRP3 adaptor protein ASC [apoptosis-associated speck-like protein containing a caspase activation and recruitment domain (CARD)] are referred to as ASC specks. During pyroptosis, ASC specks are released

from dying cells and function as DAMP signals that propagate inflammation. In this way, specks are a surrogate marker for NLRP3 inflammasome activation and pyroptotic cell death. Given that pyroptosis is the predominant mechanism of cell death in MDS and ASC specks are readily quantified by flow cytometry, we hypothesized that BM or peripheral blood (PB) plasma-derived ASC specks may be a biologically rational biomarker for the diagnosis of MDS.

The percentage of ASC specks were significantly increased in MDS BM plasma compared to normal, healthy donors, which was validated by confocal microscopy. PB plasma-derived ASC specks were significantly greater in LR- versus HR-MDS, consistent with the greater extent of cell death and myeloid-derived suppressor cell (MDSC) expansion in LR disease. As hyperglycemia induces NLRP3 inflammasome activation, plasma glucose levels were measured to adjust for this confounding variable. Subsequently, the percentage of glucose-adjusted, PB plasma-derived ASC specks was measured in a panel of specimens of varied hematologic malignancies. The corrected percentage of ASC specks was significantly increased in MDS compared to normal donors and to each other malignancy investigated, including other myeloid and lymphoid leukemias, myeloproliferative neoplasms and overlap syndromes, like chronic myelomonocytic leukemia (CMML). These data indicate that the glucose-adjusted ASC speck percentage is MDS-specific and may be a valuable diagnostic biomarker. At a cutoff of 0.039, the biomarker minimizes misclassification error and achieves 95% sensitivity and 82% specificity in classifying MDS from normal donors, other hematologic malignancies and T2D. Lastly, the biomarker declined with treatment response to lenalidomide in LR-MDS patients, but not to erythropoietin stimulating agent

(ESA) or hypomethylating agent (HMA) therapy. As such, the percentage of ASC specks represents the first biologically rational, diagnostic biomarker for MDS that can be implemented with current diagnostic practices to reduce diagnostic error.

CHAPTER 1

Background

Myelodysplastic Syndromes (MDS)

MDS Overview. Myelodysplastic syndromes (MDS) are hematopoietic stem cell malignancies characterized by ineffective hematopoiesis with marked genetic heterogeneity.¹⁻³ These disorders are clonal in nature, with the affected precursor cell restricted to the erythroid, myeloid and megakaryocytic lineage.² Resultant peripheral blood cytopenias demonstrate aberrant myeloid differentiation leading to dysplastic and ineffective blood production.^{4,5} Though prevalence is likely under-reported, MDS occur in approximately 3 or 4 individuals per 10⁵, with a significant over-representation of males.⁶⁻⁸ No significant differences are observed with respect to race, though individuals of white decent are more frequently affected.⁶

Although MDS cases are largely sporadic, rare familial clusters have been reported. To date, four familial syndromes predisposing to MDS have been described.⁹ Inherited germline mutations in the *RUNX1* or *CEBPA* genes, as well as partial or complete loss of chromosome 7 have been implicated in familial predisposition.¹⁰⁻¹⁴ Additionally, though incidence is quite rare, childhood cases of MDS are typically associated with congenital disorders and underlying bone marrow failure syndromes.^{15,16} Karyotypic abnormalities are found in approximately 55% of primary

childhood cases, with monosomy 7 most commonly detected.¹⁷

Etiology of MDS. To date, a holistic understanding of MDS etiology remains problematic. This can be attributed to a number of factors, including the lack of true MDS cell lines and inadequate animal models, slow growth of primary cells in culture and conflict over disease classification.^{4,18,19} Nevertheless, a number of predisposing factors are recognized. Incidence increases dramatically with age, suggesting that age may be the greatest risk factor for MDS development.²⁰ Individuals 80 years and older have a five-fold greater likelihood for development of MDS than individuals ages 60-69, with a median age of 77 years at diagnosis.⁶⁻⁸ Moreover, whereas 85-90% of cases arise *de novo*, 10-15% of MDS cases occur in individuals who have received prior radiation or chemotherapy.²⁰⁻²² These secondary or treatment-related cases are associated with poorer prognosis owing largely to the over-representation of unfavorable karyotypes.

Additionally, MDS may arise secondary to prolonged environmental or occupational exposures to organic solvents, including benzene or other petrochemicals and genotoxic agents such as pesticides, fertilizer and others.²⁰ In a meta-analysis of 10 case-control studies, cigarette smoking was significantly associated with MDS, with an odds ratio of 1.45, or a 45% increase in risk.²³ In a similar meta-analysis, when alcohol consumption was assessed in 5 case-control studies, the overall association of 1.31 was not significant.²³ Furthermore, in a prospective lifestyle study, obese individuals were shown to have a 2.2-fold greater risk for MDS development, illustrating a positive correlation between body mass index and MDS.²⁴ These findings suggest that smoking and obesity, but not alcohol consumption, play a role in MDS pathogenesis.

Both MDS and AML occur with greater frequency in individuals with a history of chronic infection and/or autoimmune disease, raising the notion that immune disruption precedes MDS/AML development.²⁵ As is true of childhood cases, individuals with congenital diseases or bone marrow failure conditions are also at heightened risk for MDS development.^{9,16}

Moreover, clonal drifts in hematopoietic stem cell (HSC) lineage distribution, namely myeloid skewing at the expense of lymphoid HSC, are associated with lymphoid senescence and enriched myelopoiesis with normal aging.²⁶⁻²⁸ During aging, stem cell functionality diminishes with respect to quiescence, self-renewal, differentiation and immune function, as a result of inflammatory cytokines, oxidative stress, DNA damage and telomere erosion.²⁷ As MDS are characterized by a defect in the myeloid-HSC compartment leading to aberrant myeloid maturation, senescence-dependent accumulation of alternations in hematopoietic stem and progenitor cells (HSPC), as well as cells of the surrounding microenvironment, may contribute to MDS pathogenesis and stem cell dysfunction. For instance, telomeres are shorter in MDS compared to normal donors, resulting in part from the high proliferative fraction of HSPC in MDS.²⁹ Patients who reported prior exposure to known etiologic environmental factors had significantly reduced telomeres in myeloid cells than unexposed persons.²⁹

MDS Classification. The vast degree of disease heterogeneity, both clinical and molecular, has warranted categorization of MDS into distinct, recognizable subtypes. Prior to the 1970s, what is now known as MDS was regarded as a preleukemic condition.³⁰ Patients with “preleukemia,” though at increased risk of leukemic transformation, did not always develop myeloid leukemia, and so the term

“myelodysplastic disease” was suggested instead.³¹ In the early 1970s, the French-American-British (FAB) Co-operative Group formed in an attempt to classify the acute and chronic leukemias. The seven members of the FAB described two “dysmyelopoietic syndromes,” refractory anemia with excess blasts (RAEB) and chronic myelomonocytic leukemia (CMML) in their first publication in 1976.³² It became apparent that these designations did not readily differentiate the dysmyelopoietic syndromes, or myelodysplastic syndromes, from acute myeloid leukemia (AML), illustrating the need for a new approach that would provide greater distinction between MDS subtypes.

In 1982, the FAB published a new proposal for MDS classification which was largely based on morphology and the percentage of blasts within the bone marrow (BM) and peripheral blood (PB). In total, five morphological subtypes of MDS were recognized, including refractory anemia (RA), RA with ringed sideroblasts (RARS), RA with excess blasts (RAEB), RAEB ‘in transformation’ and CMML.³³ The addition of RAEB in transformation prompted adjustment of AML diagnostic criterion from 50% blasts to at least 30%. Though the FAB acknowledged that these classification criteria did not precisely stratify MDS, it would serve as the precedent for nearly twenty years.

As understanding of the biological, molecular, immunophenotypical and clinical features of MDS pathobiology increased, so did the need for a new classification approach. In 2001, the World Health Organization (WHO) proposed an updated classification system for myeloid neoplasms, including MDS.³⁴ Definitions of RA and RARS were refined. A new subtype was added, namely refractory cytopenia with multilineage dysplasia (RCMD), which when combined with the presence of ringed sideroblasts would be called RCMD-RS and offered prognostic refinement. RAEB was

divided into two separate entities, RAEB-1 when bone marrow blast percentage was between 5-9% and RAEB-2 with blasts between 10-19%. RAEB in transformation was removed, and the AML diagnostic criterion was again lowered to 20% or more peripheral blood or bone marrow blasts. CMML was reclassified as a myelodysplastic/myeloproliferative disease (MDS/MPN), or a condition with overlapping features of both hematologic malignancy types. Lastly, the 5q- syndrome was recognized as the first and only cytogenetically defined MDS subtype, characterized by an interstitial deletion between q21 and q32 of chromosome 5.^{34,35}

In 2008, the WHO published a revision of its MDS classification system.³⁶ The previously separated RCMD-RS subtype was now captured under RCMD because of overlapping outcomes. Perhaps the greatest change was the creation of a new, overarching subtype called refractory cytopenia with unilineage dysplasia (RCUD). This includes patients with RA, and those with refractory neutropenia (RN) and refractory thrombocytopenia (RT). Finally, the WHO recently revised this classification early in 2016.³⁷ While focus in the 2016 revision remains on the percentage of blasts and the extent of dysplasia, changes in subtype nomenclature reflect that identifying the specific cytopenic lineage is not central to accurate classification.³⁷ Furthermore, cytogenetic abnormalities deemed MDS-defining remain unchanged from the previous revision. While identification of the MDS mutanome has expanded dramatically in the last decade, this updated version does not incorporate mutational information into classification with the sole exception of *SF3B1*, perhaps foreshadowing what can be expected in the next WHO revision.³⁷ A summary of the FAB and WHO classification systems is outlined in Table 1. As understanding of MDS pathobiology continues to

expand with novel findings and accumulating molecular insight, our understanding of these complex disorders will continue to be refined.

MDS Prognostication. Inasmuch as patients exhibit clinical and molecular heterogeneity, they too exhibit vast prognostic variation. Therefore, it became imperative to establish a consensus prognostic scoring system that could stratify patients into distinct risk groups and ultimately guide therapy selection. In 1997, the International Prognostic Scoring System (IPSS) was established.³⁸ The IPSS is based on three independent variables that significantly impact disease outcome with respect to risk of leukemic transformation and survival in patients with *de novo* MDS, namely cytogenetic anomalies, BM blast percentage and number of cytopenias.³⁸ Each variable is given a particular weighted score, whose sum yields a cumulative score representative of risk. The IPSS stratifies patients into four distinct risk groups: low, intermediate-1, intermediate-2 and high risk. Patients of low and intermediate-1 risk collectively represent lower-risk disease, and intermediate-2 and high risk patients collectively represent higher-risk MDS. Though the IPSS served as the fundamental scoring system for over two decades, it was not without limitations.

The revised IPSS (IPSS-R), published in 2012, aimed to address the shortcomings of the initial system while incorporating the potential prognostic impact of novel clinical and cytogenetic findings.³⁹ Although the core variables remained the same, refinements were made. Less common cytogenetic abnormalities were now included and the BM blast category was further repartitioned. Whereas less weight was given to the number of cytopenias in the IPSS, the IPSS-R recognizes the severity of cytopenias by establishing clinically relevant cutpoints. Taken together, the IPSS-R

Table 1. Overview of the FAB and WHO classification systems for MDS.

A FAB Classification			Key BM findings	
Disease	Dysplasia	Blast, %	Ring sideroblasts, %	
RA Refractory anemia	Erythroid only	<5		
RARS Refractory anemia with ring sideroblasts	Erythroid only	<5	>15	
RAEB Refractory anemia with excess blasts	≥2 or more myeloid lineages	≥5-20		
RAEB 'in transformation'	≥2 or more myeloid lineages	>20-30		
CMML Chronic myelomonocytic leukemia	≥2 or more myeloid lineages	<20		

B WHO Classification			Key BM findings	
Disease	Dysplasia	Blast, %	Ring sideroblasts, %	
RA Refractory anemia	Erythroid only	<5	<15	
RARS Refractory anemia with ring sideroblasts	Erythroid only	<5	≥15	
RCMD Refractory cytopenia with multilineage dysplasia	≥2 or more myeloid lineages	<5	<15	
RCMD-RS RCMD and ring sideroblasts	≥2 or more myeloid lineages	<5	≥15	
RAEB-1 Refractory anemia with excess blasts-1	Unilineage or multilineage	5-9		
RAEB-2 Refractory anemia with excess blasts-2	Unilineage or multilineage	10-19		
MDS-U Myelodysplastic syndrome, unclassified	Unilineage in granulocytes or megakaryocytes	<5		
5q-Syndrome MDS associated with isolated del(5q)		<5		

C 2008 Revised WHO Classification			Key BM findings	
Disease	Dysplasia	Blast, %	Ring sideroblasts, %	
RCUD: Refractory cytopenia with unilineage dysplasia: RA Refractory anemia RN Refractory neutropenia RT Refractory thrombocytopenia	Unilineage	<5	<15	
RARS Refractory anemia with ring sideroblasts	Erythroid only	<5	≥15	
RCMD Refractory cytopenia with multilineage dysplasia	≥2 or more myeloid lineages	<5	±15	
RAEB-1 Refractory anemia with excess blasts-1	Unilineage or multilineage	5-9		
RAEB-2 Refractory anemia with excess blasts-2	Unilineage or multilineage	10-19		
MDS-U Myelodysplastic syndrome, unclassified	≥1 or more myeloid lineages	<5		
5q-Syndrome MDS associated with isolated del(5q)		<5		

D 2016 Revised WHO Classification			Key BM findings	
Disease	Dysplasia	Blast, %	Ring sideroblasts, %	
MDS-SLD MDS with single lineage dysplasia	1 lineage	<5	<15	
MDS-MLD MDS with multilineage dysplasia	2 or 3 lineages	<5	<15	
MDS-RS MDS with ring sideroblasts				
MDS-RS-SLD MDS-RS with single lineage dysplasia	1 lineage	<5	≥15	
MDS-RS-MLD MDS-RS with multilineage dysplasia	2 or 3 lineages	<5	≥15	
MDS with isolated del(5q)	1-3 lineages	<5	None	
MDS-EB MDS with excess blasts				
MDS-EB-1 MDS with excess blasts-1	0-3 lineages	5-9	None	
MDS-EB-2 MDS with excess blasts-2	0-3 lineages	10-19	None	
MDS-U MDS, unclassifiable				
with 1% blood blasts	1-3 lineages	<5	None	
with single lineage dysplasia and pancytopenia	1 lineage	<5	None	
based on defining cytogenetic abnormality	0	<5	<15	
Refractory cytopenia of childhood	1-3 lineages	<5	None	

recognizes five distinct risk groups, specifically very good, good, intermediate, poor and very poor. As history has demonstrated with respect to both classification and prognosis of MDS, improved understanding of MDS biology will likely necessitate further refinement of the IPSS-R. A summary of the IPSS and IPSS-R can be found in Table 2.

Notably, both the IPSS and IPSS-R models stratify MDS patients at the time of diagnosis, illustrating a key limitation. In order to account for excluded patient populations, including patients with secondary MDS and those who have previously been treated, the MD Anderson Global Prognostic Scoring System (MDGPSS) was created.⁴⁰ This model, applicable to patients at any time during the course of their disease, was shown to add prognostic value to the IPSS. The MDGPSS includes variables not considered in the IPSS or IPSS-R, including age, performance status and prior transfusion requirement.⁴⁰ Like the IPSS, the MDGPSS stratifies patients into low, intermediate-1, intermediate-2 and high risk.

In solid tumors, the presence of a comorbidity significantly impacts therapeutic selection as well as overall survival.⁴¹ Comorbid conditions are strikingly common amongst individuals with MDS,⁸ though none of the aforementioned prognostic systems consider the impact of comorbidities on prognosis. Use of the Adult Comorbidity Evaluation-27 (ACE-27) index, demonstrated that overall survival decreased with increasing severity of comorbid conditions, prompting the creation of a novel prognostic model.⁴² Three variables, namely age, IPSS and baseline comorbidities, segregate patients into low, intermediate or high risk disease.⁴² In a similar analysis, the consideration of comorbid conditions at the time of diagnosis was shown to add to the prognostic value of the IPSS-R.⁴³

Table 2. IPSS and IPSS-R scoring systems for MDS risk stratification.

A International Prognostic Scoring System (IPSS)

Score value:	0	0.5	1	1.5	2
BM blasts, %	<5	5-10	---	11-20	21-30
Karyotype*	Good	Intermediate	Poor		
Cytopenias	0/1	2/3			

*Cytogenetic Abnormalities	
Good	Normal, -Y, del(5q), del(20q)
Intermediate	Other abnormalities
Poor	Complex (≥3 abnormalities), chromosome 7 abnormalities

Risk Group:	Total Risk Score	Median Survival, Years
Low	0	5.7
Intermediate-1	0.5-1	3.5
Intermediate-2	1.5-2	1.2
High	≥2.5	0.4

B Revised IPSS

Score value:	0	0.5	1	1.5	2	3	4
Cytogenetics**	Very good	---	Good	---	Intermediate	Poor	Very poor
BM blast, %	≤2	---	>2 - <5	---	5-10	>10	---
Hemoglobin, g/dL	≥10	---	8 - <10	<8	---	---	---
Platelets, x10 ⁹ /L	≥100	50 - <100	<50	---	---	---	---
ANC, absolute neutrophil count, x10 ⁹ /L	≥0.8	<0.8	---	---	---	---	---

**Cytogenetic Abnormalities	
Very good	-Y, del(11q)
Good	Normal, del(5q), del(12q), del(20q), double including del(5q)
Intermediate	del(7q), +8, +19, i(17q), any other single or double independent clones
Poor	-7, inv(3)/t(3q)/del(3q), double including -7/del(7q), complex (3 abnormalities)
Very poor	Complex (>3 abnormalities)

Risk Group:	Total Risk Score	Median Survival, Years
Very Low	≤1	5.4
Low	>1.5-3	4.8
Intermediate	>3-4.5	2.7
High	>4.5-6	1.5
Very High	>6	0.7

At the present time, the IPSS-R is the most commonly employed model in the hematology clinic at the H. Lee Moffitt Cancer Center and Research Institute. Nevertheless, the majority of research investigations utilize the IPSS. Typically patients

will be grouped into lower-risk (low and intermediate-1) versus higher-risk (intermediate-2 and high) disease for therapeutic trials.

MDS Treatment. Historically, treatment for MDS has largely been empirical. Unfortunately, response rates and durations of response are often limited. While three therapies have been FDA-approved for MDS to date,⁴⁴⁻⁴⁶ regrettably no novel therapies have been approved in over ten years. As the age of the American population is increasing, there is a projected increase in burden of all age-related disorders, including MDS, and consequently a heightened necessity for novel treatment approaches.⁴⁷ The lack of effective therapeutic strategies in MDS can be attributed to deficiencies in our understanding of the underlying molecular mechanisms that contribute to disease initiation and progression, underscoring the importance of developing biologically rational therapies aimed at targets relevant to disease pathobiology that will surpass the standards of care available today. Presently, clinicians use a risk-adapted approach to therapy, whereby therapy selection is made following IPSS-R-guided determination of disease prognosis.⁵ Generally, the treatment goal for lower-risk disease is to improve quality of life by managing cytopenias and symptoms. A more aggressive approach is used in higher-risk patients, whereby efforts are made to reduce risk of AML transformation and increase survival. A summary of therapeutic approaches in MDS can be found in Table 3.

Notably, the only curative treatment for patients with MDS, irrespective of risk group, is allogeneic stem cell transplantation (alloSCT).^{48,49} Unfortunately, transplantation is associated with high morbidity and mortality, and few patients are suitable candidates given their late age and the frequent presence of comorbidities.

Nevertheless, transplantation approaches are being refined to expand patient eligibility, improve survival and reduce the risk of relapse following alloSCT.⁴⁸⁻⁵⁰

Treatment of lower-risk patients. With respect to clinical manifestations, treatment of anemia remains a principal challenge. The majority of patients present with anemia, and 80-90% will require frequent red blood cell transfusions at some point during the course of the disease.⁵¹ Transfusion-dependence does have negative implications, including poorer overall survival, increased risk of AML transformation and iron overload, which results in significant morbidity and mortality.⁵¹ As an alternative to frequent transfusions, growth factor support like erythroid stimulating agents (ESAs) has been employed. Recombinant human erythropoietin (Epo) has proven effective in improving red cell production in a subset of patients with low serum erythropoietin level and transfusion-burden. Response rates range from approximately 25% to 60% depending on the study population.⁵²⁻⁵⁵ Though Epo has been the standard of care since the early 1990s, it has yet to gain FDA approval.⁵⁶ Additionally, in an attempt to augment response to Epo, others have combined Epo treatment with granulocyte- or granulocyte-macrophage colony stimulating factors (G-CSF/GM-CSF).⁵⁷ However, a meta-analysis revealed no significant response benefit of either combination therapy over Epo therapy alone.⁵⁸

Moreover, increasing evidence suggesting that immune dysfunction contributes causally to aberrant hematopoiesis in MDS has encouraged use of immunosuppressive therapies (IST), including cyclosporine A and antithymocyte globulin (ATG).^{59,60} Lenalidomide, an immune modulating but not IST, is a second-generation immunomodulatory drug (IMiD). In 2005, the FDA approved lenalidomide for the

Table 3. Standard and investigational therapeutic approaches for the treatment of MDS.

	Lower-Risk	Higher-Risk
Allogeneic stem cell transplantation (alloCST)	X	X
Erythroid stimulating agents (ESAs)	X	X
Immunosuppressive therapies:	X	
Cyclosporin A	X	
Antithymocyte globulin (ATG)	X	
Lenalidomide*	X	
Intensive chemotherapy		X
Azanucleosides	X	X
5'-Azacytidine*		X
Decitabine*		X
Investigational therapies	X	X
IDO1 inhibitor, INCB024360	X	
SMAD/TGF- β axis inhibitors	X	
TLR2 antibody	X	
p38 MAPK/Tie2 inhibitor	X	
Nucleoside analogs:		X
Clofarabine		X
Sapacitabine		X
Histone deacetylase (HDAC) inhibitors		X
Polo-like kinase 1 (PLK1) inhibitors		X
Targeted therapies of targetable mutations		X
Immune checkpoint inhibitors		X

*FDA approved therapies for MDS treatment

treatment of transfusion-dependent, lower IPSS risk patients with a chromosome 5q deletion [del(5q)].⁴⁵ This subset of patients, who typically responds poorly to Epo treatment, has remarkable response rates to lenalidomide. Approximately 76% of patients respond to therapy, 67% become transfusion-independent and 45% achieve a complete cytogenetic remission, illustrating that lenalidomide suppresses the del(5q) clone.⁴⁵ In a phase 2 study of lenalidomide in non-del(5q) MDS, approximately 46% of patients responded with 26% becoming transfusion-independent.⁶¹ These findings

suggest lenalidomide may benefit a subset of non-del(5q) patients who fail ESA therapy.⁶¹

To date, the landscape of novel therapeutic strategies is enriched with approaches aimed at inhibiting dysregulated innate immune pathways. For a number of novel agents, promising pre-clinical data has warranted further investigation in clinical trials. The selective inhibition of IDO1, an enzyme involved in tryptophan catabolism and immune modulation, with INCB024360 can reduce regulatory T cell expansion and myeloid-derived suppressor cell (MDSC) activity while concurrently increasing T cell proliferation.⁶² A phase II study of this agent has recently completed. Aberrant overactivation of the SMAD/TGF- β axis has led to a number of phase II clinical trials, including the use of a TGF- β ligand trap receptor and a TGF- β receptor 1 kinase inhibitor.⁶³⁻⁶⁵ A humanized Toll-like receptor (TLR2) antibody is currently in a phase II study. Expression of TLR2 is up-regulated 37-fold in CD34+ BM mononuclear cells (BM-MNC).^{66,67} Lastly, a dual p38 MAPK/Tie2 inhibitor has completed phase I testing, with approximately 32% of patients responding.⁶⁸ Undoubtedly, the innate immune era affords great promise for improved therapeutic strategies that may lead to durable responses and ideally cures.

Treatment of higher-risk patients. Prior to the mid-2000s, conventional care for higher-risk patients included supportive therapy, like transfusions or growth factor support, low-dose cytarabine or intensive chemotherapeutic regimens that mirrored those employed in *de novo* AML. Though complete responses to intensive chemotherapy range from 40-60%, they are neither durable nor curative.^{69,70} Moreover,

elderly patients, who represent the majority of MDS cases, poorly tolerate these aggressive regimens, evidenced by relatively high toxicity-related mortalities.⁷⁰

A major advancement in higher-risk therapy came with the understanding that DNA in MDS is largely hypermethylated, encouraging preclinical studies of hypomethylating agents (HMAs), or azanucleosides.⁷¹ In 2004 and 2006, the FDA approved the use of 5'-azacytidine and its analog decitabine, respectively, for the treatment of MDS.^{46,72} Patients treated with these therapies demonstrate more durable responses, increased median time to AML transformation, and most importantly in the case of azacitadine, increased overall survival.^{46,72-74} Given the survival benefit of azanucleoside therapy, these agents represent the standard of care for higher-risk patients, but interestingly impart no survival advantage to patients of lower-risk disease.

For higher-risk patients, novel therapeutic strategies are largely aimed at imparting benefit to patients who have failed azanucleoside therapy, or identifying therapies that may be used in combination with hypomethylating agents. Nucleoside analogues, including clofarabine and sapacitabine, have completed phase I clinical testing.⁷⁵⁻⁷⁷ These cytotoxic agents demonstrated efficacy in refractory patients, warranting further investigation as single agents or in combination therapy. As an alternative to HMAs, and also in conjunction with HMA treatment, histone deacetylase (HDAC) inhibitors have been investigated as a means of modulating aberrant epigenetic alterations in MDS. The phase I and II data have yielded encouraging response rates, whereas randomized phase II and III trials have been disappointing.⁷⁸⁻⁸⁰ Rigosertib, a kinase inhibitor with multiple targets, including polo-like kinase 1 (PLK1), also has clinical activity in HMA resistant patients.⁸¹ Moreover, molecular alterations in the *FLT3*

and *RAS* genes are associated with poor overall survival, increased risk of AML transformation and poor response to standard therapies.⁸² As these mutations are readily targetable, investigations into FLT3-specific and MAPK pathway inhibitors in higher-risk patients are warranted and underway. Lastly, immune checkpoint receptors and ligands CTLA4, PD-1, PD-L1 and PD-L2, which function to attenuate the immune response, have been shown to be overexpressed in MDS, possibly contributing to the suppressive bone marrow milieu observed in these disorders.⁸³ Notably, treatment with hypomethylating agents increases expression of these checkpoint receptors, suggesting use of blocking antibodies not only as single-agent therapies, but in combination with standard therapeutic approaches.⁸³

Molecular and Cytogenetic Alterations. In the last decade, understanding of the breadth and type of genetic lesions present in MDS has rapidly expanded, due in part to advances in sequencing technology and computational approaches aimed at managing large data sets. These data have illustrated that molecular and cytogenetic alterations are common and often complex, owing to chromosomal abnormalities, somatic gene mutations and epigenetic alterations. The vast molecular heterogeneity evident in MDS imparts biological and clinical heterogeneity in these disorders, both illustrating that genotype directly affects phenotype and contributing to the premise that multiple mechanisms of pathogenesis culminate in the MDS phenotype.⁸⁴

Cytogenetic alterations are critical in guiding diagnosis, prognosis and treatment selection in MDS, as the IPSS and IPSS-R both consider the type and clinical impact of specific karyotypic abnormalities.^{38,39} Frequently observed genetic lesions include inversions, deletions, gains or losses of whole chromosomes and copy number

alterations. Approximately 50% of *de novo* patients and up to 80% of secondary or treatment-related MDS patients present with a karyotypic anomaly.⁸⁵ With the exception of isolated 5q and 20q deletions, the presence of cytogenetic alterations negatively impacts survival, as overall survival drops dramatically from 53 months in individuals with a normal karyotype, to 17 months in those with 3 distinct lesions and just 9 months in those with 4 or more changes.⁸⁵

Moreover, somatic mutations have been discovered in a wide range of genes and gene classes, including splicing factors, epigenetic regulators, transcription factors, growth factor signaling kinases and others, illustrating profound diversity. In the last five years, three groups sought to determine the impact of mutations on disease outcome in an effort to further improve prognostic discrimination.⁸⁶⁻⁸⁸ The presence of one or more somatic mutations was observed in 78-89.5% of patients, with a median of three per patient.^{87,88} Genes most frequently found mutated included *SF3B1*, *TET2*, *SRSF2*, *ASXL1*, *DNMT3A*, *RUNX1* and *U2AF1*.^{87,88} Notably, a trend was observed in the temporal order of acquisition of somatic mutations, namely mutations in splicing factors and epigenetic regulators occurring earlier and those in transcription factors and signaling kinases occurring later with disease progression.^{87,88} The temporal order and approximate frequency of common MDS somatic mutations is summarized in Figure 1. Of interest, significant correlations were observed between specific mutations, demonstrating not only that the presence of a mutation matters, but that the specific combination imparts functional differences that can uniquely affect disease pathobiology.⁸⁸ Moreover, analysis of variant allele frequencies (VAFs) showed that while 62% of patients had clonal mutations, as much as 34-48% had subclonal

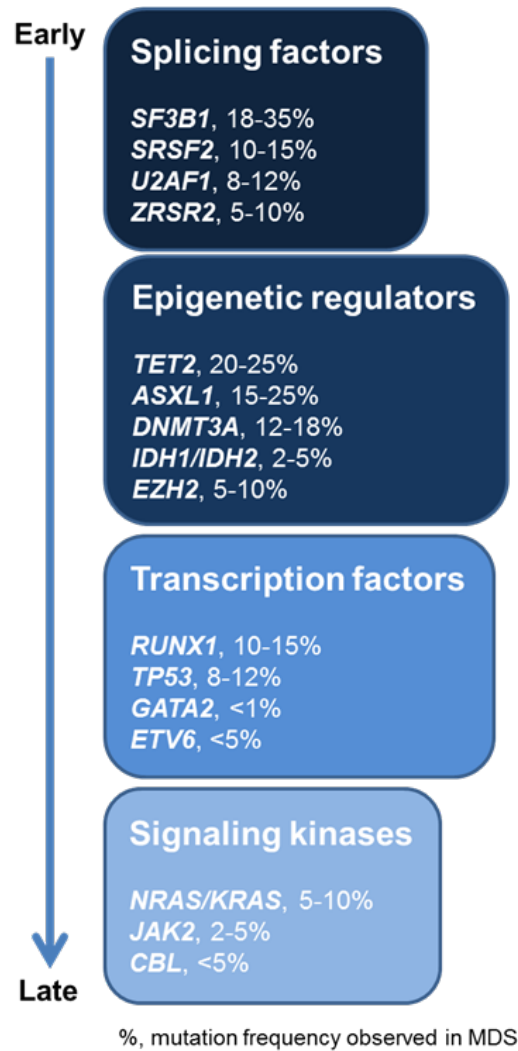


Figure 1. Temporal order and frequency of recurrent somatic gene mutations in MDS. Somatic mutations in splicing factor genes and epigenetic regulator genes are commonly observed earlier in MDS disease progression, whereas mutations in transcription factor and signaling kinase genes typically occur later. The percentage next to each gene designates the mutation frequency observed in MDS.

mutations indicative of intratumoral heterogeneity.^{87,88} In patients with higher-risk disease, the mean number of mutations per patient is typically increased, and these individuals display greater mutational diversity, increasingly complex clonal architecture and worse overall survival.⁸⁸ These findings support the notion that transformation of

MDS to AML is associated with clonal evolution, marked by the acquisition of additional, advantage-conferring mutations and clonal selection in favor of survival.⁸⁹

These studies demonstrated that the presence of a mutation in select genes independently added prognostic value to the IPSS and IPSS-R, illustrating potential clinical utility.⁸⁶⁻⁸⁸ However, recent reports have indicated that the frequency of pre-malignant, clonal hematopoiesis in the normal population can be quite high and clearly senescence-dependent.⁹⁰ This age-related clonal expansion results predominantly from the acquisition of somatic gene mutations commonly detected as founder mutations in MDS and AML, including *DNMT3A*, *TET2* and *ASXL1*.⁹⁰ Whereas mutations were nearly undetectable in younger patients (ages 40 years or below), 5.6% of persons 60-69 years of age, 11.7% of persons 80-89 years of age, and 18.4% of persons 90 years or older carried mutations by next-generation gene sequencing (NGS).⁹⁰ This phenomena, namely clonal hematopoiesis resulting from a myeloid malignancy-associated somatic gene mutation, occurs in otherwise hematologically normal individuals, and has since been named clonal hematopoiesis of indeterminate potential (CHIP).⁹¹ Persons with CHIP have 11.1-fold increased risk of developing a hematologic malignancy, as well as increased risk of type 2 diabetes, cardiovascular disease and all-cause mortality.⁹⁰ Only a small percentage of persons with CHIP progress to a hematologic neoplasm, like MDS or AML.^{90,91} Until additional studies are performed to understand the longitudinal effects of CHIP on outcome, the inclusion of mutation-based criteria into the IPSS or IPSS-R is unlikely.⁹² Nevertheless, evaluation of somatic gene mutations can help guide prognostication and offer insight into otherwise challenging diagnoses.

Aberrant Immune Activation in MDS

Autoimmune Disease and Infection. Sustained immune activation is recognized to increase the risk of hematologic malignancy. Accordingly, the literature supports a link between MDS and a number of inflammatory conditions.⁹³ For one, the presence of an autoimmune disorder significantly increases the risk of developing both MDS and AML.⁹⁴ As many as 30% of MDS cases occur concomitantly with autoimmune disorders.⁹⁵ MDS-associated rheumatoid arthritis and inflammatory bowel disease have been reported and precede development of MDS in approximately 55% of cases.^{94,96} Moreover, history of a broad range of infections, including pneumonia, upper respiratory tract infection and sinusitis, significantly increases MDS and AML risk.²⁵ When a latency analysis was performed to assess the contribution of infection three years prior to MDS or AML diagnosis, many infections retained significance.²⁵ Together, these data suggest that selective pressures associated with chronic inflammation related to infection and autoimmune conditions favor emergence of somatic mutations in HSPC, creating a fertile milieu for leukemogenesis and the development of MDS and AML. It is therefore likely that immune perturbations antecede the emergence of MDS.

Cytokine, Chemokine and Growth Factor Profile. MDS peripheral blood and bone marrow are marked by aberrant expression of inflammatory cytokines, chemokines and growth factors. Generally, lower-risk patients demonstrate marked up-regulation of pro-inflammatory mediators whereas immunosuppressive signals dominant higher-risk disease.⁹⁷ Increased interferon gamma (IFN- γ) gene expression is detectable in approximately 42% of MDS cases, with a significant overabundance of

cytokine expression within sera.^{97,98} Additionally, cytokines essential for T cell activation, differentiation and proliferation, including IL-12 and IL-7, are significantly increased in lower-risk sera, as well as the chemokine CCL5 important for lymphocyte chemotaxis.⁹⁷ Approximately 40% of early-stage MDS patients evidence significantly greater secretion of the pro-inflammatory cytokine IL-1 β within the bone marrow, which correlates positively with the degree of cell death.⁹⁹ MDS stromal cells not only express increased levels of IL-1 β , IL-6 and G-CSF mRNA, but produce mature IL-1 β and IL-6 basally without exogenous stimulation,¹⁰⁰ illustrating a pathobiologic contribution of the bone marrow microenvironment. Notably, expression of pro-angiogenic factors in solid tumors is often associated with advance stage disease and poor prognosis. In MDS, increased plasma levels of vascular endothelial growth factor (VEGF) and angiogenin (ANG) positively correlate with disease risk, suggesting a role in disease progression.¹⁰¹ Moreover, TNF α gene expression is increased in approximately 79% of cases, with a corresponding increase in the cytokine within the bone marrow.⁹⁸ Not only are TNF α levels increased in higher-risk patients, but this up-regulation correlates with lower complete response rates and reduced survival.¹⁰² Other inhibitory cytokines, including IL-10 and the soluble IL-2 receptor, are also increased in the sera of higher-risk patients,⁹⁷ and the myelosuppressive cytokine TGF- β 1 is increased in both PB plasma and the BM milieu.¹⁰³

Overview of TLR Signaling. Pattern recognition receptors (PRRs) represent a class of germline-encoded receptors recognizing both microorganism- and host-derived danger signals, or pathogen-associated molecular patterns (PAMPs) and danger-associated molecular patterns (DAMPs), respectively.^{104,105} The PRR family can

generally be divided into four receptor subfamilies. Two subfamilies, the Toll-like receptors (TLRs) and C-type lectin receptors (CLRs), are transmembrane, whereas the other two reside cytoplasmically, namely the NOD-like receptors (NLRs) and the Retinoic acid-inducible gene (RIG)-I-like receptors (RLRs).¹⁰⁴ Activation of PRRs results in activation of the innate immune response via a coordinated and fine-tuned inflammatory signal.

Undoubtedly, the TLRs are among the best-characterized PRR family, with ten members identified in humans.^{104,105} Cellular localization of the TLRs is divided between the plasma membrane (TLR-1, 2 and 4-6) and endosomal compartments (TLR-3 and 7-10), and DAMP and PAMP recognition varies between receptors.¹⁰⁶ Signaling originates at the cytoplasmic Toll/IL-1R homology (TIR) domain of the TLR following receptor engagement. Subsequently, recruitment of specific adaptor proteins allows for modified and specific responses. In total, five adaptor proteins are recognized, namely myeloid differentiation primary response gene 88 (MyD88), TIR domain containing adaptor protein (TIRAP), TIR domain-containing adaptor-inducing interferon- β (TRIF), TRIF-related adaptor molecular (TRAM) and Sterile-alpha and Armadillo motif containing protein (SARM).^{104,105}

Generally, TLR signaling can be divided into MyD88-dependent and TRIF-dependent pathways, with the majority of TLRs utilizing the former mechanism, with the exception of TLR3.^{104,105} Notably, TLR4 signaling results in activation of both pathways.¹⁰⁴ To start, MyD88 recruitment to the TIR domain results in a chain of events beginning with activation of interleukin-1 receptor-associated kinase 1 (IRAK1), then IRAK2.¹⁰⁴ Following dissociation from MyD88, the IRAK members associate with TNFR-

associated factor 6 (TRAF6), an E3 ubiquitin ligase.¹⁰⁴ Downstream signaling from TRAF6 ensues, resulting in the activation and nuclear localization of nuclear factor kappa-light-chain-enhancer of activated B cells (NF-κB).¹⁰⁴ Conversely, the TRIF-dependent signaling pathway begins with recruitment of TRAF3 and TRAF6.¹⁰⁴ While NF-κB will become activated downstream, this pathway also results in phosphorylation of interferon regulatory factor 3 (IRF3) and IRF7. Following dimerization, IRF3 and IRF7 translocate into the nucleus and induce expression of type I interferons (IFNs).¹⁰⁴ Ultimately, activation of TLR signaling culminates in activation of NF-κB, the generation of pro-inflammatory cytokines, interferons and an organized immune response (Figure 2).¹⁰⁵

TLR Signaling Dysregulation in MDS. The evidence supporting up-regulation and activation of TLR signaling in MDS is extensive and growing. Interestingly, chronic TLR4 signaling results in functional damage to long-term HSC.¹⁰⁷ The impaired repopulating potential of these HSC reflects the stem cell exhaustion observed with aging and characterized by loss of quiescence and increased cycling causing HSC depletion, accompanied by expansion of the myeloid compartment at the expense of the lymphoid.¹⁰⁷⁻¹⁰⁹ Similar findings are evident with chronic IL-1β stimulation as well.¹¹⁰ Such a phenotype is evident in MDS, suggesting TLR-driven aberrancies in hematopoiesis. Interestingly, normal BM-derived, CD34+ HSPC constitutively express TLR4 and TLR7-9, and stimulation of TLR7-8 actually skews differentiation of these cells along the myeloid lineage.¹¹¹ Moreover, gene expression of TLR1, TLR2, TLR4 and TLR6 is significantly increased in MDS BM-MNC, as well as protein expression of TLR2 and TLR4.^{67,112} Activation of TLR2 in CD34+ HSPC decreases erythropoietic

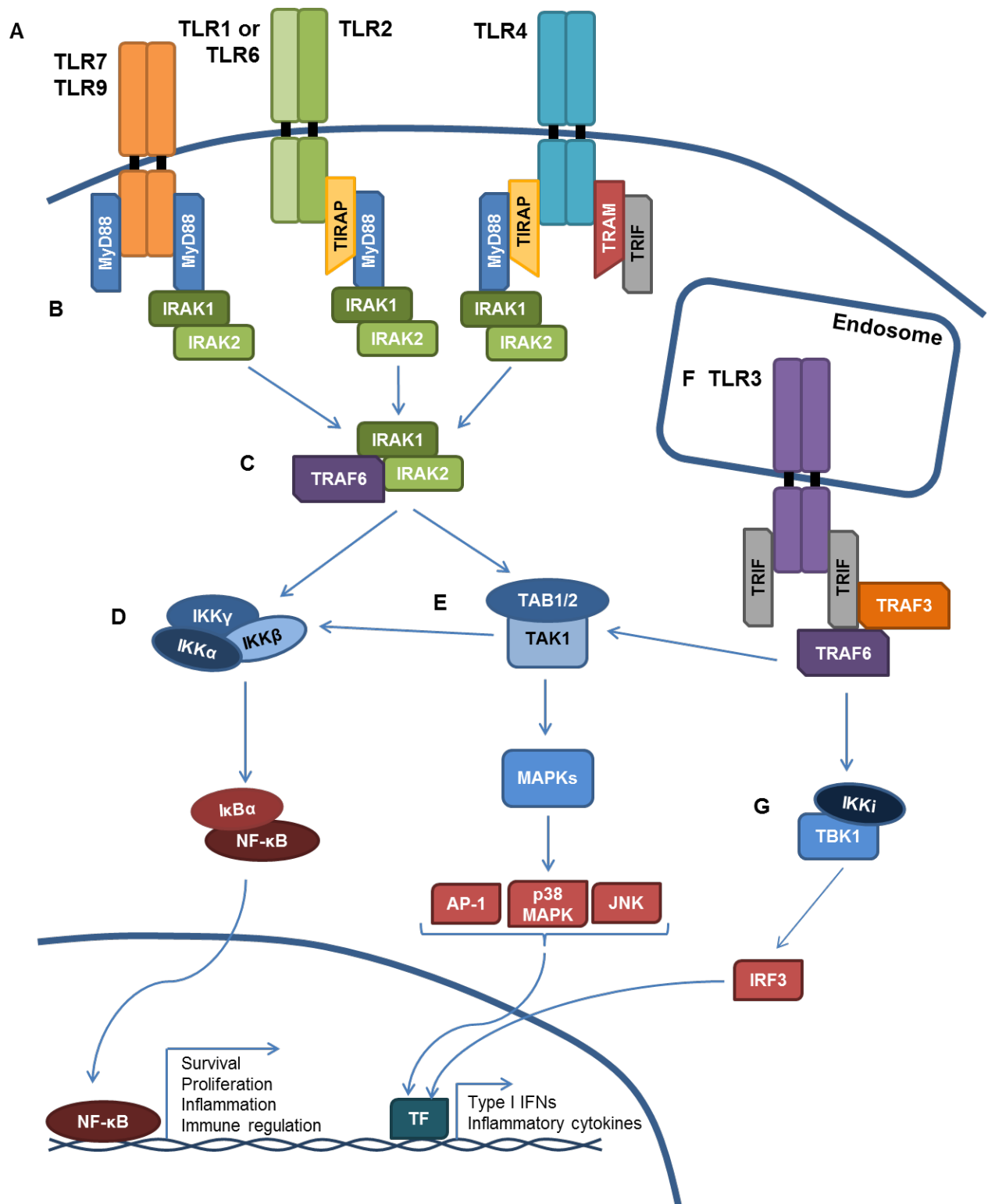


Figure 2. Overview of MyD88-dependent and TRIF-dependent TLR signaling pathways. With the exception of TLR3, all of the TLRs utilize MyD88-dependent signaling. **(A)** The TLRs located at the plasma membrane vary in the specific PAMPs and DAMPs they detect, as well as the adaptor proteins that are recruited to mediate

downstream signaling. **(B)** In MyD88-dependent signaling, MyD88 recruits and activates IRAK1 and IRAK2. **(C)** Following activation, IRAK1/IRAK2 dissociate and associate with TRAF6, an E3 ubiquitin ligase. **(D)** Once autoubiquitinated, TRAF6 recruits the IKK complex, consisting of IKK α , IKK β and IKK γ . TAK1 will phosphorylate IKK β , leading to phosphorylation and liberation of NF- κ B from the IKK complex members. NF- κ B translocates into the nucleus and induces transcription. **(E)** Activation of TAK1 results in MAPK signaling and the activation of a variety of transcription factors (TF), including AP-1, p38 MAPK and JNK. Subsequently, these TFs translocate into the nucleus and direct transcription. **(F)** TLR3, located within endosomal compartments, utilizes TRIF-dependent signaling whereby TRAF3 and TRAF6 are recruited for activation. **(G)** Activation of TBK1 results in the activation of the IRF3 transcription factor and transcription.

potential, as measured by colony forming capacity.⁶⁷ Additionally, approximately 11% of MDS patients harbor a single nucleotide polymorphism (SNP) encoding a phenylalanine to serine amino acid substitution at position 217 of *TLR2*, resulting in enhanced NF- κ B activation and signaling.⁶⁷ Notably, protein membrane expression of TLR4 is significantly increased on MDS CD34+ cells, overall 92% greater than normal HSPC, and expression on BM-MNC correlates with the extent of apoptosis as measured by annexin-V positivity.¹¹²

Comparative gene expression analyses of 84 TLR-related genes in BM-derived, CD14+ monocytes demonstrated that approximately 63% of these genes were significantly over-expressed in MDS compared to normal controls.¹¹³ Subsequent gene set enrichment analysis elucidated that up-regulated genes belonged to both the MyD88-dependent and -independent pathways, as well as TLR signaling adaptors and downstream pathway mediators, illustrating widespread network dysregulation.¹¹³ In accordance with these findings, while no mutations in MyD88 are demonstrable in MDS, increased gene expression has been shown in both BM-MNC and CD34+ HSPC.¹¹⁴ Lower-risk patients have greater over-expression than those with higher-risk disease,

and this up-regulation directly correlates with reduced survival and diminished erythroid colony forming capacity.¹¹⁴ Additionally, the genomic regions harboring TIRAP and TRAF6, the downstream target of the IRAK1 kinase, are amplified in a subset of patients.¹¹⁵ Furthermore, approximately 10-30% of MDS cases manifest over-expressed and hyperactive IRAK1 adaptor protein.¹¹⁶ Silencing of IRAK1 by RNA interference or pharmacologic inhibition of the kinase resulted in reduced proliferation and colony forming capacity in MDS, illustrating the importance of this target in these disorders.¹¹⁶ Notably, deletion of the long arm of chromosome 5 in patients with del(5q) MDS results in haploinsufficiency for a number of genes, including two microRNAs (miRNAs) within the commonly deleted region (CDR), namely miR-145 and miR-146a.^{117,118} These miRNA, which target TIRAP and TRAF6, respectively, are normally expressed in CD34+ HSPC and function to fine-tune the innate immune response.¹¹⁷ Loss of miR-145 and miR-146a recapitulates the del(5q) phenotype, elegantly demonstrating that aberrant activation of TLR- and innate immune-driven signaling has pathobiological effects in MDS.¹¹⁷

Bone Marrow Microenvironment Abnormalities. Like hematopoietic stem cells, mesenchymal stromal cells (MSC) reside within the bone marrow whose stem cell component is characterized by multipotency, self-renewal and the ability to differentiate into cells of the adipocytic, chondrocytic and osteocytic lineages (Figure 3).¹¹⁹ Together, these cells constitute the BM microenvironment and fulfill the crucial function of supporting normal hematopoiesis.

Undoubtedly, complex and dynamic interactions exist between cells of the hematopoietic and stromal lineages. Dysfunction in either dichotomy, namely the

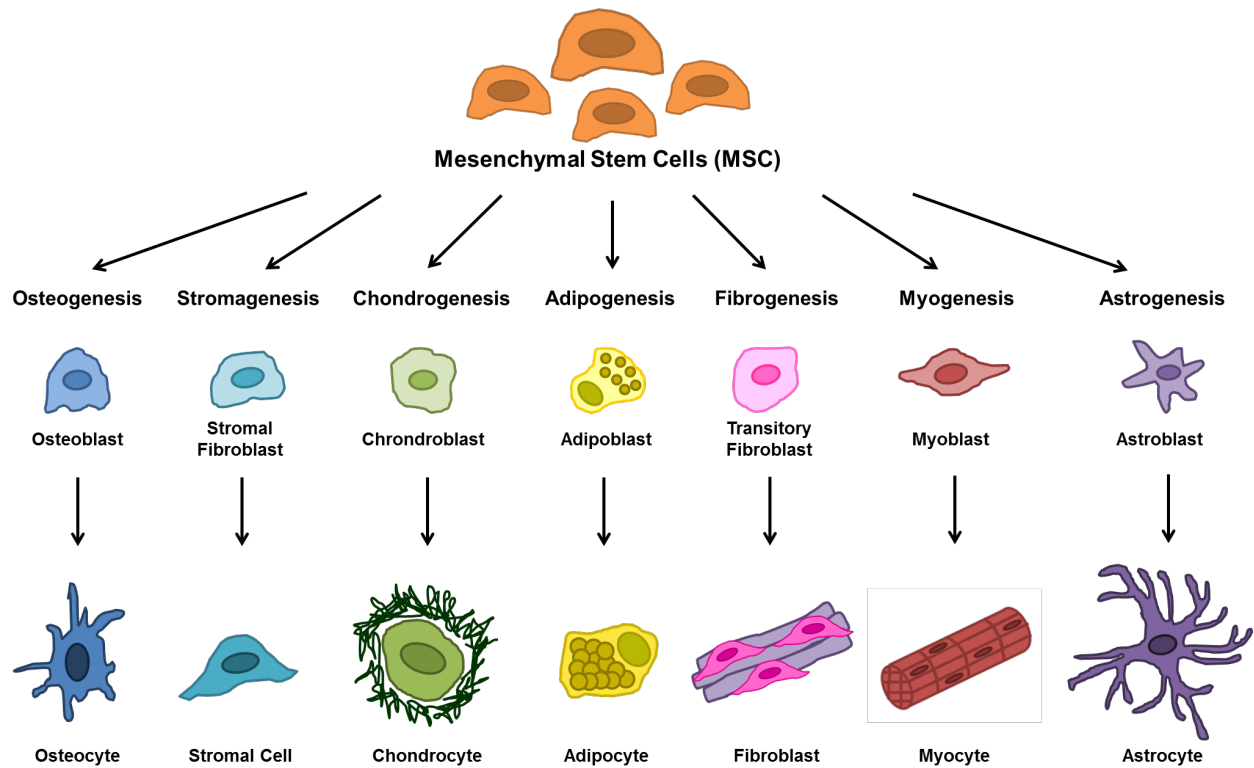


Figure 3. Hierarchy of the mesenchymal lineage. Mesenchymal stem cells (MSC) propagate cells of the mesenchymal lineage through a number of differentiation pathways, like osteogenesis, stromagenesis, etc. The precursor cells of these pathways will terminally differentiate into mesenchymal cells, including osteocytes, stromal cells, chondrocytes, adipocytes, fibroblasts, myocytes and astrocytes.

hematopoietic cells or the surrounding stroma, has implications for disease pathogenesis, as an abnormality in either typically translates to abnormalities in the other.^{84,120} For one, co-culture studies of the F-36P AML cell line with MDS-derived stromal layers illustrated the defective ability of the stroma to support hematopoiesis, as evidenced by increased cell death of the cell line.¹²¹ In a sophisticated animal model, disruption of the microenvironment was sufficient to initiate neoplastic change in a cell type of non-mesenchymal origin.¹²² Specifically, osteoprogenitor-specific deletion of Dicer1, an RNase III family endonuclease, resulted in myelodysplastic features with dysplasia, increased rate of transformation to AML and clonal genetic events in the

hematopoietic compartment.¹²² The role of the BM microenvironment in initiating disease was further supported by studies using the NUP98-HOXD13 (NDH13) animal model, which phenocopies MDS and is generated by hematopoietic cell-specific expression of the NUP98-HOXD13 transgene.¹²³ Not only was the NDH13 stroma defective in supporting hematopoiesis, but transplantation of NDH13 BM-MNC into WT recipients resulted in increased survival and reduced leukemic transformation compared to transplantation into NDH13 transgenic recipients.¹²³ These findings illustrate that normalizing the diseased BM microenvironment improves general hematopoietic function.¹²³ Conversely, the instructive reprogramming of the microenvironment by MDS-derived BM-MNC has also been demonstrated.¹²⁰ In the presence of MDS BM-MNC, normal MSC actually acquire an abnormal phenotype, with features similar to MDS-derived MSC.¹²⁰

Not only are BM-derived MSC phenotypically and functionally abnormal in MDS, they are also genetically unstable.¹²⁴ Germline genetic alterations in MSC have been described in MDS.¹²⁵ Moreover, clonal chromosomal abnormalities in MSC have also been reported and confirmed in approximately 34% of MDS patients, and these are of distinct origin from the MDS clone.¹²⁴ Patients harboring a clonal MSC abnormality have significantly reduced overall survival compared to those without MSC-specific genomic changes.¹²⁶ Although the precise biological consequence of these genetic alterations is largely unknown, they confer neither a proliferative nor a survival benefit.¹²⁴

Overview of Hematopoiesis. Though largely regarded today as an oversimplification, hematopoiesis, or the process resulting in the formation of all types of blood cells, is typically depicted as a hierarchy (Figure 4). Hematopoietic stem cells

(HSC), found atop of the hematopoietic pyramid, reside within the bone marrow as a rare, and largely quiescent, multipotent cell population.¹²⁷ HSC are characterized according to two unique attributes, namely the ability to self-renew, or generate additional HSC through cell division, and secondly, the ability to propagate all cells of the hematopoietic system.¹²⁸ In a simplistic view, HSC give rise to slightly more differentiated progenitor cells, which then differentiate further along specific hematopoietic lineages into fully mature and terminally differentiated cells.¹²⁸ In this way, self-renewal potential dramatically decreases as cell maturation increases. Two populations of HSC have been recognized, the long-term (LT-HSC) and short-term (ST-HSC) hematopoietic-initiating cells which differ in their self-renewal ability. Perhaps self-evident from their designation, LT-HSC retain life-long ability to reconstitute the hematopoietic system, whereas ST-HSC are more limited and can only do so short-term.¹²⁹ Therefore, LT-HSC give rise to ST-HSC, which then continue on to differentiate into multipotent progenitor cells (MPP).¹²⁹ MPP differentiate either into common myeloid progenitor (CMP) or common lymphoid progenitor (CLP) cells, which then produce cells of the entire myeloid and lymphoid lineages, respectively.^{128,129} In this way, MPP serve as the divergence point for the two main branches of hematopoiesis.¹²⁹ The CMP is also referred to as the colony forming unit (CFU)-granulocyte, erythrocyte, monocyte/macrophage, megakaryocyte (CFU-GEMM), as it gives rise to these myeloid cell populations.¹²⁹ Red blood cells are formed following maturation of the CFU-GEMM into burst forming unit-erythroid (BFU-E) and then CFU-erythroid (CFU-E).¹²⁹ Differentiation of CFU-GEMM into CFU-granulocyte-macrophage (CFU-GM) results in the production of mature neutrophils and macrophages.¹²⁹ The myeloid lineage also

includes megakaryocytes, which form platelets, mast cells, and the granulocytic basophil and eosinophil populations. Conversely, the CLP generates mature T and B lymphocytes, as well as natural killer (NK) cells.¹²⁹ A basic representation of hematopoiesis is illustrated in Figure 4. In MDS, aberrant hematopoiesis typically results in peripheral blood cytopenias, or the loss of cells of a particular lineage from premature cell death. Although loss of mature red blood cells, or anemia, is the most frequently observed cytopenia in MDS, other forms include neutropenia, loss of neutrophils, thrombocytopenia, loss of platelets, and leukopenia, general loss of white blood cells.⁴

Lymphoid Cell Lineage Involvement. Aberrant expression, activation and function of specific lymphocytic lineage cells is well documented in MDS, linking this branch of hematopoiesis to immune-mediated pathobiology. For one, natural killer (NK) cell cytolytic activity is globally impaired, with reduced expression of activating receptors resulting in impaired and deficient immunosurveillance.¹³⁰ Importantly, reduced function significantly correlated with disease progression, as the greatest functional defects were observed in higher-risk patients, those with increased BM blast count and abnormal karyotype.¹³⁰ These findings suggest that NK cells may function to eliminate aberrant hematopoietic cells in lower-risk disease, and that the progressive loss of cytotoxic ability results in expansion and escape of the leukemic clone.¹³⁰ Alternatively, biological events associated with genetic evolution of the clone may further impair NK cell function. Moreover, genes associated with the B cell lineage are significantly reduced in MDS CD34+ BM-MNC compared to normal controls, potentially contributing to the apparent myeloid lineage bias in MDS.¹³¹ Accordingly, B cell precursors are markedly reduced in MDS compared to normal.¹³¹

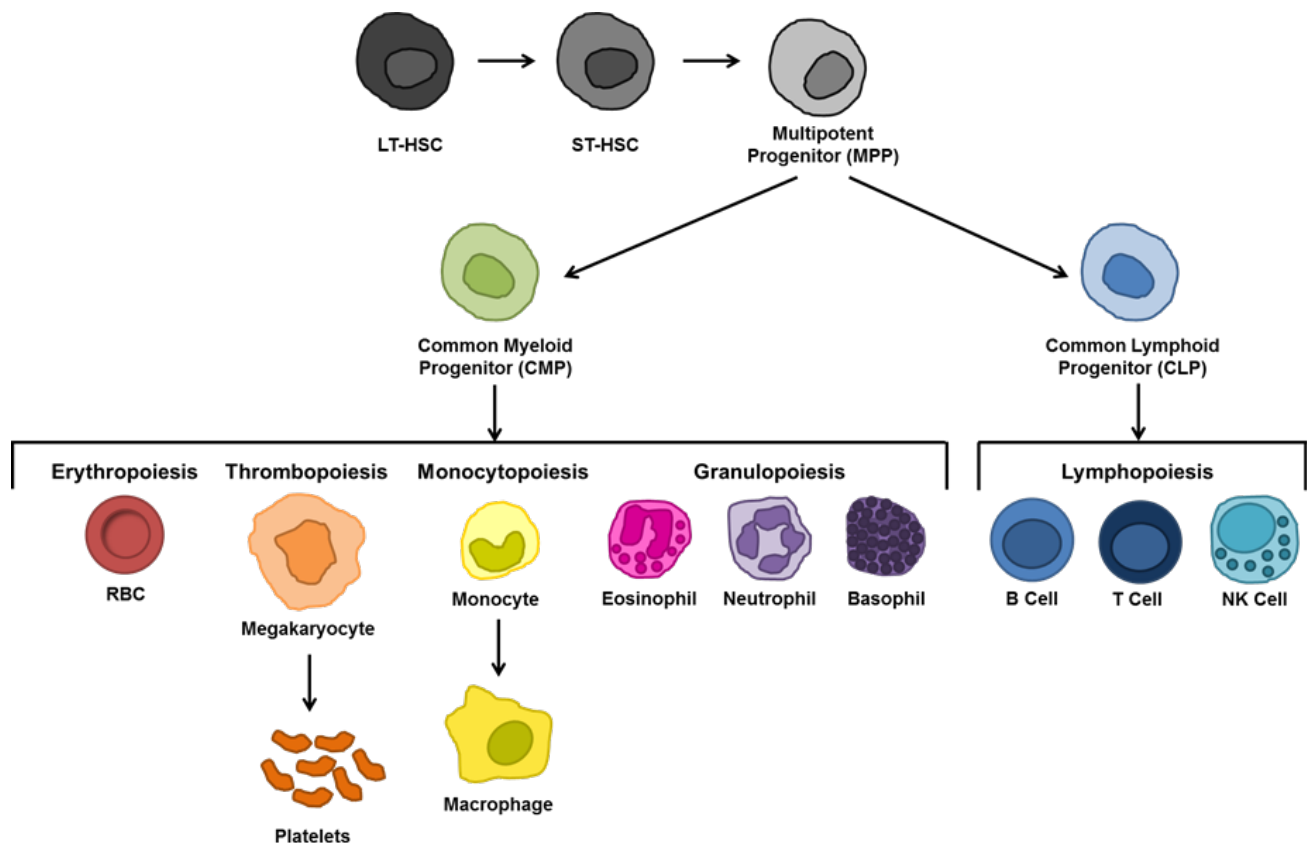


Figure 4. Overview of hematopoiesis. Long-term (LT) hematopoietic stem cells (HSC) differentiate into short-term (ST)-HSC, which have reduced self-renewal capacity. ST-HSC differentiate into multipotent progenitor cells (MPP), which can either differentiate into precursor cells of the myeloid or lymphoid lineages, namely common myeloid progenitors (CMP) or common lymphoid progenitors (CLP). The CMP will propagate all cells of the myeloid lineage, including red blood cells (RBC), megakaryocytes and platelets, monocytes and macrophages, and the granulocytes, including eosinophils, neutrophils and basophils. The CLP will generate B cells, T cells and natural killer (NK) cells through lymphopoiesis.

Conversely, cytotoxic T lymphocytes are expanded in MDS, retain potent cytolytic activity and appear to be reduced upon response to treatment.¹³² Depletion of CD8+CD57+ effector T cells from long-term cultures of BM-MNC resulted in a marked increase in colony forming capacity, albeit to a lesser extent than that observed in normal controls.¹³³ While MDS-derived CD8+ cell add-back had no effect on normal control colonies, no colonies formed in all 33 MDS samples where autologous CD8+

cells were added back into culture, illustrating an antigen-specific autologous response.¹³³ In support of this observation, in patients with an abnormal karyotype, depletion of this effector lymphocyte population increased the proportion of genetically abnormal cells by approximately 12.5%, indicating that the biological effects of the CD8+ cells is largely surveillant and involved in direct clonal suppression.¹³³ Accordingly, isolated CD8+ cells are typically oligoclonal, likely a result of selective expansion in response to self-recognition of an abnormal hematopoietic progenitor.¹³⁴

While CD4+ helper T cells are also aberrantly expanded in MDS, isolated populations are typically polyclonal.¹³⁴ Expansion of regulatory T cells (Tregs), defined as CD4+CD25+FOXP3+, is evident in the PB and BM of MDS patients with higher-risk disease.^{135,136} In lower-risk patients, autoimmune reactions targeting dysplastic hematopoietic cells may be the result of diminished Treg function and localization to the BM in this subset of patients.^{135,136} On the contrary, in higher-risk patients, Treg expansion aids in immunologic escape of the MDS clone, permitting disease progression.^{135,136} Indeed, PB Treg expression is associated with reduced survival and poor prognosis.¹³⁷ Lastly, IL-17 producing CD4+ T cells, or Th17 cells, have known pathobiological roles in autoimmune conditions and other inflammatory responses whereby they function as potent inducers of cytokine production.⁹⁷ Th17 cells are markedly expanded in lower-risk MDS, which is likely indicative of an inflammatory reaction.⁹⁷ Moreover, Th17 and Treg cells have an inverse relationship in lower- versus higher-risk MDS and this pattern reflects that observed in autoimmune conditions.⁹⁷ These findings may indicate why autoimmune diseases are significantly associated with MDS, particularly in lower-risk patients.

The Role of Myeloid-Derived Suppressor Cells (MDSC) and S100A9. Named appropriately, myeloid-derived suppressor cells (MDSC) represent a phenotypically distinct, immature myeloid cell population that remains in an activated and highly immunosuppressive state.¹³⁸ A block in myeloid lineage differentiation results in the accumulation of MDSC, which are often expanded in pathological conditions, including cancer, autoimmunity, inflammation and infection, as well as in the normal process of aging.¹³⁸ MDSC modulate both the innate and adaptive immune responses through two general modes of action, namely cell-to-cell, contact-based interactions and also the release of soluble mediators.¹³⁸ MDSC produce a number of factors that contribute to immune suppression, including substantial amounts of reactive oxygen species (ROS), nitrous oxide (NO), arginase and inducible nitric oxide synthase (iNOS), as well as direct release of granzyme granules.¹³⁸ These factors are highly suppressive of NK and T cell responses, which in conjunction with the known role of MDSC in promoting Treg expression, demonstrates clearly the role of MDSC in fostering immune tolerance.^{138,139} To date, two populations of MDSC have been identified and differ in morphology, with one appearing more granulocytic and the other more monocytic.¹³⁸ These subsets display inversed expression of ROS and NO, with low levels of ROS and high NO evident in the monocytic subset and high ROS and low NO in the granulocytic.¹³⁸ Understanding of the distinct functions of these subsets is presently under investigation.

While MDSC regulation is complex, a number of mediators have key roles in MDSC activation and expansion, including pro-inflammatory cytokines like IFN- γ and TGF- β , and signaling through TLRs.¹³⁸ Recently, the danger-associated molecular pattern (DAMP) proteins S100A8 and S100A9, or migration inhibitory factor-related

protein 8 (MRP8) and MRP14, respectively, have been implicated in MDSC activation and expansion.^{140,141} S100A8 and S100A9 are just two of the twenty-five members of the S100 calcium-binding protein family with known roles in tumorigenesis, infection and inflammation.¹⁴² These proteins are highly expressed by neutrophils and monocytes, and secretion of S100A8/A9 into the extracellular milieu represents a pro-inflammatory signal of cell damage.¹⁴³ Generally, S100A8 and S100A9 function as a heterodimer that is also known as calprotectin, expression of which is significantly increased in a number of cancer types, including breast, prostate, lung and stomach cancers.¹⁴² Both intracellular and extracellular roles have been described for S100 family members. Extracellular S100A8/A9 functions akin to cytokine signaling, whereby engagement of specific cell surface receptors results in signal transduction and an inflammatory response.¹⁴² To date, S100A8/A9 has been shown to serve as a ligand for TLR4, RAGE and surface receptors with carboxylated N-glycan moieties.¹⁴⁴⁻¹⁴⁶ S100A9-induced activation of TLR4 results in a similar signaling cascade as is observed with lipopolysaccharide (LPS) stimulation, namely through I κ B α - and MAPK-mediated pathways resulting in robust activation of NF- κ B and generation of inflammatory cytokines.¹⁴⁷ In a murine model of human breast cancer, ligation of S100A8/A9 with surface receptors on MDSC was shown to induce NF- κ B-dependent peripheral blood MDSC expansion.¹⁴¹ S100A8/A9 is actively produced by MDSC, which upon secretion, functions in an autocrine circuit to further sustain MDSC expansion.¹⁴¹ In an alternative murine model, the constitutive secretion of IL-1 β by fibrosarcoma cells results in highly metastatic and aggressive tumors through IL-1 β -directed immune suppression.¹⁴⁸ Interestingly, the IL-1 β receptor, a member of the IL-1/TLR family, directs the

accumulation of murine MDSC, defined as CD11b+/Gr-1+ cells, resulting not only in T cell inactivity but also hematopoietic abnormalities, such as anemia.¹⁴⁸

Importantly, we reported that MDSC are significantly expanded in the BM of lower-risk, but not higher-risk MDS patients compared with normal, age-matched controls as well as patients with solid tumors.¹⁴⁰ Subsequent fluorescence *in situ* hybridization (FISH) analyses and targeted quantitative PCR (qPCR) for commonly observed MDS somatic gene mutations confirmed that the expanded MDSC population was distinct from the MDS clone.¹⁴⁰ MDSC depletion from BM-MNC cultures resulted in increased T cell proliferation and improved progenitor colony forming capacity, illustrating the pathobiological role of MDSC in the aberrant hematopoiesis of MDS. Furthermore, MDSC highly express the surface receptor glycoprotein CD33, which belongs to the sialic acid-binding immunoglobulin-type lectin (Siglec) family of receptors with known roles in inflammation.¹⁴⁹ Surface receptor density of CD33 is significantly greater in MDSC from MDS compared to those from normal donors, suggesting an aberrant role of CD33-driven signaling in MDS.¹⁴⁰ We found that the primary MDS-specific ligand for CD33 is the DAMP protein S100A9, which is actively produced and secreted by MDSC.¹⁴⁰ Engagement of S100A9 with CD33 results in CD33-dependent signaling, culminating in MDSC activation and expansion.¹⁴⁰ Notably, S100A9 transgenic (S100A9Tg) mice phenocopy human MDS, evidenced by progressive multilineage cytopenias and cytological dysplasia, hypercellular marrows and age-dependent expansion and accumulation of MDSC.¹⁴⁰ Treatment of the transgenic mice with all-trans retinoic acid (ATRA) resulted in the forced differentiation of MDSC to mature myeloid cells with corresponding improvement in blood counts and

hematopoiesis.¹⁴⁰ Together, these data illustrate that aberrant inflammation driven by S100A9 and the expansion of MDSC together create a suppressive and inflammatory microenvironment that is sufficient to direct the development of MDS. A summary of general MDSC immunosuppressive mechanisms and our findings related to MDSC and S100A9 in MDS can be found in Figure 5.

The 5q- Syndrome.

Overview. Though the 5q- syndrome was initially described in 1974 in the seminal publication by Van den Berghe et al., it was not acknowledged as a distinct subset of Myelodysplastic Syndromes until 2001 with the release of the first WHO classification system.^{34,35} To date, it represents the sole MDS subtype characterized by the presence of a cytogenetic abnormality, namely the isolated, interstitial deletion of the long arm of chromosome 5 (del(5q) MDS).³⁷ With respect to the clinical phenotype, patients with del(5q) MDS present with a progressive, macrocytic, hypoplastic anemia despite the presence of a normo- or hypercellular bone marrow (BM).¹⁵⁰ Conversely, platelet and megakaryocyte counts are generally normal or increased, illustrating that only the erythroid compartment suffers from worsening blood counts.¹⁵⁰ Both BM and peripheral blood (PB) blast percentages are below 5%.³⁷ Of interest, the 5q- syndrome is more common in females, with a 7:3 prevalence versus males.¹⁵¹ Overall, patients with del(5q) MDS have a favorable prognosis, with a median survival of 63 months and a lower chance for leukemic transformation.¹⁵¹

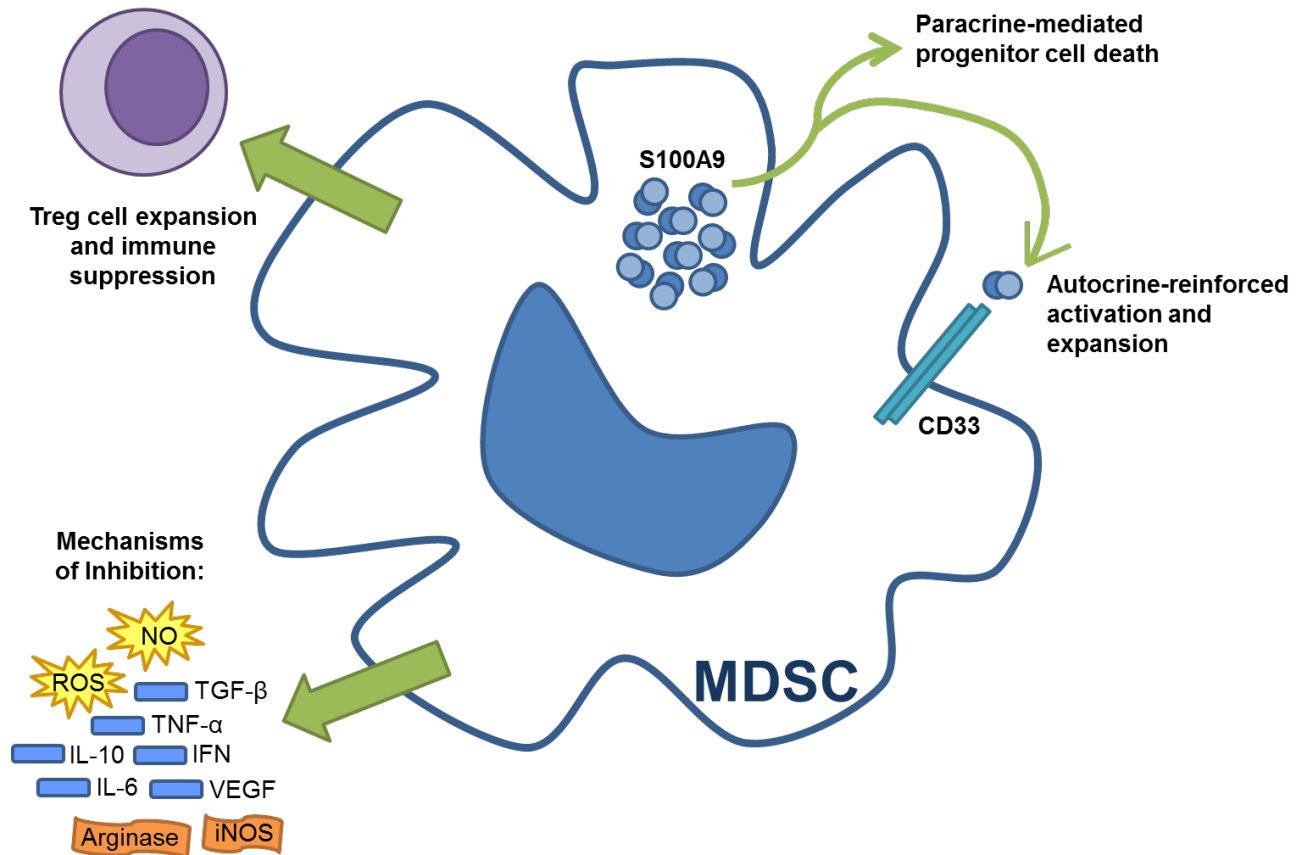


Figure 5. General mechanisms of hematopoietic inhibition by MDSC and the role of the MDSC/S100A9 axis in MDS. (A) MDSC mediate the suppression of a number of immune cells, including NK and T cells, and also promote the expansion of regulatory T cells (Treg). **(B)** Through the release of soluble factors, MDSC are highly suppressive and have a number of mechanisms of inhibition. These include release of reactive oxygen species (ROS) and nitrous oxide (NO), arginase and inducible nitric oxide synthase (iNOS), and inflammatory cytokines, like TGF- β , IFN- α , IL-10 and others. **(C)** MDSC robustly express the surface receptor glycoprotein CD33. **(D)** The DAMP protein S100A9 is a native ligand for CD33 and is actively produced by MDSC. Upon secretion, S100A9 functions **(E)** in a paracrine manner to mediate progenitor cell death. Additionally, S100A9 **(F)** reinforces MDSC activation and expansion through autocrine signaling and binding to CD33.

Moreover, this particular clonal abnormality is restricted to the myeloid lineage, as both myeloid and erythroid progenitors harbor the chromosomal deletion but generally not cells of the lymphoid compartment.¹⁵² Both proximal (5q12-14) and distal (5q31-33) deletions are typically reported, with breakpoints having been recognized at

each band between 5q11 and 5q35.¹⁵³ Unmistakably, this particular genetic loss is large and substantial. The majority of the long arm of chromosome 5 is lost, and with it a gene-rich area.¹⁵³ In the early 2000s, considerable efforts in molecular mapping identified the del(5q) commonly deleted region (CDR), or the smallest region lost in patients with the 5q- syndrome.¹⁵⁴ Specifically, the CDR spans a genomic region of 1.5-megabases and 40 genes, bordered by marker D5S413 and the gene *GLRA1*.¹⁵⁴ Comprehensive array-based transcriptome analyses of CD34+ HSPC illustrated that 536 genes are differentially expressed in del(5q) patients compared to normal donors.¹⁵⁵ Of interest, mutations in the CDR genes are rare, implicating gene dosage effects in the pathobiology of the 5q deletion.¹⁵⁵ Accordingly, expression levels of the CDR genes are approximately 60-80% of normal.¹⁵⁵ This range is not characteristic of a two-hit model of gene loss, and is reminiscent instead of haploinsufficiency stemming from loss of a single allele.¹⁵⁵ Indeed, Boulwood et al. suggested that *casein kinase 1 alpha 1 (CSNK1A1)* or *ribosomal protein S14 (RPS14)* may be candidate haploinsufficient genes implicated in del(5q) MDS pathobiology.¹⁵⁵

Treatment of Del(5q) MDS. Anemia is the major therapeutic challenge for patients with del(5q) MDS. Approximately 80% of patients are transfusion-dependent proximate to the time of diagnosis, and 93% of patients will be at some point during their disease.¹⁵¹ Historically, patients with del(5q) MDS received supportive therapy, as other treatment approaches were largely disappointing. While lenalidomide, a second-generation immunomodulatory drug (IMiD), is currently FDA approved for the treatment of del(5q) MDS, the path to this designation is rather unique. Thalidomide, the parent compound of lenalidomide, is a known teratogenic agent responsible for widespread

birth defects or phocomelia in the 1950s.¹⁵⁶ Despite this, thalidomide has unique biological effects including the enhancement of antigen-induced T cell proliferation and activity and inhibition of angiogenesis, illustrating the ability of this agent to modulate the immune response.^{156,157} In a study performed in lower- and higher-risk MDS, approximately 19% of patients responded to thalidomide.¹⁵⁸ Though no cytogenetic or complete responses were observed, the drug did improve blood counts and reduce cytopenias in a subset of lower-risk patients.¹⁵⁸ The negative connotation of the IMiDs was lessened with the identification of lenalidomide, a 4-amino-glutarimide analogue of thalidomide.¹⁵⁶ Lenalidomide has greater potency than its parent compound with less toxic effects.¹⁵⁶ Seminal work by List et al. demonstrated the therapeutic efficacy of lenalidomide in del(5q) MDS.⁴⁵ Approximately 83% of del(5q) patients had a fast hematologic response associated with transfusion-independence.^{45,159} Additionally, lenalidomide was cytotoxic to the del(5q) clone as evidenced by frequent cytogenetic responses.¹⁵⁹ Lenalidomide received FDA approval in 2005 and still remains the standard of care in patients with deletion of chromosome 5q MDS.

Pathobiology of the 5q- Syndrome.

Ribosomal protein S14 (RPS14). Major advances in the understanding of 5q-syndrome biology were made by Ebert and colleagues in 2008, with the identification of ribosomal protein S14 (RPS14) haploinsufficiency in the pathobiology of del(5q) MDS anemia.¹⁶⁰ In an elaborate set of knockdown experiments, normal CD34+ HSPC were lentivirally transduced with shRNAs targeting each of the 40 genes in the CDR.¹⁶¹ Knockdown of one gene, namely *RPS14*, to haploinsufficient levels (~60% expression) recapitulated the 5q- phenotype, namely erythroid-specific proliferative arrest and cell

death.¹⁶⁰ The group additionally demonstrated that no mutations were detectable in the remaining *RPS14* allele in del(5q) patients, confirming the pathological effects of *RPS14* loss in MDS were attributable to a *RPS14* gene dosage effect.¹⁶⁰ Moreover, a murine model of the 5q- syndrome was generated by the syntenic deletion of the del(5q) CDR, which translates to the *Cd74-Nid67* interval in mice.¹⁶² Mice harboring the deletion phenocopy human del(5q) MDS, with severe anemia, erythroid dysplasia and reduced red blood cell counts.¹⁶² Notably, *Cd74-Nid67* BM erythroid cells demonstrated significantly increased expression of p53.¹⁶² Crossing of the *Cd74-Nid67* mice with p53 deficient mice rescued the hematologic phenotype and improved erythropoiesis, illustrating that the molecular pathobiology of the 5q- syndrome is p53-dependent.¹⁶²

In support of these findings, *RPS14* gene haploinsufficiency in del(5q) MDS was shown to result in the erythroid lineage-specific activation and accumulation of p53.¹⁶³ *RPS14*, a central component of the 40S ribosome, has essential roles in RNA processing and maturation.¹⁶⁰ Mechanistically, decreased *RPS14* expression disrupts ribosome assembly, triggering the degradation of MDM2, an E3 ubiquitin ligase and the central negative regulator of p53 activation.^{160,163} Indeed, BM biopsies from del(5q) patients confirm increased nuclear expression of p53 and reduced expression of MDM2 in erythroid progenitors.¹⁶⁴ Stabilized and activated p53 triggers p21-dependent cell cycle arrest, erythroid progenitor-specific cell death and anemia.¹⁶³ Abnormal activation of the p53 pathway in MDS can additionally be attributed to the role of p53 in monitoring ribosome function, as ribosomal stress can directly activate p53.¹⁶⁵ Interestingly, in a recent investigation, reduced expression of *RPS14* was identified in 83 of 156 non-

del(5q) MDS patient specimens, and was associated with increased apoptosis of erythroid precursors.¹⁶⁶

Perhaps the findings demonstrating a key role for the RPS14/MDM2/p53 pathway in driving ineffective erythropoiesis in del(5q) MDS are best corroborated by studies performed in the *Rps14* haploinsufficient mouse model.¹⁶⁷ Inactivation of *Rps14* results in p53-dependent defects in erythropoiesis, age-dependent, progressive anemia and other defining features of human disease.¹⁶⁷ Using a quantitative proteomics-based approach, 26 proteins were identified as differentially expressed in the *Rps14* haploinsufficient versus wild-type littermates.¹⁶⁷ As expected, many of these were ribosomal-related proteins, which functioned as a positive control for the experiment. Most important, though, S100A8 and S100A9 were the highest differentially expressed proteins in the context of *Rps14* haploinsufficiency.¹⁶⁷ Wild-type HSPC, defined as LSK (Lin⁻Sca-1⁺c-Kit⁺) positive, treated with recombinant murine S100A8 failed to differentiate properly along the erythroid lineage, which was rescued by CRISPR-Cas9-mediated knockdown of *S100a8*.¹⁶⁷ Furthermore, S100A8 and S100A9 can signal to increase p53 activation, and multiple p53 binding sites have been identified within the *S100A9* gene promoter, linking these proteins in a positive feedback loop.^{167,168} Indeed, p53 activation was increased in the context of *Rps14* haploinsufficiency, impairing differentiation and increasing erythroid progenitor cell death.¹⁶⁷ These data link innate immune mediators in the pathobiology of del(5q) MDS through an S100A8/A9/Rps14/p53 pathway.

Casein kinase 1A1 (CSNK1A1). In addition to *RPS14*, Boulwood et al. hinted at a potential pathobiologic role for haploinsufficiency of *casein kinase 1A1 (CSNK1A1)* in

del(5q) MDS, as expression levels of CSNK1A1 were reduced to approximately 50% in this cohort of patients.¹⁵⁵ Indeed, this hypothesis was recently confirmed using a murine model of *CSNK1A1* haploinsufficiency.¹⁶⁹ CK1 α , which is encoded by *CSNK1A1*, is a key regulator of β -catenin given its membership in the β -catenin destruction complex. Haploinsufficiency of *CSNK1A1* increased β -catenin activation in HSPC, resulting in enhanced survival and proliferation of the stem cell population.¹⁶⁹ These data suggest that loss of *CSNK1A1* expression provides a proliferative advantage to the del(5q) clone, and highlight an additional mechanism of pathobiology conferred by the chromosome 5q deletion.

TLR4/TRAFF6/NF- κ B-dependent signaling axis. Intriguing work by Starczynowski and colleagues implicated, for the first time, microRNAs in the pathobiology of the 5q- syndrome.¹¹⁷ MicroRNAs (miRNAs), highly conserved, ~22-nucleotide-long, small non-coding RNAs, mediate post-transcriptional gene regulation to exert widespread repressive changes in gene expression.¹⁷⁰ Following parallel sequencing and qPCR validation, miR-145 and miR-146a were shown to be significantly reduced in del(5q) patients compared to normal controls.¹¹⁷ miR-145 lies within the CDR whereas miR-146a is just outside this region.¹¹⁷ In lethal irradiation and transplantation experiments, overexpression of miR-145 and miR-146a recapitulated the del(5q) phenotype, confirming a role for the miRNA in disease biology.¹¹⁷ Moreover, toll-interleukin 1 receptor (TIR) domain containing adaptor protein (TIRAP) and TNF receptor-associated factor 6 (TRAF6) were identified as the targets of miR-145 and miR-146a, respectively.¹¹⁷ Loss of miR-145 and miR-146a derepressed expression of these downstream targets which aberrantly drives innate immune activation, as both

TIRAP and TRAF6 have central roles in TLR4 and NF- κ B signaling.¹¹⁷ As proof of concept, forced expression of TRAF6 significantly reduced blood cell counts, impaired myeloid lineage differentiation and induced bone marrow failure and risk of AML progression.¹¹⁷

Notably, these data are strongly supported by recent findings related to *TRAF-interacting protein with forkhead-associated domain B (TIFAB)*, a gene located at 5q31.1 that is also haploinsufficient in del(5q) MDS.¹⁷¹ Transplantation experiments of germline *Tifab* knockout BM cells into wild-type recipients showed that loss of *Tifab* confers hematopoietic defects.¹⁷¹ Recipient mice developed bone marrow failure and cytopenias with impaired myeloid differentiation.¹⁷¹ Mechanistically, TIFAB complexes with TRAF6 to promote its degradation, which in turn inhibits NF- κ B.¹⁷¹ Therefore, haploinsufficient loss of *TIFAB* in del(5q) MDS increases TRAF6 activity, enhancing TLR4-mediated signaling and activation of NF- κ B.^{117,171}

Finally, the aberrant TLR4/TRAF6/NF- κ B pathway in del(5q) MDS is additionally dysregulated by p62, also known as sequestosome 1 (SQSTM1), a mitochondrial adapter indispensable for autophagy.¹⁷² Paradoxically, despite the presence of p62 within the 5q chromosome deletion in MDS, expression levels of p62 are often normal or even increased.¹⁷² Normally, p62 helps activate NF- κ B by recruitment and activation of TRAF6. This allows for TRAF6-mediated signaling and activation of NF- κ B.¹⁷² In del(5q), where expression of miR-145 and miR-146a are reduced, overexpression of p62 exacerbates signaling along this pathway.¹⁷² Additionally, p62 is a transcriptional target of NF- κ B, illustrating a feedforward mechanism of expression.

Diaphanous related formin 1 (DIAPH1). Located at 5q31.3, *DIAPH1* flanks the CDR of chromosome 5 in del(5q) MDS.¹⁷³ *DIAPH1* encodes the mDia1 protein with known roles in actin polymerization and Rho GTPase signaling.¹⁷³ Importantly, mDia1 has been shown to facilitate activation of a number of innate immune cells, including T cells, macrophages and neutrophils, linking mDia directly to innate immunity.¹⁷⁴⁻¹⁷⁶ Gene expression of mDia1 was reduced approximately 50% in del(5q) MDS patients compared to normal controls, which is consistent with the degree of knockdown of other CDR genes.¹⁷³ In mice, the *Drf1* gene encodes for mDia1, and mice heterozygous and homozygous for *Drf1* loss evidence dramatic hematologic defects.^{173,174} Specifically, the mice phenocopy human MDS and share features of murine models from other CDR genes, including *Rps14*.^{173,174} In mechanistic murine model studies, loss of mDia correlated with a significant increase in expression of the TLR4 co-receptor CD14 on granulocytes.¹⁷⁴ These findings were corroborated by flow-based measurements of CD14 expression, whereby expression was significantly increased in del(5q) patients compared to both normal donors and patients with non-del(5q) MDS.¹⁷⁴ Understandably, overexpression of CD14 results in hypersensitive activation of TLR4 to agonists, driving aberrant innate immune activation.

Programmed Cell Death

Caspases. Programmed cell death (PCD) describes tightly-regulated, intrinsic suicide mechanisms utilized by cells during processes related to normal development, tissue maintenance and even aberrantly in the context of disease, including cancer and

autoimmune disorders. Apoptosis, described in a later section of this manuscript, is the best-characterized mechanism of PCD, mainly because it was among the first forms of PCD identified. As a consequence, substantial work performed in model organisms as well as in mammalian cells has elegantly deconvoluted the pathway culminating in apoptotic cell death.¹⁷⁷ Nonetheless, other distinct forms of PCD are now recognized, including autophagy, necroptosis and pyroptosis. Each mechanism has unique morphological and biological hallmarks, as well as general attributes common to many PCD pathways. Mechanisms of PCD, as well as a number of inflammatory processes, are largely mediated by cysteine proteases, called caspases.¹⁷⁸

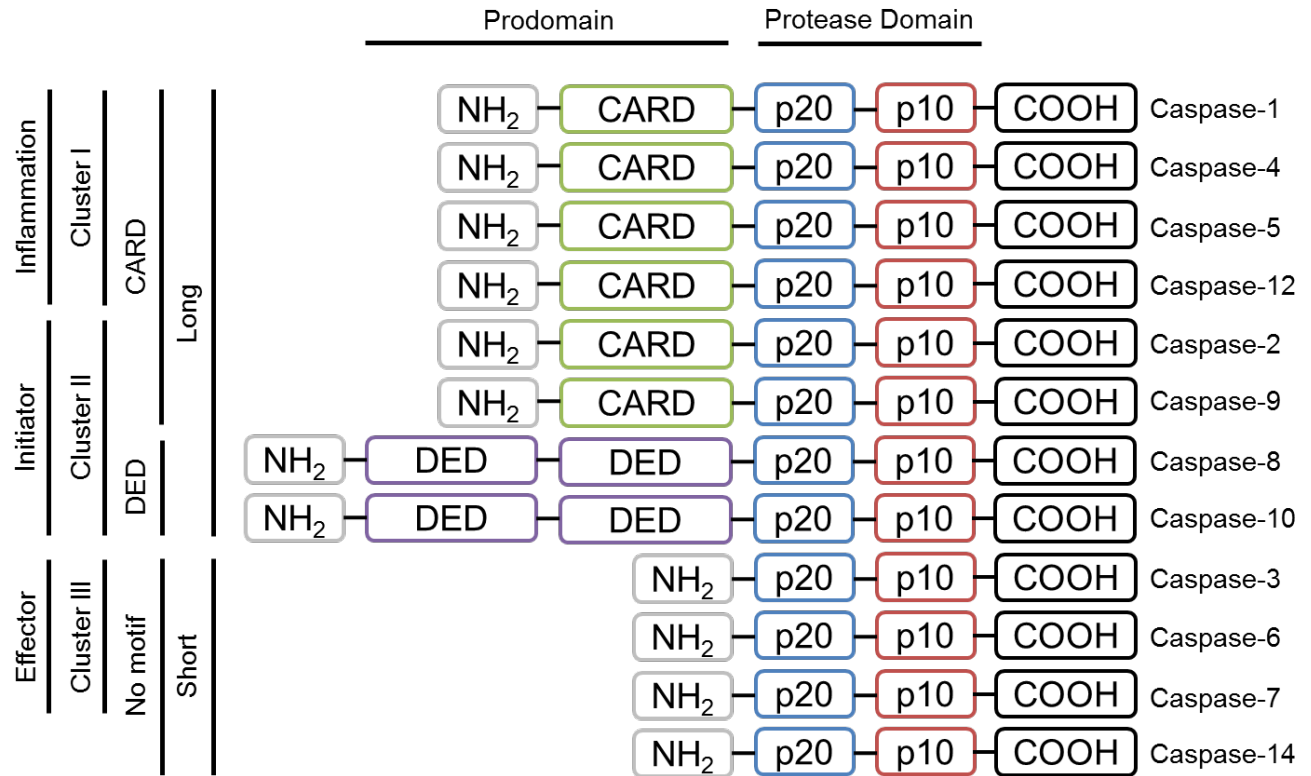
Expansion of the caspase (cysteine-dependent aspartate-specific protease) family name highlights two key catalytic functions that each member of this enzymatic family possesses: first, a cysteine-histidine catalytic mechanism and second, specificity for substrate cleavage after an aspartic acid residue.^{179,180} Caspases vary in the four amino acid sequence that dictates substrate recognition, and synthetic peptide inhibitors to particular caspases are typically created with activity against the respective recognition motif.¹⁸¹ To date, twelve human caspases have been identified.^{182,183} The human genome contains eleven or twelve caspases, the variability a consequence of a single nucleotide polymorphism in caspase-12, resulting either in a truncated protein or full-length enzyme. Full-length caspase-12, however, appears confined to populations of African descent.¹⁸²

Generally, pro-caspases share a similar structure, each composed of an N-terminal prodomain of variable length and a C-terminal protease domain. Within the protease domain, a large, p20 subunit is joined to a smaller, p10 subunit by means of a

short linker region. The p20 subunit has been implicated in catalytic activity, while the p10 confers substrate specificity.¹⁸¹ Despite this basic organization, caspases can be categorized into distinct subsets, and historically a number of criteria have been applied to do so. Notably, and overlooking a few exceptions, caspases segregate into the same subfamilies, regardless of what factor is used in categorization (Figure 6).

By simpler means, caspases can be classified according to the length of their prodomains. Contrary to shorter domains, longer prodomains house homotypic protein-protein interaction motifs of the death domain (DD) superfamily, with caspase activation and recruitment domain (CARD), death effector domain (DED), and pyrin domain (PYD) subfamilies.¹⁸⁴ These interaction motifs aid in caspase activation by allowing for the recruitment of pro-caspases to signaling platforms where they undergo proximity-induced auto-activation.^{181,184} Furthermore, phylogenetic analysis of the complete mRNA sequence of each caspase establishes three main clusters, which perhaps not surprisingly, coincide with the general function that each performs. Cluster I contains caspases with known roles in inflammation, whereas clusters II and III relate to apoptosis, with the initiator caspases comprising the former group, and the effectors the latter.

Apoptosis. Apoptotic cell death can be triggered by two distinct pathways, the intrinsic and extrinsic, both of which converge on a similar signaling event, namely activation of caspase-3 (Figure 7).^{105,185} The intrinsic pathway is predominantly governed by mitochondrial integrity and specifically, the balance between pro- and anti-apoptotic Bcl-2 family members. Beyond a particular threshold, cytochrome c is released from the mitochondria, triggering activation of the initiator caspase-9 which



CARD, caspase activation and recruitment domain; DED, death effector domain

Figure 6. Classification of human caspases. A number of classification approaches exist for classifying the twelve human caspases that have been identified. Generally, the caspases group into the same sub-families irrespective of the classification approach employed. The main approaches used to date include general function (inflammation, initiator, effector), phylogenetic (cluster I, II or III), death domain (DD) interaction motif (no motif, DED, CARD) and prodomain length (short, long).

subsequently cleaves and activates caspase-3, culminating in apoptosis.¹⁸⁶ Conversely, the extrinsic pathway is dependent on cell extrinsic ligand interaction with plasma membrane-bound death receptors of the tumor necrosis factor (TNF) superfamily.^{105,185}

Ligation of TNF to TNF receptor (TNFR), TNF-related apoptosis-inducing ligand (TRAIL) to TRAIL receptor (TRAIL-R) and Fas to Fas receptor (FasR) results in activation of the initiator caspase-8 and activation of caspase-3.¹⁸⁷ Ultimately, apoptosis is a non-immunogenic mechanism of cell death. Following nuclear condensation and

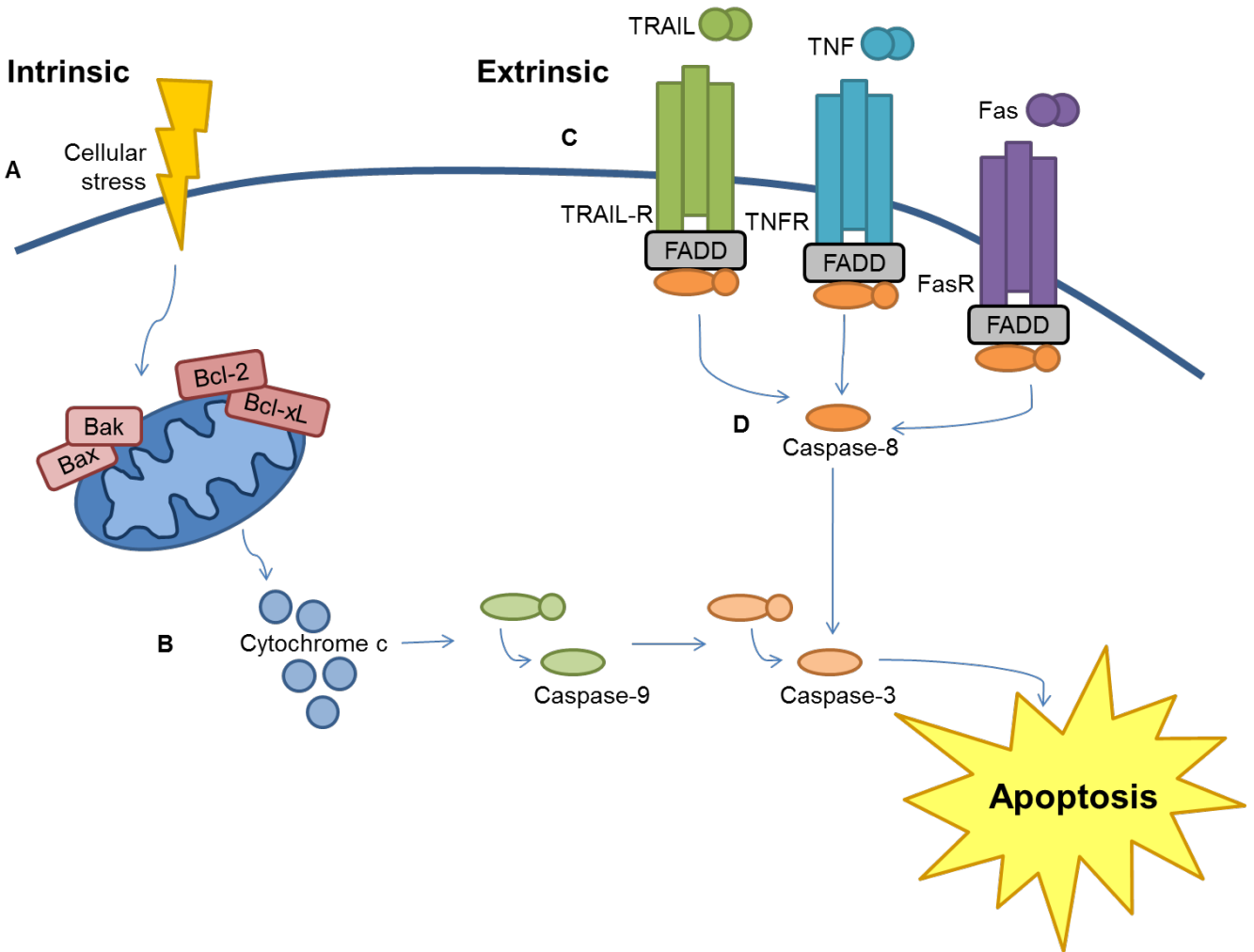


Figure 7. Simplistic overview of the intrinsic and extrinsic apoptotic pathways. The intrinsic apoptotic pathway is largely governed by mitochondrial integrity. **(A)** Cellular stresses alter the balance between pro- and anti-apoptotic Bcl-2 family members, resulting in **(B)** the release of cytochrome c from the mitochondria. This in turn triggers activation of caspase-9, an initiator caspase. Caspase-9 will activate caspase-3, and subsequent signaling events will result in apoptotic death. **(C)** The extrinsic apoptotic pathway initiates with external ligation of TNF superfamily surface receptors, specifically TNFR, TRAIL-R and FasR. **(D)** Caspase-8 will be cleaved and activated, resulting in downstream activation of caspase-3 and apoptosis.

DNA fragmentation, cellular contents are packaged into apoptotic bodies which result from blebbing of the plasma membrane. During this process, cytosolic phosphatidyl serine is exposed extracellularly, marking the apoptotic bodies for phagocytosis by

neighboring cells.¹⁸⁵ The cell shrinks and is removed without generation of inflammatory signals.

Autophagy. As an evolutionarily conserved and tightly-regulated process, autophagy represents a cytoprotective mechanism to maintain cellular energy homeostasis through the catabolism of long-lived, damaged or excessive proteins or organelles.¹⁸⁸ A conserved set of thirty or more core proteins, the autophagy-related proteins (Atg), mediate the formation of a double-membrane vacuole, called the autophagosome, which sequesters cytosolic material to provide energy and recycle nutrients.^{188,189} The autophagosome fuses with the lysosome, whereby its contents are degraded by lysosomal hydrolases, or cathepsins (Figure 8). Autophagy can occur non-selectively as a stress-adaptation mechanism so that the cell can avoid death. Alternatively, selective or cargo-specific autophagy results in the removal of select proteins or organelles to control number and ensure quality.¹⁸⁹ Mitophagy, for instance, the autophagic removal of mitochondria, occurs normally during red blood cell maturation but also occurs upon detection of damaged or noxious mitochondria (Figure 8).¹⁸⁹ While autophagy is driven in response to stress, over stimulation can trigger autophagic, or type II cell death.¹⁸⁸

Moreover, interplay exists between autophagy and apoptosis as a means of regulating cell death. In some contexts, autophagy suppresses apoptotic cell death providing the cell an opportunity to survive. Conversely, autophagy can also promote apoptosis. For instance, caspase-mediated cleavage of beclin 1, an essential autophagic protein, results in its mitochondrial accumulation and accelerated cell death.^{190,191} Additionally, the autophagosomal membrane can act as a platform for the

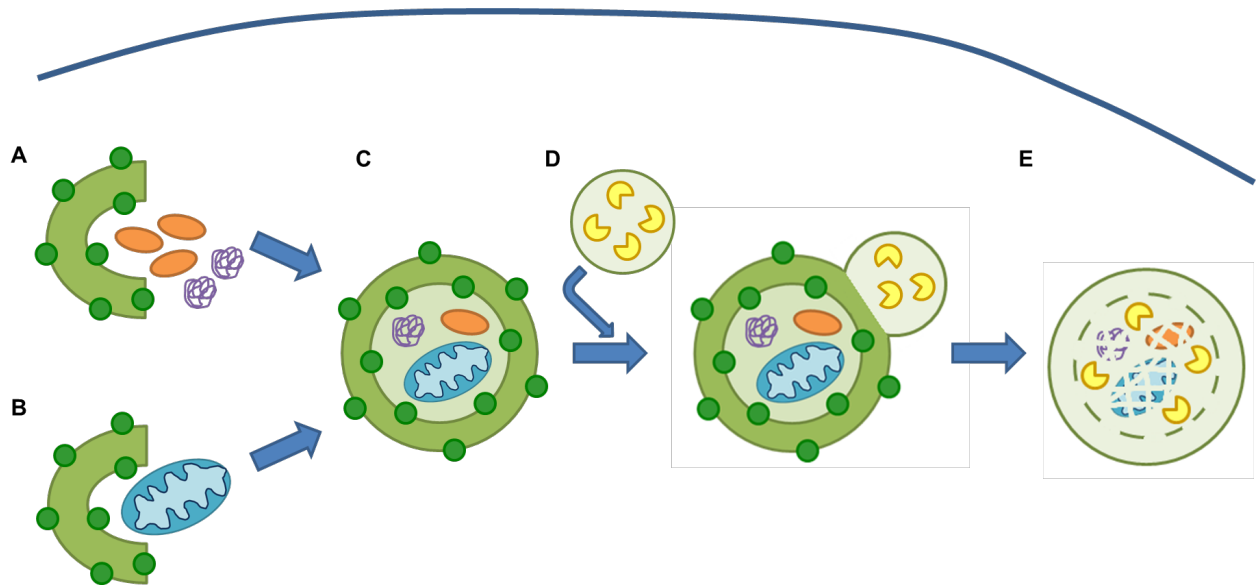


Figure 8. Autophagy and mitophagy maintain cellular homeostasis through catabolism. (A) Long-lived, damaged or unnecessary proteins or organelles will be degraded and recycled through the process of autophagy. (B) Mitophagy, or the recycling of damaged mitochondria, is a specialized form of autophagy. Both autophagy and mitophagy initiate with the formation of the (C) autophagosome, a double membrane vacuole. The autophagosome sequesters the unwanted cellular material, allowing for (D) lysosomal hydrolases to fuse with the autophagosome and (E) degrade the contents.

formation of an intracellular death-inducing signaling complex (iDISC), resulting in the recruitment and activation of caspase-8 to initiate apoptosis.¹⁹² Similar to apoptosis, a complex interaction exists between autophagy and pyroptosis, discussed in a later section of this manuscript. Under basal conditions, autophagy and pyroptosis are antagonistic. Reduced autophagic activity and the accumulation of damaged mitochondria result in release of mitochondrial DNA (mtDNA), thereby activating the NLRP3 inflammasome to mature caspase-1 and interleukin (IL)-1 β .¹⁹³ In contrast, formation of NLRP3 inflammasome complexes triggers formation of autophagosomes.¹⁹⁴ In this context, both pro-IL-1 β and active NLRP3 inflammasome

complexes can undergo degradation, illustrating autophagy-mediated dampening of the inflammatory response.^{194,195}

Historic View of Cell Death in MDS. For over two decades, apoptotic cell death potentiated by inflammatory cytokines has long been considered a fundamental feature of MDS. Despite the presence of normo- or hypercellular marrows, MDS patients typically present with peripheral blood cytopenias involving one or more lineages, an apparent paradox that in retrospect was reconciled incorrectly by apoptosis. In lower-risk disease, BM-MNC and CD34+ stem and progenitor cells were shown to exhibit a heightened rate of proliferation, which occurred concurrently with apoptosis.^{196,197} Apoptosis was demonstrable in the erythroid, myeloid and megakaryocytic lineages, as well as in cells of the surrounding stroma by a number of methodologies, including *in situ* end labeling of fragmented DNA and annexin-V and PI staining.¹⁹⁶⁻¹⁹⁸ Even though the marrow is highly engaged in DNA synthesis, the rapid turnover of precursor cells prohibits their maturation and differentiation, thereby accounting for the presence of cytopenias and the hematopoietic deficiency observed in MDS. Though unknown at the time, these markers are not faithful and specific indicators of apoptotic cell death and as a consequence, the principal mechanism of cell death in MDS has been incorrectly labeled. This was demonstrated by our group in 2016, over twenty years later, effectively changing the paradigm for these disorders.¹⁹⁹ These data are described in detail in Chapter 2.

Though it is not the predominant programmed cell death pathway, apoptosis does play a role in MDS, as dysregulation of both the intrinsic and extrinsic pathways have been reported.¹⁰⁵ In early-stage disease, pathobiology favors a pro-apoptotic

phenotype. Death-inducing ligands TNF- α and Fas are up-regulated, as well as death receptors and the signaling adaptor Fas-associated death domain (FADD), required for caspase-8 activation.^{98,200-202} Additionally, spontaneous mitochondrial release of cytochrome c into the cytosol is observed in MDS, which is hypothesized to not only drive activation of caspase-9 and caspase-3 but also to sensitize cells to extrinsically-induced apoptosis.²⁰³ In late-stage disease, a shift to an anti-apoptotic phenotype is observed with reduced cell death and increased survival signals. Whereas pro-apoptotic Bcl-2 family members, like Bad and Bax, are over-expressed in lower-risk patients, higher-risk patients over-express anti-apoptotic members, including Bcl-2 and Bcl-xL.^{197,204} NF- κ B-dependent up-regulation of FLICE-inhibitory protein (FLIP), a negative regulator of death receptor signaling, also occurs with disease progression.^{200,205}

Anemia, a consequence of ineffective erythropoiesis, is evident in approximately 90% of MDS patients at some point in the course of their disease.²⁰⁶ Given the role of mitophagy in normal erythroid maturation and the aberrances observed in the erythroid compartment in MDS, dysregulated mitophagy has been implicated in MDS pathobiology.¹⁰⁵ Though loss of autophagic pathway genes has not been reported in MDS to date, a number of genes are lost in AML, suggesting a possible role in disease progression.²⁰⁷ Cytochrome c oxidase, encoded by mtDNA, is enzymatically involved in the electron transport chain and iron metabolism in the mitochondria.²⁰⁸ Approximately 75% of MDS patients harbor mutations in cytochrome c oxidase, resulting in the accumulation of iron in the mitochondrial matrix.²⁰⁸ Accordingly, MDS mitochondria are characteristically enlarged and iron-laden, and the presence of abnormalities increases with prognostic risk.²⁰⁹ Pathologic iron accumulation not only increases oxidative stress,

leading to increased mutations of both mtDNA and nuclear DNA, but exacerbates impaired mitochondrial integrity and homeostasis.²⁰⁹ Indeed, enhanced mitophagy is manifest in early-stage disease.²¹⁰ MDS-derived erythroblasts undergo mitophagy earlier than normal erythroid progenitors, evidenced by five-time greater formation of iron-positive autophagosomes.²¹⁰ Though mitophagy may be a protective mechanism in lower-risk disease to clear iron-laden mitochondria and safeguard against further genetic damage, activation of this mechanism occurs at the expense of the normal erythroid program.

Pyroptotic Cell Death

History and Hallmarks of Pyroptosis. First identified nearly two decades ago, pyroptosis was described as a caspase-1-dependent necrosis.²¹¹ At the time, Brennan and Cookson had classified the death of macrophages post *Salmonella typhimurium* infection as a more specialized, albeit unusual, form of necrosis.²¹¹ However, the inherent dependence upon caspase-1 warranted a distinct cell death designation, one that encompassed the inflammatory, but more importantly, the programmed nature of this pathway. Just a year after their initial discovery, the pair amended their conclusion and coined the term pyroptosis, whose roots stem from the Greek word 'pyro,' meaning fire, and 'ptosis,' a falling.²¹² Today, pyroptosis is regarded as a pro-inflammatory programmed cell death mechanism mediated by the formation of cytosolic inflammasome complexes which function to catalyze maturation of caspase-1, resulting in caspase-1-dependent signaling events that culminate in cytolysis (Figure 9).

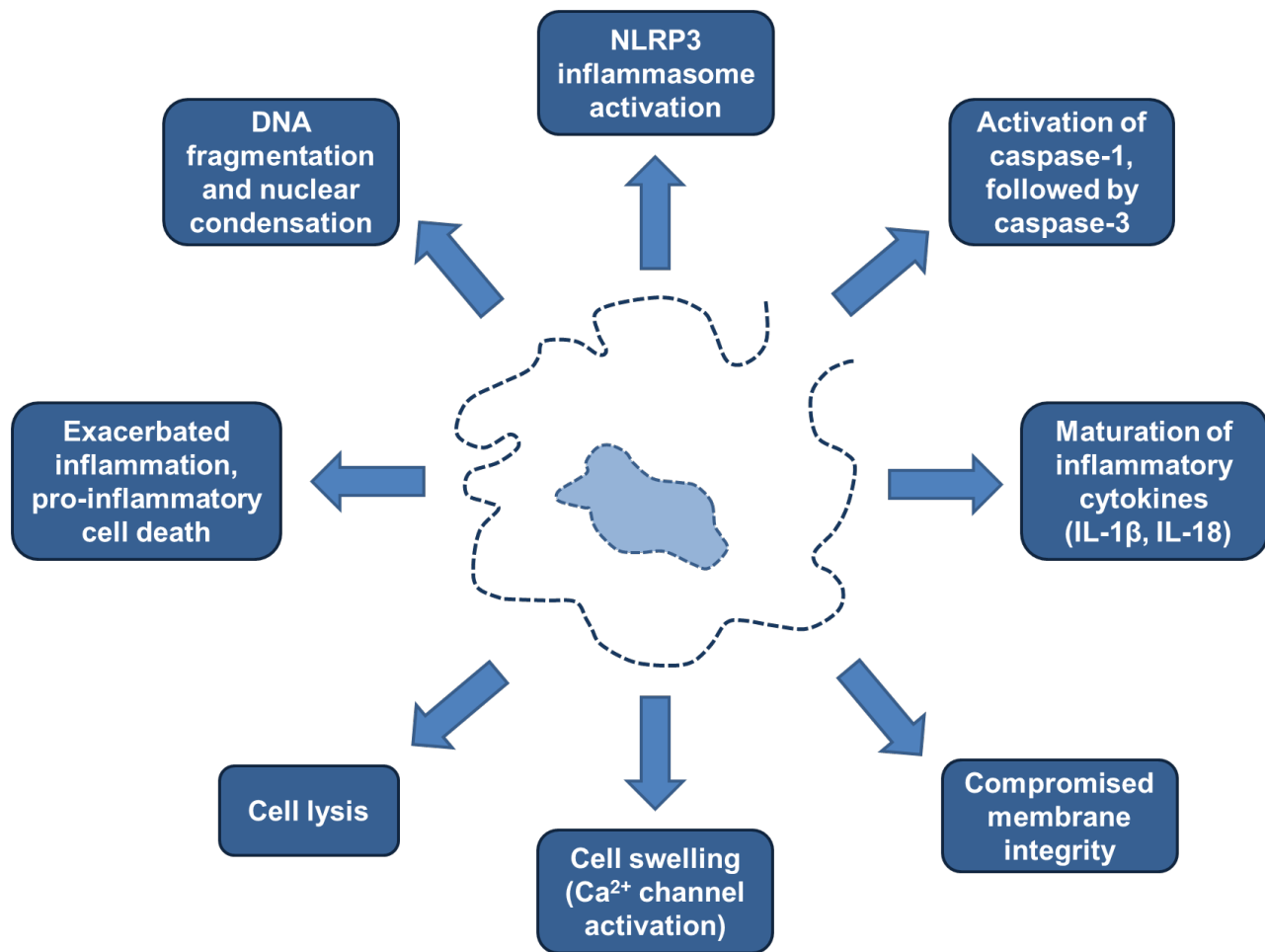


Figure 9. The hallmarks of pyroptosis. While some hallmarks of pyroptosis are shared with apoptotic cell death, most are uniquely specific, including activation of NLRP3 inflammasome complexes, caspase-1-dependency and cell lysis.

Of note, pyroptosis does share features characteristic of apoptosis, which may be attributable to the fact that in addition to cleavage of other pro-caspases, including caspase-4, -5 and -7, caspase-1 can activate caspase-3, the canonical apoptotic caspase.²¹³ While also common to apoptosis, nuclear condensation and DNA fragmentation occur but through a distinct mechanism, namely by means of a caspase-1-activated nuclease.²¹⁴ Furthermore, poly(ADP-ribose) polymerase 1 (PARP1) cleavage is similarly observed in both cell death mechanisms. During pyroptosis,

caspase-1 cleaves caspase-7, which translocates into the nucleus to cleave PARP1.²¹⁵ PARP1, which serves to negatively regulate certain NF-κB-specific gene targets, is subsequently released, leading to transcription induction.²¹⁵

Generally, spillage of intracellular content into the extracellular environment, membrane pore formation, release of activated pro-inflammatory cytokines and cell lysis speak to the many distinct facets of pyroptosis that contribute to its inflammatory nature.^{213,214} At earlier time points, caspase-1 mediates formation of plasma membrane pores, which measure approximately 15-20 nanometers in diameter.²¹⁴ These pores compromise membrane integrity, resulting in the dissipation of cellular ionic gradients, a net increase in osmotic pressure, intake of water and cell swelling.^{214,216} Additionally, activation of the cell surface cation channel transient receptor potential melastatin 2 (TRPM2) may contribute to cell swelling during pyroptosis. TRPM2 is a calcium permeable channel expressed by a number of cell types, but most importantly, hematopoietic cells including CD34+ HSPC and immature erythroid and myeloid cells.²¹⁷ Activation of TRPM2 by TNF-α or oxidative stress results in a significant increase in the intracellular concentration of Ca²⁺, leading to cell volume expansion and increased cell death.²¹⁸ Reduced viability was attributed to cleavage of both extrinsic and intrinsic apoptotic caspases, like caspase-7 and caspase-3, both of which are known to be cleaved and activated by caspase-1.^{213,218} These findings suggest that in the context of oxidative stress or excess inflammatory cytokines, cell death of hematopoietic cells may be regulated in part by activation of TRPM2.²¹⁸ Accordingly, mice deficient in both alleles of *Trpm2* demonstrate not only reduced calcium influx and

signaling, but significant reductions in caspase-1 activation and IL-1 β production.²¹⁷ TRPM2 activation and subsequent calcium mobilization may contribute to inflammasome activation, leading to maturation of caspase-1. Irrespective of the mechanism resulting in cell swelling, both apoptosis and pyroptosis are marked by compromised membrane integrity. Historically, annexin-V and 7-AAD positivity have labeled cells as apoptotic. However, cells undergoing pyroptosis additionally stain positive for these same markers,²¹¹ illustrating that caution should be exercised when identifying and characterizing a particular cell death mechanism.

In accordance with one of its central roles in pyroptosis, specifically the maturation of pro-inflammatory cytokines, caspase-1 was initially identified for its ability to convert pro-interleukin-1 β (pro-IL-1 β) to its mature, active form.^{219,220} Actually, until a system of caspase nomenclature was implemented, caspase-1 was known as ICE, or interleukin-1 β -converting enzyme, highlighting the importance of this particular role. Furthermore, caspase-1 catalyzes maturation of pro-IL-18, and together IL-1 β and IL-18 represent the prototypical cytokines that are activated during pyroptosis.²²¹ These pro-inflammatory cytokines are released following cell lysis, or execution of the pyroptotic program. However, secretion also occurs prior to cell lysis, specifically through non-conventional secretory mechanisms.²¹⁴ As both IL-1 β and IL-18 are leaderless cytokines, their release does not follow the conventional endoplasmic reticulum (ER)-Golgi apparatus pathway.²²² Though the mechanism is not entirely understood, these pro-inflammatory targets, in addition to seventy-five other proteins, are targeted for non-conventional secretion by active caspase-1.^{214,223} As potent inflammatory mediators, expression of IL-1 β and IL-18 is tightly regulated to prevent unwarranted and damaging

inflammation. Foremost, expression of pro-IL-1 β and pro-IL-18 is dependent on NF- κ B activation for transcriptional priming.²¹³ Next, maturation occurs only following cleavage of the cytokine prodomain by active caspase-1.²¹³

Indeed, many of the hallmarks of pyroptosis can be attributed to processes that occur as a result of caspase-1 activation (Figure 9). Inasmuch as pyroptosis is dependent on caspase-1, it remains as dependent on inflammasome complexes, the functional complex that matures pro-caspase-1 to drive cell demise.

NLR Proteins. The nomenclature of the nucleotide-binding oligomerization domain (NOD)-like receptors (NLRs) has since been reformed for unity and clarity.²²⁴ Named for the presence of two receptor family-defining domains, the NLRs are now more accurately known as the nucleotide-binding domain and leucine-rich repeat containing receptors (NLRs).²²⁴ These germline-encoded receptors belong to the pattern recognition receptor family (PRR) with central roles in innate immunity. Specifically the NLRs function to recognition both microorganism and host-derived danger signals, or pathogen-associated molecular patterns (PAMPs) and danger-associated molecular patterns (DAMPs), respectively.²²⁵ Subsequent signaling results in activation of both the innate and adaptive immune responses. The twenty-two known members of the NLR family share structural similarities and can generally be divided into three main parts.²²⁶ First, the N-terminal domain is variable and mediates protein-protein interactions.²²⁶ In total, four different domains exist, namely the acidic transactivating domain, the Baculovirus inhibitor of apoptosis repeat (BIR) domain, the caspase activation and recruitment domain (CARD) and the pyrin domain (PYD).²²⁶

Downstream signaling is largely dependent on the N-terminus, as the domains participate in key homotypic protein-protein interactions.²²⁶ Following activation, receptor oligomerization occurs through the NACHT domain located centrally on the NLR.²²⁵ Lastly, the C-terminus contains a leucine-rich repeat (LRR) domain responsible for PAMP and DAMP detection.²²⁵ The new system of nomenclature divides the NLR family into five main subfamilies according to each receptor's variable N-terminal domain, specifically, (1) NLRA, acidic transactivating domain containing, (2) NLRB, BIR domain containing, (3) NLRC, CARD domain containing, (4) NLRP, PYD domain containing and (5) NLRX, unclassifiable N-terminal domain (Figure 10).²²⁴ Activation of NLR signaling is highly interactive with and complementary to TLR signaling, and certain signaling intermediates overlap between the two pathways.²²⁶ Typically three targets may become activated following NLR pathway activation, including NF- κ B, MAPKs and caspase-1.²²⁶ Only five NLR family members function to mature pro-caspase-1 to its active form, and these do so through self-oligomerization into large, multi-protein complexes called inflammasomes.²²⁶

Inflammasome Complexes and Canonical Activation and Signaling. Critical to innate immunity and the generation of an immune reaction is the efficient detection of pathogens that have gained entry into the cytosol, as well as the recognition of host-derived signals of danger or damage. Five specific NLR family members mediate these detection events, namely NLRC4, pyrin (also known as marenastrin or TRIM20), absent in melanoma 2 (AIM2), NLRP1 and NLRP3.²²⁷ Upon detection of an activating signal within the cytosol, these NLR members self-oligomerize into wheel-like macromolecular

complexes called inflammasomes, which are named for the NLR protein by which they form (Figure 11A).²²⁷

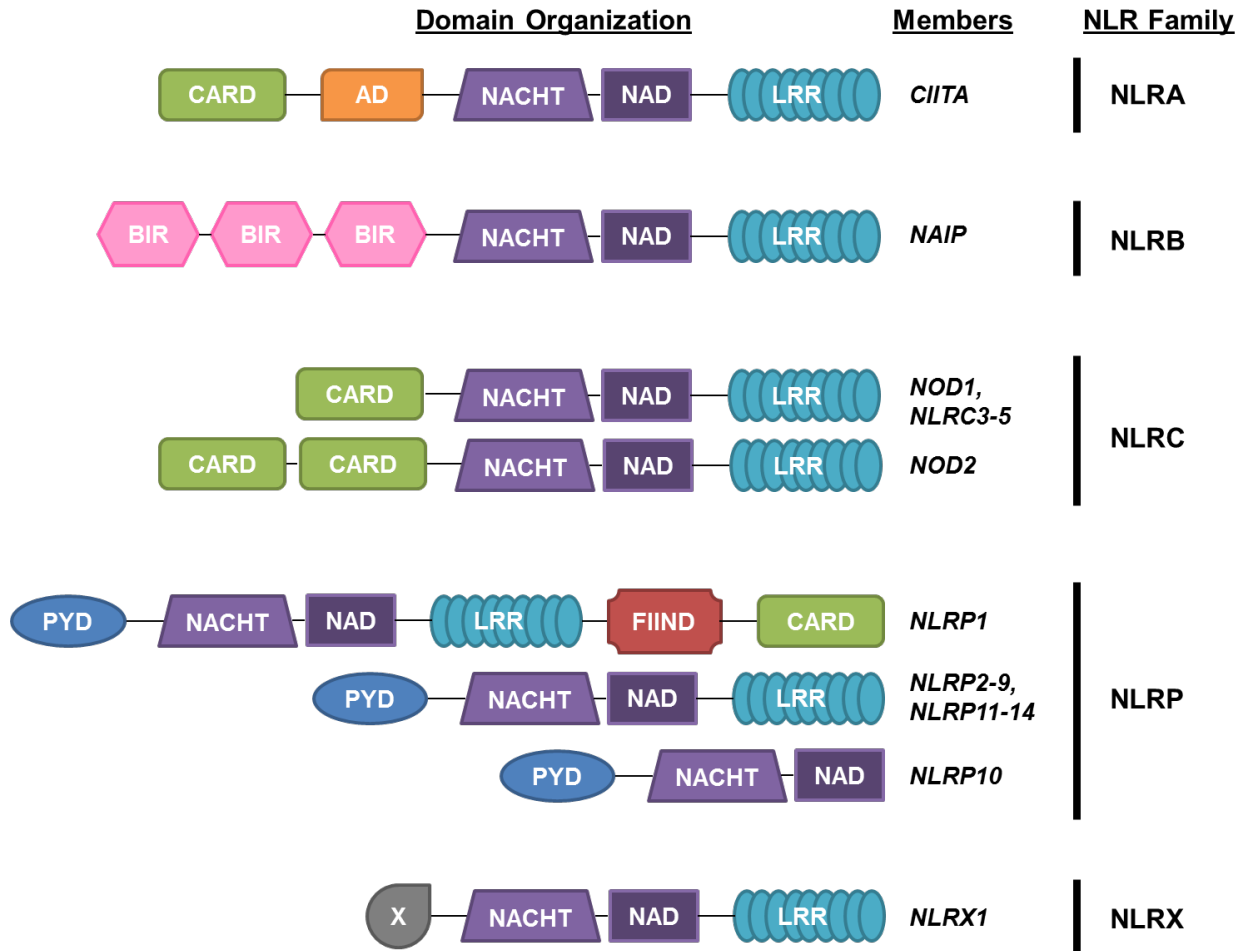


Figure 10. Domain organization of the nucleotide-binding oligomerization domain (NOD)-like receptors (NLRs). The NLRs are classified into five distinct families according to the variable N-terminal domain possessed by each receptor. Four distinct N-terminal domains exist, namely CARD (caspase activation and recruitment domain), AD (acidic transactivating), BIR (Baculovirus inhibitor of apoptosis repeat) and PYD (pyrin domain). Other abbreviations include NACHT (NAIP, CIITA, HET-E, and TP-1), NAD (NACHT-associated domain), LRR (leucine-rich repeat), FIIND (function to find) and X (unknown).

In 2002, Martinon et al. identified a multi-protein complex responsible for activating caspase-1, producing mature pro-inflammatory cytokines and mediating a

cytolytic, inflammatory cell death, called pyroptosis.²²⁸ This complex was coined the inflammasome, and the group specifically identified NLRP1.²²⁸ While mice have three paralogs of Nlrp1, namely Nlrp1a-1c, the human genome encodes a single NLRP1 gene.²²⁹ A variety of PAMPs activate NLRP1, including anthrax lethal toxin, muramyl dipeptide, and even metabolic changes like reductions in intracellular ATP levels.²²⁹ Perhaps most relevant for this manuscript, NLRP1 expression is high within the hematopoietic compartment, in both the myeloid and lymphoid lineages.²³⁰ Masters et al. demonstrated that a point mutation in Nlrp1a (Q593P), resulting in a constitutively active inflammasome complex, leads to aberrant activation of caspase-1.²³¹ Homozygous Nlrp1^{Q593P/Q593P} mice succumb to a highly lethal inflammatory phenotype, with death ensuing at approximately 4 months of age.²³¹ Prolonged activation of Nlrp1 resulted in severe cytopenias, aberrant myeloid lineage maturation, immune suppression and HSPC death.²³¹ Notably, this phenotype was also evidenced in mice subjected to sustained hematopoietic stress.²³¹ Together, these data suggest that the NLRP1 inflammasome may play an important role in aberrant hematopoiesis.

Since the discovery of NLRP1, four additional inflammasome complexes have been identified. Not only do the activating signals vary between inflammasome complexes, but so too does expression, suggesting that particular complexes are most pertinent in certain tissues.²³⁰ The absent in melanoma 2 (AIM2) inflammasome binds cytoplasmic double stranded DNA (dsDNA) and some dsDNA viruses through its oligonucleotide/oligosaccharide-binding domain.^{232,233} This HIN-200 domain is unique to the AIM2 inflammasome as compared to other inflammasome-forming NLR family

members. Activation of caspase-1 follows AIM2^{PYD}-dependent recruitment of ASC.^{232,233} Moreover, the NLRC4 inflammasome responds to a variety of bacterial components, including flagellin, Gram-negative bacteria-derived needle proteins and type III secretion system (TTSS) rod components.²³⁴ NLRC4 inflammasome assembly requires a physical association with NAIP in humans, and NAIP2 and NAIP5 in mice, which function as the sensor of these cytoplasmic bacterial products.²³⁴ The binding of NAIP members to NLRC4 results in inflammasome assembly, caspase-1 activation and the generation of an immune response.²³⁴ Furthermore, pyrin, also known as TRIM20, is the most recently discovered inflammasome complex.²³⁵ Caspase-1 is generated in response to the pyrin-dependent detection of bacterially-mediated modifications of Rho GTPase family members.²³⁵ More specifically, monoglycosylation of Rho family members on a particular threonine residue prevents GTP binding, resulting in Rho inactivation.²³⁵ Interestingly, the PRY/SPRY domain of pyrin that is located at its N-terminus, interacts directly with NLRP1, NLRP3 and pro-caspase-1.²³⁶ This interaction mediates the autophagy-specific degradation of these inflammasome components, illustrating direct regulation of one inflammasome complex over another.²³⁶ Lastly, the best characterized inflammasome-forming protein is undoubtedly NLRP3, which will be discussed in more detail in another portion of this manuscript.

Inflammasome complexes function to drive the maturation of caspase-1 and the generation of pro-inflammatory cytokines IL-1 β and IL-18.^{227,237} Pro-caspase-1, which contains a caspase recruitment domain (CARD), will be recruited to the site of the assembled inflammasome complex through homotypic death domain fold motif

interactions. Specifically, the CARD and pyrin domain (PYD) motifs are important for caspase-1 activation.²³⁸ NLR proteins that contain a CARD domain, specifically NLRC4 and NLRP1, can directly recruit pro-caspase-1 through NLR^{CARD} and pro-caspase-1^{CARD} interactions (Figure 11B).²³⁹ Interestingly, pro-caspase-1 polymerization in the inflammasome was shown to occur through the interaction of CARD domains, leading to enhanced cleavage and proteolytic activity.²³⁹

Alternatively, the other inflammasome forming proteins, specifically pyrin, AIM2 and NLRP3, lack a CARD domain and instead express a PYD motif.²³⁹ These receptors rely on the adaptor protein apoptosis-associated speck-like protein containing a CARD (ASC) (Figure 11C).²³⁸ Specifically, the PYD-only receptors and NLRP1, which contains both a CARD and a PYD domain, use an ASC-dependent mechanism for inflammasome oligomerization and caspase-1 activation.²³⁸ In support, mice deficient in ASC mature significantly less active caspase-1 and IL-1 β than both wild-type and heterozygous counterparts.²⁴⁰ Murine ASC is highly homologous to human ASC, both in structure and function, suggesting evolutionary conservation.²⁴¹ ASC has a bipartite domain structure, with an N-terminal PYD domain and a C-terminal CARD domain.²³⁸ The active NLR receptors recruit ASC through NLR^{PYD} and ASC^{PYD} interactions, resulting in the nucleation and polymerization of ASC at the site of the inflammasome complex (Figure 11D).²³⁹ The PYD-PYD interactions are rather rigid in nature, allowing for the subsequent nucleation and polymerization of pro-caspase-1 (Figure 11D).²⁴¹ Specifically, ASC will recruit pro-caspase-1 to the inflammasome complex, whereby ASC^{CARD} and pro-caspase-1^{CARD} domain interactions allow for pro-caspase-1

nucleation.²³⁹ The CARD-CARD interactions do maintain more flexibility than the rather inflexible PYD cores, which helps regulate the density of pro-caspase-1 at the site of activation.²⁴¹ Once in appropriate proximity, pro-caspase-1 will auto-cleave and activate, resulting in downstream signaling. Both the ASC-dependent and ASC-independent mechanisms of caspase-1 activation fall under canonical inflammasome signaling.

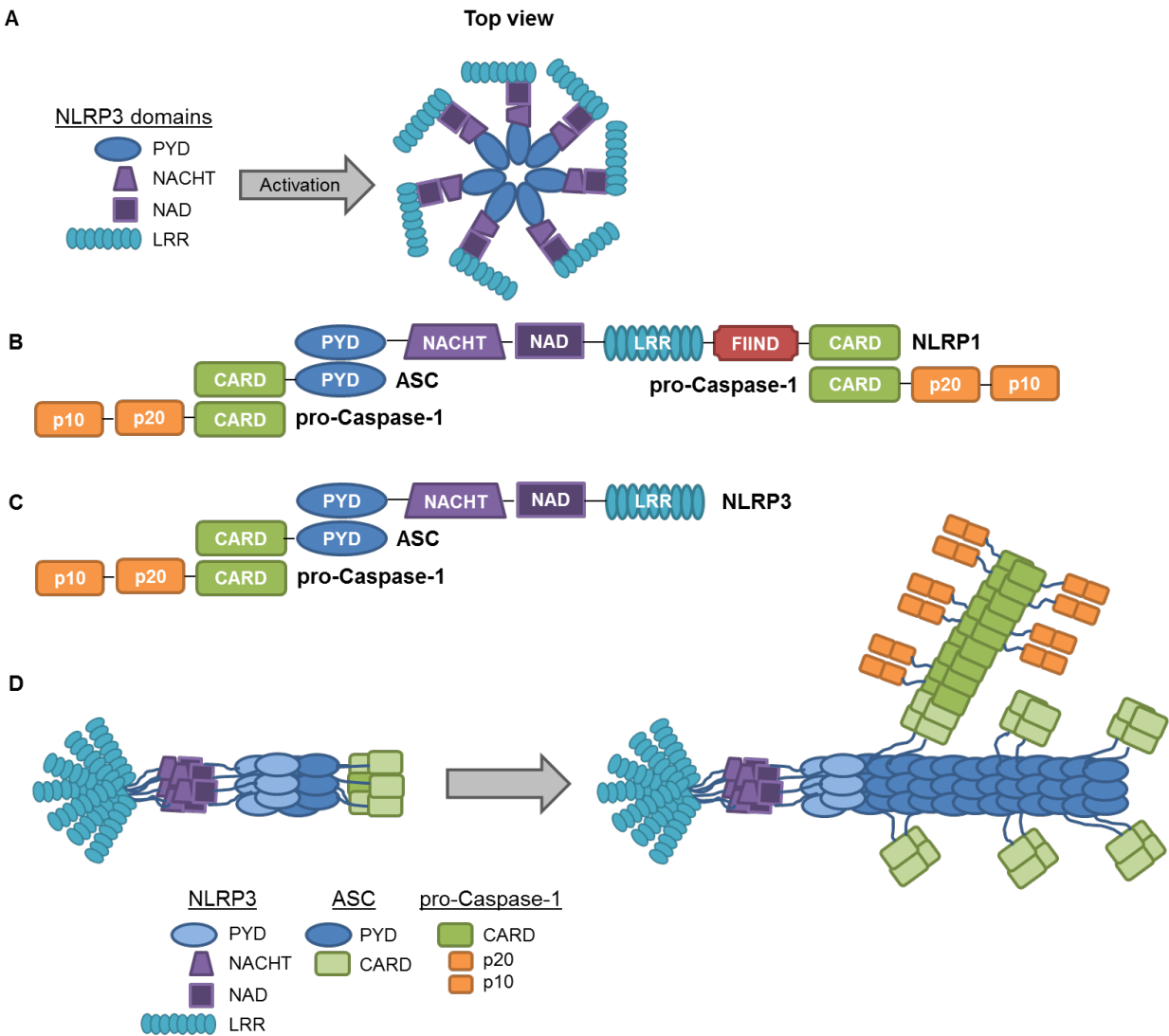


Figure 11. Activation of pro-caspase-1 by inflammasome complexes requires ASC-dependent or ASC-independent nucleation and polymerization. (A) Depicted in the schematic is the NLRP3 inflammasome. Once an activating PAMP/DAMP signal is detected, the inflammasome will oligomerize into a cytosolic, wheel-like complex called the inflammasome. **(B)** Inflammasome-forming NLRs that contain a CARD

domain can directly recruit pro-caspase-1 through NLR^{CARD} and pro-caspase-1^{CARD} interactions. The domain structure of NLRP1 is depicted. As NLRP1 additionally contains a PYD motif, it can also recruit pro-caspase-1 via the adaptor protein ASC. **(C)** The other inflammasome forming proteins, namely pyrin, AIM2 and NLRP3, which is depicted in the schematic, contain a PYD domain motif only. These receptors recruit pro-caspase-1 indirectly through ASC, which subsequently recruits pro-caspase-1 through ASC^{CARD} and pro-caspase-1^{CARD} homotypic interactions. **(D)** NLRP3-mediated activation of pro-caspase-1 is detailed here. Activated NLRP3 recruits ASC through NLRP3^{PYD} and ASC^{PYD} domain interactions. ASC will nucleate and polymerize into a filamentous structure that is rather rigid in nature. Next, ASC will recruit pro-caspase-1 through CARD-CARD domain interactions, leading to nucleation of pro-caspase-1. As the homotypic CARD interactions are more flexible, they help regulate the density of pro-caspase-1, leading to facilitated and enhanced auto-cleavage and activation of the caspase.

Non-Canonical Inflammasome Signaling. Most basically, the processing of pro-caspase-1 and the generation of pro-inflammatory cytokines through inflammasome-dependent mechanisms defines canonical inflammasome signaling. Approximately five years ago, the non-canonical inflammasome was identified in mice through a series of experiments using *caspase-11*^{-/-} BM-derived macrophages (BMDM).²⁴² Caspase-11 activation drives two central signaling events that together characterize the non-canonical inflammasome.²⁴² Specifically, activation of caspase-11 results in (i) NLRP3-independent pyroptotic cell death and (ii) concurrent NLRP3-dependent activation of caspase-1, which is necessary to generate the mature forms of IL-1 β and IL-18 (Figure 12).²⁴² Murine caspase-11-directed signaling is matched in humans by its pro-inflammatory caspase orthologs, namely caspase-4 and caspase-5.²⁴³ Furthermore, in myeloid cells, caspase-4, -5 and -11 were shown to be activated in response to gram-negative bacteria whereby they detect the presence of cytoplasmic LPS.^{243,244} Detection of LPS is mediated by the caspase CARD domain, leading to auto-

activation and dimerization of the caspase into its mature, proteolytically active form.^{243,244} Alternative activators of caspase-4, -5 or -11 are still under investigation.

In canonical inflammasome signaling, activation of caspase-1, the initiator caspase, stems from NLR-dependent PAMP/DAMP detection, leading to inflammasome complex assembly and activation. Contrary to this mechanism, in non-canonical inflammasome signaling, caspase-4, -5, or -11 function as both the PAMP/DAMP detection 'receptor' as well as the initiating caspase.^{243,245} Although these caspases are capable of directly triggering pyroptosis, they are unable to mature pro-IL-1 β and IL-18 independently. Instead, using potent NLRP3 activators, like nigericin, as well as small molecule inhibitors of NLRP3, specifically compound MCC950, Baker et al. reported that cytokine maturation occurs downstream of caspase-4, -5 or -11 activation through an NLRP3-dependent mechanism that results in activation of caspase-1 followed by cytokine processing.²⁴⁵ More specifically, the dramatic drop of intracellular potassium concentration triggers NLRP3 inflammasome assembly and activation (Figure 12).^{246,247} Whether caspase-4, -5 or -11 directly or indirectly trigger changes in potassium concentration remains to be determined.^{246,247}

In non-canonical inflammasome signaling, caspase-4-, -5- or -11-dependent induction of pyroptotic cell death occurs through gasdermin D (GSDMD) cleavage and activation (Figure 12).^{244,248} GSDMD belongs to the gasdermin family of proteins whose physiological roles are still poorly understood.²⁴⁸ Murine and human GSDMD maintain approximately 72% sequence homology, which results in similar functionality.²⁴⁸ Murine GSDMD is cleaved by active inflammatory caspases after amino acid 276 and human

GSDMD after 275.²⁴⁸ This results in two GSDMD cleavage products, namely the inactive C-terminal (~22 kDa) and the active N-terminal (~31 kDa) fragments.²⁴⁴ Whereas full-length (~53 kDa) GSDMD and the C-terminal fragment cannot induce pyroptosis, the N-terminal fragment drives cell death.²⁴⁴ Intramolecular interactions between the C-terminal and N-terminal portion of pro-GSDMD maintain the protein in an inactive state.²⁴⁸ Cleavage relieves this suppressive mechanism, releasing the N-terminal fragment.²⁴⁸ The N-terminal p30 fragment serves as the executioner responsible for membrane pore formation. Recent investigations have shown that the GSDMD N-terminal p30 fragment oligomerizes before binding to phosphatidylinositol phosphates and phosphatidyl serines restricted to the cell membrane inner leaflet to create non-selective membrane pores with an inner diameter of 10-20 nanometers in size.²⁴⁹⁻²⁵² Interestingly, GSDMD has been identified as a substrate of caspase-1, suggesting that the physiological functioning of GSDMD overlaps between canonical and non-canonical inflammasome signaling.²⁴⁴ A summary of non-canonical inflammasome signaling is found in Figure 12.

The NLRP3 Inflammasome

NLRP3 Agonists. Undoubtedly, NLRP3 is the best characterized and most highly understood inflammasome-forming protein. Expression of NLRP3 largely overlaps with NLRP1 and may be found in numerous cell types.²³⁰ Most importantly, NLRP3 is readily expressed in the myeloid and lymphoid lineages of the hematopoietic

system.²³⁰ Over a decade ago, murine BM-derived macrophages deficient in Nlrp3 were shown to lack caspase-1 activation.²⁵³ These data elegantly illustrate, from the most basic of viewpoints, that NLRP3 functions to activate caspase-1, elaborate inflammatory cytokines and generate an effective and potent innate immune response.²⁵³ Nevertheless, many questions remain regarding the complete biology governing the functionality of this receptor, including its mechanism of activation, mode of agonist sensing, regulation and therapeutic targeting, among others.

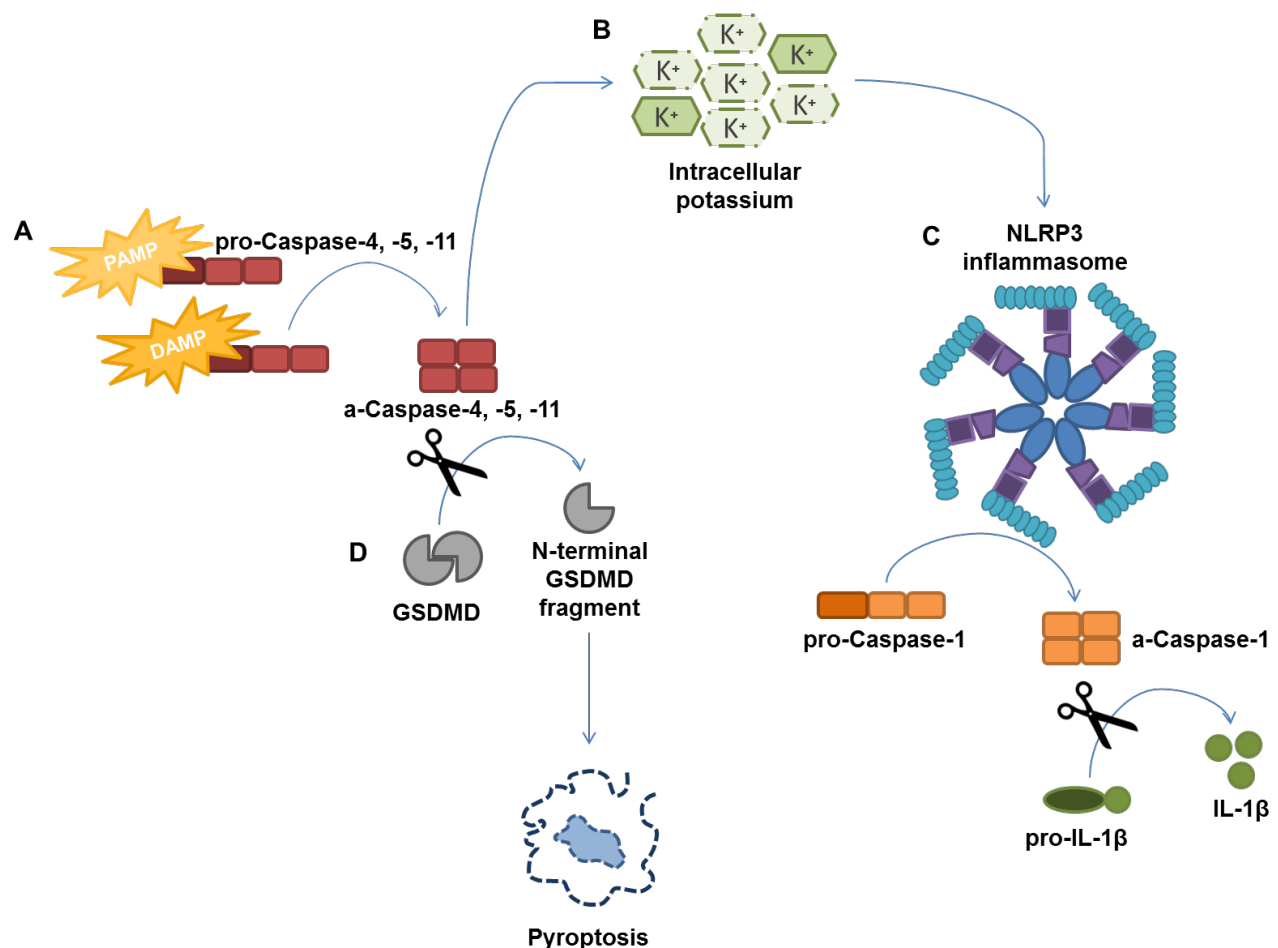


Figure 12. The non-canonical inflammasome signaling pathway. (A) Non-canonical signaling begins with the PAMP/DAMP-specific detection by pro-caspase-4, -5 or -11. Detection is mediated by direct interaction of the PAMP/DAMP with the CARD domain

of the caspase, leading to caspase dimerization and activation. **(B)** Through a direct or indirect mechanism, active (a)-caspase-4, -5 or -11 mediate a dramatic reduction in intracellular potassium concentration. This serves as a trigger for **(C)** NLRP3 inflammasome activation. The inflammasome mediates activation of pro-caspase-1, which subsequently matures pro-IL-1 β and pro-IL-18, leading to cytokine release. **(D)** Concurrently, a-caspase-4, -5 or -11 cleave gasdermin D (GSDMD), which releases the active N-terminal fragment. This fragment is necessary to signal pyroptotic cell death.

With respect to activation signals, NLRP3 is unique from other inflammasome-forming proteins. Whereas other complexes mainly detect PAMPs, NLRP3 predominantly detects DAMP signals.²⁵⁴ Furthermore, NLRP3 detects a very extensive set of both physically and structurally diverse and dissimilar agonists, which is highly unusual compared to the activators detected by other complexes.^{254,255} Generally, NLRP3 is activated by three types of agonists, including extracellular microbial products or toxins (LPS, nucleic acids, muramyl dipeptide, nigericin), environmental irritants and inorganic crystals (asbestos, silica, alum), and DAMPs (ROS, ATP, hyaluronan, S100A9).^{254,255} The mechanism by which such diverse proteins and products activate NLRP3 is still largely unknown and represents one of the most important unanswered questions in the field to date.

NLRP3 Inflammasome Activation: Signal 1. It is generally accepted that NLRP3 inflammasome activation requires two steps, namely an initiating, priming signal followed by a secondary, activation signal.^{255,256} This two-step mechanism is conserved between mice and humans, and represents just one of many regulatory mechanisms that prevent unwarranted and damaging inflammasome activation.²⁵⁶ Surface and cytoplasmic receptor signaling culminating in NF- κ B activation primes the inflammasome and functions to provide signal 1.²⁵⁵ In the absence of transcriptional

priming, NLRP3 will generate an inadequate or simply no inflammatory response, even in the presence of an appropriate signal 2.²⁵⁵ IL-1R, CD33, various TLRs and NLRs represent just a few receptors that can prime the inflammasome.²⁵⁵ As basal cellular concentrations of both *NLRP3* and *pro-IL-1 β* are insufficient for the generation of an inflammasome-mediated immune response, NF- κ B-dependent transcriptional priming must occur prior to the detection of signal 2.²⁵⁶ Conversely, levels of *pro-caspase-1*, *IL-18* and *ASC* are basally sufficient, and therefore do not require priming.²⁵⁵ Notably, NF- κ B-dependent priming of NLRP3 occurs upstream of ASC recruitment, as inflammasome activation fails to occur in the context of ASC overexpression.²⁵⁶

Once primed, NLRP3 is maintained in an ubiquitinated, auto-repressed and inactive configuration within the cytosol.^{254,255} This additional regulation of NLRP3 at the post-transcriptional level prevents exposure of the nucleotide-binding domain (NBD) of NLRP3, effectively preventing oligomerization into mature inflammasome complexes.²⁵⁴ Upon detection of an appropriate activating signal, the leucine-rich repeat (LRR) domain of NLRP3 is deubiquitinated by BRCA1-BRCA2-containing complex 3 (BRCC3) in mice, and BRCC36 (also known as BRCC3) in humans.²⁵⁷ Subsequently, NLRP3 opens its configuration permissive to oligomerization. While transcriptional priming, or signal 1, occurs independently of BRCC3, it is indispensable for NLRP3 inflammasome activation following detection of signal 2.²⁵⁷

NLRP3 Inflammasome Activation: Signal 2. Given that NLRP3 is activated by such a diverse set of agonists, it is unlikely that direct binding is responsible for inflammasome activation.²⁵⁴ Generally, three hypotheses exist for signal 2, or the signal

that induces NLRP3 activation and oligomerization into the inflammasome complex.²⁵⁴ Foremost, reactive oxygen species (ROS) have been shown to induce both priming and activation of the NLRP3 inflammasome.²⁵⁸ This can occur through an NADPH oxidase (NOX)-dependent mechanism.²⁵⁸ The NOX proteins, of which there are six homologs in humans, are ubiquitously expressed and function to generate superoxide and ROS by the transfer of electrons across the plasma membrane.²⁵⁹ Both siRNA-directed silencing as well as pharmacologic inhibition of NOX using diphenyleneiodonium (DPI) results in a significant reduction in *NLRP3* priming, caspase-1 activation and IL-1 β production.²⁵⁸

Using a yeast two-hybrid approach, thioredoxin-interacting protein (TXNIP) was shown to bind to and negatively regulate thioredoxin (TRX), a protein with roles in multiple biological processes.²⁶⁰ Binding of TXNIP to TRX is redox-dependent, as TRX is oxidized in the presence of high ROS concentration, liberating TXNIP from TRX.²⁶¹ Subsequently, TXNIP was shown to bind to the LRR of NLRP3, resulting in inflammasome assembly and activation.²⁶¹ Suppression of TXNIP in the THP-1 cell line using siRNAs resulted in a significant reduction in caspase-1 activation and IL-1 β secretion.²⁶¹ Additionally, BMDM from *Txnip*^{-/-} mice corroborate these findings, illustrating that the TXNIP/NLRP3 axis is significant *in vivo* and functionally activates NLRP3 downstream of ROS.²⁶¹ Interestingly, in a model of type 2 diabetes, Masters et al. was unable to demonstrate neither binding of TXNIP to NLRP3, nor a role of TXNIP in the maturation of IL-1 β .²⁶² Perhaps these conflicting data may be reconciled by the possibility of cell- or context-specific mechanisms leading to NLRP3 activation

downstream of secondary activating signals. To date, the precise mechanism leading to NLRP3 inflammasome activation downstream of ROS production is still unknown.

Notably, in the context of MDS, genomic alterations increase ROS in a NOX-dependent manner.²⁶³ The extent of ROS production increases with the number of mutations, as well as with disease progression.²⁶³ Moreover, the DAMP proteins S100A8 and S100A9, which have been shown to be increased in lower-risk MDS,¹⁴⁰ are scaffold proteins for the assembly and activation of the NOX complex within neutrophils.^{264,265} S100A8/A9 physically interact with cytosolic NOX complex members, resulting in enhanced oxidase activity and enzyme kinetics.²⁶⁵ Studies in PB mononuclear cells (PB-MNC) demonstrated that S100A8/A9 induce NF- κ B-mediated transcriptional priming of *NLRP3* and *pro-IL-1 β* via NOX-dependent generation of ROS.²⁶⁶ Additionally, treatment of PB-MNC with S100A8/A9 increased NLRP3 inflammasome activation, with subsequent caspase-1 activation and IL-1 β secretion.²⁶⁶ Lastly, mitochondria-derived ROS also activate NLRP3, resulting in caspase-1 activation and cell death.^{267,268}

Within the cytosol, ROS can trigger permeabilization of the mitochondrial membrane as well as of the lysosomal membrane, which both trigger NLRP3 inflammasome activation.²⁶⁷ Indeed, NLRP3 appears to be a sensor of organelle dysfunction.^{267,269} A lysosome/cathepsin B-dependent mechanism represents the second hypothesis allowing for NLRP3 inflammasome activation. In PB-MNCs, phagocytosis of crystalline substances, like silica and alum, results in lysosomal swelling, damage and spillage of lysosomally-contained material into the cytosol.²⁶⁹ This

results in the release of the lysosomal protease cathepsin B, which by a direct or indirect mechanism activates the NLRP3 inflammasome, triggering caspase-1 activation with IL-1 β secretion.²⁶⁹ A conserved mechanism is evident in Alzheimer's disease, contributing to disease pathobiology.²⁷⁰ Phagocytosis of amyloid β , an endogenous DAMP peptide, by microglial cells damages lysosomes, resulting in cathepsin B release and activation of the NLRP3 inflammasome complex.²⁷⁰ Undoubtedly, phagocytosis of other DAMPs capable of triggering lysosomal membrane permeabilization and spillage of lysosomal contents into the cytosol would also activate NLRP3.

Lastly, the final hypothesis for NLRP3 inflammasome activation is characterized by upstream changes in intracellular cation concentrations.²⁵⁴ Potassium efflux may be elicited by a variety of NLRP3 agonists, resulting in NLRP3 inflammasome formation, caspase-1 activation and IL-1 β generation.²⁷¹ The opening of ion channels or alternatively, the formation of pores by bacterial or pathogenic toxins likely mediates K⁺ efflux.^{254,271} Conversely, increased cytoplasmic concentration of Ca²⁺ modulates NLRP3 inflammasome activation.²⁷² ER stress frequently results in rapid increases in Ca²⁺, recently identified to trigger inflammasome formation.²⁷² Moreover, lysosomal membrane permeabilization as well as overt rupture function to mobilize Ca²⁺, which can mediate subsequent plasma membrane pore permeability and the efflux of K⁺.^{271,272} In this way, both K⁺ and Ca²⁺ activate NLRP3 inflammasome complexes at the level of signal 2.

Endogenous Regulation of the NLRP3 Inflammasome. In addition to the requisite two signals necessary for NLRP3 inflammasome assembly and activation, a

number of decoy proteins have originated from gene duplication events that further regulate NLRP3 activation.²⁷³⁻²⁷⁷ To start, three genes have originated adjacent to one another on chromosome 11q22, near *caspase-1*, and serve as negative regulators of caspase-1-dependent activation of IL-1 β .²⁷³⁻²⁷⁵ Specifically, ICEBERG, inhibitory CARD (INCA) and CARD only protein (COP) share 52%, 81% and 97% sequence identity to the CARD domain, located within the prodomain of pro-caspase-1.^{274,275} These proteins are induced by pro-inflammatory stimuli, resulting in their expression and the subsequent extinction of caspase-1-dependent responses.²⁷³⁻²⁷⁵ Through directly binding to the prodomain of pro-caspase-1, ICEBERG, INCA and COP inhibit the activation of caspase-1 by blocking dimerization, which is required for conversion of the zymogen to its active form.²⁷³⁻²⁷⁵ In this way, these endogenous inhibitors prevent unwarranted, exacerbated and accidental caspase-1 activation and limit IL-1 β -induced inflammation.²⁷³⁻²⁷⁵

Additionally, pyrin-domain (PYD) only protein 1 (POP1) represents an alternative negative regulator of NF- κ B, ASC and NLRP3.^{276,277} POP1 is thought to have generated from gene duplication events, as it shares approximately 88% sequence identity to the PYD of the NLRP3 adaptor protein ASC. Foremost, POP1 directly interacts with the IKK complex responsible for activating NF- κ B in response to cytokine stimulation.²⁷⁶ This results in the inhibition of NF- κ B activation, as well as the repression of NF- κ B-inducible target genes.²⁷⁶ Moreover, POP1 directly binds to ASC^{PYD}, which blocks ASC^{PYD} and NLRP3^{PYD} domain interactions, effectively preventing NLRP3 assembly, ASC nucleation and polymerization, caspase-1 activation and the release of mature IL-1 β and IL-18.²⁷⁷

While these negative regulatory mechanisms function to limit and fine-tune inflammasome-dependent responses, excessive and prolonged activation of the NLRP3 inflammasome has been pathobiologically implicated in a wide range of autoimmune diseases and inflammatory conditions.²⁵⁴

Evidence of Pyroptosis in the MDS Literature. Over two decades ago, Mundle et al. demonstrated that approximately 40% of lower-risk MDS cases demonstrate significantly increased IL-1 β secretion within the bone marrow, which positively correlated with the amount of DNA fragmentation.⁹⁹ More importantly, treatment of BM-MNC with a caspase-1-specific inhibitor reduced DNA fragmentation and IL-1 β secretion, implicating caspase-1 activation in the cell death observed in MDS.⁹⁹ In corroboration of these findings, caspase-3 activation was shown to occur downstream of caspase-1 activation in MDS, illustrating a sequence of caspase activation consistent with pyroptosis rather than apoptosis.²⁷⁸ More recently, a non-canonical role for NLRP3 was described in regulating receptor-mediated apoptosis in epithelial cells. In response to TNF- α /TNFR signaling, NLRP3, ASC and pro-caspase-8 are recruited to the mitochondria where NLRP3-dependent processing of pro-caspase-8 occurs.²⁷⁹ As TNF- α is overexpressed in MDS and the extrinsic apoptotic pathway is activated, it is likely that such a mechanism additionally occurs within this context.

Beyond basal activation, in overstimulated or overstressed conditions, autophagy synergizes with inflammasome activation to augment the inflammatory response.²⁸⁰ Accordingly, non-canonical roles of autophagy-related proteins are continually being described, including atypical roles in antigen presentation and non-conventional secretion.¹⁸⁸ Stimulation of autophagy in the context of NLRP3 inflammasome activation

results in co-localization of autophagosomes with IL-1 β and HMGB1. Subsequently, through non-conventional secretion, the autophagic machinery mediates secretion of inflammasome substrates, like IL-1 β and IL-18, as well as potent DAMPs into the extracellular milieu.²⁸¹ As a consequence of mitochondrial damage, mitochondrial-derived ROS are increased, which can enhance NLRP3 inflammasome activation and thereby activation of caspase-1 and generation of IL-1 β .²⁶⁸ These findings help vindicate why mitochondrial dysfunction is often linked to inflammatory disease, both of which are manifest in MDS. Furthermore, in the context of oxidative stress, caspase-1 augments mitophagic flux by promoting up-regulation of beclin 1.²⁸² A recent publication illustrated that both mRNA and protein expression of beclin 1 are increased in lower-risk MDS.²⁸³ Although the findings in this manuscript are the first to link NLRP3 inflammasome activation and pyroptotic cell death to the pathobiology of MDS, the literature supports, both directly and indirectly, the role of caspase-1 and NLRP3 activation in these disorders.

β -Catenin

Canonical Wnt/ β -Catenin Signaling. The canonical Wnt/ β -catenin signaling pathway, which was first identified in *Drosophila*, is implicated in supporting self-renewal, proliferation and cell survival.²⁸⁴ This is accomplished through the activation of β -catenin, which will translocate into the nucleus and bind transcriptional activators, resulting in gene transcription.²⁸⁴ Understandably so, mutations in this signaling pathway are commonly observed in human cancer.²⁸⁴

In the basal state, β -catenin activation is repressed by the β -catenin destruction complex. The complex consists of two tumor suppressors, Axin and adenomatous polyposis coli (APC), as well as two constitutively active serine/threonine kinases, or casein kinase 1 (CK1) and glycogen synthase kinase 3 (GSK3).²⁸⁴ Axin, the main scaffold for the destruction complex, directly interacts with β -catenin. CK1 and GSK3 will deliver phosphorylation marks on β -catenin, resulting in its recognition by the E3 ubiquitin ligase, beta-transducin repeat containing protein (β -TrCP).²⁸⁴ Ubiquitination of β -catenin by β -TrCP targets it for proteasomal degradation, effectively eliminating β -catenin-mediated transcription effects in the absence of appropriate pathway activation. Wnt/ β -catenin pathway inactivation is summarized in Figure 13A-D.

Conversely, canonical Wnt/ β -catenin signaling initiates with the binding of a Wnt ligand to a transmembrane receptor complex consisting of Frizzled (Fz) and low-density lipoprotein receptor-related protein 5 (LRP5) or 6 (LRP6).²⁸⁴ Next, Dishevelled (Dvl) will bind the cytoplasmic part of Fz, allowing for recruitment of Axin to the LRP5/6 tail.²⁸⁴ These recruitment events sequester Axin, preventing the formation of the destruction complex and subsequently allow for the accumulation of cytoplasmic β -catenin.²⁸⁴ Ultimately, β -catenin translocates into the nucleus and binds transcriptional activators, like T cell factor (TCF) and lymphoid enhancing factor (LEF), resulting in gene transcription.²⁸⁴ The signaling cascade resulting from Wnt/ β -catenin pathway activation is summarized in Figure 13E-G. Though β -catenin activation vastly alters gene expression, cyclin D1 and c-myc are among the best characterized downstream targets. Notably, in a cohort of sixteen MDS patients, approximately 90% of all CD34+ BM-MNC

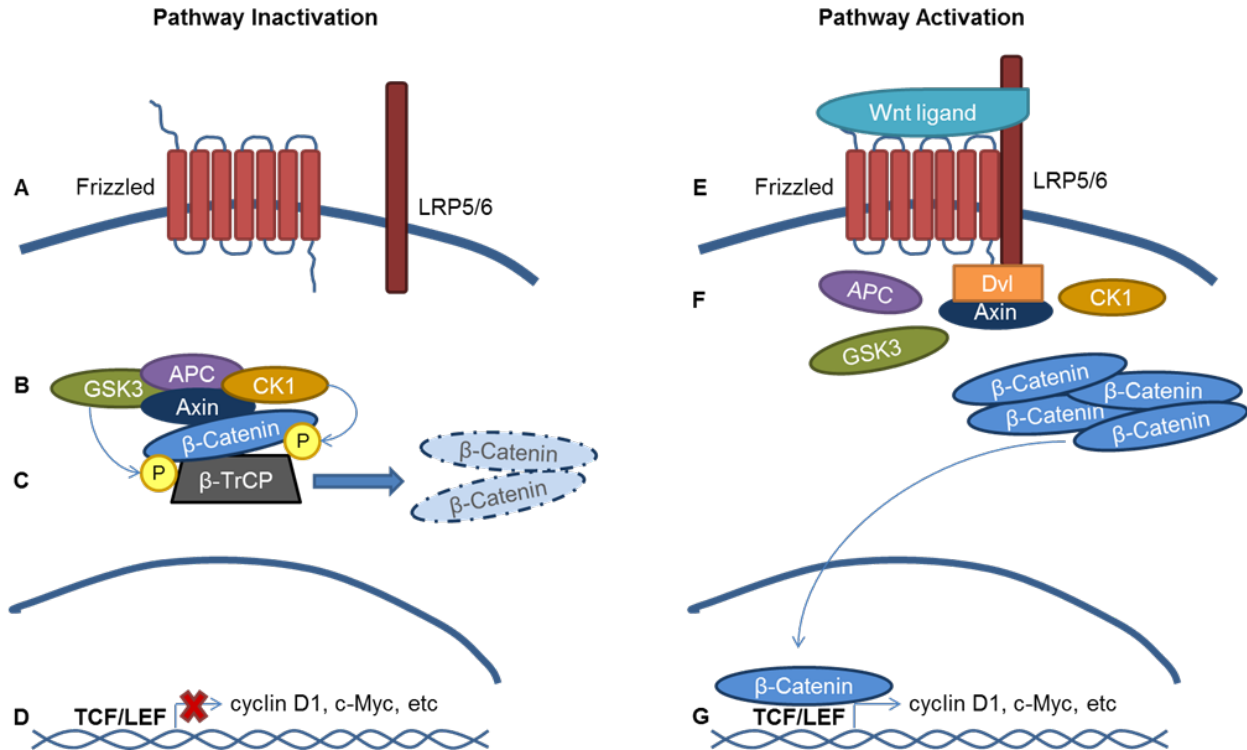


Figure 13. Canonical Wnt/ β -catenin signaling depicted in the context of pathway inactivation and activation. The signaling events resulting from the lack of a pathway activating signal are shown in A-D. **(A)** Without ligand binding to the transmembrane Frizzled (Fz) or LRP5/6 receptors, the **(B)** β -catenin destruction complex, consisting of Axin, APC, CK1 and GSK3, will initiate degradation of β -catenin. The serine/threonine kinases CK1 and GSK3 phosphorylate β -catenin, which is recognized by **(C)** β -TrCP, an E3 ubiquitin ligase. Ubiquitination of β -catenin targets it for proteasomal degradation. **(D)** β -catenin-mediated transcriptional activation of TCF/LEF controlled genes is repressed. The signaling events resulting from pathway activation are shown in E-G. **(E)** Binding of a Wnt ligand to Frizzled/LRP5/6 allows for recruitment of Dishevelled (Dvl) and Axin to the cytoplasmic tails of Fz and LRP5/6, respectively. **(F)** The destruction complex will not form, allowing for the cytoplasmic accumulation of β -catenin. **(G)** Translocation of β -catenin into the nucleus results in activation of TCF/LEF controlled genes, leading to gene transcription.

were c-myc+, as measured by flow cytometry.¹⁹⁸ Expression of c-myc was greater in MDS compared to normal controls, and increased with disease risk.¹⁹⁸ These findings suggest a role for aberrant β -catenin activation in MDS, likely contributing to survival of the MDS clone during disease progression.

Activation of β -Catenin is Regulated by Oxidative Stress. Extensive evidence indicates that oxidative stress enhances activation of β -catenin, resulting in increased expression of its downstream target genes, including c-myc. Notably, Rac proteins, members of the Rho family of small GTPases, associate with NADPH oxidase (NOX) complexes and enhance NOX activation.²⁸⁵ Rac1 activation was shown to be a requisite for the nuclear translocation of β -catenin.²⁸⁵ NOX members, who function to generate ROS through the transfer of electrons across membranes, are central producers of ROS.²⁵⁹ Therefore, NOX activation and NOX-dependent production of ROS would be expected to promote β -catenin activation. Accordingly, not only are β -catenin gene targets markedly suppressed in NOX1^{KO} mice, activity of the β -catenin destruction complex member GSK3 is significantly increased.²⁸⁶ These data are particularly interesting, given that S100A8/A9, the DAMP signals increased in lower-risk MDS,¹⁴⁰ function as a scaffold for the membrane assembly and activation of the NOX complex, and additionally increase NOX function.²⁶⁵

Moreover, an unbiased, mass spectrometry pull-down approach to identify additional binding partners of dishevelled (Dvl) identified nucleoredoxin (NRX) as a novel interaction partner.²⁸⁷ NRX, related to thioredoxin (TRX), was confirmed through immunoprecipitation experiments to bind Dvl directly.²⁸⁷ Binding of NRX-Dvl is Wnt ligand-independent, but rather redox-dependent. In the absence of oxidative stress, NRX specifically binds Dvl, illustrating a mechanism whereby NRX negatively regulates β -catenin activation.²⁸⁷ In contrast, oxidation of NRX liberates Dvl, allowing Dvl to inhibit

the β -catenin destruction complex and enhance β -catenin nuclear translocation.²⁸⁷

These effects of oxidative stress on β -catenin activation are summarized in Figure 14.

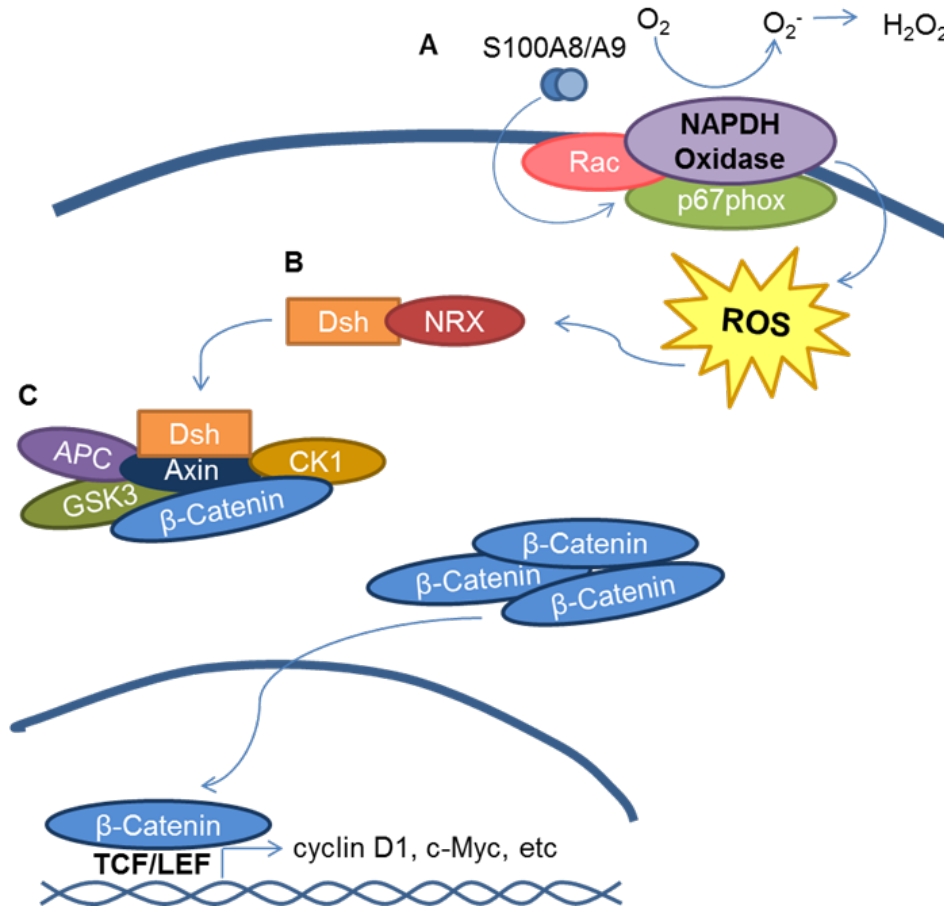


Figure 14. Oxidative stress positively regulates β -catenin activation and signaling. (A) Activation of the NADPH oxidase (NOX) complex is enhanced by the DAMP proteins S100A8/A9 as well as Rac proteins. NOX generates reactive oxygen species (ROS) by the transfer of electrons across the plasma membrane. (B) NOX-derived ROS can oxidize nucleoredoxin (NRX), a binding partner and negative regulator of dishevelled (Dvl) and β -catenin signaling. Once oxidized, NRX dissociates from Dvl, allowing Dvl to (C) bind to Axin and prevent the formation of the β -catenin destruction complex. As a result, β -catenin accumulates within the cytoplasm and can translocate into the nucleus and alter gene transcription.

CHAPTER 2

The NLRP3 Inflammasome Functions as a Driver of the Myelodysplastic Syndromes (MDS) Phenotype

Note: This chapter has been previously published in the journal *Blood*, Basiorka et al. *Blood*. 2016 Oct 13, and has been reproduced in this manuscript with permission from the publisher.

Introduction

Myelodysplastic syndromes (MDS) are hematopoietic stem cell malignancies characterized by dysplastic and ineffective hematopoiesis. MDS bone marrow precursors typically display larger cell size, deregulated proliferation and maturation, and accelerated attrition by programmed cell death.^{45,288,289} Despite these shared phenotypes, MDS harbor a spectrum of clonal chromosome abnormalities and somatic gene mutations, the latter most commonly involving genes encoding RNA splicing and epigenetic regulatory proteins.^{84,290} How such diverse genetic alterations initiate a common MDS phenotype is unexplained. Apoptosis, a non-inflammatory form of programmed cell death, has been implicated in the ineffective hematopoiesis in MDS based upon membrane externalization of phosphatidylserine, mitochondrial depolarization and DNA fragmentation.^{196,197,203} However, the cytokine profile and cellular milieu in MDS instead support aberrant innate immune activation.²⁹¹ Indeed, inflammatory cytokines such as interleukin-1 β (IL-1 β), tumor necrosis factor- α , transforming growth factor- β , IL-6 and others are generated in excess in MDS,

accompanied by bone marrow expansion of hematopoietic-inhibitory, myeloid derived suppressor cells (MDSC) activated by the danger associated molecular pattern (DAMP) S100A9, a Toll-like receptor (TLR)-4 and CD33 ligand.^{99,140,144,292} Furthermore, MDS hematopoietic stem and progenitor cells (HSPC) overexpress TLRs accompanied by activation of respective signaling intermediates, which have been implicated in the aberrant proliferation of MDS HSPC and in the pathogenesis of peripheral blood cytopenias.^{112,116,293}

Recent studies have shown that activation of TLRs by select DAMPs can trigger pyroptosis, a novel caspase-1-dependent pro-inflammatory cell death that involves the activation of ion gradients, cell swelling, the release of IL-1 β and IL-18, intracellular DAMPs and other pro-inflammatory cytokines.^{211,212,292,294} Pyroptosis is mediated by the formation of inflammasome complexes, which are cytosolic heptameric oligomers composed of nucleotide-binding domain and leucine-rich repeat containing pattern recognition receptors (NLRs). The best characterized NLR, NLRP3, is a redox-sensitive cytosolic sensor that undergoes a conformational change in response to DAMP interaction to recruit the ASC (apoptosis-associated speck-like protein containing a caspase-recruitment domain) adaptor protein. This interaction in turn triggers ASC polymerization and nucleation of large cytoplasmic aggregates referred to as ASC specks.²³⁹ ASC specks serve as a platform recruiting pro-caspase-1 monomers that are activated by proximity-induced autocatalysis to initiate proteolytic processing of pro-IL-1 β and pro-IL-18 to their mature, active forms.²¹¹ Inflammasome activation involves two steps beginning with NF κ B-induced transcriptional priming of inflammasome proteins, followed by cation channel activation, cell volume expansion and inflammasome

component assembly.^{211,212,294} NLRP3 is activated by diverse DAMP signals, including S100A9 homodimers and S100A8/9 heterodimers that function as alarmins to induce NADPH oxidase and generate reactive oxygen species (ROS).^{266,295,296}

Here we show that S100A9 and ROS, generated in response to NLRP3 inflammasome activation or somatic gene mutations, serve as DAMP signaling intermediates responsible for inflammasome-mediated pyroptosis and β -catenin activation in MDS. Remarkably, disabling this inflammasome circuit restores effective hematopoiesis in MDS. Collectively, these findings define key biological effectors of the MDS phenotype and suggest novel strategies for therapeutic intervention.

Results

MDS HSPC manifest inflammasome activation and pyroptosis. To determine if pyroptosis was primed in MDS, expression of genes encoding inflammasome proteins was evaluated in BM-MNC isolated from MDS patients (n=10) compared to age-matched normal controls (n=5). MDS specimens displayed marked up-regulation of inflammasome transcripts (Figure 15A) where *caspase-1* (*CASP1*) mRNA levels were increased 209-fold and *NLRP3* 48.1-fold in MDS; in contrast, levels of *caspase-3* (*CASP3*) mRNA, the canonical apoptotic caspase, were similar in MDS and normal BM-MNC. Further, mRNAs encoding the inflammatory cytokines *IL-1 β* and *IL-18* were increased 3.7-fold and 29.6-fold in lower-risk MDS (n=5) versus normal BM-MNC (n=5), whereas expression was only increased 1.1-fold and 9.2-fold in higher-risk MDS specimens (n=5). Confocal fluorescence microscopy confirmed selective activation of

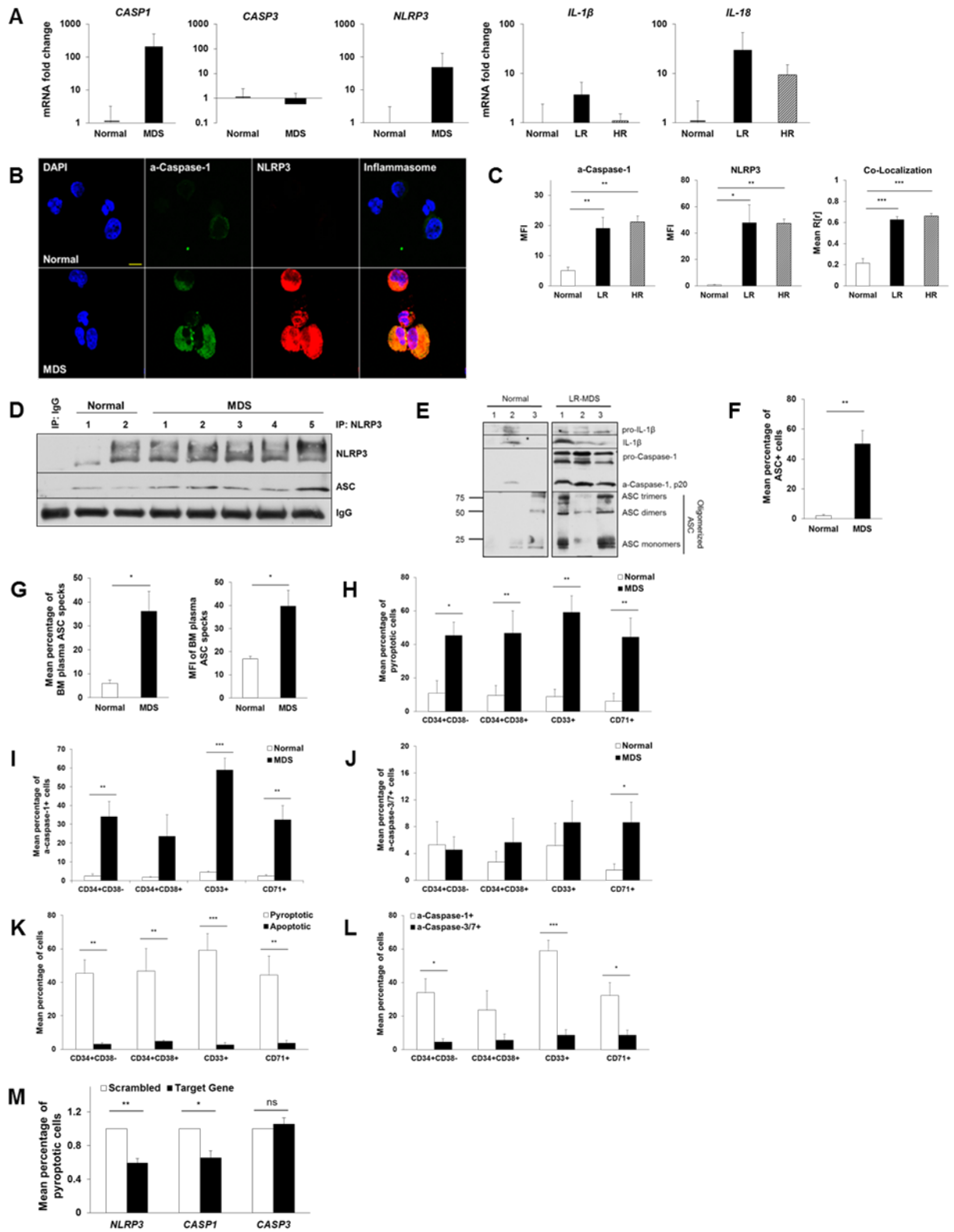


Figure 15. Fulminant pyroptosis is manifest in HSPC and progeny in MDS. (A) qPCR analyses of expression of pyroptosis-associated genes in BM-MNC isolated from

MDS patient specimens (n=10 total; n=5 lower- and n=5 higher-risk disease) compared to normal BM-MNC (n=5). **(B)** Representative confocal fluorescence micrograph (2520x magnification, 7.5 μm scale) of (active) a-caspase-1 and NLRP3 expression in MDS versus normal BM-MNC. DAPI (blue), a-caspase-1 (green), NLRP3 (red); merged images show inflammasome formation. **(C)** Quantitative analysis of confocal images of BM-MNC isolated from MDS patients [lower-risk (n=7), higher-risk (n=3)] and normal donors (n=6). **(D)** Binding of ASC to NLRP3 in lower-risk MDS BM-MNC compared to normal donors (IP: NLRP3, IB: NLRP3, ASC). Data are representative of three independent experiments. **(E)** Immunoblot following chemical crosslinking of BM-MNC cell lysates derived from normal donors (n=3) and LR-MDS patients (n=3). **(F)** Quantitation of inflammasome activation based on ASC oligomerization in BM-MNC from lower-risk MDS (n=5) versus normal BM-MNC (n=3). **(G)** Mean percentage of ASC specks and speck MFI in the BM plasma of lower-risk MDS specimens (n=6) compared to normal BM plasma (n=3). **(H)** The mean percentage of pyroptotic cells by hematopoietic lineage in lower-risk MDS (n=8) versus normal donors (n=8). **(I-J)** Mean percentage of **(I)** total a-caspase-1⁺ and **(J)** a-caspase-3/7⁺ cells assessed by hematopoietic lineage in lower-risk MDS (n=8) and normal donors (n=5). **(K)** Comparison of the mean percentage of pyroptotic versus apoptotic cells by hematopoietic lineage in lower-risk MDS specimens (n=8). **(L)** Comparison of the mean percentage of a-caspase-1⁺ versus a-caspase-3/7⁺ cells in the same lower-risk MDS patients (n=8). **(M)** Mean percentage of pyroptotic cells following knockdown of *NLRP3*, *CASP1* and *CASP3* by shRNA-directed silencing of lower-risk MDS BM-MNC (*NLRP3*, n=4; *CASP1* and *CASP3*, n=3). Error bars: SE, *p<0.05, **p<0.01 and ***p<0.001.

NLRP3 inflammasome complexes in MDS specimens versus age-matched normal BM-MNC, evidenced by co-localization and increased active (a)-caspase-1 (MFI 3.7-fold increase in lower-risk [$p=7.1 \times 10^{-3}$] versus 4.1-fold in higher-risk MDS [$p=6.0 \times 10^{-3}$]) and NLRP3 (MFI 69.1-fold increase in lower-risk [$p=0.013$] and 68.2-fold in higher-risk disease [$p=5.1 \times 10^{-3}$]) (Figure 15B and 15C). NLRP3 oligomerization and activation was confirmed by increased binding of NLRP3 to ASC in MDS compared to normal donors (Figure 15D), and by robust formation of ASC monomers and higher-order oligomer complexes, which are indispensable for inflammasome activity and evident following DSS-crosslinking (Figure 15E). MDS BM-MNC also displayed increased levels of pro- and a-caspase-1, pro-IL-1 β and a-IL-1 β compared to normal BM-MNC (n=3) (Figure 15E). Finally, inflammasome formation was confirmed by alternate methods of

assessment of ASC oligomerization, where ASC incorporation into inflammasome complexes is detected by flow cytometric changes in fluorescence pulse height and area (Figure 15F).²⁹⁷ MDS specimens also displayed significantly greater inflammasome assembly compared to controls, irrespective of IPSS risk group (Figure 15C). Specifically, NLRP3 inflammasome assembly was increased 2.9-fold in lower-risk ($p=3.9 \times 10^{-5}$) and 3.1-fold in higher-risk ($p=7.1 \times 10^{-5}$) MDS patients. Active ASC specks are released into the extracellular space following cytolysis and specifically following execution of pyroptotic pore formation and cytolysis.²⁹⁸ Notably, analysis of ASC specks in BM plasma from lower-risk MDS specimens (n=6) confirmed a profound increase in the percentage and MFI of ASC specks in MDS compared to normal BM plasma (n=3) (mean, MDS 36.2 ± 1.4 vs. 6.0 ± 8.4 , Figure 15G). Finally, immunofluorescence and flow cytometry analyses of other hematologic malignancies suggest that inflammasome activation is specific for MDS (Figure 16).

Caspase-1 activation by the inflammasome is followed by mitochondrial depolarization and caspase-3 activation, a secondary cleavage target of caspase-1, as late events in pyroptosis. To specifically assess pyroptosis versus apoptosis in MDS, the percentage of pyroptotic cells, defined as the percentage of α -caspase-1⁺/ α -caspase-3/7⁺/annexin-V⁺ cells, was determined in phenotypically distinct hematopoietic lineages by flow cytometry. Normal (n=5) and lower-risk MDS BM-MNC (n=8) were incubated with autologous BM plasma for 24 hours prior to flow cytometry analysis. MDS HSPC demonstrated profound increases in pyroptosis, where the fraction of pyroptotic cells was increased 4.1-fold in CD34⁺CD38⁻ stem cells ($p=0.035$), 4.9-fold in

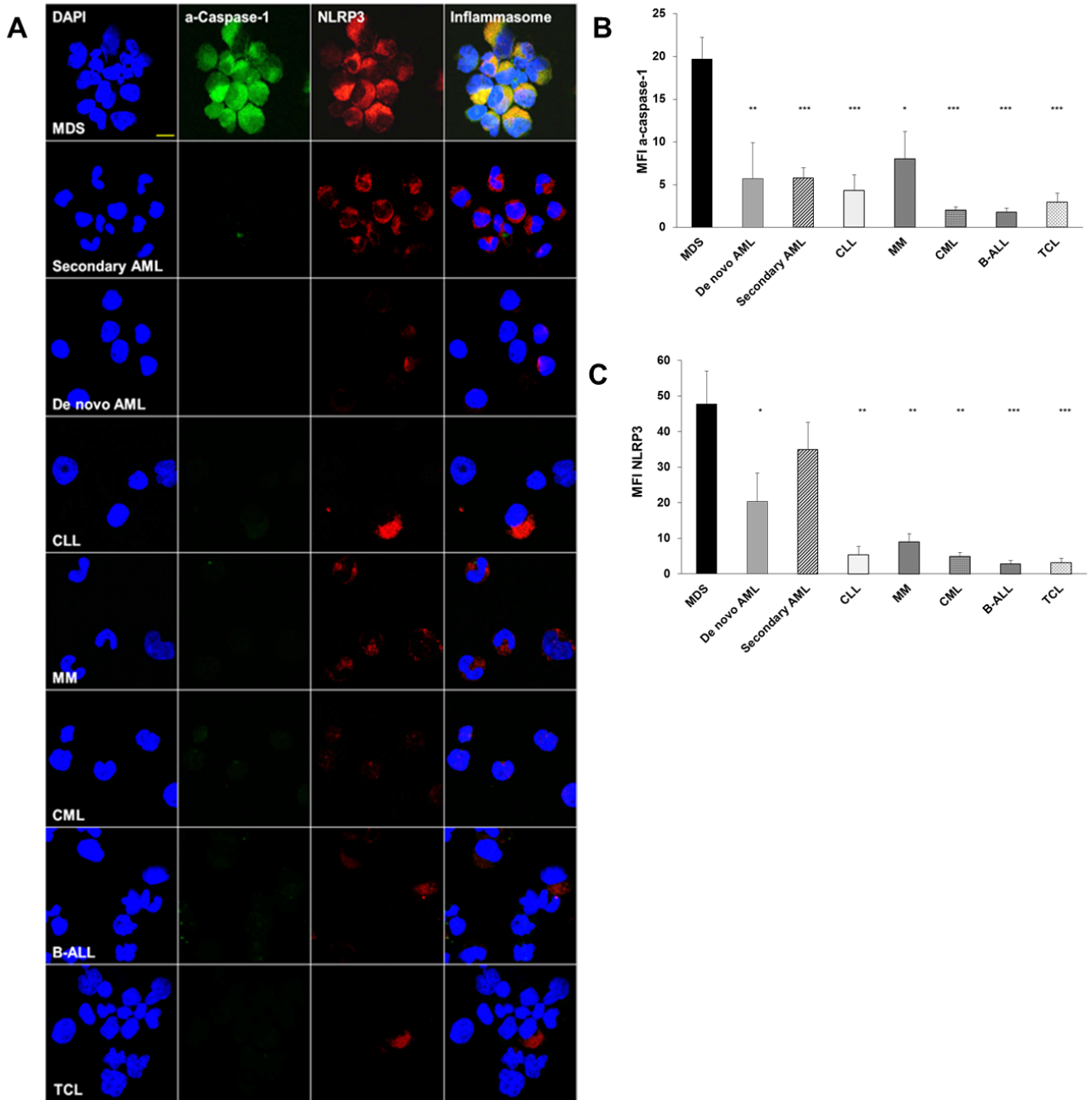


Figure 16. NLRP3 inflammasome assembly may be MDS-specific. (A) Representative confocal fluorescence micrograph (2520x magnification, 7.5 μm scale) of a-caspase-1 and NLRP3 expression in MDS (n=10), de novo AML (n=5), secondary AML (n=8), chronic lymphocytic leukemia (CLL, n=5), multiple myeloma (MM, n=5), chronic myeloid leukemia (CML, n=3), acute B lymphoblastic leukemia (B-ALL, n=3) and T cell lymphoma (TCL, n=3) BM-MNC. DAPI (blue), a-caspase-1 (green), NLRP3 (red); merged images show inflammasome formation. (B-C) Quantitative analysis of (B) a-Caspase-1 MFI and (C) NLRP3 MFI. Error bars: SE, * $p < 0.05$, ** $p < 0.01$ and *** $p < 0.001$.

progenitor cells (CD34⁺CD38⁺, $p=6.8 \times 10^{-3}$), 6.6-fold in immature myeloid cells (CD33⁺, $p=1.5 \times 10^{-3}$), and 7.3-fold in erythroid cells (CD71⁺, $p=2.8 \times 10^{-3}$) compared to normal controls (Figure 15H). Additionally, the percentage of a-caspase-1⁺ cells was increased 14.2-fold in the stem cell fraction ($p=8.0 \times 10^{-3}$), 13.2-fold in progenitors, 12.9-fold in immature myeloid cells ($p=1.3 \times 10^{-4}$), and 13.0-fold in CD71⁺ erythroid precursors ($p=7.7 \times 10^{-3}$) (Figure 15I). A-caspase-1 MFI directly correlated with NLRP3 MFI, inflammasome assembly and the percentage of pyroptotic stem cells. Notably, the latter was directly associated with the percentage of a-caspase-1⁺ CD33⁺ myeloid progenitors (Figure 17). In contrast, there were no significant differences in the apoptotic indices (i.e., a-caspase-3/7⁺/a-caspase-1⁻/annexin-V⁺) in lower-risk MDS specimens (n=8) versus normal progenitors in any of the four hematopoietic cell subsets investigated (Figure 15J). Indeed, the pyroptotic cell fraction was 14.4-fold ($p=9.7 \times 10^{-3}$), 9.7-fold ($p=2.3 \times 10^{-3}$), 21.9-fold ($p=9.5 \times 10^{-4}$), and 12.1-fold ($p=1.6 \times 10^{-3}$) increased in stem cells, progenitor cells, immature myeloid and erythroid cells when compared to the apoptotic cell fraction (Figure 15K). Finally, the fraction of a-caspase-1⁺ cells was significantly greater than the corresponding a-caspase-3/7⁺ cell fraction, confirming that caspase-1 activation (pyroptosis) exceeds caspase-3 activation (apoptosis) in MDS (Figure 15L).

To confirm that NLRP3 inflammasome activation and caspase-1 are essential for hematopoietic cell death in MDS, shRNA-directed knockdown of *NLRP3*, *CASP1* and *CASP3* was performed by lentivirus transfection of lower-risk BM-MNC (*NLRP3*, n=4; *CASP1* and *CASP3*, n=3) (Figure 15M). Protein levels of NLRP3 were reduced 54%, whereas expression of *CASP1* and *CASP3* were reduced 34% and 40%, respectively. Knockdown of NLRP3 and caspase-1 significantly decreased the fraction of pyroptotic

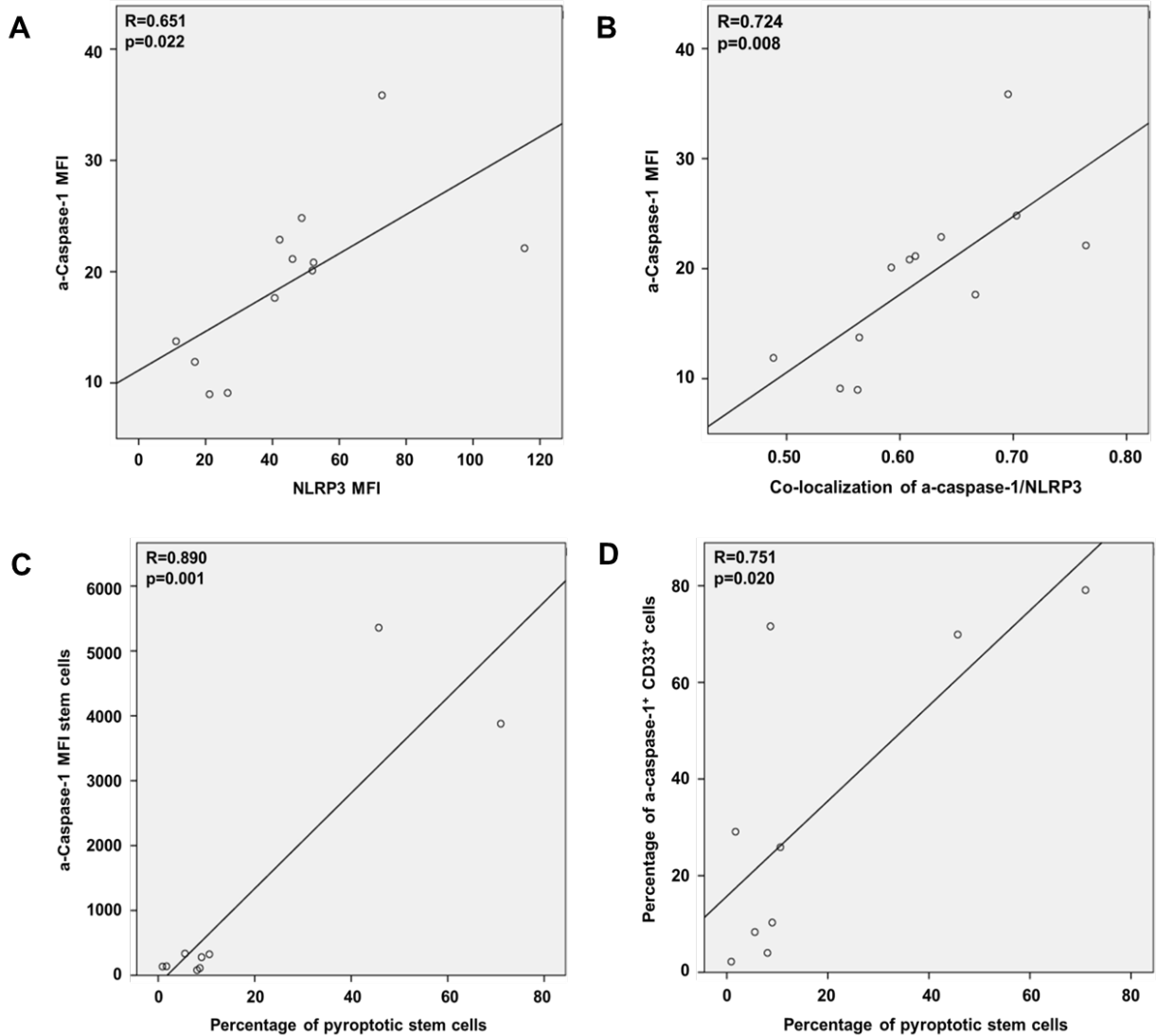


Figure 17. Caspase-1 activation significantly correlates with the extent of pyroptosis detected in MDS BM-MNC. (A-B) A-caspase-1 MFI, NLRP3 MFI and NLRP3 inflammasome formation measured by co-localization of a-caspase-1/NLRP3, were determined by analysis of confocal immunofluorescence images. **(C-D)** The percentage of pyroptotic stem cells and MFI of a-caspase-1 in the stem cell and CD33⁺ population were determined by flow cytometry.

cells versus scrambled transfected controls ($p=5.7 \times 10^{-3}$ and 0.038, respectively) (Figure 15M). In contrast, knockdown of caspase-3 had no discernible effect (Figure 15M), confirming selective NLRP3- and caspase-1-dependence.

The alarmin S100A9 initiates pyroptosis. As we previously reported,¹⁴⁰ BM plasma concentration of S100A9 was significantly higher in lower-risk MDS patient specimens (n=33) compared to normal controls (n=12; $p=1.5 \times 10^{-4}$) (Figure 18A). Analysis of S100A9 BM plasma concentration by International Prognostic Scoring System (IPSS) risk category showed a 2.3- and 2.2-fold increase in low risk (n=10, $p=2.3 \times 10^{-5}$) and intermediate-I risk MDS (n=23, $p=1.0 \times 10^{-3}$), compared to normal controls (n=12), whereas there were no significant differences among controls and intermediate-II (n=17) or high risk (n=10) disease (Figure 18B). Notably, BM S100A9 concentrations were significantly higher in lower-risk versus higher-risk MDS ($p=0.013$) (Figure 18A), consistent with the reduced fraction of MDSC and acquisition of survival signals in higher-risk MDS that mitigates cell death and DAMP elaboration.^{84,197}

In addition, the BM plasma concentration of HMGB1, a nuclear DAMP and TLR4 ligand, was significantly increased in MDS (n=55) versus normal controls (n=11) ($p=2.6 \times 10^{-3}$) (Figure 18C), consistent with intracellular DAMP release upon cytolysis.^{113,299} Moreover, *S100A9* and *HMGB1* transcripts were up-regulated 104.5-fold and 1.5-fold in MDS, respectively, compared to normal controls (Figure 18D and 18E). Further, flow cytometry analyses of phenotypically distinct hematopoietic lineages confirmed a corresponding increase in the intracellular levels of S100A9 protein in MDS stem cells and progeny (Figure 18F and 18G).

As TLRs and NLRs are sensors of DAMP signals, we tested if S100A9 would directly trigger pyroptosis in HSPC. Normal BM-MNCs were treated with 1 $\mu\text{g/mL}$ rhS100A9 and changes in gene expression were assessed by qPCR. The expression of pyroptosis-associated genes was significantly induced by rhS100A9, and indeed

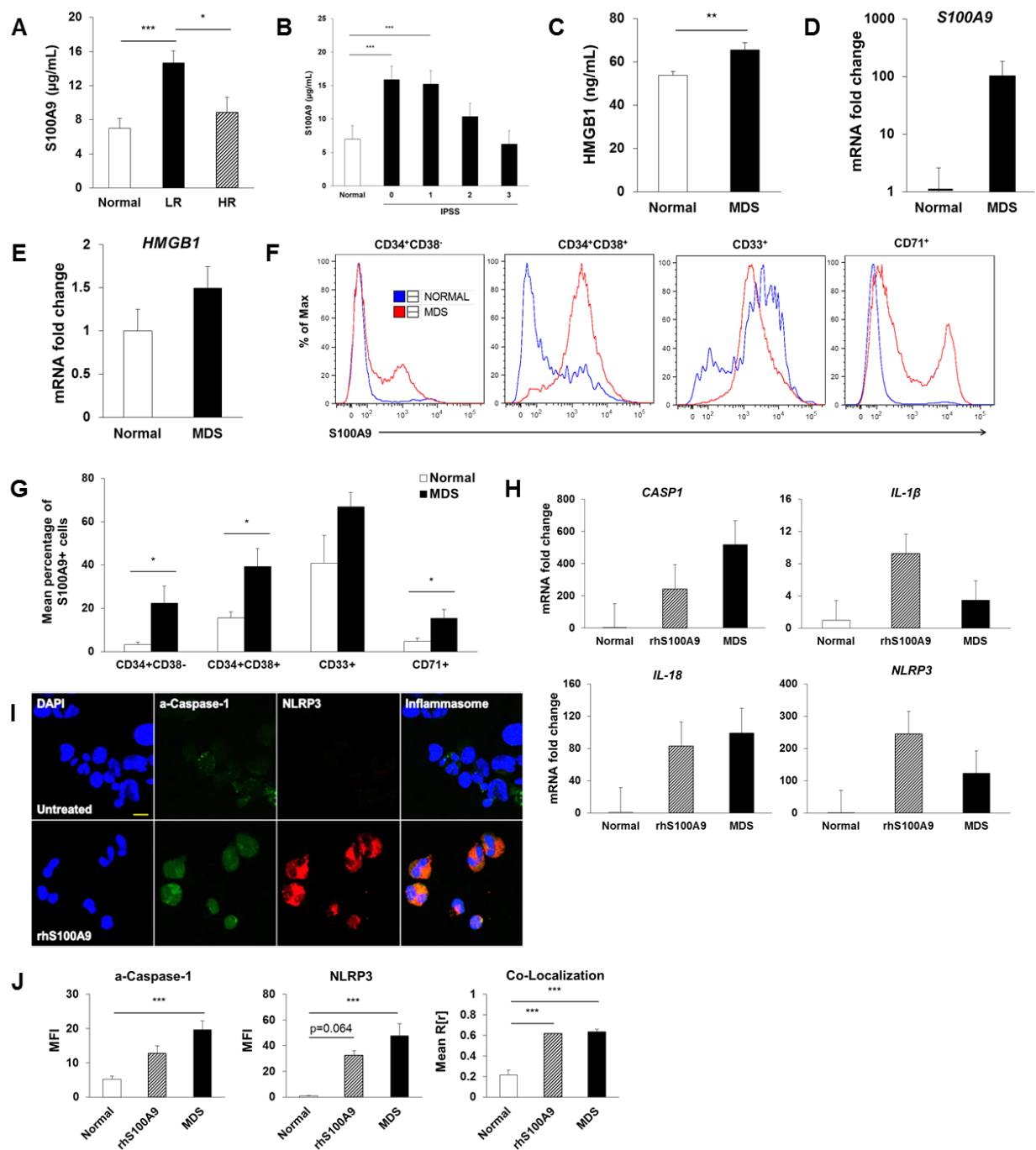


Figure 18. S100A9 initiates pyroptosis in MDS. (A) ELISA assessment of BM plasma concentration of S100A9 in normal donors (n=12) versus MDS [lower-risk (n=33), higher-risk (n=27)]. **(B)** S100A9 BM plasma concentration analyzed according to IPSS risk score. **(C)** HMGB1 BM plasma concentration assessed by ELISA in normal donors (n=11) and MDS (n=55). **(D)** qPCR analysis of *S100A9* mRNA levels in normal (n=2) versus lower-risk MDS BM-MNC (n=8). **(E)** *HMGB1* mRNA levels in normal (n=6) versus MDS BM-MNC (n=10). **(F)** Representative histograms of intracellular levels of S100A9 by hematopoietic lineage in BM-MNC isolated from MDS patients (n=6) and

from normal donors (n=5). **(G)** Mean percentage of S100A9⁺ cells by hematopoietic lineage. **(H)** qPCR analysis of untreated normal BM-MNC (n=3), normal BM-MNC treated with 1 µg/mL rhS100A9 for 24 hours (n=2) and MDS patient specimens (n=5). **(I)** Representative micrograph (2520x magnification, 7.5 µm scale) depicting inflammasome formation in normal, untreated BM-MNC or normal BM-MNC treated with 5 µg/mL rhS100A9 for 24 hours. DAPI (blue) a-caspase-1 (green), and NLRP3 (red); merged images show inflammasome formation. **(J)** Quantitative analysis of confocal images of BM-MNC from normal donors (n=6), normal BM-MNC treated with 5 µg/mL rhS100A9 (n=2), and MDS patients (n=10). Error bars: SE, *p<0.05, **p<0.01 and ***p<0.001.

exceeded those found in MDS (Figure 18H). Accordingly, treatment of normal BM-MNC with 5 µg/mL rhS100A9 was sufficient to induce a-caspase-1 and NLRP3 (Figure 18I) by 2.5-fold and 47.1-fold (p=0.064), respectively, as well as NLRP3 inflammasome assembly (2.9-fold, p=3.1x10⁻⁴) (Figure 18J). Although rhS100A9 induced inflammasome assembly and caspase-1 activation in normal BM-MNC, MDS patient BM-MNC displayed greater activation of these effectors. Notably, treatment of normal BM-MNC with MDS-derived bone marrow plasma did not induce pyroptosis, as measured by the mean percentage of pyroptotic cells, a-caspase-1⁺ cells or a-caspase-1 MFI (data not shown), indicating that MDS HSPCs are selectively primed for the pyroptotic response.

Inflammasome-activated cation channels increase the size of MDS progenitors. Cell swelling is a hallmark of pyroptosis following activation of plasma membrane cation channels, which compromise membrane integrity and trigger mitochondrial membrane depolarization.²¹⁴ Confocal image analyses of MDS BM-MNC cells revealed a significantly larger mean cell area compared to normal BM-MNC (Figure 19A). Further, this phenotype was accentuated in lower-risk MDS patients

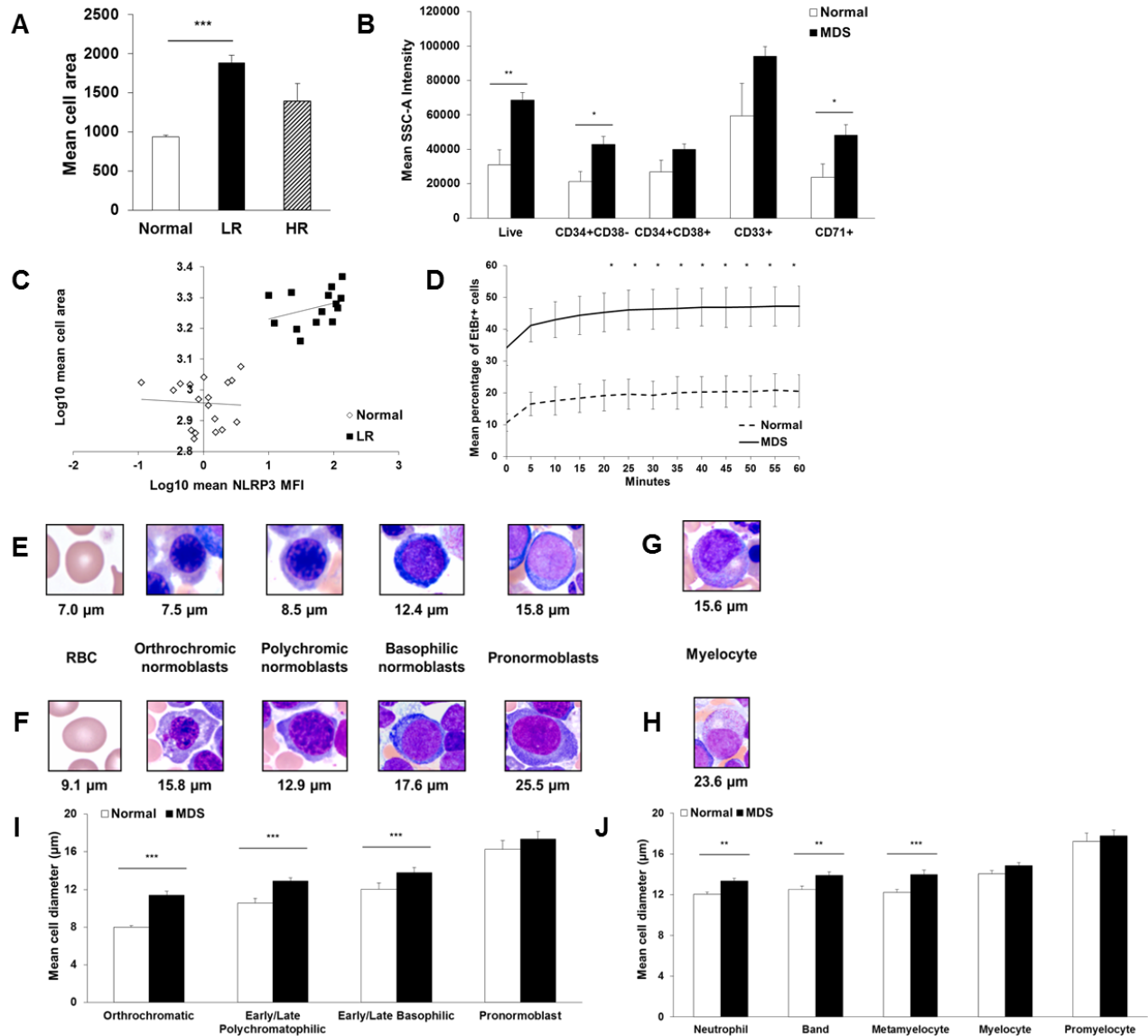


Figure 19. MDS precursors evidence cell swelling, a pyroptotic hallmark. (A) Mean cell area was quantified from confocal images of BM-MNC from normal donors (n=6) versus MDS patient specimens [lower-risk (n=7), higher-risk (n=3)]. **(B)** Flow cytometric analysis of mean SSC-A intensity of BM-MNC isolated from normal donors (n=6) or lower-risk MDS patients (n=7). MDS BM-MNC have 2.0-fold greater mean cell area of live, ungated BM-MNC (p=0.017), 2.2-fold of stem cells (CD34⁺CD38⁻, p=0.019), 1.5-fold of progenitor cells (CD34⁺CD38⁺), 1.6-fold of immature myeloid progenitors (CD33⁺) and 2.0-fold of erythroid progenitors (CD71⁺, p=0.038). **(C)** NLRP3 MFI correlates with BM-MNC area in lower-risk MDS patients (r=0.49, n=7). **(D)** Ethidium bromide dye incorporation in BM-MNC from normal donors (n=3) and MDS patients (n=3) was measured at 5 minute intervals by flow cytometry. **(E)** *Left to right*, photomicrograph images from normal donors illustrating normal red blood cell (RBC, 7.0 μm) followed by normal erythroid lineage maturation of nucleated BM precursors with corresponding cell diameter. **(F)** Corresponding images from MDS BM aspirates, demonstrating an oval

macrocyte (RBC, 9.1 μm) followed by dysplastic and megaloblastic erythroid lineage maturation. **(G)** Normal myelocyte. **(H)** Enlarged dysplastic myelocyte with mild hypogranulation in MDS. **(I-J)** **(I)** Erythroid and **(J)** myeloid lineage maturation comparison of mean cell diameter in normal donor (n=4) versus MDS patient (n=4) BM. Maturation is depicted as most to least mature cell populations from left to right. Error bars: SE, *p<0.05, **p<0.01 and ***p<0.001.

versus normal controls ($p=6.0 \times 10^{-5}$), whereas there were no significant differences in higher-risk patients. These findings were corroborated using SSC-A flow cytometric measurements, a validated reference for cell size,³⁰⁰ in ungated BM-MNC derived from lower-risk MDS patients (n=7) and normal donors (n=6), as well as in antigenically distinct hematopoietic cell subsets (Figure 19B). Finally, mean NLRP3 MFI correlated with mean cell area in lower-risk but not higher-risk MDS patients ($r=0.49$) ($p=7.8 \times 10^{-3}$) (Figure 19C).

To assess ion channel activation, influx of the membrane-impermeable, cationic dye ethidium bromide (EtBr) was assessed by flow cytometry. MDS specimens incubated with autologous bone marrow plasma displayed rapid and sustained EtBr influx compared to that of normal BM-MNC (Figure 19D). This was detected as early as 20 minutes in MDS specimens ($p=0.041$), and was sustained through 1 hour of dye exposure ($p=0.014$). Finally, analysis of normal and MDS BM morphology confirmed the larger cell size by maturation stage and lineage in MDS (Figure 19E-J).

Inhibition of pyroptosis promotes effective hematopoiesis in MDS. To assess the role of S100A9 in pyroptosis in MDS, we tested if S100A9 neutralization in autologous BM plasma using a high-affinity chimeric (CD33-IgG₁) decoy receptor could ameliorate the phenotypes manifest in MDS BM-MNC. Notably, treatment with the CD33-IgG₁ chimera markedly reduced the fraction of pyroptotic cells without altering the

fraction of apoptotic cells (Figure 20A and 20B). Overall, short-term incubation with the chimera was sufficient to reduce the fraction of pyroptotic cells across lineages, with an 81% reduction in stem cells, 57% in progenitor cells, 90% in CD33⁺ and 42% in CD71⁺ erythroid progenitors. Short-term treatment with CD33-IgG₁ also significantly reduced the MDSC fraction, confirming that blocking S100A9 function impairs survival of MDSC (data not shown). Consistent with this, the CD33-IgG₁ chimera reduced S100A9 transcriptional priming, evidenced by a concentration-dependent reduction in the expression of *CASP1*, *IL-1β*, *IL-18*, and *NLRP3* transcripts in MDS BM-MNC versus treatment with autologous BM plasma alone (n=5) (Figure 20C). *CASP3* expression was also markedly reduced, consistent with late, secondary caspase-3 activation.²⁷⁸ Note that as a result of the IgG₁-Fc conjugation, high concentrations of the chimera led to cross-linking of the Fc domains and aggregation that masked dose-dependent transcriptional effects of S100A9 neutralization.

To test if S100A9 neutralization could improve hematopoiesis in MDS, colony forming capacity was assessed after plating MDS BM-MNC in autologous BM plasma and increasing concentrations of CD33-IgG₁ (Figure 20D) or of MCC950 (Figure 20E), a small molecule inhibitor of the NLRP3 inflammasome.³⁰¹ Notably, neutralization of S100A9 or inhibition of the NLRP3 inflammasome markedly improved colony forming capacity of MDS progenitors (up to 6.6-fold greater than controls). Thus, pyroptotic pathway inhibition abrogates MDS hematopoietic cell death and promotes effective hematopoiesis.

S100A9 is sufficient to provoke HSPC pyroptosis *in vivo*. To test if forced expression of S100A9 is sufficient to induce pyroptosis *in vivo*, we assessed

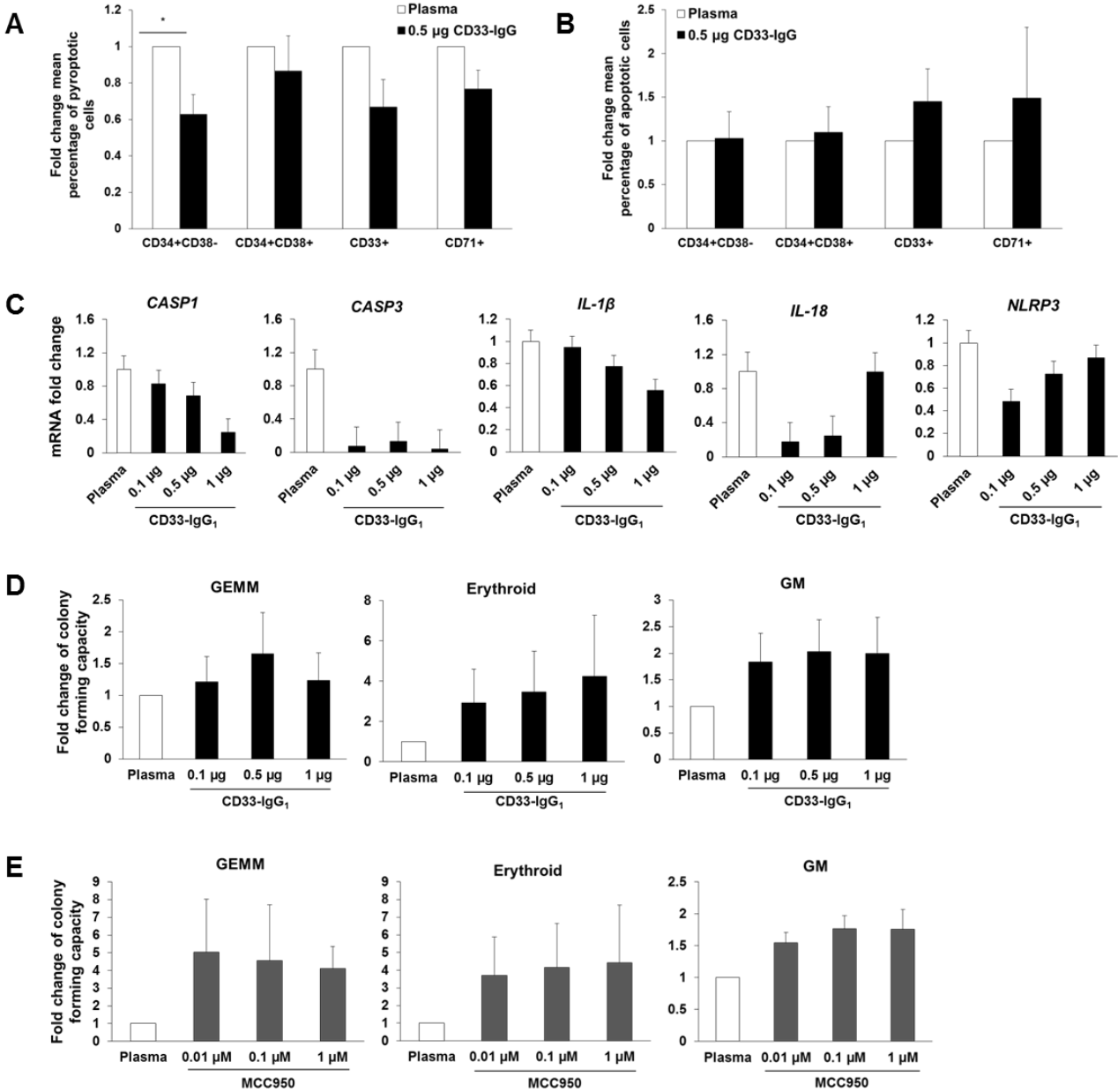


Figure 20. Inhibition of pyroptosis abrogates MDS HSPC death and augments colony forming capacity. (A-B) Fold change in the mean percentage of **(A)** pyroptotic or **(B)** apoptotic cells in each respective lineage in lower-risk MDS BM-MNC (n=6) incubated with autologous BM plasma and 0.5 µg CD33-IgG₁ chimera for 24 hours. Values are normalized to autologous BM plasma-incubated MDS BM-MNC. **(C)** qPCR analysis of BM-MNC isolated from lower-risk MDS patients (n=5) treated for 24 hours with CD33-IgG₁. **(D)** Colony forming capacity was assessed in BM-MNC from lower-risk MDS patient specimens (n=3) treated with increasing concentrations of CD33-IgG₁ or **(E)** the inflammasome inhibitor MCC950. Error bars: SE, *p<0.05.

phenotypes manifest in an S100A9 transgenic (S100A9Tg) mouse model that phenocopies human MDS.¹⁴⁰ Confocal fluorescence microscopy analyses of BM cells from the tibia and femurs of S100A9Tg versus wild type (WT) mice at 2 (n=4), 6 (n=4), and 11 (n=5) months of age showed that caspase-1 activation increased with age in the BM cells of S100A9 transgenics, with a 2.1-fold up-regulation at 2 months, 2.4-fold at 6 months ($p=3.3 \times 10^{-3}$), and 2.5-fold at 11 months ($p=0.010$). Similarly, NLRP3 levels were increased in S100A9Tg mice, with a 21.1-fold up-regulation at 2 months ($p=0.059$), 25.6-fold at 6 months ($p=2.2 \times 10^{-4}$), and 12.1-fold at 11 months ($p=0.018$) (Figure 21A). Accordingly, formation of NLRP3 inflammasome complexes also significantly increased with age, with 2.6-fold greater co-localization in the 2-month-old S100A9Tg transgenic mice ($p=0.017$), 3.3-fold in 6 month ($p=1.0 \times 10^{-6}$), and 3.2-fold in 11-month-old mice ($p=1.2 \times 10^{-3}$) (Figure 21A).

To determine if S100A9 was sufficient to trigger pyroptosis in mouse hematopoietic cells, BM cells isolated from WT mice were treated with 5 $\mu\text{g/mL}$ recombinant murine S100A9 and inflammasome formation was assessed by confocal microscopy (Figure 21B and 21C). As predicted, MFI of α -caspase-1 and NLRP3 significantly increased after rmS100A9 treatment (n=2) versus controls (n=2) ($p=7.5 \times 10^{-3}$ and 0.017, respectively). Notably, MFI values from rmS100A9-treated WT BM cells were comparable to those manifest in the BM cells of S100A9 transgenic mice (n=13), and rmS100A9 treatment of WT BM cells markedly induced assembly of inflammasome complexes ($p=0.023$) (Figure 21C).

To assess the extent of pyroptosis versus apoptosis *in vivo*, BM cells were isolated from 7-month-old WT (n=6) and 9-month-old S100A9Tg (n=6) mice and active

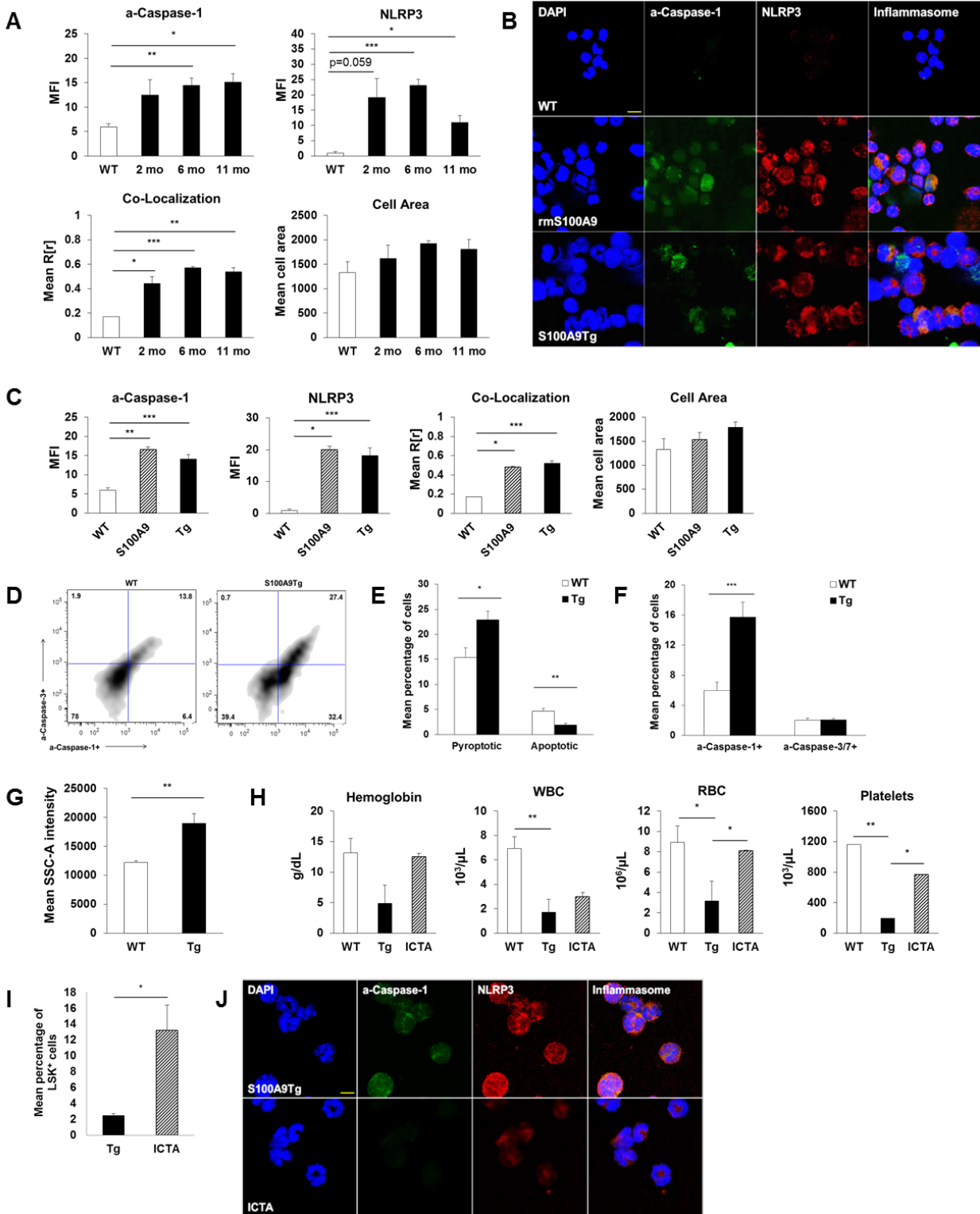


Figure 21. Pyroptosis is the principal mechanism of HSPC death in S100A9 transgenic mice. (A) Confocal image analysis of BM cells isolated from WT (n=2), 2 month (n=4), 6 month (n=5) and 11 month (n=4) old S100A9Tg mice. **(B)** Representative micrograph (2520x magnification, 7.5 μm scale) depicting

inflammasome formation in BM cells from WT, WT cells treated for 24 hours with 5 $\mu\text{g}/\text{mL}$ S100A9 and BM cells from S100A9Tg mice. DAPI (blue), a-caspase-1 (green) and NLRP3 (red); merged images show inflammasome formation. **(C)** Quantitative analysis of confocal images of BM cells isolated from WT (n=2) mice, from WT BM cells treated for 24 hours with 5 $\mu\text{g}/\text{mL}$ rmS100A9 (n=2) or BM cells from S100A9Tg mice (n=13). **(D)** Representative scatter plots of pyroptotic and apoptotic LSK (Lin⁻Sca-1⁺c-Kit⁺) cells isolated from WT and transgenic mice. **(E)** Mean percentage of pyroptotic versus apoptotic LSK cells in WT (n=6) and S100A9Tg mice (n=6). **(F)** Mean percentage of total a-caspase-1⁺ and a-caspase-3/7⁺ LSK cells isolated from WT (n=6) and S100A9Tg mice (n=6). **(G)** Flow cytometric analysis of mean SSC-A intensity of BM cells isolated from WT (n=6) and S100A9Tg mice (n=6) ($p=1.0 \times 10^{-2}$). **(H)** At six months of age, S100A9Tg mice were treated with 50 mg/kg of ICTA. Shown are changes in hemoglobin, white blood cell (WBC), RBC and platelet counts in WT (n=4), S100A9Tg (n=5) and ICTA-treated S100A9Tg mice (n=5). **(I)** Mean percentage of LSK⁺ HSPC in untreated versus ICTA-treated S100A9Tg mice. **(J)** Representative micrograph (2520x magnification, 7.5 μm scale) depicting inflammasome formation in BM cells harvested from untreated S100A9Tg mice or mice treated with ICTA by oral gavage for a total of eight weeks. DAPI (blue), a-caspase-1 (green), and NLRP3 (red); merged images show inflammasome formation. Error bars: SE, * $p < 0.05$, ** $p < 0.01$ and *** $p < 0.001$.

caspase-1 and a-caspases-3/7 were assessed by flow cytometry in the LSK (Lin⁻Sca-1⁺c-Kit⁺) HSPC population. The mean percentage of pyroptotic LSK cells was significantly increased in the S100A9Tg versus WT mice ($p=0.052$), whereas WT BM cells had a higher apoptotic index ($p=7.1 \times 10^{-3}$) (Figure 21D and 21E). Additionally, the percentage of a-caspase-1⁺ LSK cells was increased 2.6-fold in the S100A9Tg mice compared to WT mice ($p=4.2 \times 10^{-3}$), while there was no significant difference in the a-caspase-3/7⁺ LSK cells in the two cohorts (Figure 21F). S100A9Tg BM cells also had a significant increase in mean cell area, as assessed by SSC-A intensity measurements (Figure 21G). Finally, to test if *in vivo* inflammasome inhibition also improves hematopoiesis in S100A9Tg mice, aged S100A9Tg mice (n=5) were treated with ICTA, an icariin derivative that inhibits NLRP3 inflammasome activation, every other day for eight weeks (Figure 22). ICTA treatment markedly improved peripheral blood counts, and increased

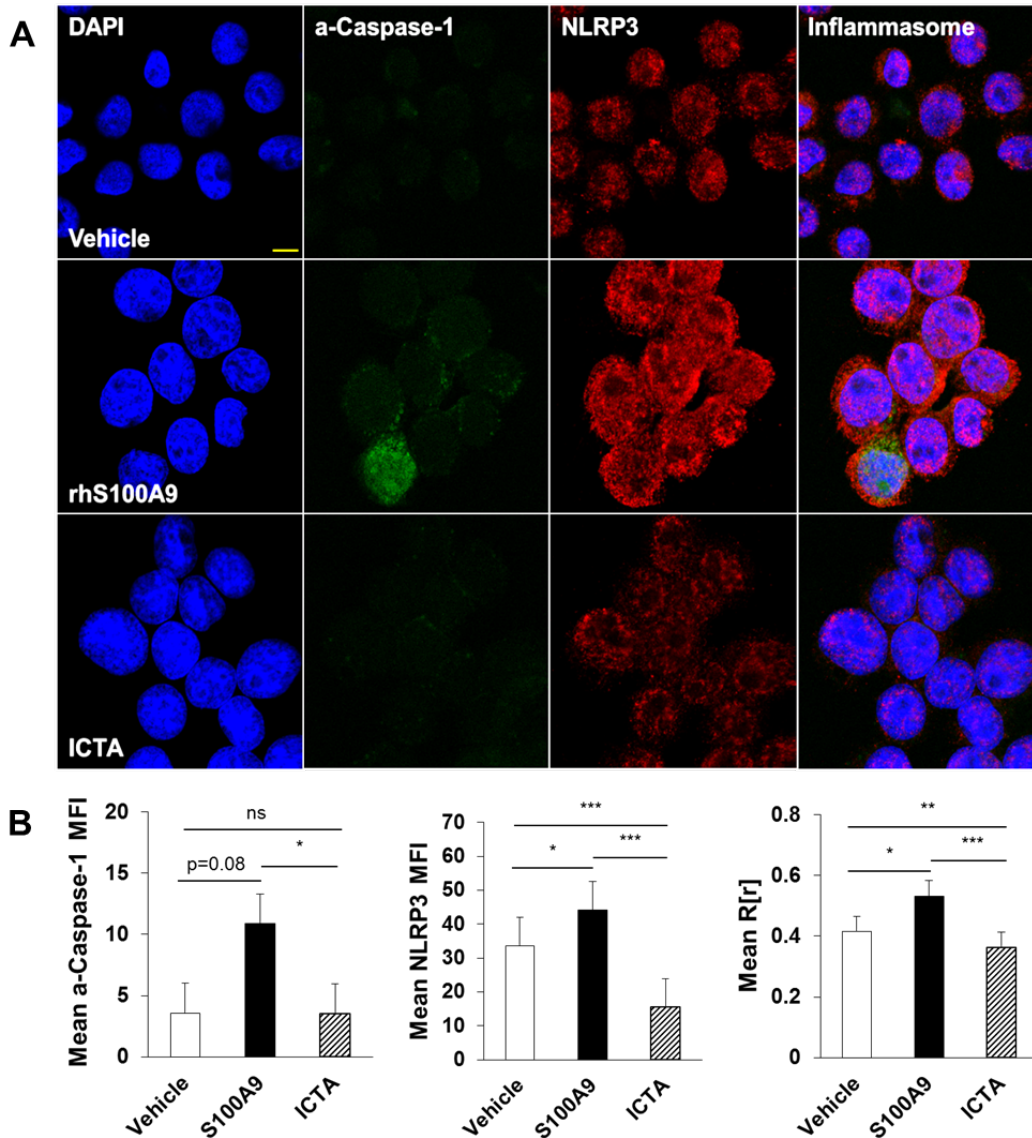


Figure 22. ICTA inhibits inflammasome activation. (A) Representative micrograph (1890x magnification, 10 μ m scale) depicting inflammasome formation in U937 cells following 24 hr treatment with vehicle or 5 μ g/mL rhS100A9 alone or with ICTA (20 μ g/mL). DAPI (blue), a-caspase-1 (green), NLRP3 (red); merged image shows formation of inflammasome complexes. (B) Quantitative analysis of confocal images. Error bars: SE, * $p < 0.05$, ** $p < 0.01$ and *** $p < 0.001$.

hemoglobin, leukocyte count, red blood cells and platelet counts in the transgenic mice (Figure 21H), accompanied by a significant increase in the percentage of LSK⁺ HSPC ($p = 0.047$) (Figure 21I), consistent with restored effective hematopoiesis. Finally, NLRP3

activation was dramatically reduced in BM cells from ICTA-treated S100A9Tg mice (Figure 21J). Thus, pyroptosis is the principal mechanism driving HSPC cell death in MDS and S100A9Tg mice.

S100A9 and MDS somatic gene mutations trigger pyroptosis and β -catenin activation via ROS. ROS act as DAMP intermediates that activate the Wnt/ β -catenin axis, which is known to be activated in MDS.³⁰²⁻³⁰⁶ Thus, we hypothesized that ROS generated by either S100A9 or somatic gene mutations would direct activation of β -catenin in MDS. In accord with this notion, the mean percentage of ROS positive cells was increased in MDS BM-MNC (n=5) 16.5-fold compared to normal BM-MNC (n=2) (p=0.011) (Figure 23A), with corresponding significant increases in ROS MFI (p=0.028) (Figure 23B). Further, MDS BM-MNC displayed increased nuclear β -catenin (n=6) compared to normal donors (n=3), as well as in normal BM-MNC treated with 5 μ g/mL rhS100A9 versus untreated BM-MNC (p=0.043 and p=6.38x10⁻⁷, respectively) (Figure 23C and 23D). Finally, β -catenin mRNA levels were increased 9.5-fold in the BM cells of S100A9Tg mice versus WT BM cells, with corresponding up-regulation of Wnt/ β -catenin target genes (Figure 23E). As expected, this phenotype was associated with significant increases in nuclear β -catenin in S100A9Tg-derived BM cells versus WT BM cells, and levels of nuclear β -catenin were reduced following *in vivo* treatment with ICTA (Figure 23F), which led to corresponding reductions in the expression of Wnt/ β -catenin target genes (Figure 23E). Similarly, treatment of MDS BM-MNC with ICTA suppressed nuclear β -catenin as well as Wnt/ β -catenin target gene expression (Figure 23G). Thus, the S100A9-to-NLRP3 inflammasome circuit is necessary and sufficient to drive activation of β -catenin in MDS.

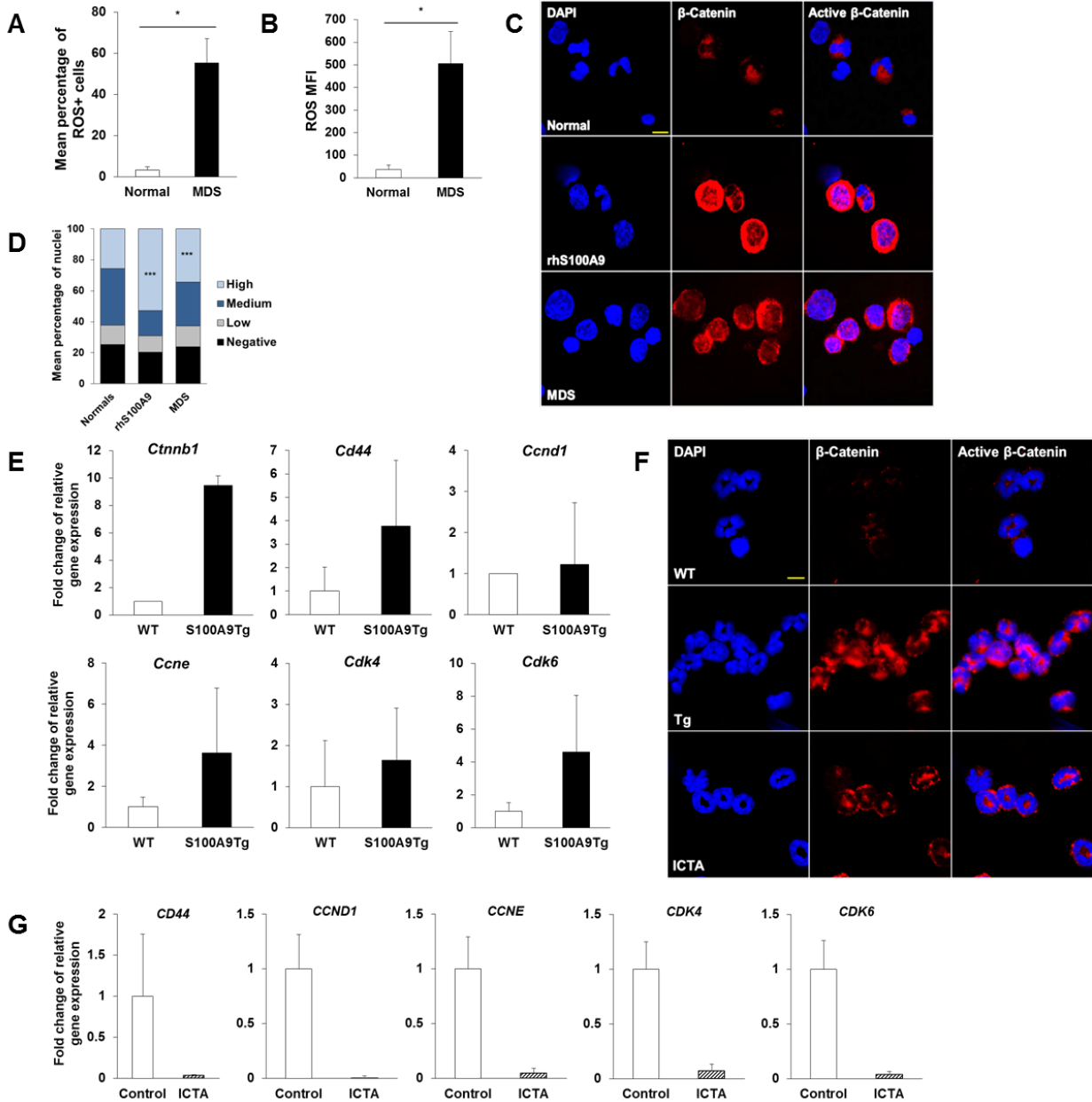


Figure 23. S100A9 induces ROS through NADPH oxidase to activate β -catenin. (A-B) The percentage of (A) ROS positive cells and (B) ROS MFI assessed by flow cytometry in BM-MNC isolated from MDS patients (n=5) and normal donors (n=2). (C) Representative micrograph (2520x magnification, 7.5 μ m scale) of β -catenin expression in normal BM-MNC (n=3), normal BM-MNC treated with 5 μ g/mL rhS100A9 (n=3) and MDS BM-MNC (n=6). DAPI (blue), β -catenin (red); merged images show nuclear β -catenin localization. (D) Quantitation and scoring of confocal images based on the presence of no, low, medium or high nuclear β -catenin. (E) Wnt/ β -catenin target gene expression in WT and S100A9Tg BM cells. (F) Representative micrograph (2520x magnification, 7.5 μ m scale) of β -catenin expression in WT (n=5), S100A9Tg (n=5) and S100A9Tg that were treated with ICTA (n=5) by oral gavage for a total of eight weeks.

DAPI (blue), β -catenin (red); merged images show nuclear β -catenin localization. **(G)** Wnt/ β -catenin target gene expression in MDS BM-MNC (n=4) treated for 48 hours with ICTA. Error bars: SE, * p <0.05 and *** p <0.001.

To determine if somatic gene mutations in MDS also trigger activation of the NLRP3 inflammasome, increased ROS, pyroptosis and β -catenin activation, we first investigated these phenotypes in TF-1 myeloid leukemia cells engineered to express GFP-labeled wild type or mutants of the *U2AF1* splicing factor gene.²⁹⁰ The percentage of pyroptotic cells was increased 4.6-fold in *U2AF1-S34F* mutant versus *U2AF1-WT*-expressing cells, which was associated with increased levels of a-caspase-1 ($p=0.044$) and annexin-V ($p=0.021$) (Figure 24A-24H). Further, there was increased ASC oligomerization and NLRP3 inflammasome activation in the *S34F*-expressing cells, as evidenced by increased binding of NLRP3:ASC (Figure 24I), maturation of caspase-1 and IL-1 β (Figure 24J) and the generation of ASC monomers and higher-order ASC complexes (Figure 24K).

ROS generation by NADPH oxidase-1 (NOX1) has been linked to Wnt/ β -catenin activation.^{302,303} Treatment of the *S34F*-expressing cells with the NOX1/4-specific inhibitor GKT137831 or with the pan-NOX inhibitor DPI profoundly reduced ASC oligomerization and thereby NLRP3 inflammasome assembly; thus, NLRP3 activation in response to somatic gene mutation is NOX1/4-dependent (Figure 24B). Moreover, elevated levels of ROS in *U2AF1-S34F*-expressing cells were abrogated by GKT137831 or DPI treatment (Figure 24N and 24O). *U2AF1-S34F*-expressing cells also displayed significant increases in mean cell area ($p=0.035$), ethidium bromide influx (Figure 24L and 24M), mean percentage of ROS⁺ cells ($p=1.5 \times 10^{-3}$) and ROS MFI ($p=0.032$) (Figure 24N and 24O), accompanied by nuclear localization of β -catenin

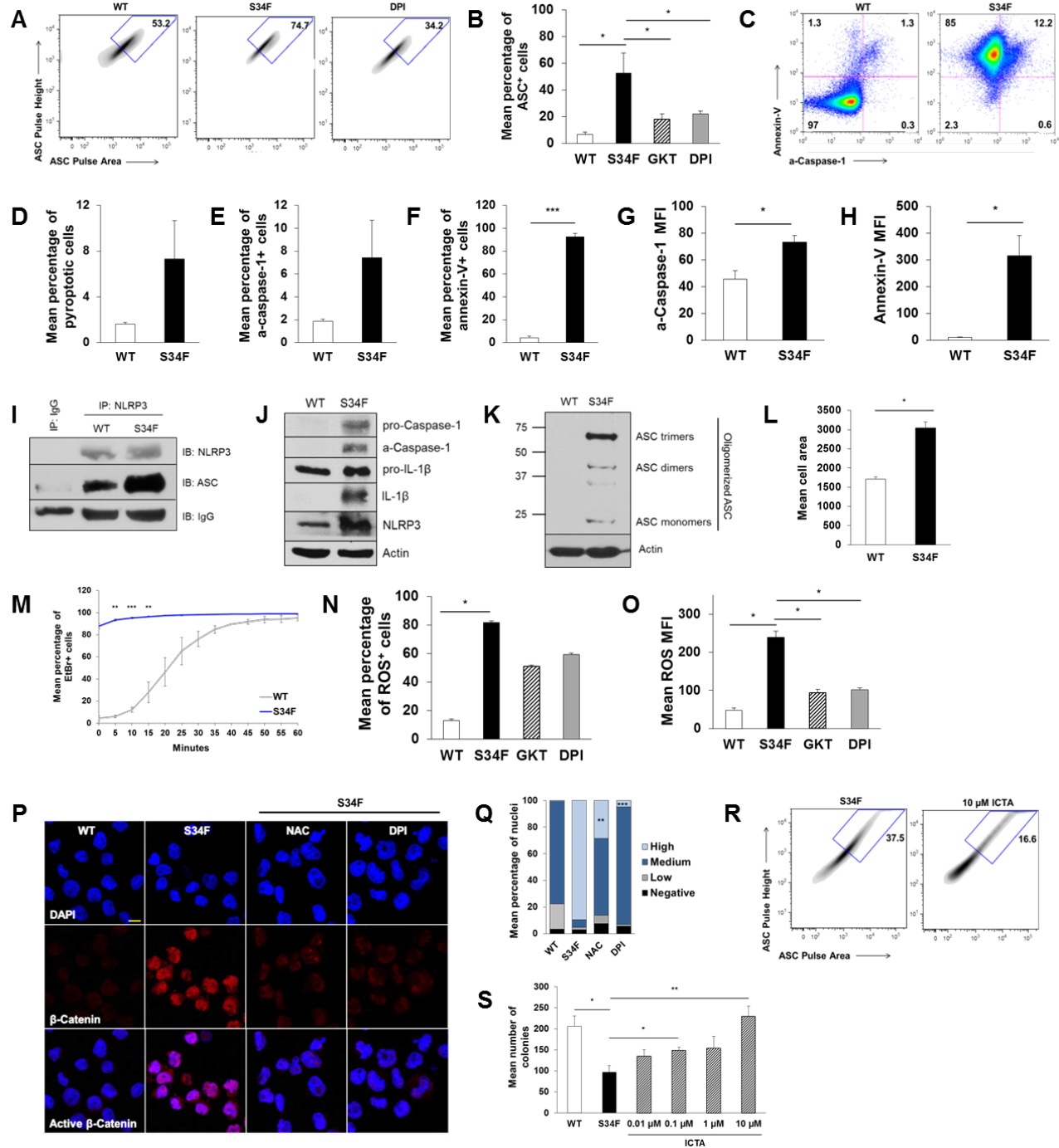


Figure 24. *U2AF1* mutations manifest in MDS provoke pyroptosis and induce NOX-dependent activation of β -catenin. (A) Representative density plot of inflammasome formation based on ASC oligomerization. **(B)** Quantitation of ASC in WT, S34F and S34F cells treated with DPI for 24 hours. **(C)** Representative scatter plots of pyroptotic cells by flow cytometry. **(D)** Mean percentage of pyroptotic cells in mutant and WT cells. **(E-H)** Mean percentage of total **(E)** a-caspase-1⁺ and **(F)** annexin-V⁺ cells, as well as the MFI of **(G)** a-caspase-1 and **(H)** annexin-V assessed by flow cytometry. **(I)**

Binding of ASC to NLRP3 (IP: NLRP3, IB: NLRP3, ASC). **(J)** Western blot of cleaved caspase-1 and IL-1 β maturation. **(K)** Immunoblot of ASC monomers and higher-order ASC complexes following chemical crosslinking of cell lysates. **(L)** Mean cell area quantitated from confocal images. **(M)** Incorporation of ethidium bromide measured by flow cytometry at 5 minute intervals. **(N-O)** Mean percentage of **(N)** ROS positive cells and **(O)** ROS MFI assessed by flow cytometry. **(P)** Representative micrograph (1890x magnification, 10 μ m scale) of β -catenin expression in *U2AF1* WT cells, *S34F* or *S34F*-expressing cells treated with NAC or DPI for 24 hours prior to staining. DAPI (blue), β -catenin (red); merged images show nuclear β -catenin localization. **(Q)** Quantitation and scoring of confocal images based on the presence of no, low, medium or high nuclear β -catenin. **(R)** Representative density plot of inflammasome formation based on ASC oligomerization in *S34F* cells treated with 10 μ M ICTA. **(S)** Colony forming capacity assessed in WT, *S34F* and *S34F* cells treated with increasing concentrations of ICTA (0.01-10 μ M). The mean number of colonies is representative of four replicates per condition. Error bars: SE, * p <0.05, ** p <0.01, and *** p <0.001. Data are representative of three independent experiments.

(Figure 24P and 24Q). Notably, treatment of *U2AF1-S34F* mutant cells with the anti-oxidant N-acetylcysteine (NAC) or the NOX inhibitor DPI effectively reduced β -catenin activation in *U2AF1-S34F*-expressing cells ($p=3.8 \times 10^{-3}$ and $p=2.5 \times 10^{-6}$, respectively) (Figure 24P and 24Q); thus, β -catenin activation is initiated by NOX-derived ROS generation. Finally, treatment of the *U2AF1-S34F*-expressing mutant cells with the NLRP3 inflammasome inhibitor ICTA suppressed inflammasome activation, as evidenced by a reduction in ASC polymerization, and restoration of colony forming capacity to levels commensurate with that of WT BM cells (Figure 24R and 24S). Thus, the reduced survival of cells harboring this MDS splicing mutation is driven by NLRP3 inflammasome-directed pyroptosis, while β -catenin activation may support propagation of the clone.

This circuitry was also evaluated in BM cells from the conditional knock-in *Sf3b1-K700E* mouse model, which expresses an RNA splicing subunit gene mutation found in MDS and displays an MDS phenotype.³⁰⁷ *Sf3b1-K700E* BM cells ($n=6$) displayed similar

increases in the percentage of pyroptotic versus apoptotic cells, with a significant increase in total a-caspase-1⁺ cells ($p=0.014$) versus WT BM ($n=6$) (Figure 25A and 25B). Further, a-caspase-1 and a-caspase-3/7 MFI were both significantly increased in the *Sf3b1-K700E* mutant BM cells ($p=0.030$ and $p=6.92 \times 10^{-3}$, respectively) (Figure 25C) accompanied by increased inflammasome assembly (Figure 25D). Accordingly, NLRP3 protein expression was increased 1.9-fold in the *Sf3b1-K700E* cells ($p=0.063$) in accordance with NLRP3 inflammasome formation (Figure 25E).

Inflammasome activation in *Sf3b1-K700E* mutant BM cells was confirmed by assessment of ASC oligomerization, demonstrating marked ASC polymerization associated with inflammasome assembly versus WT BM ($p=8.4 \times 10^{-3}$). Further, this was dependent upon NOX-generated ROS, as (i) ASC oligomerization was significantly reduced in *Sf3b1-K700E* mutant-expressing BM cells following treatment with NAC ($p=2.68 \times 10^{-3}$) or DPI (Figure 25F-G); and (ii) the mean percentage of ROS⁺ cells and ROS MFI were markedly increased in *Sf3b1-K700E*-expressing mutant BM cells, which was extinguished by treatment with NAC or DPI (Figure 25H-I). Finally, nuclear localization of β -catenin was also significantly increased in *Sf3b1-K700E* mutant BM compared to WT BM ($p=0.04$), which was also reduced by treatment with NAC ($p=2.0 \times 10^{-3}$) or DPI ($p=1.8 \times 10^{-2}$) (Figure 25J-K).

Notably, pharmacologic inhibition of the NLRP3 inflammasome in *Sf3b1-K700E* mutant BM cells restored colony forming capacity, illustrating the importance of inflammasome activation in the attrition of mutant cells (Figure 25L). Similar findings were also manifest in mutant versus WT *SRSF2*-expressing HEK293T cells (Figure 26), as well as in BM cells obtained from MDS murine models driven by epigenetic

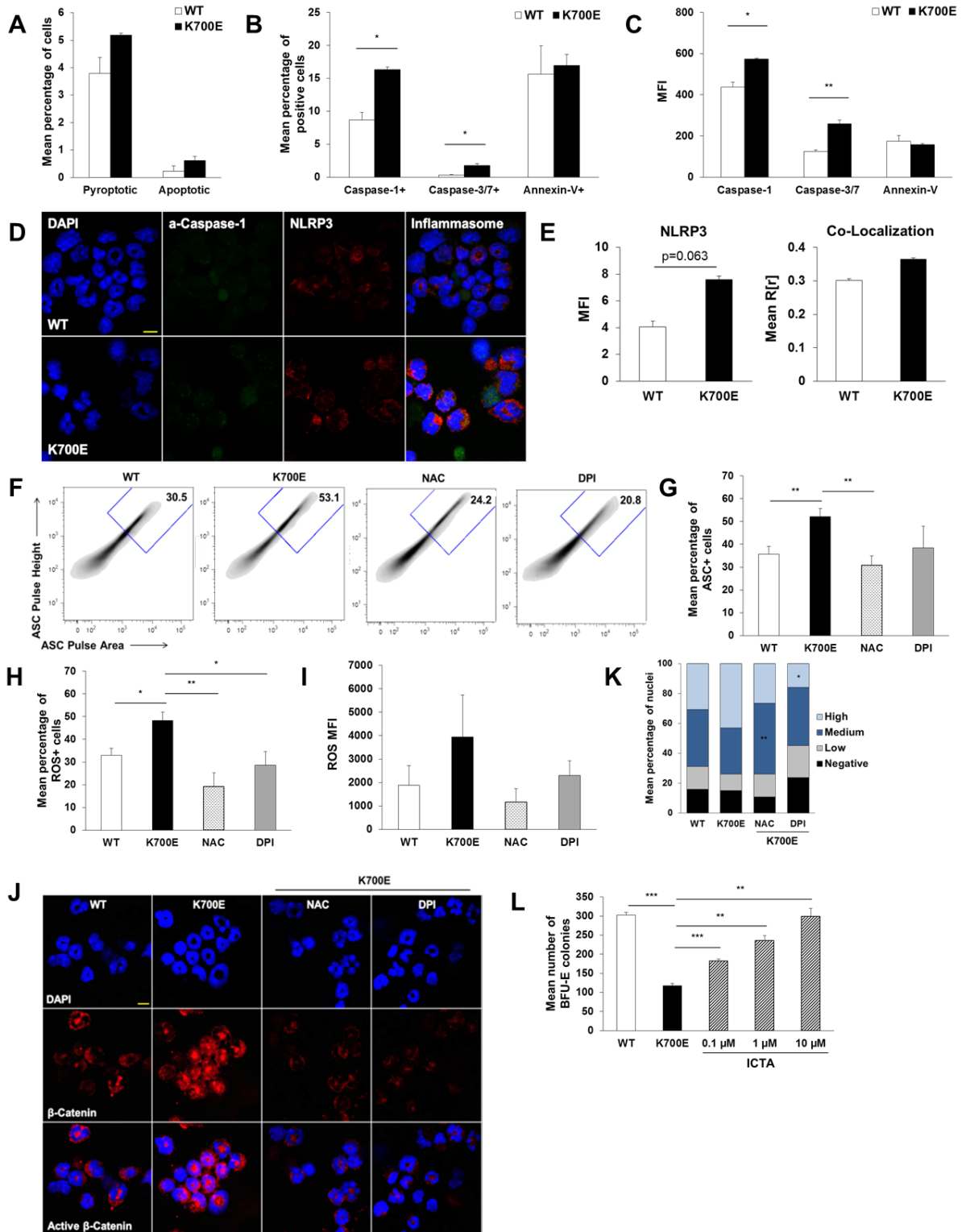


Figure 25. *Sf3b1*-K700E induces pyroptosis and supports self-renewal through β -catenin activation. Data are representative of BM cells harvested from wild type (WT) ($n=6$) and *Sf3b1*-K700E mutant ($n=6$) mice. **(A)** Quantitation of the percentage of

pyroptotic versus apoptotic cells. **(B)** Mean percentage of total a-caspase-1⁺, a-caspase-3/7⁺, and annexin-V⁺ cells. **(C)** MFI values for a-caspase-1, a-caspase-3/7, and annexin-V⁺ cells. **(D)** Representative micrograph (2520x magnification, 7.5 μm scale) depicting inflammasome formation in the WT and K700E mutant cells. DAPI (blue), a-caspase-1 (green), NLRP3 (red); merged image shows inflammasome formation. **(E)** Quantitative analysis of a-caspase-1/NLRP3 confocal images. **(F)** Representative density plot of inflammasome formation based on the detection of fluorescence pulse differences in ASC. **(G)** Quantitation of ASC in WT, K700E and K700E cells treated with NAC or DPI for 24 hr. **(H-I)** Mean percentage of **(H)** ROS positive cells and **(I)** ROS MFI assessed by flow cytometry. **(J)** Representative micrograph (2520x magnification, 7.5 μm scale) of β-catenin expression. DAPI (blue), β-catenin (red), and the merged images show nuclear localization of β-catenin. **(K)** Quantitation and scoring of β-catenin confocal images based on the presence of no, low, medium, or high nuclear β-catenin in WT, K700E and K700E cells treated with NAC or DPI for 24 hr. **(L)** Colony forming capacity was assessed in WT, K700E or K700E cells treated with increasing concentrations of ICTA (0.1-10 μM). Mean number of BFU-E colonies is representative of BM cells isolated from four mice per condition, and four replicates per mouse. Error bars: SE, *p<0.05, **p<0.01 and ***p<0.001.

regulatory gene mutations (*Asx1*, *Tet2*)^{308,309} (Figure 27). To confirm that somatic gene mutations prime HSPC for pyroptosis in MDS, we performed comparative analyses of published gene expression profiles from human and murine *SRSF2* (GSE65349) and *U2AF1* mutants (GSE30195, GSE66793) versus WT, *TET2* knock-out (GSE27816) and primary MDS (GSE19429) versus normal HSPC, demonstrating uniform up-regulation of pyroptosis effectors consistent with transcriptional priming.³⁰⁹⁻³¹³

Importantly, in MDS BM specimens, BM plasma concentration of S100A9 positively correlated with NLRP3 MFI, percentage and MFI of plasma ASC specks, and with the presence of spliceosome gene mutations and variant allele frequency (VAF) (Figure 28). Furthermore, both the percentage and MFI of plasma ASC specks were significantly increased in MDS patients harboring somatic gene mutations (Figure 28D-E). Finally, the percentage of pyroptotic erythroid precursors significantly increased in

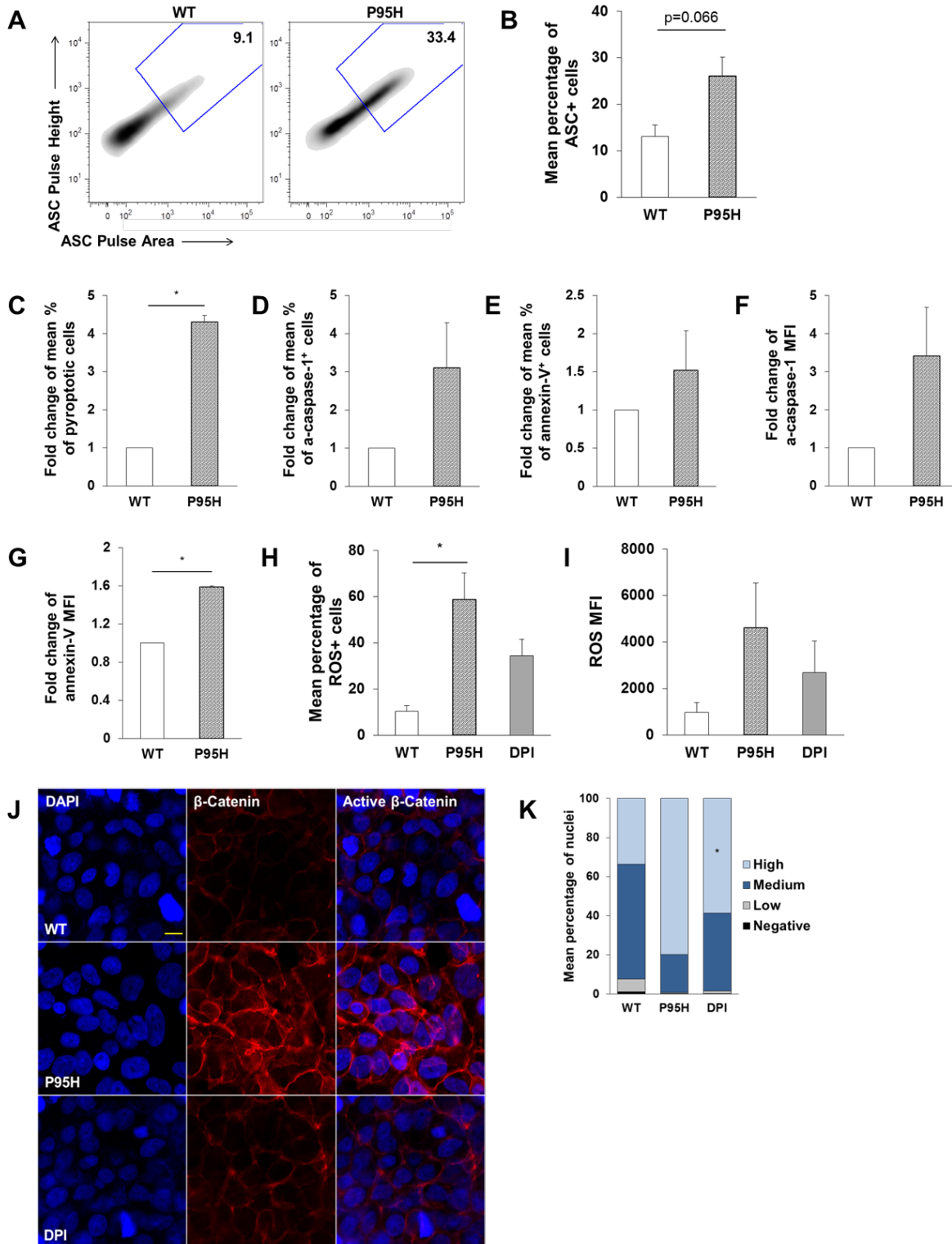


Figure 26. *SRSF2* mutants induce pyroptosis and support self-renewal through β -catenin. HEK293T cells were transiently transfected with wild type (WT) and P95H mutant *SRSF2* expression plasmids. Data shown of the GFP⁺ transfected populations

are representative of three independent experiments. **(A)** Representative density plot of inflammasome formation based on the detection of fluorescence pulse differences in ASC. **(B)** Quantitation of ASC positive cells. **(C-G)** Fold change of the mean percentage of **(C)** pyroptotic cells, **(D)** total a-caspase-1⁺ cells, **(E)** total annexin-V⁺ cells, and MFI values for **(F)** a-caspase-1 and **(G)** annexin-V, normalized to WT transfected cells. **(H-I)** Mean percentage of **(H)** ROS positive cells and **(I)** ROS MFI. **(J)** Representative micrograph (1890x magnification, 10 μm scale) of β-catenin expression. DAPI (blue), β-catenin (red), and the merged images show nuclear localization of β-catenin. **(K)** Quantitation and scoring of β-catenin confocal images based on the presence of no, low, medium, or high nuclear β-catenin. Error bars: SE, *p<0.05.

parallel with splicing gene mutation VAF and with the number of somatic gene mutations. Thus, MDS somatic gene mutations prime cells to undergo pyroptosis, which promotes self-renewal and contributes to an inflammatory microenvironment that is driven by NOX-derived ROS.

MDS HSPC are primed for NLRP3 inflammasome activation. Given the increased oxidative stress in MDS, we investigated the contribution of redox-proteins in mediating NLRP3 inflammasome activation. ROS oxidize thioredoxin (TRX) triggering its dissociation from thioredoxin-interacting protein (TXNIP). Recent studies suggest that liberated TXNIP serves as a redox sensitive ligand that binds NLRP3 and activates inflammasome complex assembly.²⁶¹ *TXNIP* gene expression was 9.6-fold increased in lower-risk MDS BM-MNC (n=9) compared to normal donors (n=4), and increased 3.4-fold in *U2AF-S34F*-expressing cells compared to WT *U2AF1*-expressing cells (Figure 29A). Further, there was increased binding of TXNIP to NLRP3 in MDS and *S34F*-expressing cells, compared to normal donors and WT cells, respectively (Figure 29B and 29C). Notably, increased NLRP3 oligomerization and activation was confirmed through binding of NLRP3:ASC (Figure 29B and 29C). Moreover, mRNA and protein levels of the pyrin domain-only protein (POP)-1, a key negative regulator of NLRP3

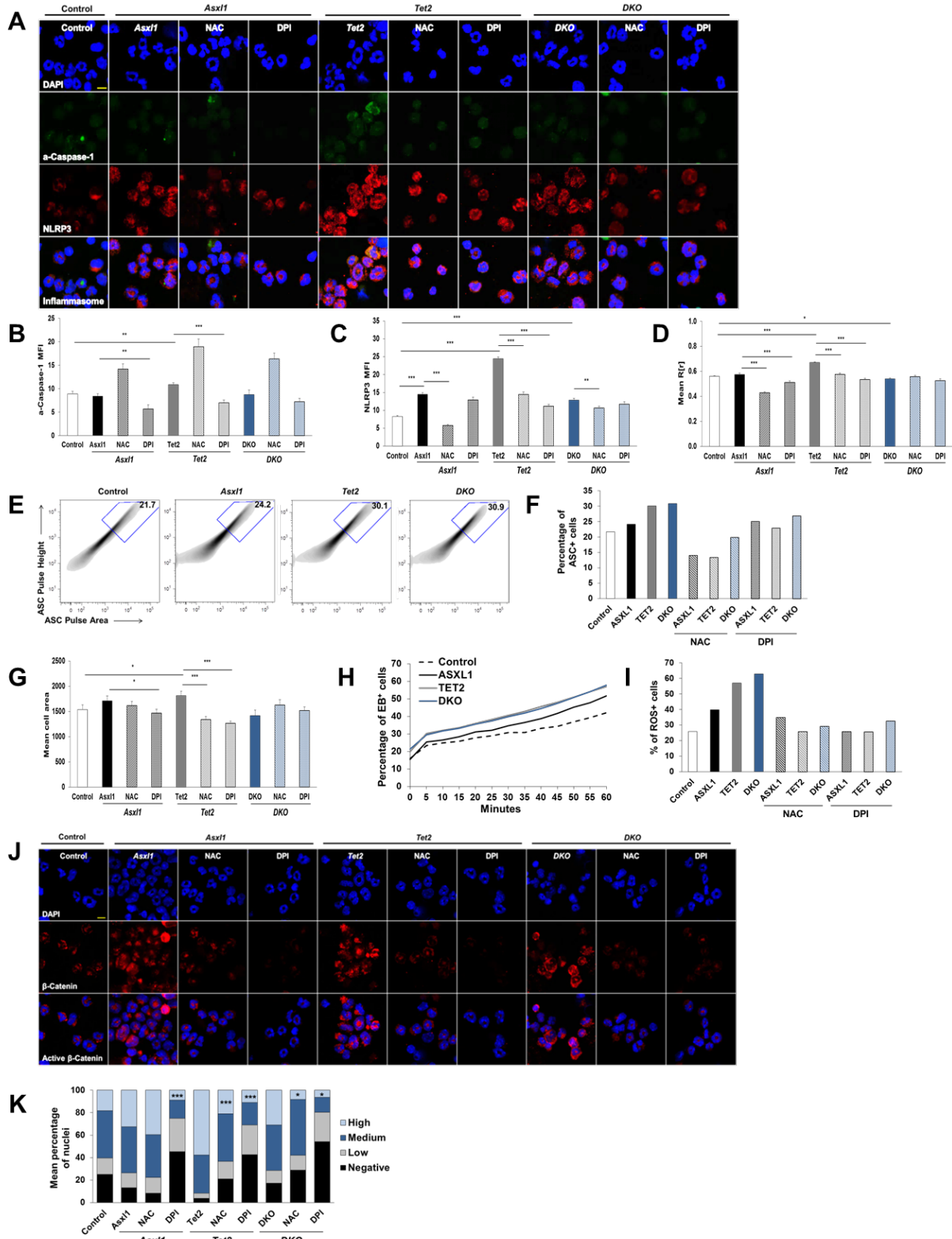


Figure 27. *Asx1f* and *Tet2* deletions are sufficient to induce pyroptosis and drive self-renewal through β -catenin activation. BM cells were isolated from *Asx1f* KO,

Tet2 KO and *DKO* mice and were compared to BM from wild type mice. **(A)** Representative micrograph (2520x magnification, 7.5 μ m scale) depicting inflammasome formation in control and KO cells that were untreated, or treated with NAC or DPI for 24 hr. DAPI (blue), a-caspase-1 (green), NLRP3 (red); merged images show inflammasome formation. **(B-D)** Quantitative analysis of a-caspase-1/NLRP3 confocal images. Cells were pooled for analysis. **(E)** Representative density plot of inflammasome formation based on the detection of fluorescence pulse differences in ASC. **(F)** Quantitation of percentage of ASC positive cells. **(G)** Quantitation of mean cell area. **(H)** Ethidium bromide dye incorporation was measured by flow cytometry at 5 min intervals. **(I)** Percentage of ROS positive cells was assessed by flow cytometry. **(J)** Representative micrograph (2520x magnification, 7.5 μ m scale) of β -catenin expression. DAPI (blue), β -catenin (red), and the merged images show nuclear localization of β -catenin. **(K)** Quantitation and scoring of β -catenin confocal images based on the presence of no, low, medium, or high nuclear β -catenin. Cells were pooled for analysis. Measurements of significance were made on untreated KO cells compared to NAC or DPI treated KO cells. Error bars: SE, * p <0.05, ** p <0.01 and *** p <0.001.

inflammasome activation that functions as a dominant-negative ASC antagonist blocking ASC oligomerization,²⁷⁷ was profoundly reduced in both lower-risk MDS BM-MNC (n=9) and *U2AF1-S34F*-expressing cells (Figure 29D and 29E). To determine if NLRP3 inflammasome activation is reinforced in MDS by reduced expression of POP-1, *U2AF1-S34F* cells were transfected with *POP-1* expression vectors. Significant increases in POP-1 expression were associated with a 40% reduction in NLRP3 activation, as measured by ASC oligomerization (Figure 29F). Collectively, these findings indicate that MDS HSPCs are primed for NLRP3 inflammasome activation.

MDS MSC and stromal-derived lineages undergo pyroptosis. It is well established that a dynamic and complex interplay exists between hematopoietic cells and the surrounding mesenchymal stromal cells (MSC) in the MDS bone marrow.¹²⁰⁻¹²² Specifically, dysfunction in one compartment, namely hematopoietic cells or MSC, reinforces dysfunction in the other compartment.¹²⁰ Of note, co-culture of MDS-derived

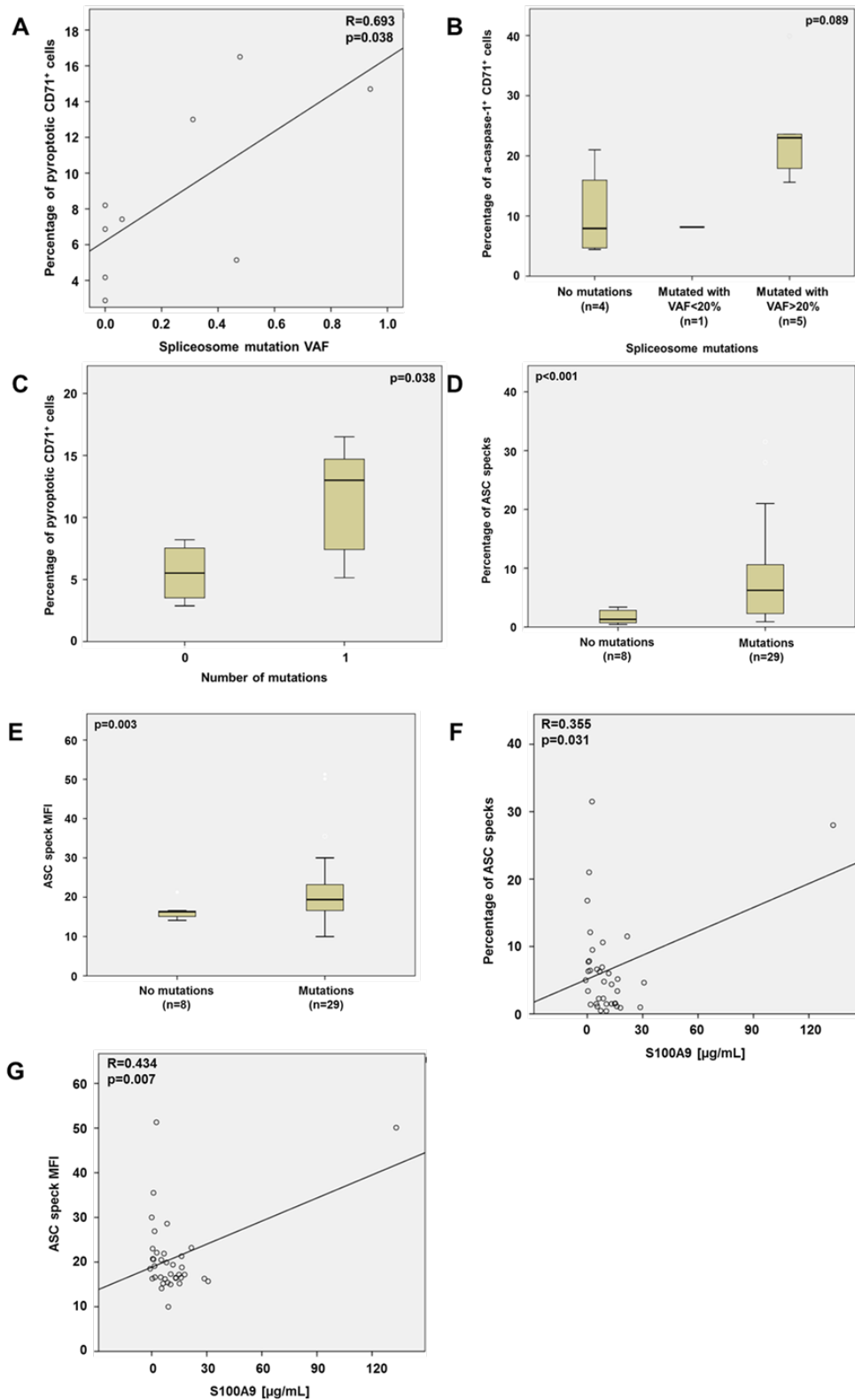


Figure 28. Somatic gene mutations and mutation variant allele fraction correlate with the extent of pyroptosis in MDS. (A) The percentage of pyroptotic CD71⁺ cells

significantly increases with spliceosome mutation VAF. **(B)** There is a trend toward increased a-caspase-1⁺ CD71⁺ cells with VAF. **(C)** The percentage of pyroptotic CD71⁺ cells increases with the number of mutations. **(D-E)** The **(D)** percentage and **(E)** MFI of plasma ASC specks significantly increases with the presence of a somatic gene mutation. **(F-G)** The **(F)** percentage and **(G)** MFI of plasma ASC specks significantly and positively correlate with BM plasma S100A9 concentration.

stromal cells with the F-36P AML cell line resulted in increased hematopoietic cell death, measured by 7-aminoactinomycin D (7-AAD) staining.¹²¹ Given the inflammatory nature of pyroptosis, with the release of DAMP signals, pro-inflammatory cytokines, and cellular debris following lysis, we hypothesized that pyroptotic cell death of HSPC triggers pyroptosis within MSC and stromal-derived lineages. As such, pyroptosis of stromal cells could account for the defective ability of the MDS stroma to support normal, effective hematopoiesis.

Foremost, we measured the extent of pyroptosis versus apoptosis in MSC and MSC-derived lineages from lower-risk MDS (n=6) compared to normal (n=6) BM donors. MSC were defined as CD45⁻CD105⁺, endothelial cells as CD31⁺ and osteoblasts as CD34⁻osteocalcin(OCN)⁺. The mean percentage of pyroptotic MSC (p=4.1x10⁻³), endothelial cells (p=0.034) and osteoblasts (p=1.0x10⁻³) were significantly increased in MDS compared to normal donors (Figure 30A). While the apoptotic fraction across the three lineages was markedly increased in MDS compared to normal, these findings are consistent with activation of caspase-3 downstream of caspase-1 activation during pyroptosis execution (Figure 30B). Moreover, MDS specimens displayed 13.9-fold and 7.6-fold increases in the mean percentage of a-caspase-1⁺ MSC (p=6.6x10⁻⁵) and endothelial cells (p=0.05) compared to normal donors (Figure 30C). Though a-caspase-1⁺ osteoblast cells were increased 7.1-fold in MDS, this level only approached

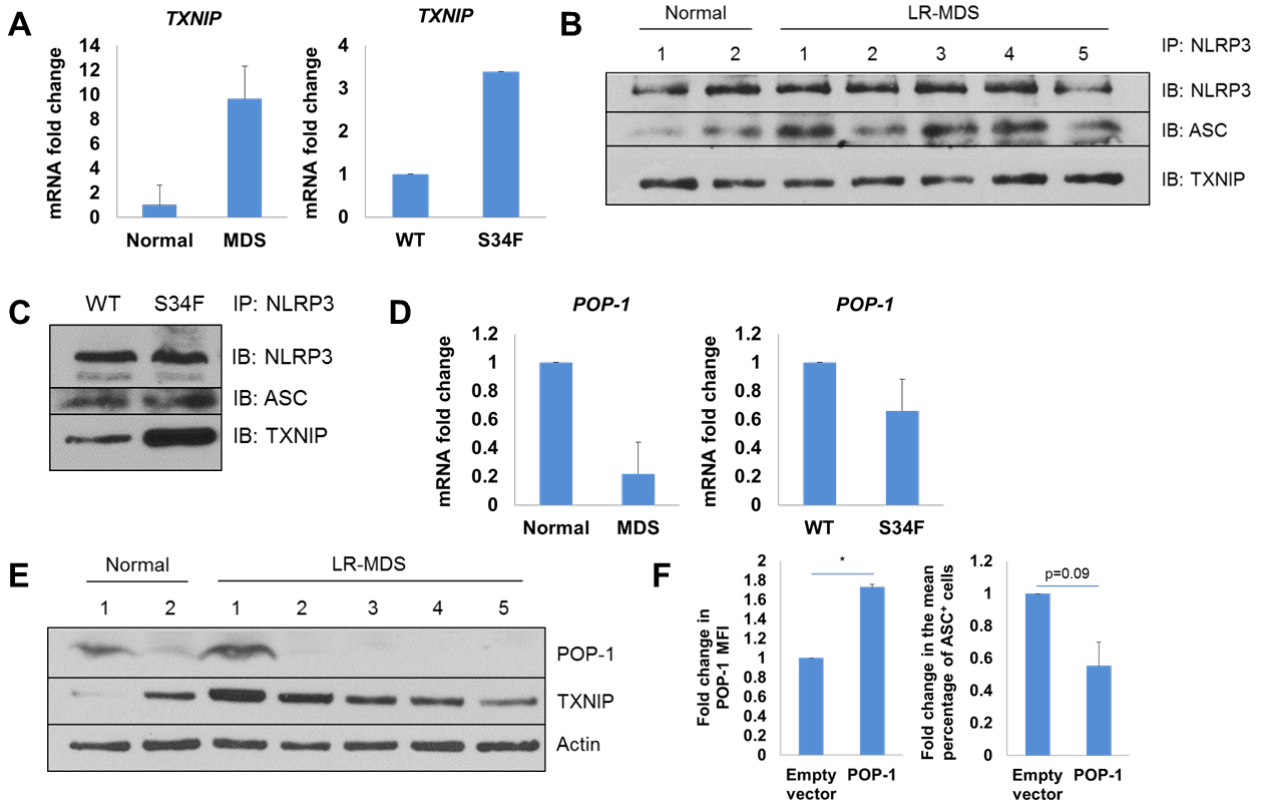


Figure 29. Inflammasome activation occurs via up-regulation of TXNIP and down-regulation of POP-1. Data are representative of three independent experiments. **(A)** qPCR analyses show markedly increased expression of *TXNIP* in lower-risk MDS BM-MNC (n=9) compared to normal donor controls (n=4), as well as in *U2AF1-S34F*-expressing cells compared to WT. **(B-C)** Binding of TXNIP and ASC to NLRP3 is increased in **(B)** lower-risk MDS BM-MNC and **(C)** *U2AF1-S34F* cells (IP: NLRP3, IB: NLRP3, ASC, TXNIP). **(D)** *POP-1* gene expression is dramatically reduced in lower-risk MDS BM-MNC (n=9) compared to normal donor controls (n=4), as well as in *U2AF1-S34F*-expressing cells compared to WT. **(E)** Western blot of POP-1 and TXNIP protein expression in lower-risk MDS BM-MNC compared to normal donors. **(F)** *U2AF1-S34F*-expressing cells were transiently transfected with *POP-1* expression vectors by electroporation method. POP-1 expression is increased following transfection, which corresponds with a pronounced reduction in ASC oligomerization as measured by flow cytometry. Error bars: SE, *p<0.05.

statistical significance (Figure 30C). To a lesser extent, a-caspase-3/7⁺ cells were increased across each stromal-derived lineage in MDS compared to normal (Figure 30D). Similar observations were made with respect to a-caspase-1 MFI (Figure 30E) and a-caspase-3/7 MFI (Figure 30F). When the extent of pyroptosis versus apoptosis

was compared across lineages in MDS, the pyroptotic cell fraction significantly exceeded the corresponding apoptotic cell fraction (Figure 30G). Specifically, pyroptotic MSC, endothelial cells and osteoblasts were 7.3-fold ($p=4.6 \times 10^{-3}$), 10.3-fold ($p=0.03$) and 16.2-fold ($p=1.1 \times 10^{-4}$) more frequent than apoptotic cells of the same cell type (Figure 30G). When a similar comparison was made in the fraction of a-caspase-1⁺ versus a-caspase-3/7⁺ cells of each lineage, a-caspase-1⁺ cells were predominant (Figure 30H). Lastly, cell swelling, a hallmark of pyroptosis, can be measured by SSC-A flow cytometric measurements.³⁰⁰ MDS-MSC had significantly larger cell area ($p=0.03$) compared to normal donors (Figure 30I). While MDS endothelial cells and osteoblasts did display a larger cell area compared to normal, these data did not reach statistical significance. Together, these findings indicate that MDS-MSC and MSC-derived lineages, specifically endothelial cells and osteoblasts, predominantly undergo pyroptotic cell death.

Discussion

Heretofore, ineffective hematopoiesis in MDS has been attributed to high fractions of proliferating BM progenitors undergoing apoptotic cell death within an unexplained inflammatory microenvironment.^{196,288} Nearly two decades ago it was reported that MDS HSPC generate IL-1 β in short term cultures, which directly correlated with the extent of cell death as measured by DNA fragmentation.⁹⁹ We present evidence that these and other biological features of MDS are explained by the activation of the NLRP3 pattern recognition receptor by S100A9 and ROS DAMP intermediates that

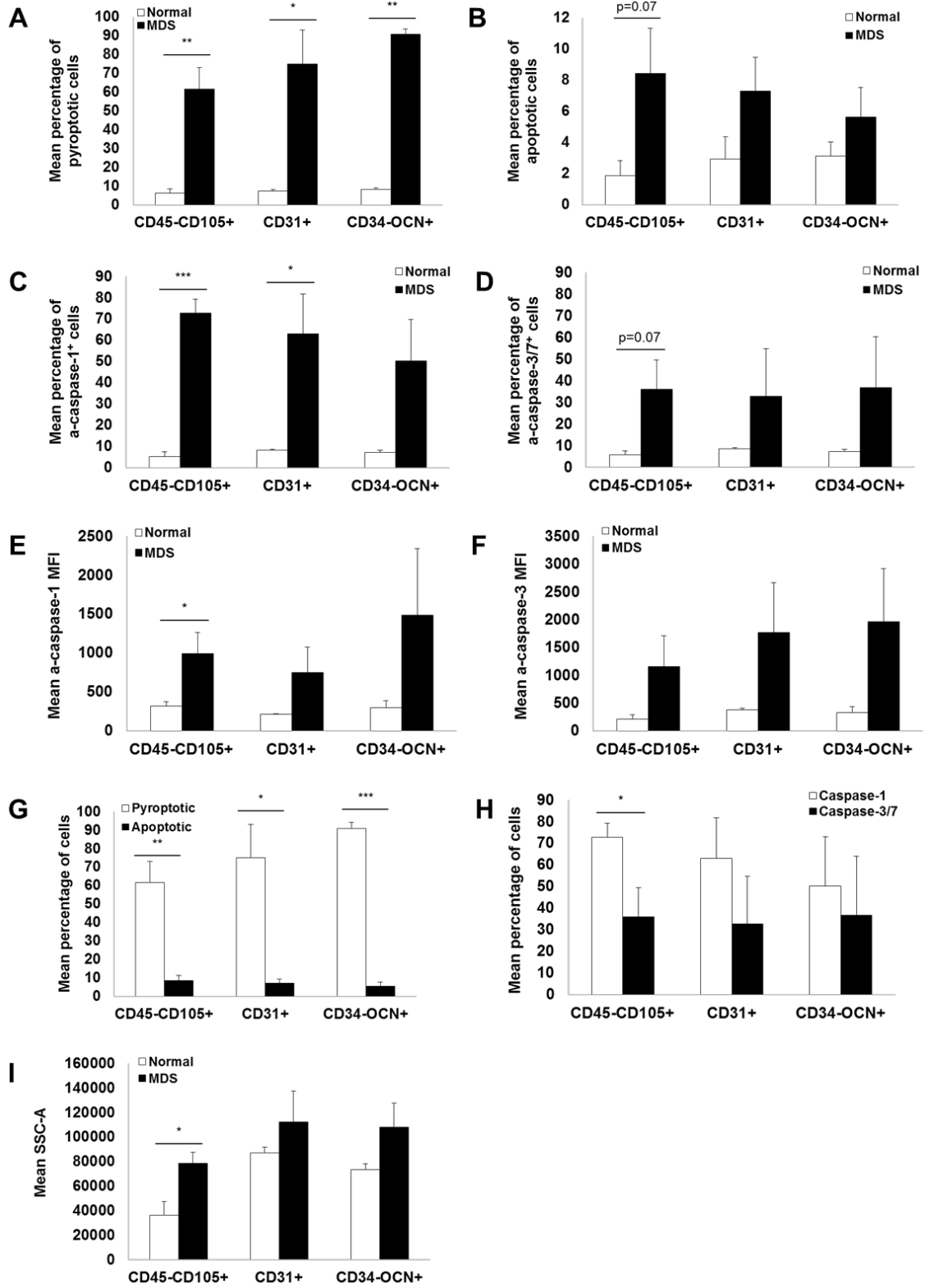


Figure 30. Pyroptosis is manifest in MSC and stromal-derived lineages in MDS. (A-B) The mean percentage of (A) pyroptotic and (B) apoptotic cells by mesenchymal

lineage in lower-risk MDS (n=6) versus normal donors (n=6). **(C-D)** Mean percentage of **(C)** total a-caspase-1⁺ and **(D)** a-caspase-3/7⁺ cells in lower-risk MDS (n=6) versus normal donors (n=6). **(E-F)** Mean **(E)** a-caspase-1 MFI and **(F)** a-caspase-3/7 MFI. **(G)** Comparison of the mean percentage of pyroptotic versus apoptotic cells in lower-risk MDS specimens (n=6). **(H)** Comparison of the mean percentage of a-caspase-1⁺ versus a-caspase-3/7⁺ cells in the same lower-risk MDS patients (n=6). **(I)** Flow cytometric analysis of mean SSC-A intensity of BM-MNC by mesenchymal lineage isolated from normal donors (n=6) or lower-risk MDS patients (n=6). Error bars: SE, *p<0.05, **p<0.01 and ***p<0.001.

induce inflammasome assembly, β -catenin nuclear translocation and pyroptotic cell death. Notably, pyroptosis-associated gene transcripts and inflammasome assembly are profoundly up-regulated in MDS independent of genotype. Moreover, pyroptotic but not apoptotic cells are markedly increased in MDS stem cells, progenitors and erythroid precursors. Accordingly, knockdown of NLRP3 and caspase-1, but not caspase-3, significantly reduced the pyroptotic cell fraction in MDS BM-MNC. MDS HSPCs are also selectively primed to undergo pyroptosis, due in part to up-regulation of pattern recognition receptors directing pyroptotic cell death, the expansion of MDSCs¹⁴⁰ and transcriptional priming of inflammasome components. Importantly, neutralization of S100A9 in MDS BM plasma or pharmacologic inhibition of inflammasome assembly suppressed pyroptosis and restored effective hematopoiesis *in vitro* and in the S100A9Tg mouse model of MDS. Thus, pyroptosis, a caspase-1-dependent inflammatory cell death, impairs HSPC survival in MDS.

S100A8/S100A9 heterodimers activate both NF- κ B and NLRP3 inflammasome assembly via an NADPH oxidase (NOX)/ROS-dependent mechanism.^{258,266,267,314} Intracellularly, S100A8/9 heterodimers serve as a scaffold for the membrane assembly and activation of the NOX complex,^{264,265} which generates ROS via transfer of electrons

across membranes to generate superoxide.²⁵⁹ As also shown here, NOX activity regulates both priming and activation of NLRP3 inflammasomes, including the activation of caspase-1 and IL-1 β maturation.²⁵⁸ Moreover, transcription and nuclear localization of β -catenin are redox- and NOX1-dependent.^{285,286} Although MDSC are a key paracrine source of S100A9 in the MDS BM microenvironment,¹⁴⁰ here we show that MDS HSPC also express high intracellular levels of S100A9 across lineages, suggesting that inflammasome activation may be sustained by intracrine DAMP stimulation which following cytolysis, may be reinforced by paracrine TLR4 activation and expansion of BM MDSC. Indeed, Schneider et al. recently reported that *Rps14* haploinsufficiency induces S100A8/9 expression to direct TLR4-dependent, cell-intrinsic death of polychromatic erythroblasts.¹⁶⁷ Comparative transcriptome analysis also shows that S100A8/9 is highly up-regulated in *Srsf2* P95H mutant as well as *Ezh2*-deleted mouse models.^{315,316} Additionally, our findings that catalytically-active pyroptotic ASC specks are released from the cytosol into the extracellular space suggest that specks may continue to reinforce bystander inflammation in the microenvironment in a non-cell autonomous fashion.^{298,317} Importantly, NOX1/4 inhibition suppresses the activation of the inflammasome and β -catenin in both MDS patient-derived BM-MNC and in cells harboring varied classes and types of MDS founder gene mutations. Thus, S100A9 induces NOX1/4 activity to drive ROS-dependent inflammasome assembly, pyroptosis, and β -catenin activation, explaining the proliferation and inflammatory cell death manifest in MDS.

Another hallmark of MDS is the larger cell size of BM precursors, or macrocytosis. A characteristic feature of NLRP3 inflammasome activation is cell

swelling due to the activation of cation channels in the plasma membrane.²¹⁴ We show that activation of pattern recognition receptors triggers expansion in size and volume of MDS progenitors via influx of cations by membrane channels that are activated by NOX-derived ROS.^{217,318-320} Our findings show that MDS BM-MNC display increased influx of the membrane impermeable, cationic dye ethidium bromide, confirming ion channel activation. Additionally, quantitation of BM cells according to lineage and stage of maturation confirmed a significantly larger size of MDS BM precursors versus normal controls that increased directly with NLRP3 mean fluorescence intensity. Thus, S100A9-mediated NOX activation and inflammasome-initiated pyroptosis explain the characteristic larger cell size, proliferation and inflammatory cell death manifest in MDS.

Somatic gene mutations in MDS trigger Rac1/NOX-dependent ROS generation,^{263,321} which we show activates both inflammasomes and Wnt/ β -catenin signaling, a pathway known to promote leukemia stem cell self-renewal. NOX-derived ROS stabilize and activate β -catenin by oxidation and dissociation of nucleoredoxin (NRX) from disheveled (Dvl), which in turn inactivates the β -catenin destruction complex.²⁸⁷ Here we show that ROS and β -catenin nuclear localization are profoundly increased in MDS HSPC, and that S100A9 treatment of normal BM-MNC is sufficient to trigger NOX/ROS-dependent nuclear translocation of β -catenin and the activation of Wnt/ β -catenin target genes. Similarly, BM-MNC from S100A9Tg mice, and BM progenitors that express varied RNA splicing gene mutations (*U2AF1*, *SF3B1*, *SRSF2*) and epigenetic regulatory gene mutations (*ASXL1*, *TET2*) found in MDS similarly undergo pyroptosis, pore formation, cell volume expansion and express high levels of nuclear β -catenin and Wnt/ β -catenin target genes, which can be suppressed by

inhibition of the NLRP3 inflammasome or NOX1/4. Moreover, the proportion of pyroptotic erythroid progenitors in primary MDS specimens increases with somatic gene mutation allele burden and mutation complexity. Mechanistically, we show that the thioredoxin-interacting protein, TXNIP, serves as a redox sensitive ligand activating the NLRP3 inflammasome upon oxidative dissociation from thioredoxin in both MDS and splicing gene mutant cells. Inflammasome nucleation in MDS is further reinforced by reduced expression of the pyrin domain-only protein (POP)-1, a dominant-negative ASC antagonist preventing NLRP3 and ASC polymerization. The forced expression of POP-1 reduced NLRP3 inflammasome activation, indicating that MDS HSPCs are primed for NLRP3 inflammasome activation. Thus, both S100A9-induced NOX activation and MDS gene mutations initiate pyroptosis through superoxide generation to drive β -catenin activation and enable a proliferative advantage to the MDS clone.

Lastly, the MDS stroma is known to be impaired in its ability to support normal, effective hematopoiesis. Murine models generated by MDS-related stromal abnormalities demonstrate that stromal defects can induce aberrances and dysplasia in otherwise normal hematopoietic cells.¹²² Conversely, normal MSC co-cultured with MDS patient-derived CD34+ HSPC adopt a phenotype characteristic of MDS-MS.^{120,121} These findings illustrate the complex interplay that exists between the hematopoietic and stromal cell compartments in MDS. Given that pro-inflammatory cytokines and DAMP signals are released upon cytolysis in pyroptosis, we hypothesized that cell death of hematopoietic cells can induce pyroptosis of neighboring stromal cells, resulting in cell death or injury of stromal lineages and consequent deficient support of hematopoiesis. Indeed, our data indicate that pyroptosis is significantly increased in

MSC, endothelial cells and osteoblasts in MDS compared to normal donors. Similar increases were observed in the percentage of a-caspase-1⁺ cells and a-caspase-1 MFI. Moreover, the pyroptotic cell fraction significantly exceeded the corresponding apoptotic cell fraction across stromal-derived lineages in MDS, indicating that the MDS stroma predominantly undergoes pyroptotic cell death.

In conclusion, despite genetic heterogeneity, inflammasome activation underlies the biological phenotype in lower-risk MDS, whereby DAMP signals and MDS gene mutations license a common redox-sensitive inflammasome platform to drive pyroptotic death, elaborate inflammatory cytokines, activate cation influx, and support propagation of the MDS clone through β -catenin activation (Figure 31). These findings provide a common platform that accounts for the biological features of MDS and suggest that strategies targeting S100A9 neutralization or inhibition of pyroptosis signaling offer therapeutic promise in lower-risk MDS.

Methods

MDS patient specimens. MDS patients consented on The University of South Florida Institutional Review Board approved protocols were recruited from the Malignant Hematology Clinic at H. Lee Moffitt Cancer Center & Research Institute, and the Eastern Cooperative Oncology Group (ECOG) E2905 trial (NCT00843882). Pathologic subtype of MDS was reported according to World Health Organization (WHO) criteria and prognostic risk assigned according to the International Prognostic Scoring System

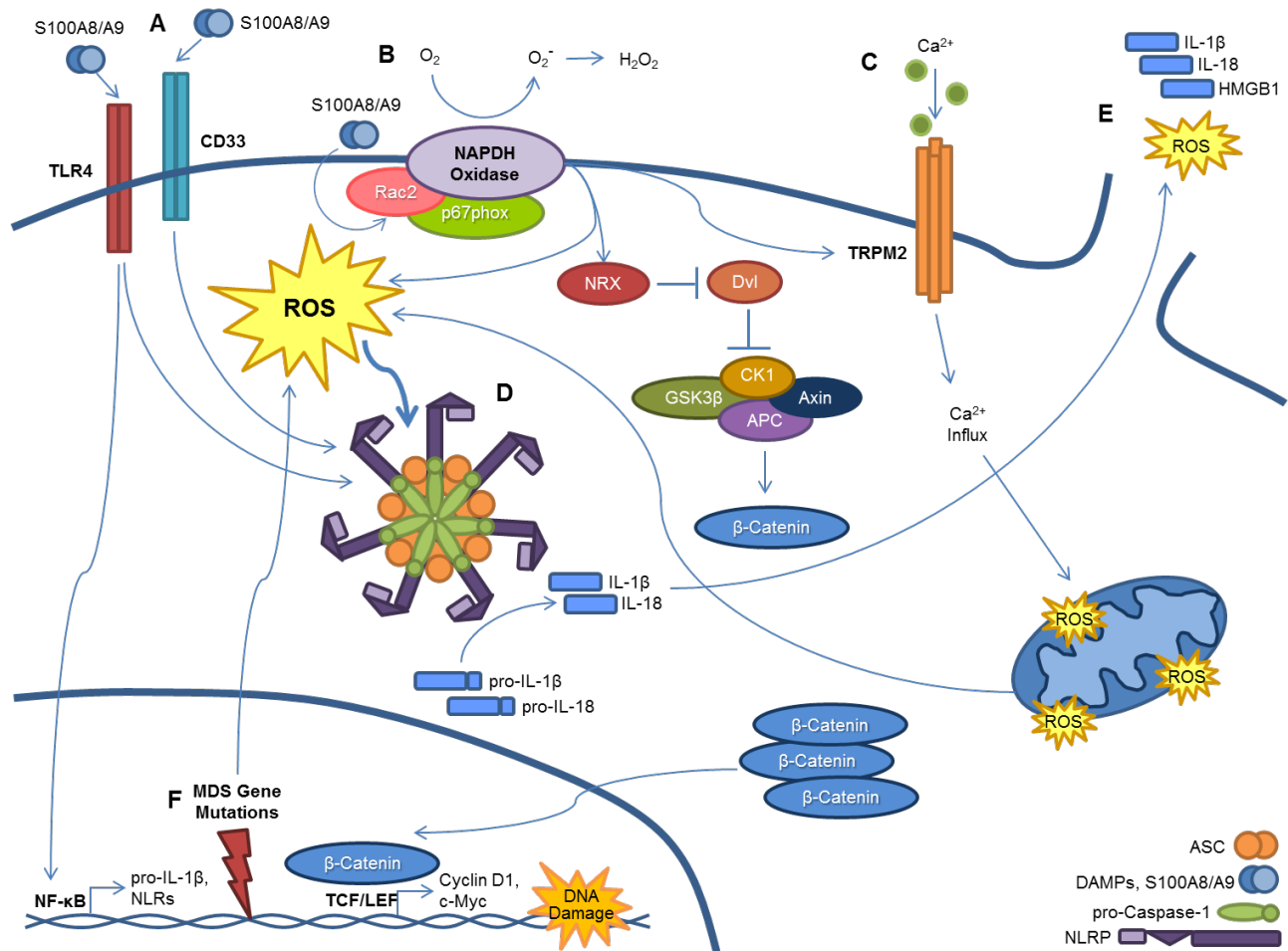


Figure 31. An S100A9/pyroptosis circuit provokes phenotypes manifest in MDS. (A) S100A8/A9 binds both CD33 and TLR4, resulting in inflammasome assembly. Ligation of S100A8/A9 to TLR4 results in NF- κ B-mediated transcription and subsequent production of pro-inflammatory cytokines such as pro-IL-1 β and pro-IL-18, along with inflammasome components. (B) Through interaction with Rac2 and p67phox, S100A8/A9 promotes activation of NOX, which results in a dual function. First, NOX proteins generate ROS, which serve to activate NLRs and inflammasome assembly. Second, NOX-derived ROS oxidize NRX, leading to its dissociation from Dvl. Once dissociated, Dvl suppresses the β -catenin destruction complex (GSK β /CK1/APC/Axin), resulting in stabilization of β -catenin. This allows β -catenin to enter the nucleus and induce transcription of TCF/LEF controlled genes, including *Cyclin-D1* and *c-Myc*, which are essential to self-renewal. (C) Transient receptor potential melastatin 2 (TRPM2), a calcium-permeable cation channel in hematopoietic cells, is activated by NOX-derived ROS via oxidation of a single channel methionine residue, Met²¹⁴. Upon activation, TRPM2 causes an influx of calcium leading to mitochondrial depolarization and further release of ROS, which activate the inflammasome complex. (D) Formation of the inflammasome complex occurs as a consequence of ROS activation and DAMP signaling. Once activated, inflammasomes mediate conversion of pro-caspase-1 to its mature and catalytically active form. Active caspase-1 cleaves pro-IL-1 β and pro-IL-18

to their mature forms. **(E)** Pyroptosis ensues with loss of membrane integrity resulting in release of pro-inflammatory cytokines and other intracellular contents into the extracellular milieu. **(F)** MDS-related gene mutations activate NF- κ B and NLRP3 via NOX-generated ROS.

(IPSS). Patients were segregated as lower- (low, intermediate-1) and higher-risk (intermediate-2, high) MDS.

Mice. S100A9Tg mice have been described.¹⁴⁰ Wild type FVB/NJ mice were purchased from Jackson Laboratories (Bar Harbor, Maine). Bone marrow (BM) cells were isolated from tibias and femurs of male and female mice.

Reagents and cells. Parental TF-1 cells and TF-1 cells engineered to express mutant *U2AF1* were cultured in RPMI-1640 supplemented with 10% FBS and 2 ng/mL recombinant human GM-CSF. Normal, heparinized BM aspirates were purchased from Lonza Walkersville or AllCells, LLC. Normal and MDS BM mononuclear cells (BM-MNC) were isolated from heparinized BM aspirates using Ficoll-Hypaque Plus gradient centrifugation (GE Healthcare). Recombinant human S100A9 and the CD33/Siglec 3 chimeric fusion protein were generated as described.¹⁴⁰ NAC and DPI were purchased from Sigma. Active caspase-1 and caspase-3/7 were detected using FAM-FLICA® Caspase-1 and Caspase-3/7 activity kits, (ImmunoChemistry Technologies). NLRP3 antibodies were purchased from Abcam (ab4207) or AdipoGen (AG-20B-0014), and β -catenin antibodies from BD Biosciences (610154). Caspase-1 antibodies (#3866) were purchased from Cell Signaling Technology, Inc. IL-1 β antibodies (AF-201-NA) were acquired from R&D Systems, Inc.

Immunofluorescence confocal microscopy. MDS BM-MNC, normal donor BM-MNC and mouse BM cells were stained with 30x FAM-FLICA® Caspase-1 solution

at a ratio of 1:30 for 2 hr at 37°C. Cells were washed and cytopins were generated using a 5 min centrifugation at 450 rpm. Slides were fixed at 37°C for 10 min using BD Cytotfix Fixation Buffer (BD Biosciences), and then washed with PBS. Cells were permeabilized with 0.1% Triton X-100/2% BSA in PBS for 15 min at room temperature. After washing with PBS, cells were blocked using 2% BSA in PBS for 30 min at room temperature and washed again. Cells were incubated with the appropriate primary antibody overnight (1:400 for NLRP3, 1:20 for β -catenin) at 4°C. The next day, cells were washed with PBS and incubated with the appropriate secondary antibodies (1:500) for 1 hr at room temperature. After washing, cells were covered with ProLong Gold Antifade Reagent with DAPI prior to the addition of a coverslip (Life Technologies).

Co-localization of a-caspase-1 with NLRP3 inflammasomes was assessed using a Leica TCS SP5 AOBS Laser Scanning Confocal microscope (Leica Microsystems). Analysis of images was performed with Definiens Developer 2.0 (Definiens AG), which distinguishes cells based on brightness and size thresholds, followed by a watershed segmentation algorithm. Intensity values and Pearson's correlation coefficient were extracted from the segmented cells. For β -catenin image analysis, confocal images were imported into Definiens Tissue Studio v3.0, 64 Dual in .tif format. Cells were separated from background using the RGB thresholds. Nuclei were identified by setting thresholds in the DAPI channel. β -catenin intensity in the nucleus and cytoplasm was established by setting thresholds to low, medium and high in the red channel on a scale of 0-255.

Flow cytometry analyses. For human samples, treated and untreated BM-MNC were incubated overnight in IMDM, supplemented with 10% autologous BM plasma.

Cells were then harvested, washed twice in PBS, and stained with LIVE/DEAD Violet fluorescent reactive dye (Life Technologies) and Zombie NIR Viability dye (BioLegend) according to the manufacturer's protocols. Cells were resuspended in 1x PBS with 2% BSA, and incubated at room temperature for 15 min to block non-specific binding. After washing, cells were stained with 30x FAM-FLICA® Caspase-1 and Caspase-3/7 solution at a ratio of 1:30 for 2 hr at 37°C. For flow cytometry analyses of phenotypically distinct hematopoietic lineages, human cells were washed and stained for cell surface receptors using CD38:PE-CF594, CD33:BV711, CD34:APC (BD Biosciences, 562288, 563171, 555824, respectively), and CD71:PE-Cyanine7 (eBioscience, 25-0719-42). For analyses of phenotypically distinct stromal cell lineages, human cells were washed and stained for cell surface receptors using CD105:BUV395, CD31:FITC, CD34:BUV395 (BD Biosciences, 563803, 553372, 563778, respectively) and osteocalcin:Alexa Fluor 488 (R&D Systems, IC1419G). Mouse cells were washed and stained for cell surface receptors using Lineage Cocktail:V450, CD117:BUV395, and Ly-6A/E:BV786 (BD Biosciences, 561301, 564011, 563991, respectively). All antibodies were diluted 1:20, and cells were stained for 30 min at 4°C. Cells were washed, resuspended in 1x binding buffer, and stained with Annexin-V:PE or Annexin-V:V500 at a dilution of 1:20 for 15 min at room temperature (BD Biosciences, 556421) for hematopoietic and stromal cell lineage panels, respectively. 1x binding buffer was added to a final volume of 400 µL.

ASC staining was carried out as described.²⁹⁸ Briefly, cell pellets were resuspended in 1 mL of prewarmed BD Permeabilization Buffer III, and incubated on ice for 30 min. Cells were washed 2x with staining buffer. Following washing, cells were stained with rabbit-anti-ASC primary antibodies at a 1:1500 dilution and incubated for 90

min (Santa Cruz, sc-22514-R). Cells were washed, stained with secondary antibodies at a dilution of 1:1500, and incubated for 45 min. Cells were washed, and sample acquisitions were carried out using a BD LSR II flow cytometer and FACSDiva software.

For ASC speck detection, 400 µg of protein in BM plasma from normal donors and MDS patients was stained with rabbit-anti-ASC primary antibodies at a 1:1500 dilution and incubated for 90 min. Secondary antibodies were added at a dilution of 1:1500 and incubated for 45 min. Sample acquisitions were carried out using a BD FACSCalibur flow cytometer. Threshold for FSC and SSC were set to zero to allow detection of specks.

Sample acquisitions were carried out using a BD LSR II flow cytometer and FACSDiva software (BD Biosciences). Calibration was carried out prior to each experiment using Rainbow Mid-Range Fluorescent Particles (BD Biosciences). To establish compensation settings, ArC Amine Reactive Compensation Beads were used for viability staining (Life Technologies), and BD CompBead Plus Anti-Mouse Ig κ/Negative Control (BSA) Compensation Plus Particles and Anti-Rat and Anti-Hamster Ig κ/Negative Control Compensation Particles Set were used for surface receptor conjugates for human and murine studies, respectively (BD Biosciences). Data were analyzed using FlowJo 9.7.5 software (FlowJo, LLC). Gating strategies for evaluating the extent of pyroptosis versus apoptosis in normal/MDS specimens and WT/S100A9Tg mice are illustrated in Figure 32.

Lentiviral infection of primary mononuclear cells. Lentiviral constructs were purchased from Origene. NLRP3 (TL30582b), Caspase-1 (TL305640), Caspase-3 (TL305638b) and scrambled (TR30021) HuSH™ shRNA plasmids were amplified by

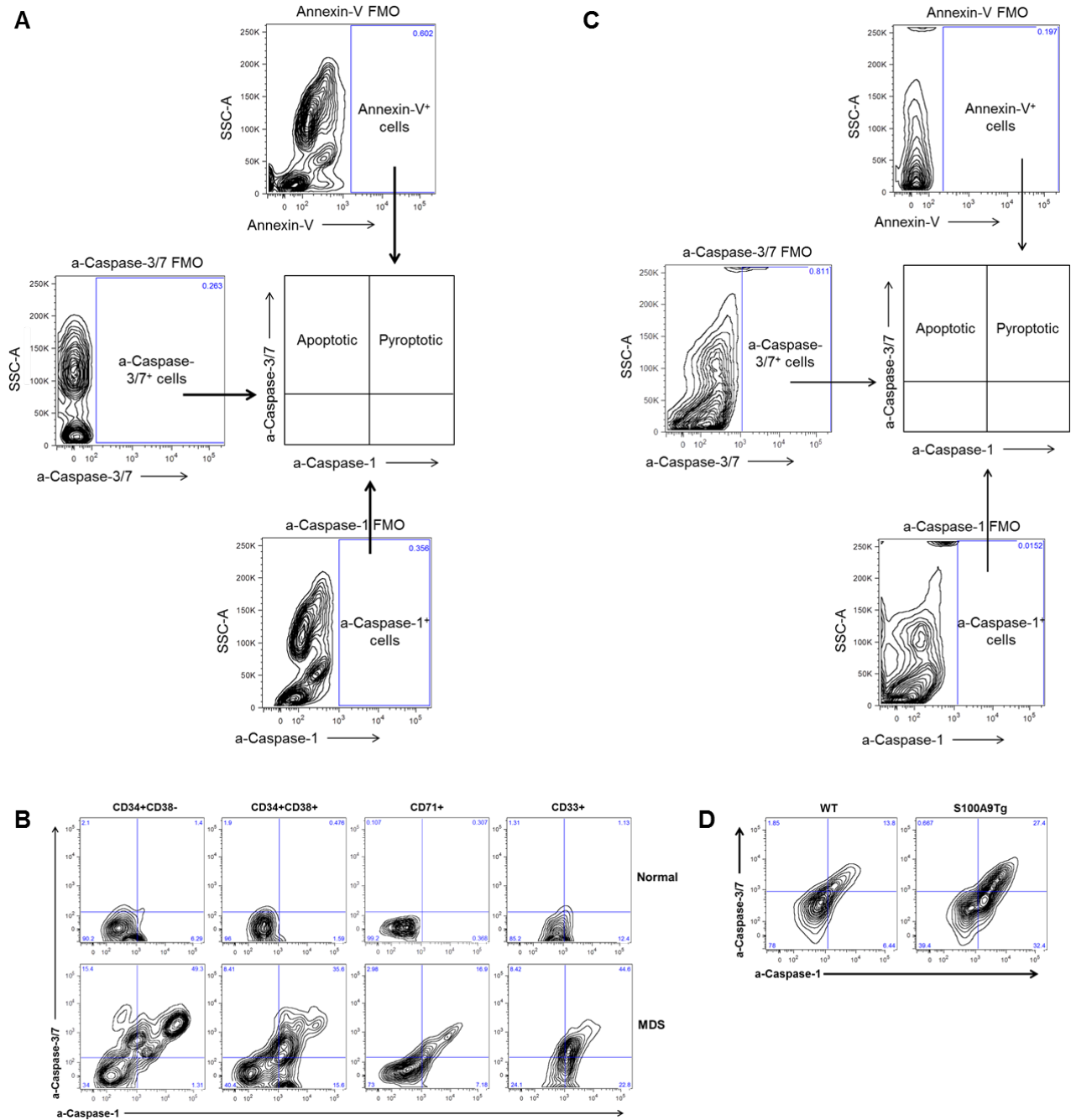


Figure 32. Flow cytometry gating strategies for evaluating the extent of pyroptosis versus apoptosis in normal/MDS specimens and WT/S100A9Tg mice. The gating strategies depicted take place after gating for cell lineage was carried out. (A) For normal donors and MDS specimens, the gates for annexin-V, a-caspase-1 and a-caspase-3/7 positivity were identified using fluorescence minus one (FMO) controls. The annexin-V positive cells were then stratified by a-caspase-1 and a-caspase-3/7 positivity. Using the gates identified for a-caspase-1 and a-caspase-3 positivity, a quadrant plot was made. Apoptotic cells were defined as annexin-V⁺/a-caspase-1⁻/a-caspase-3/7⁺ and pyroptotic cells annexin-V⁺/a-caspase-1⁺/a-caspase-3/7⁺. (B)

Representative density plots from a normal BM donor versus an MDS specimen. Annexin-V positive cells from the stem cell (CD34⁺CD38⁻), progenitor (CD34⁺CD38⁺), immature myeloid (CD33⁺) and erythroid (CD71⁺) populations were stratified according to a-caspase-1 and a-caspase-3/7 positivity, allowing for the characterization of the extent of pyroptotic versus apoptotic cell death. (C) For WT/S100A9Tg mice analyses, the gates for annexin-V, a-caspase-1 and a-caspase-3/7 positivity were identified using FMO controls and a quadrant plot stratifying the annexin-V positive cells according to a-caspase-1 and a-caspase-3/7 expression was created as described in (A). (D) Representative density plot from a WT versus a S100A9Tg sample. The plot depicts the extent of pyroptosis versus apoptosis in the LSK positive HSPC population.

transforming One Shot® Top10 competent cells (Life Technologies) according to manufacturer's protocol. Single colonies were expanded and plasmid DNA prepared using the Qiagen QIAprep® Mini Prep Kit. HEK293T cells were transfected by incubating 2600 ng of shRNA plasmid, 30 µL Lipofectamine® 2000 (Invitrogen) and 26 µL MISSION™ Lentiviral Packaging Mix (Sigma) in 500 µL of Opti-MEM® (Life Technologies) for 15 min at room temperature. This mixture was then added to 70% confluent HEK293T cells with 4 mL Opti-MEM® medium without serum in a 100 mm dish. After 6 hr, 6 mL of DMEM with 10% FBS (Mediatech) was added. After 16 hr, medium was changed and 10 mL fresh DMEM was added. Virus was collected at 48 and 72 hr using 0.45 µm filters. The titer was at least 5 x 10⁵ IFU/mL and virus was stored at 4 °C.

For primary cell infections with caspase-1 and caspase-3 lentivirus, 2.5x10⁶ cells were plated in a 100 mm dish with 1.25 mL virus, 1.25 mL opti-MEM® and 8 µg/mL polybrene. Cells were incubated overnight, then 5 mL of fresh IMDM with 10% FBS (Mediatech) was added. RNA was isolated 72 hr after infection using Qiagen RNeasy Isolation Kit. mRNA levels were analyzed by qPCR using *GAPDH* mRNA levels as a control. For primary cell infections with NLRP3 lentivirus, 2x10⁶ cells were plated in a 24

well plate with 500 μ L fresh virus, 500 μ L Opti-MEM® and 8 μ g/mL polybrene. The plate was spun at 2,200 rpm for 90 min. After 1 hr, 5 mL of fresh IMDM was added. Knockdown efficiency of NLRP3 protein was determined by flow cytometry. For both infection protocols, 10% v/v of autologous BM plasma was added to the cells at 72 hr. Cells were stained with annexin-V, 7-AAD, and FAM-FLICA® Caspase-1 and analyzed using a BD FACSCalibur flow cytometer 24 hr after plasma was added.

Enzyme-linked immunosorbent assays (ELISA). Human S100A9 DuoSet ELISA kit was purchased from R&D Systems and HMGB1 ELISA kit was purchased from MYBioSource. ELISA assays were performed according to manufacturer's protocol.

Intracellular S100A9 flow cytometry. BM-MNC were incubated overnight in IMDM medium with 10% autologous BM plasma. Cells were then harvested, washed twice in 1x PBS, fixed with BD Cytofix Fixation Buffer at 37°C for 10 min, and stored at -80°C until staining. For staining, cells were warmed to 37°C, spun down, and washed twice with staining buffer. Cells were suspended in 1 mL of pre-warmed BD Permeabilization Buffer III, incubated on ice for 30 min, washed twice with staining buffer and stained with antibodies at a 1:20 dilution for 30 min at 4°C (S100A9:FITC [BioLegend]; CD38:PE-CF594; CD33:BV711; CD34:APC [BD Biosciences]; and CD71:PE-Cyanine7 [eBioscience]). Cells were washed and resuspended in 400 μ L staining buffer. Sample acquisitions were performed using a BD LSR II flow cytometer and FACSDiva software (BD Biosciences).

Pore formation assay. MDS and normal donor BM-MNC were incubated in 10% autologous BM plasma at 37°C overnight. Cells were then washed and suspended in 1

mL of PBS with 12.5 µg/mL ethidium bromide (Fisher Scientific). Sample acquisitions were acquired using a BD FACSCalibur flow cytometer at 5 min intervals.

Real-time quantitative PCR. RNA was isolated from BM-MNC using the RNeasy Mini Kit (Qiagen). cDNA was produced using the iScript cDNA Synthesis Kit (Bio-Rad). Sequences for primers can be found in Table 4. *GAPDH* mRNA was used for transcript normalization. cDNA was amplified using the iQ SYBR Green Supermix and the CFX96 Real-Time PCR Detection System (Bio-Rad). PCR conditions were as follows: 10 min at 95°C, followed by 40 cycles of amplification (15 seconds at 95°C and 1 min at 60 °C). Relative gene expression was calculated using the $-2^{\Delta\Delta Ct}$ method.

Table 4. Primer sequences used for real-time quantitative PCR.

Gene	Forward	Reverse
<i>CASP1</i>	5'-TGAGCAGCCAGATGGTAGAGC-3'	5'-TCACTTCCTGCCACAGACAT-3'
<i>CASP3</i>	5'-GTGAGGCGTTGTAGAAGAGTTTC-3'	5'-TGAGCAGGGCTCGCTAACTC-3'
<i>IL-1β</i>	5'-CTCTTCGAGGCACAAGGCAC-3'	5'-CAAGTCATCCTCATTGCCACTGT-3'
<i>IL-18</i>	5'-ACTGCCTGGACAGTCAGCAA-3'	5'-GCAGCCATCTTTATTCTGAGA-3'
<i>NLRP3</i>	5'-CAATGGGGAGGAGAAGGCGT-3'	5'-TCTGAACCCCACTTCGGCTC-3'
<i>S100A9</i>	5'-CTCGGCTTTGACAGAGTGCAA-3'	5'-CTGGTTCAGGGTGTCTGGGT-3'
<i>HMGB1</i>	5'-CCCTCCCAAAGGGGAGACAAA-3'	5'-AGAGGAAGAAGGCCGAAGGAG-3'
<i>TXNIP</i>	5'-GGGCCTCTGGGAACATCCTT-3'	5'-CTCGGGCGGTCAAGAAAAGC-3'
<i>POP1</i>	5'-TCGCGGAGGCTTGTCAATTCT-3'	5'-TCTTGGCGTGTTCCTTTCTTTTG-3'
<i>GAPDH</i>	5'-GAAGGTGAAGGTCGGACT-3'	5'-GAAGATGGTGATGGGATTTTC-3'

Colony formation assays. For MDS assays, 4 replicates of 3.5×10^5 BM-MNC/mL were resuspended in 10% autologous BM plasma and plated in MethoCult methylcellulose medium (Stemcell Technologies) supplemented with 1% v/v penicillin-streptomycin and 3 units/mL erythropoietin (Epo). CD33-IgG and MCC950 were added directly to the medium prior to plating. BFU-E, CFU-GM and CFU-GEMM colonies were scored using an inverted light microscope 14 days after plating. For assays of TF-1 cells expressing mutant *U2AF1*, 4 replicates of 3×10^4 cells/mL were plated in medium supplemented with 1% v/v penicillin-streptomycin and increasing concentrations of

ICTA. Colonies were counted 7 days after plating. For colony assays of primary *Sf3b1-K700E* mouse BM cells, BM cells were isolated from 4 mice per condition and 4 replicates of 3.5×10^5 BM cells/mL were plated in MethoCult with increasing concentrations of ICTA. Colonies were scored 14 days after plating.

ROS detection. ROS levels were determined using CellROX® Deep Red Reagent using the manufacturer's protocol (Life Technologies).

ICTA mouse treatment studies. ICTA was synthesized by the Drug Discovery Core Facility at H. Lee Moffitt Cancer Center & Research Institute. Six month old S100A9Tg (n=5) were dosed every other day with 50 mg/kg ICTA by oral gavage, for a total of eight weeks.

SRSF2 transfection of HEK293T cells. HEK293T cells were transfected by incubating 4 µg of *SRSF2* expression plasmid with 10 µL Lipofectamine® 2000 in 100 µL of Opti-MEM®I for 20 min at room temperature. This mixture was added to 70% confluent HEK293T cells with 2 mL Opti-MEM®I medium without serum in a 6 well plate. Cells were incubated at 37°C for 4 hr in a humidified chamber, then medium was replaced with 2 mL of DMEM with 10% FBS. Cells were treated with NAC and DPI 24 hr later, and subsequent analyses were carried out 48 hr following transfection.

Immunoblotting. *U2AF1-S34F*-expressing TF-1 cells were treated for 24 hr as indicated and harvested. Normal and lower-risk MDS BM-MNC were thawed and pelleted. Samples were lysed in 1x RIPA buffer (250 µM NaO₄, 2 µg/mL aprotinin, 2 µg/mL leupeptin, 0.2 µg/mL pepstatin A and 500 µM PMSF), and proteins were resolved by SDS-PAGE and transferred to PVDF membranes. Membranes were blocked for 30 min in 5% dry milk PBS-T solution (1x PBS, Tween®20), and incubated overnight with

the indicated antibody. For caspase-1 detection, the membrane and indicated antibody were incubated in TBS-T solution (1x TBS, 5% w/v BSA, 0.1% Tween®20). The next day, membranes were washed and secondary antibodies were incubated for 3 hr. Membranes were developed using ECL or ECL+ according to manufacturer's protocol (Thermo Scientific).

Immunoprecipitation. Following lysis, 200 µg of protein were incubated with 2 µg of the indicated antibody on ice for 2 hr. 50 µL of Protein A Agarose beads (EMD Millipore) were added to each sample, and bead-lysate slurries were incubated overnight at 4°C on a rotator. The next day, samples were washed with 500 µL of lysis buffer three times. Beads were dissociated at 95°C for 5 min following addition of sample buffer. Proteins were separated by SDS-PAGE and analyzed by immunoblotting.

ASC crosslinking. For normal and MDS BM-MNC, 10×10^6 cells were incubated overnight in autologous plasma. Cells were harvested, washed twice with 1x PBS and lysed with 100 µL of 1x RIPA buffer containing 1 tablet of Complete PhosStop (Roche Diagnostics, Indianapolis, IN) for 10 min on ice. Samples were spun down at 5,000 rpm for 10 min at 4°C, and cell lysates were removed and saved. Cell pellets were washed twice with 1x PBS, spun at 5,000 rpm for 10 min at 4 °C for each wash, and cells were resuspended in 100 µL of 1x PBS. Disuccinimidyl suberate (2 mM) (DSS, ThermoScientific) was then added, samples were incubated on a rotator for 30 min at room temperature, and then spun down at 5,000 rpm for 10 min at 4°C. The supernatant was removed and saved. 20 µL of sample buffer was added to the saved

lysate and supernatant samples, and the crosslinked pellet was resuspended in 30 μ L. Samples were boiled at 99°C for 5 min and proteins resolved by SDS-PAGE.

Next-generation sequencing and mutation identification. DNA was extracted from 40 total PB and BM samples. Target amplification of DNA for each sample was performed using the GeneRead DNAseq Panel PCR Kit V2 (Qiagen). Target regions of 26 common genes and genotype fingerprint regions were enriched using the Human Colorectal Cancer Panel according to manufacturer instructions. Samples were barcoded using NEXTflex-96™ DNA Barcodes (Bioo Scientific) and pooled in equal amounts before running on an Illumina MiSeq 2000. Sequence reads were aligned to the human genome using the GeneRead Targeted Exon Enrichment Panel Data Analysis (Qiagen). Sample data with synonymous variants, noncoding variants and variants present in databases of normal genomes (*i.e.*, ESP6500) were discarded. Remaining variants were filtered to contain more than 50x coverage and variant frequencies greater than 0.2. Of these variants, those that were present in COSMIC, or those not present in COSMIC but having SIFT scores ≤ 0.05 and Polyphen scores ≥ 0.909 , were considered candidate somatic mutations. Clinical and mutational patient characteristics are summarized in Table 5.

POP-1 overexpression. PYDC1 expression (RC211240) and empty control (PS100001) vectors were purchased from Origene Technologies, Inc. 5 μ g of plasmid was added to 6 million cells suspended in 100 μ L electroporation solution (Ingenio® Solution, Mirus Bio LLC.) and electroporated using Amaxa Nucleofector® program T-20 (Lonza Cologne AG, Germany). Cells were resuspended in 30 mL of appropriate

Table 5. Clinical and genotypic characteristics of sequenced patients. Bone marrow (BM) or peripheral blood (PB) samples were obtained for DNA extraction and sequencing. Patients were characterized according to WHO diagnostic classifications: (i) refractory anemia with ring sideroblasts (RARS); (ii) refractory anemia (RA); (iii) refractory cytopenia with multilineage dysplasia (RCMD); and (iv) refractory anemia with excess blasts (RAEB). Risk stratification was determined by IPSS classification: 0, low; 1, intermediate-1; 2, intermediate-2; 3, high risk. For each patient, genes without mutations are blank, and those harboring mutations are identified by a plus (+). Data that was unavailable is listed as NA.

Sample Number	Sample Type	Age	Sex	WHO Diagnosis	Cytogenetics	IPSS	ZRSR2	EZH2	BCORL1	RAD21	RUNX1	SF3B1	SRSF2	TET2	NRAS	TP63	JAK2	MPL	KRAS	ASXL1	UZAF1	DNMT3A	MLL	
1	BM	72	M	RARS	46,XY	0																		
2	BM	66	M	RA	46,XY	0																		
3	BM	71	F	RARS	46,XX,der(7)t(1;7)(q21;q22)[cp5]/46,XX[15]	0																		
4	BM	77	M	RARS	46,XY[20]	0																		
5	BM	77	M	RARS	46,XY[20]	0																		
6	BM	70	M	RARS	46,XY[20]	0																		
7	BM	65	M	RARS	46,XY[20]	0																		
8	BM	61	M	RCMD	46,XY[20]	0																		
9	BM	76	M	RCMD	46,XY[20]	0																		
10	BM	32	F	RA	46,XX[20]	0																		
11	PB	63	M	RCMD	46,XY	0																		
12	PB	64	F	RCMD	46,XX[20]	0																		
13	PB	63	F	RCMD	46,XX[20]	0																		
14	BM	75	M	RCMD-RS	46,XY,del(11)(q21)[20]	1																		
15	BM	69	F	RARS	46,XX[20]	1																		
16	BM	69	M	RCMD	46,XY[20]	1																		
17	BM	NA	NA	RAEB-2	46,XY,del(11)(q13q23)[cp20]	1																		
18	BM	78	M	RCMD	46,XY[20]	1																		
19	BM	80	M	RCMD	46,XY	1																		
20	BM	67	M	RAEB-1	46,XY[3]	1																		
21	BM	67	M	RCMD	47,XY+8 [15]/91XXY,-7 [5]	1																		
22	BM	71	M	RCMD	46,XY	1																		
23	BM	75	M	RCMD	46,XY[20]	1																		
24	BM	72	M	RCMD	NA	1																		
25	BM	45	M	RCMD	46,XY,del(20)(q11.2q12)[20]	1																		
26	PB	57	F	RCMD	46,XX	1																		
27	PB	73	F	RAEB-1	46,XX	1																		
28	PB	71	F	RA	46,XX	1																		
29	PB	70	M	RA	47,XY,+8[20]	1																		
30	BM	83	M	RAEB-1	46,X,der(Y)t(Y,-1)(q12;q10)[3]/46,XY,der(15)t(1;15)(q10;p11.2)[5]/46,XY,der(18)t(1;19)(q10;q23)[4]	2																		
31	BM	63	F	RAEB-2	46,XX	2																		
32	BM	83	M	RAEB-2	46,XY,del(7)(q22)[17]/46,XY[3]	2																		
33	PB	77	F	RAEB-2	46,XX,del(11)(q13q23)[3]/46,XX[17]	2																		
34	BM	68	M	RAEB-1	46,XY,add(5)(q11.2),add(8)(p12),del(11)(q21)-	3																		
35	BM	68	F	RAEB-2	13,add(14)(p11.2),-18,-19,-3mar[cp15]/46,XY[5] 47,XX,+8[20]	3																		
36	BM	69	M	RAEB-2	46,XY,der(4)t(4;5)(q25;q33),der(5)del(5)(q22q33) (4;5)(q25;q33)[17]/46,del(7)(p11.2),del(15)(q11.2q15)[cp3]	3																		
37	PB	74	M	RAEB-1	44,XY,del(5)(q12),add(7)(q36),-11,-13,-17, add(18)(q21),7add(20)(q12),-21,+2mar[cp20]	3																		
38	BM	NA	NA	NA	NA	NA																		
39	BM	74	M	RARS	45,X,-Y[20]	NA																		
40	BM	NA	NA	NA	NA	NA																		

growth medium. Expression and functional assays were performed 48 hr after transfection.

Statistical analyses. Data are expressed as means \pm standard error. Statistical analyses were carried out in Microsoft Excel using student's *t*-test. *P values <0.05 , ** $p<0.01$, and *** $p<0.001$ were considered to be statistically significant. Correlations were performed using chi-squared test for non-continuous variables and logistic regression for continuous variables. Comparisons of all pyroptotic parameters and somatic gene mutation variant allele frequency (VAF) were performed using chi-squared test for binary variables and Mann-Whitney and Kruskal-Wallis tests for continuous variables. These analyses were performed using SPSS software v22 (SPSS, Inc.).

CHAPTER 3

Pyroptosis of Erythroid Progenitors Accounts for the Erythroid Defect Characteristic of the 5q- Syndrome

Introduction

Identified in 1974, the 5q- syndrome represents a distinct subtype of myelodysplastic syndromes (MDS) characterized by a clonal, interstitial deletion of the long arm of chromosome 5 [del(5q)].³⁵ Patients with del(5q) MDS generally present with a progressive, macrocytic and hypoplastic anemia with normal or elevated platelet count and dysplastic, oligonuclear megakaryocytes,¹⁵⁰ suggesting that the major hematopoietic defect lies within the erythroid compartment. Accordingly, anemia remains the principal therapeutic challenge for patients with del(5q) MDS, as approximately 93% of patients will become transfusion-dependent in the course of their disease.¹⁵¹ Lenalidomide, a second-generation immunomodulatory drug (IMiD), is FDA-approved for del(5q) MDS and represents the standard of care for this subset of patients for over a decade.⁴⁵ Although approximately 83% of lenalidomide-treated patients respond quickly and become transfusion-independent, 50% of these will develop resistance within two or three years,³²² illustrating the need for novel therapeutic agents.

The commonly deleted region (CDR) in del(5q) MDS encompasses a gene-rich area on chromosome 5, spanning approximately 1.5-megabases or 40 genes.¹⁵⁴ Using array-based transcriptome analyses together with gene sequencing, haploinsufficiency

of select 5q- genes has been implicated in disease pathobiology, as no mutations have been described in the other allele to date.¹⁵⁵ Subsequent studies have confirmed that haploinsufficient loss of ribosomal protein S14 (*RPS14*), casein kinases 1A1 (*CSNK1A1*), TRAF-interacting protein with forkhead-associated domain B (*TIFAB*), diaphanous related formin 1 (*DIAPH1*, also known as *mDia1*) and the microRNAs (miR)-145 and -146a contribute to disease biology.^{117,160,169,171,173} Notably, haploinsufficient loss of these key target genes in murine models results in marrow-related changes characteristic of MDS, but more importantly, a severe and progressive anemia, confirming that the hemizygous loss of these genes contributes to the erythroid defect observed in MDS.

Mechanistically, these murine models implicate activation of p53 (*RPS14*), β -catenin (*CSNK1A1*) and the TLR4/TRAF6/NF- κ B signaling axis (miR-145/miR-146a, *TIFAB*, *DIAPH1*) in the pathobiology of del(5q) MDS. Although these individual mechanisms are well supported, a unifying mechanism by which loss of a diverse set of genes allows for del(5q) MDS development remains unclear. Recently, we reported that danger associated molecular pattern (DAMP) signals, like S100A9, and a diverse set of somatic gene mutations (including *U2AF1*, *SRSF2*, *SF3B1*, *ASXL1* and *TET2*) activate the redox-sensitive NLRP3 inflammasome pathway in non-del(5q) MDS.¹⁹⁹ NLRP3 inflammasome activation drives pyroptotic cell death and activation of β -catenin, effectively accounting for the central hallmarks of non-del(5q) disease, specifically significant cell death in the context of proliferation. Given that haploinsufficiency of a diverse set of genes results in del(5q) MDS, we hypothesized that activation of the NLRP3 inflammasome in these patients may function as a unifying pathobiologic

mechanism, akin to that observed in non-del(5q) disease. To this end, we investigated the role of NLRP3 inflammasome activation in two distinct murine models of del(5q) MDS, namely in the context of *Rps14* haploinsufficiency and concurrent loss of mDia1 and microRNA (miR)-146a, as well in a preliminary cohort of del(5q) patient specimens.

Results

***Rps14* haploinsufficiency induces NLRP3 inflammasome activation in erythroid progenitors but not HSPC.** NLRP3 inflammasome activation was assessed in a murine model of *Rps14* haploinsufficiency, whereby *Rps14* is conditionally reduced to haploinsufficient levels in hematopoietic cells, specifically.¹⁶⁷ Whole bone marrow (BM) cells were isolated from *Rps14* and wild type (WT) littermates. Using confocal fluorescence microscopy, NLRP3 activation was measured by the co-localization of cleaved or active (a)-caspase-1 and NLRP3 (Figure 33A). BM cells from *Rps14* mice evidenced robust formation of NLRP3 inflammasome complexes, warranting further investigation of NLRP3-mediated signaling events.

For one, NLRP3 activation results in pyroptosis, a caspase-1-dependent, pro-inflammatory cell death. Typical cell death markers, like annexin-V and propidium iodide (PI), cannot distinguish apoptosis from pyroptosis. Instead, these types of programmed cell death are reliably distinguishable by flow cytometry using the markers annexin-V, a-caspase-1 and a-caspase-3.¹⁹⁹ Specifically, apoptotic cells are defined as a-caspase-1⁻/a-caspase-3/7⁺/annexin-V⁺ and pyroptotic cells as a-caspase-1⁺/a-caspase-3/7⁺/annexin-V⁺. We first investigated pyroptosis of the hematopoietic stem and

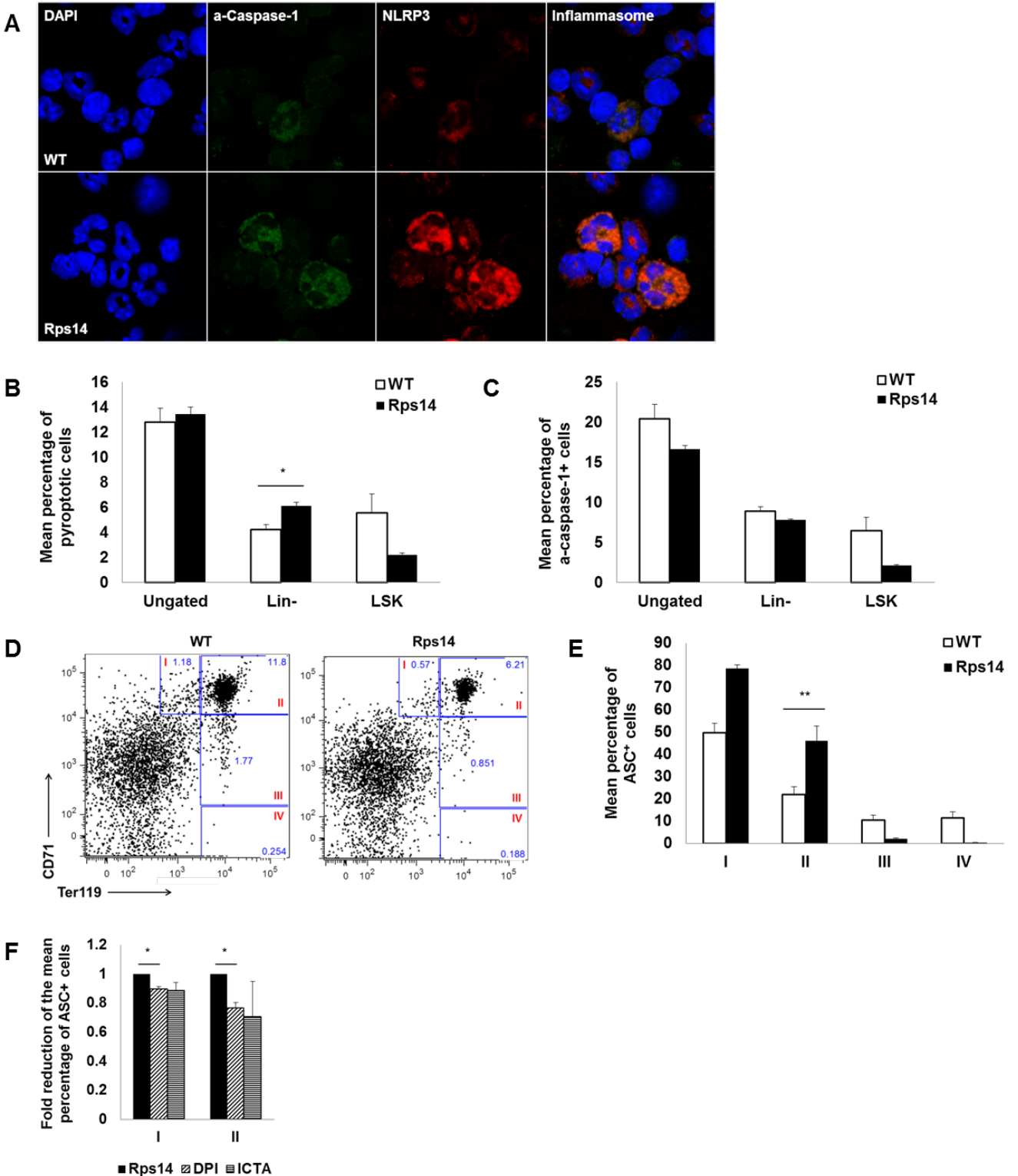


Figure 33. *Rps14* haploinsufficiency induces NLRP3 inflammasome activation in erythroid progenitors but not HSPC. Data are representative of BM cells harvested from WT (n=5) and *Rps14* haploinsufficient (n=7) mice. **(A)** Representative confocal fluorescence micrograph (2520x magnification) of active (a)-caspase-1 and NLRP3

expression in *Rps14* haploinsufficient BM cells versus WT controls. DAPI (blue), a-caspase-1 (green), NLRP3 (red); merged images show inflammasome formation. **(B-C)** The mean percentage of **(B)** pyroptotic and **(C)** a-caspase-1⁺ cells in ungated, lineage negative (Lin⁻) and LSK (Lin⁻Sca-1⁺c-Kit⁺) positive hematopoietic stem and progenitor (HSPC) cells. **(D)** Representative scatter plots of RI-RIV erythroid progenitor BM cells isolated from WT and *Rps14* haploinsufficient mice. Erythroid populations are gated according to expression of CD71 and Ter119. **(E)** Quantitation of inflammasome activation based on ASC oligomerization in BM RI-RIV erythroid progenitors from WT and *Rps14* haploinsufficient mice. **(F)** Fold reduction in the mean percentage of ASC⁺ RI and RIV erythroblasts following treatment of *Rps14* BM cells with DPI [2 μM] and ICTA [20 μM] for 24 hours *in vitro*. Error bars: SE, *p<0.05 and **p<0.01.

progenitor cell (HSPC) population in the *Rps14* haploinsufficient versus the WT bone marrow, as pyroptotic cell death of this population is characteristic of non-del(5q) MDS.¹⁹⁹ HSPC are identifiable in mice as LSK (Lin⁻Sca-1⁺c-Kit⁺) positive. Notably, the mean percentage of pyroptotic (Figure 33B) and a-caspase-1⁺ (Figure 33C) HSPC did not differ in *Rps14* haploinsufficient and WT mice.

Since this model is characterized by a progressive anemia,¹⁶⁷ we next investigated NLRP3 inflammasome activation in erythroid progenitors from four month-old mice. Maturation of murine erythroid precursors is readily assayed by flow cytometry through the differential expression of the markers CD71 and Ter119, which are also referred to as transferrin receptor protein 1 (TfR1) and lymphocyte antigen 76 (Ly76), respectively.¹⁶⁷ Four distinct erythroid populations can be characterized from least to most mature: RI, basophilic/early chromatophilic (CD71⁺Ter119⁺); RII, polychromatophilic (CD71^{intermediate}Ter119⁺); RIII, orthochromatophilic (CD71^{low}Ter119⁺); RIV, enucleated erythrocytes (CD71⁻Ter119⁺). Compared to WT controls, *Rps14* haploinsufficient mice demonstrated dramatic reductions in erythroid populations, particularly the RIII and RIV subsets (Figure 33D).

Notably, assessment of NLRP3 inflammasome oligomerization and activation can be measured by flow cytometric changes in fluorescence pulse height and area measurements of the inflammasome adaptor protein ASC.²⁹⁷ ASC functions to recruit pro-caspase-1 to the site of the inflammasome, whereby its incorporation and oligomerization forms mature complexes, effectively serving as a surrogate marker of NLRP3 activation.²⁹⁷ The percentage of ASC⁺ RI and RII erythroblasts was significantly increased in *Rps14* haploinsufficient BM compared to WT controls (Figure 33E), suggesting that NLRP3 inflammasome activation is manifest in early stage erythropoiesis. As NLRP3 is redox-sensitive and is activated in response to NADPH oxidase (NOX)-derived ROS, we next tested whether inhibition of NOX using diphenyleneiodonium (DPI) or inhibition of NLRP3 using the icariin derivative ICTA can reduce NLRP3 activation in the context of *Rps14* haploinsufficiency. Indeed, treatment with DPI or ICTA resulted in approximately 15-30% reduction in the proportion of ASC⁺ RI and RII erythroblasts, respectively (Figure 33F).

***Rps14* haploinsufficient erythroid precursors predominantly undergo pyroptosis.** Next, we aimed to investigate the extent of pyroptosis versus apoptosis in the context of *Rps14* haploinsufficiency within erythroid subsets. The mean percentage of pyroptotic RI-RIII erythroblasts was significantly increased in the *Rps14* haploinsufficient mice compared to normal controls (Figure 34A), whereas no significant differences were detected in the corresponding apoptotic cell fraction (Figure 34B). Accordingly, the mean percentage of a-caspase-1⁺ cells (Figure 34C) and a-caspase-1 mean fluorescent intensity (MFI) (Figure 34D) were significantly increased in *Rps14* RI-RIII erythroblasts compared to WT controls. Though a-caspase-3/7 MFI was

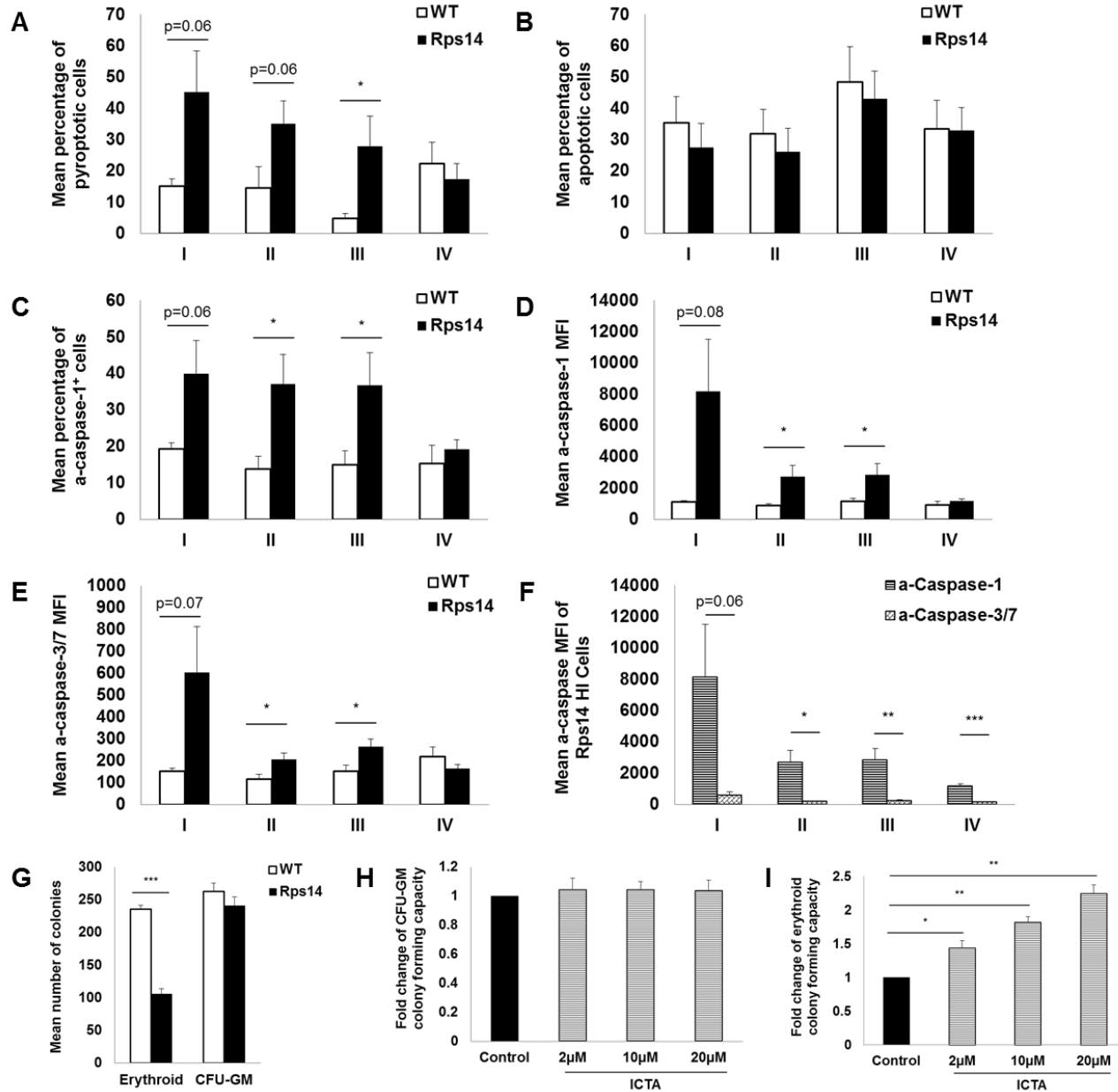


Figure 34. *Rps14* haploinsufficient erythroid progenitors predominantly undergo pyroptotic cell death. Data are representative of BM cells harvested from WT (n=5) and *Rps14* haploinsufficient (n=7) mice. **(A-C)** The mean percentage of **(A)** pyroptotic, **(B)** apoptotic and **(C)** a-caspase-1⁺ RI-RIV erythroid progenitors in *Rps14* haploinsufficient BM cells compared to WT controls. **(D-E)** Mean fluorescence intensity (MFI) of **(D)** a-caspase-1 and **(E)** a-caspase-3/7 in RI-RIV erythroblasts in *Rps14* haploinsufficient BM cells compared to WT controls. **(F)** Comparison of the mean percentage of a-caspase-1 versus a-caspase-3/7 MFI in the RI-RIV populations in *Rps14* haploinsufficient mice. **(G)** Colony forming capacity was assessed in BM cells isolated from WT versus *Rps14* haploinsufficient mice. The mean number of erythroid and granulocyte-macrophage (CFU-GM) colonies are represented. **(H-I)** Fold change of

(H) CFU-GM and **(I)** erythroid colony forming capacity in *Rps14* haploinsufficient BM cells treated with increased concentrations of the NLRP3 inhibitor ICTA [2-20 μ M]. Error bars: SE, * $p < 0.05$, ** $p < 0.01$ and *** $p < 0.001$.

significantly increased in *Rps14* BM RI-RIII compared to normal (Figure 34E), these data are not surprising as caspase-3 is activated downstream of caspase-1 during pyroptosis. More importantly, comparison of α -caspase-1 and α -caspase-3/7 MFI in *Rps14* haploinsufficient RI-RIV erythroblasts confirms that caspase-1 activation significantly exceeds caspase-3/7 activation in each erythroid population (RI-RIV) (Figure 34F). Together, these data demonstrate that attrition of erythroid progenitors in *Rps14* haploinsufficient BM is mediated primarily by pyroptotic cell death.

Lastly, the erythroid defect in the *Rps14* haploinsufficient mice was corroborated in colony formation assays, whereby a significant reduction in erythroid colony forming capacity was evidenced in the *Rps14* mice compared to WT controls (Figure 34G). No difference was observed in granulocyte/monocyte (CFU-GM) colony forming capacity (CFC) between the two groups (Figure 34G). Notably, while treatment of *Rps14* BM cells with ICTA had no effect on granulocyte-macrophage CFC (Figure 34H), ICTA treatment significantly increased erythroid CFC in a concentration-dependent manner (Figure 34I). These findings indicate that NLRP3 inhibition can rescue erythropoiesis in the context of *Rps14* haploinsufficiency, a mechanism distinct from the cytotoxic effect of lenalidomide in del(5q) MDS.

ROS and β -catenin activation are significantly increased in *Rps14* haploinsufficient erythroid progenitors. Somatic gene mutations are known to increase levels of reactive oxygen species (ROS), which like DAMP signals, can direct activation of β -catenin.³⁰²⁻³⁰⁵ In non-del(5q) MDS, we demonstrated that NOX-derived

ROS activate the redox-sensitive NLRP3 inflammasome, triggering not only pyroptosis, but also activation of β -catenin.¹⁹⁹ We hypothesized that the loss of genetic material through chromosome 5 deletion in del(5q) MDS would additionally trigger increased ROS production and consequent nuclear localization of β -catenin. The percentage of ROS⁺ cells (Figure 35A) and ROS MFI (Figure 35B) were significantly increased in the BM of *Rps14* mice compared to controls. Investigation of the RI-RIV erythroid lineage populations illustrated that the early RI erythroblasts in the *Rps14* haploinsufficient mice had a significant increase in the percentage of ROS⁺ cells (Figure 35C) and ROS MFI (Figure 35D) versus normal controls. No significant differences were observed in the RII-RIV populations. Notably, treatment of *Rps14* haploinsufficient BM cells with DPI or ICTA resulted in a dramatic reduction in the percentage of ROS⁺ cells (Figure 35E) and ROS MFI (Figure 35F), demonstrating that inhibition of NOX or NLRP3 can reduce ROS. Lastly, nuclear localization of β -catenin, representative of its transcriptionally active form, was assessed using confocal fluorescence microscopy in BM cells harvested from WT mice, *Rps14* haploinsufficient mice or *Rps14* cells treated with DPI. Whereas *Rps14* haploinsufficient cells evidenced significant nuclear localization of β -catenin, nuclear expression was negligible in WT littermates (Figure 35G). Importantly, treatment of *Rps14* cells with DPI reduced active β -catenin to levels similar to WT controls (Figure 35G). These data demonstrate that ROS and β -catenin activation are increased in the context of *Rps14* haploinsufficiency in a NOX- and NLRP3-dependent manner.

Concurrent loss of *mDia1* and *miR-146a* results in pyroptotic cell death of erythroid precursors. Next, we investigated an alternative murine model of del(5q)

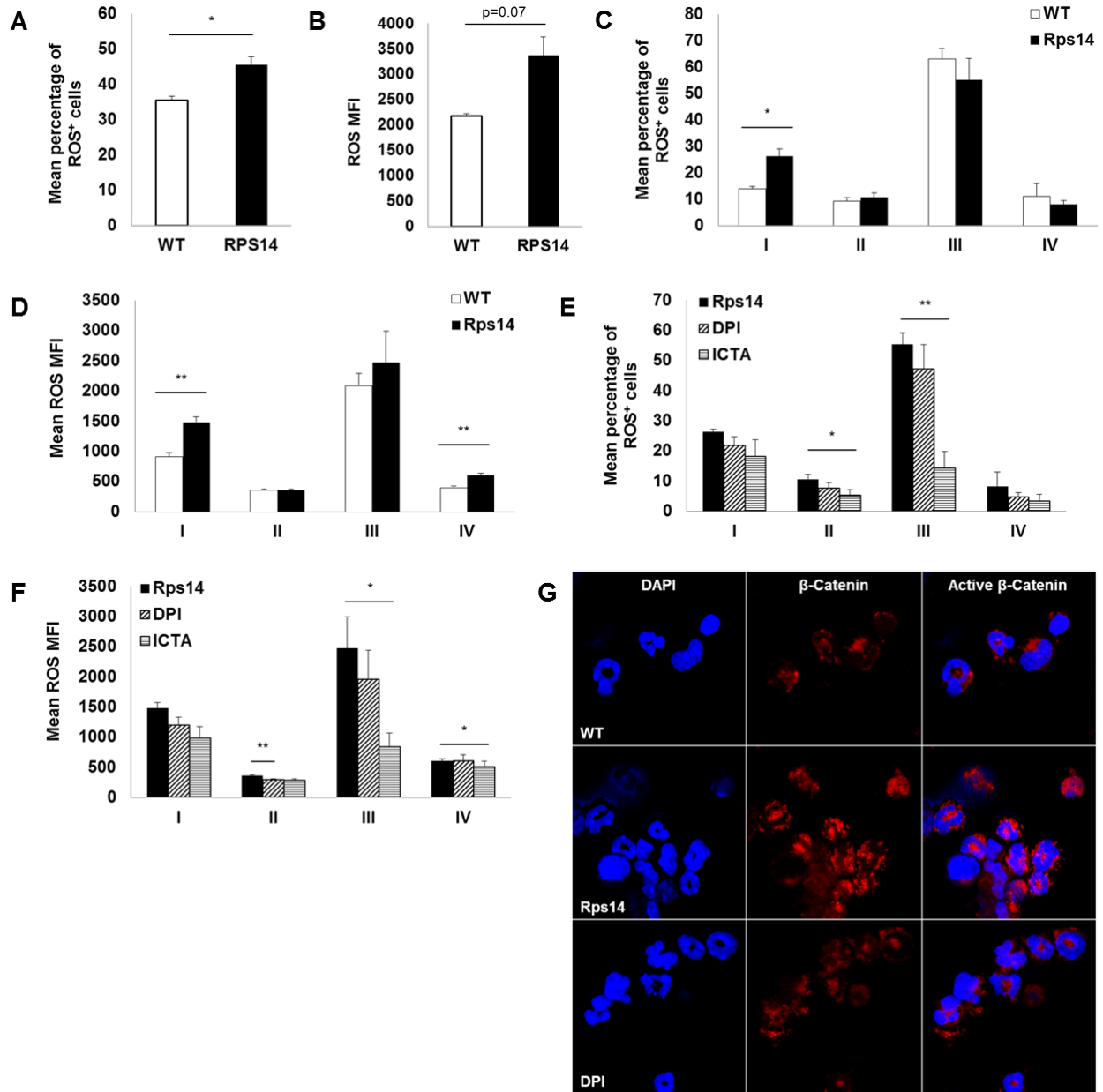


Figure 35. ROS and β -catenin activation are markedly increased in erythroid progenitors in the context of *Rps14* haploinsufficiency. Data are representative of BM cells harvested from WT (n=5) and *Rps14* haploinsufficient (n=7) mice. **(A-B)** Mean **(A)** percentage and **(B)** MFI of ROS in ungated WT and *Rps14* haploinsufficient BM cells. **(C-D)** Mean **(C)** percentage and **(D)** MFI of ROS in RI-RIV erythroid progenitors from WT and *Rps14* haploinsufficient BM cells. **(E-F)** Mean **(E)** percentage and **(F)** MFI of ROS in RI-RIV erythroid progenitors from *Rps14* haploinsufficient BM cells treated for 24 hours with DPI [2 μ M] and ICTA [20 μ M]. **(G)** Representative micrograph (2520x magnification) of β -catenin expression in BM cells from WT, *Rps14* haploinsufficient or *Rps14* cells treated with DPI [2 μ M] for 24 hours. DAPI (blue), β -catenin (red); merged images show nuclear β -catenin localization. Error bars: SE, *p<0.05 and **p<0.01.

MDS, namely the concurrent loss of both *mDia1* and *miR-146a*, two genes located within or near the CDR and haplodeficient in del(5q) MDS. Loss of these 5q- genes results in hypersensitivity to the TLR4/TRAF6/NF- κ B signaling axis, which is deregulated in both non-del(5q) and del(5q) MDS.^{117,174} More specifically, *mDia1* has known roles in innate immune cell activation.¹⁷⁴⁻¹⁷⁶ Loss of *mDia1* results in a significant increase of the TLR4 co-receptor CD14 on granulocytes, sensitizing cells to TLR4 ligands such as LPS and resulting in aberrant innate immune activation.¹⁷⁴ Furthermore, as *miR-146a* targets TNF receptor-associated factor 6 (TRAF6) for degradation, haploinsufficiency in del(5q) MDS results in increased expression of this TLR4 signaling intermediate.¹¹⁷ Increased expression of TRAF6 drives abnormal activation of NF- κ B, reduced blood cell counts and bone marrow failure.¹¹⁷ Together, the dual loss of *mDia1* and *miR-146a* represents an applicable model of del(5q) disease.

First, following isolation of BM cells from double wild-type (DWT) and double knockout (DKO) mice, NLRP3 inflammasome formation was assessed via ASC oligomerization in RI-RIV erythroid progenitors by flow cytometry. The percentage of ASC⁺ cells was increased in ungated BM cells from DKO mice compared to DWT, but more importantly in the RI and RII erythroblast populations (Figure 36A), suggesting an aberrant activation of the NLRP3 inflammasome in early erythropoiesis. Accordingly, pyroptotic cell death was dramatically increased in the RI-RIV erythroid populations in the DKO mice compared to DWT controls (Figure 36B). The extent of apoptosis was not different between the DWT and DKO RI-RIV populations (Figure 36C). Indeed, when the percentage of pyroptotic versus apoptotic RI-RIV DKO cells was compared, the pyroptotic fraction significantly exceeded the corresponding apoptotic cell fraction

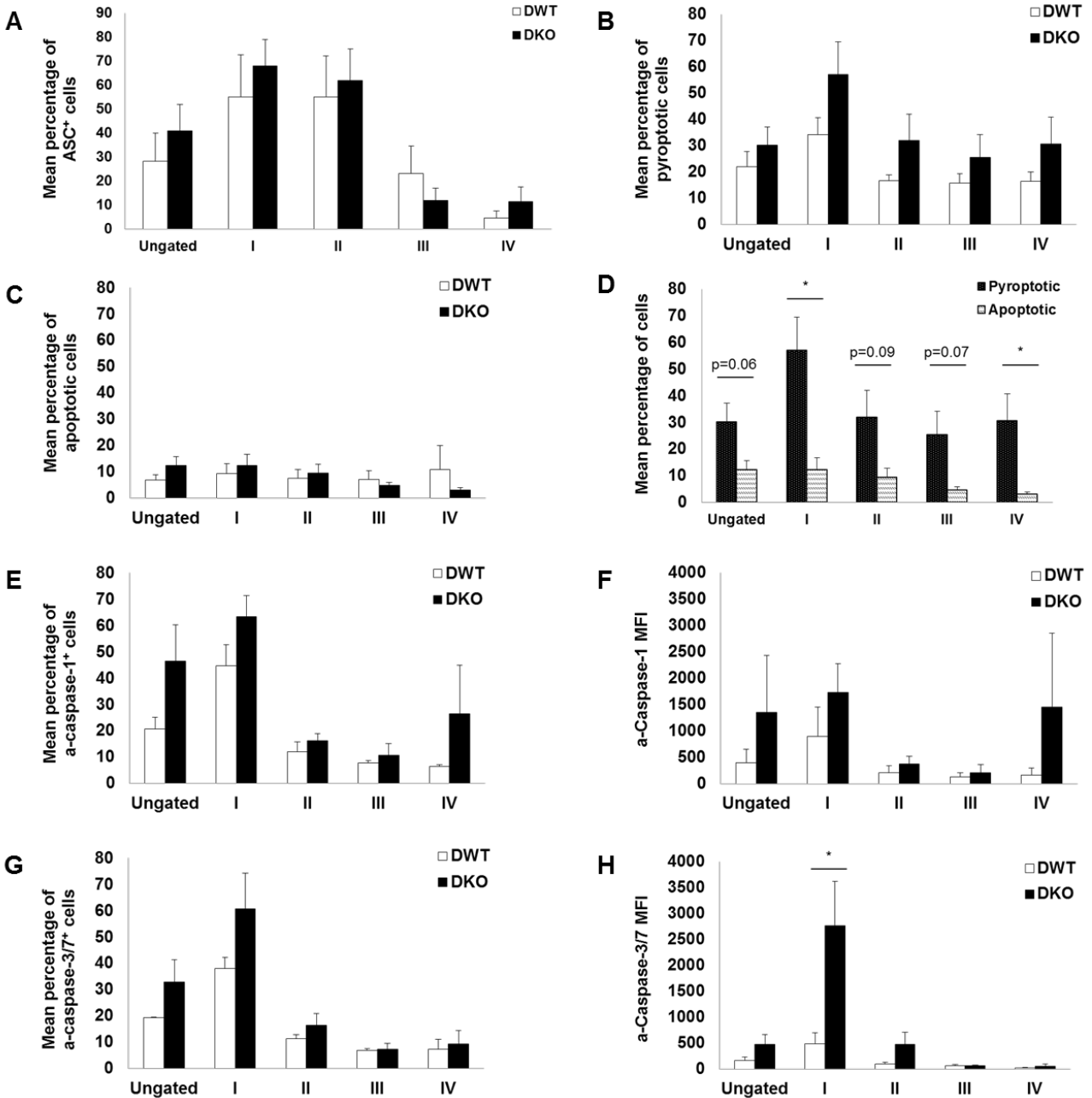


Figure 36. Concurrent loss of *mDia1* and *miR-146a* results in pyroptotic cell death of erythroid progenitors. Data are representative of BM cells harvested from DWT (n=3) and DKO (n=5) mice. **(A)** Quantitation of inflammasome activation based on ASC oligomerization in ungated BM cells and RI-RIV erythroid progenitors from DWT and DKO mice. **(B-C)** The mean percentage of **(B)** pyroptotic and **(C)** apoptotic ungated BM cells and RI-RIV erythroid progenitors from DWT and DKO mice. **(D)** Comparison of the mean percentage of pyroptotic versus apoptotic ungated BM and RI-RIV cells isolated from DKO mice. **(E-F)** Mean **(E)** percentage of a-caspase-1⁺ cells and **(F)** a-caspase-1 MFI in ungated BM and RI-RIV cells from DWT and DKO mice. **(G-H)** Mean **(G)**

percentage of a-caspase-3/7⁺ cells and **(H)** a-caspase-3/7 MFI in ungated BM and RI-RIV cells from DWT and DKO mice. Error bars: SE and *p<0.05.

(Figure 36D). These data suggest that DKO mice predominantly undergo a pyroptotic, not apoptotic, cell death. In support of these findings, the percentage of a-caspase-1⁺ cells (Figure 36E) and a-caspase-1 MFI (Figure 36F) were profoundly increased in RI DKO erythroblasts compared to DWT controls. While the percentage of a-caspase-3/7⁺ cells (Figure 36G) and a-caspase-3/7 MFI (Figure 36H) were additionally increased in the RI DKO cells, this likely occurs downstream of caspase-1 activation in accordance with execution of the pyroptotic program. Taken together, these data illustrate that early erythroid progenitors from DKO mice undergo pyroptotic cell death, with marked activation of caspase-1.

ROS and β -catenin activation are significantly increased in *mDia1/miR-146a* double knockout mice. We hypothesized that dual loss of *mDia1* and *miR-146a* would increase ROS generation with activation of β -catenin. Accordingly, the mean percentage of ROS⁺ cells (Figure 37A) and ROS MFI (Figure 37B) were significantly increased in ungated BM cells from DKO mice compared to DWT controls. ROS were also significantly increased across the RI-RIV erythroid populations in the DKO mice compared to controls (Figure 37A and 37B), indicating that deletion of these genes increases ROS production in the DKO mice. Moreover, nuclear localization of β -catenin was significantly increased in the BM of DKO mice compared to DWT controls (Figure 37C). Therefore, these data corroborate findings of NLRP3 inflammasome-induced ROS generation and β -catenin activation following the loss of central 5q- genes.

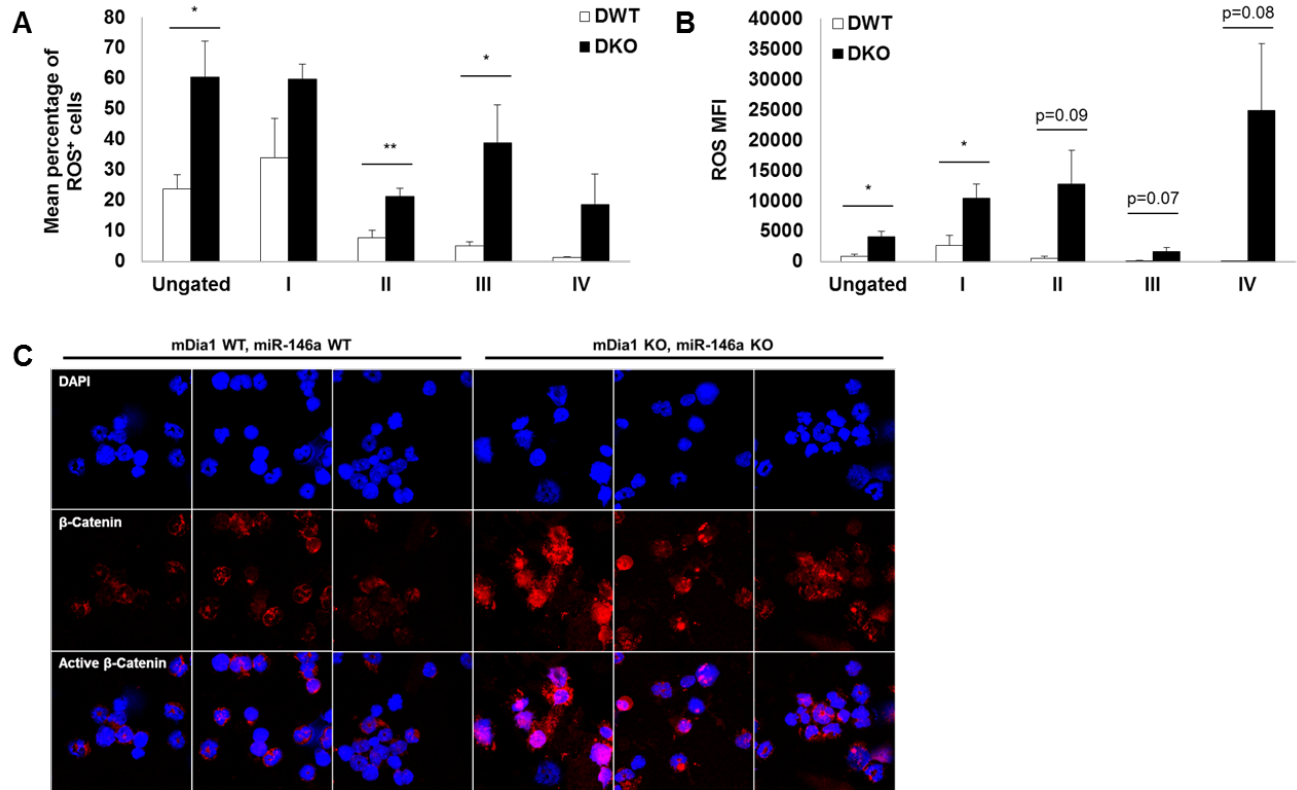


Figure 37. ROS and β -catenin activation are significantly increased with dual loss of *mDia1* and *miR-146a*. Data are representative of BM cells harvested from DWT (n=3) and DKO (n=5) mice. **(A-B)** Mean **(A)** percentage and **(B)** MFI of ROS in ungated BM cells and RI-RIV erythroid progenitors isolated from DWT and DKO mice. **(C)** Representative micrograph (2520x magnification) of β -catenin expression in BM cells from DWT and DKO mice. DAPI (blue), β -catenin (red) and merged images show nuclear β -catenin localization. Error bars: SE and *p<0.05.

NLRP3 inflammasome inhibition restores effective erythropoiesis in del(5q)

MDS. NLRP3 inflammasome formation and activation was markedly increased in a preliminary cohort of del(5q) MDS patient BM-MNC specimens (n=2) compared to normal controls (n=6) (Figure 38A). Importantly, short-term treatment of del(5q) BM-MNC with 10 μ M ICTA significantly reduced inflammasome activation, as well as protein expression of both a-caspase-1 and NLRP3 (Figure 38A). To determine if NLRP3 inflammasome inhibition could improve hematopoiesis, colony forming capacity was assessed after plating del(5q) MDS BM-MNC in autologous BM plasma and increasing

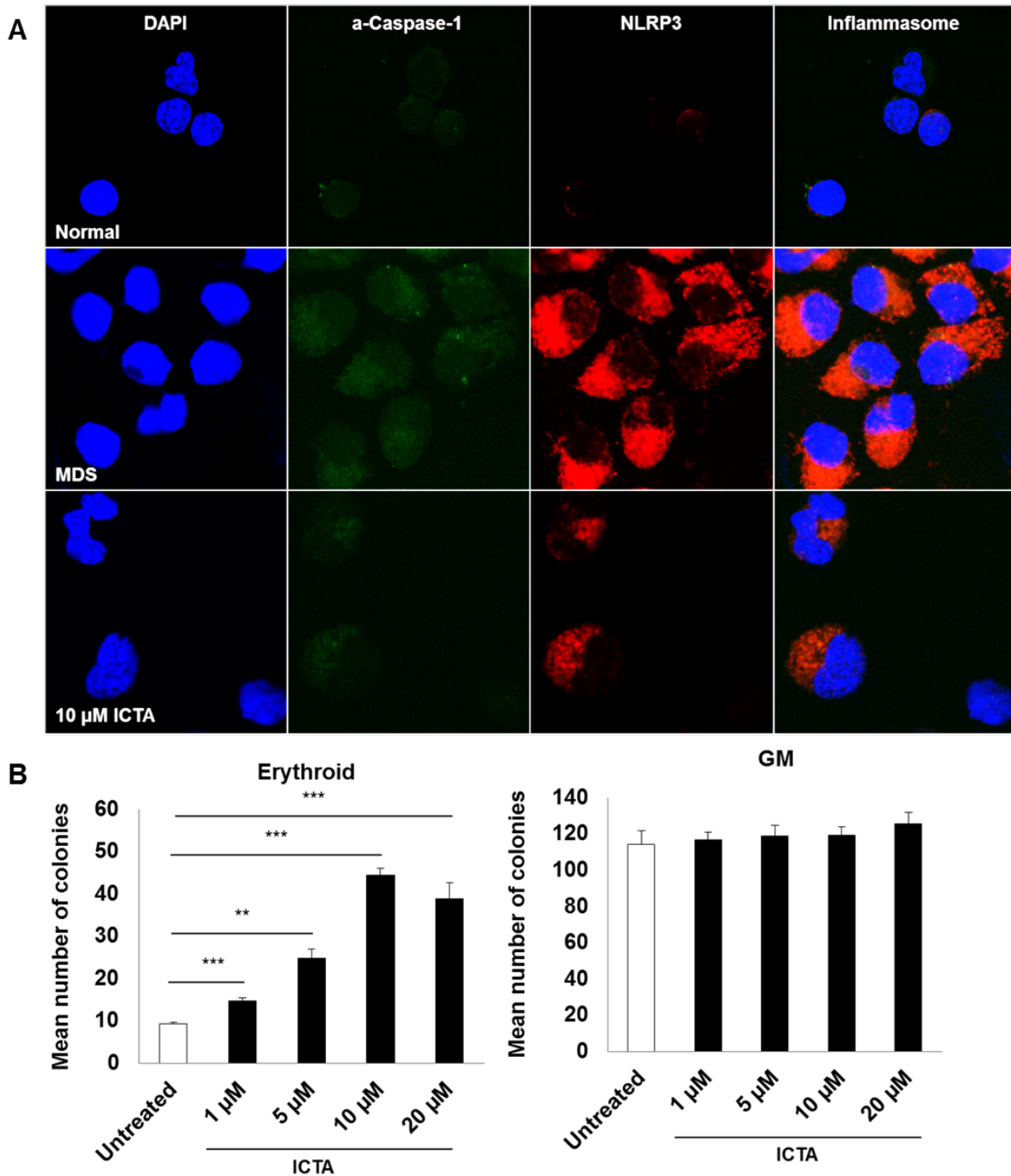


Figure 38. NLRP3 inflammasome inhibition restores effective erythropoiesis in patients with del(5q) MDS. (A) Representative confocal fluorescence micrograph (2520x magnification) of active (a)-caspase-1 and NLRP3 expression in normal BM-MNC (n=6) compared to del(5q) MDS BM-MNC (n=2) untreated or treated with 10 μM ICTA for 24 hours. DAPI (blue), a-caspase-1 (green), NLRP3 (red); merged images show inflammasome formation. **(B)** Colony forming capacity was assessed in BM-MNC from a del(5q) MDS specimen treated with increasing concentrations of ICTA. Error bars: SE, *p<0.05, **p<0.01 and ***p<0.001.

concentrations of ICTA. Whereas ICTA treatment had no effect on granulocyte-macrophage (GM) CFC, ICTA treatment significantly increased erythroid CFC in a concentration-dependent manner (Figure 38B). These data are consistent with findings observed in the *Rps14* haploinsufficiency model (Figure 33H and 33I), and indicate that inflammasome inhibition restores effective erythropoiesis in primary MDS specimens.

Discussion

We recently reported that central hallmarks of the non-del(5q) MDS phenotype, including cell death in the context of proliferation, can be attributed to aberrant activation of the NLRP3 inflammasome complex.¹⁹⁹ This complex functions to drive caspase-1-dependent pyroptotic cell death of hematopoietic stem and progenitor cells (HSPC) and the simultaneous activation of β -catenin, which can augment cell proliferation and survival. In this way, activation of β -catenin supports propagation and proliferation of the MDS clone. Of note, both recurrent somatic gene mutations and over-expressed DAMP proteins, like S100A9, trigger activation of the redox-sensitive NLRP3 inflammasome pathway.¹⁹⁹ Most important, neutralization of S100A9 and inhibition of the NLRP3 inflammasome complex was able to augment normal hematopoiesis in non-del(5q) MDS patients, suggesting novel strategies for therapeutic intervention.¹⁹⁹

To date, the ineffective erythropoiesis characteristic of del(5q) MDS, resulting in severe and progressive hypoplastic anemia, has been attributed to cooperative haploinsufficiency of a number of genes encoded in the deleted portion of chromosome 5q, including, but not limited to, *RPS14*, *DIAPH1* (*mDia1*) and *miR-146a*.^{117,160,169,171,173}

We hypothesized that the widespread loss of genetic material on chromosome 5q in del(5q) MDS would share a similar pathobiological mechanism of NLRP3 inflammasome activation as is observed in non-del(5q) disease. Accordingly, this hypothesis was corroborated in two distinct murine models of del(5q) MDS, namely in the context of *Rps14* haploinsufficiency and the dual loss of *mDia1* and *miR-146a*, as well as in primary del(5q) MDS specimens. While NLRP3 inflammasome activation and pyroptotic cell death of hematopoietic stem and progenitor cells (HSPC) was not observed in these models, this was not surprising. We anticipated that defects in hematopoiesis would largely be restricted to the erythroid compartment, as the 5q-syndrome is characterized by severe macrocytic anemia. Indeed, in both models, the early erythroid progenitor populations, identified by CD71 and Ter119 staining as the RI and RII subsets, demonstrated significant NLRP3 inflammasome formation with caspase-1 activation. These populations predominantly underwent pyroptosis, rather than apoptotic cell death. Additionally, NLRP3 inflammasome activation was robustly increased in primary del(5q) specimens. ICTA-mediated inflammasome inhibition not only reduced inflammasome activation and protein expression of a-caspase-1 and NLRP3, but significantly improved erythroid colony forming capacity. Taken together, our findings suggest that the aberrant activation of NLRP3 in early erythroid progenitors prevents their maturation to mature, enucleated erythrocytes, effectively driving the anemia that is clinically manifest in MDS.

Moreover, the two murine models demonstrated that ROS are significantly increased in the early RI and RII erythroblast populations. ROS, which are increased with somatic gene mutation and in the context of gene loss, function to activate the

NLRP3 inflammasome, triggering pyroptosis. Additionally, ROS can increase nuclear localization of β -catenin, which occurs through an NADPH oxidase (NOX)-dependent mechanism. In each model, ROS were dramatically reduced in the RI and RII erythroid progenitor populations following NOX or NLRP3 pharmacological inhibition. Active β -catenin, which was increased in BM cells harboring genetic loss compared to WT controls, was significantly reduced following NOX inhibition. These data support the hypothesis that the del(5q) clone is propagated through activation of β -catenin, which occurs through a NOX-dependent mechanism.

Murine models of del(5q) MDS have described mechanisms of pathobiology, including implication of p53 activation, β -catenin and TLR4 signaling. Here, our findings illustrate a common mechanism of pathobiology that is shared in non-del(5q) and del(5q) MDS, specifically activation of the NLRP3 inflammasome complex. Our data indicate that loss of central 5q- genes, irrespective of the gene in question, triggers NLRP3 activation and leads to pyroptosis and β -catenin activation. These data unify previous mechanisms of del(5q) pathobiology, as reduced expression of each gene is linked to activation of the NLRP3 inflammasome complex. Foremost, *RPS14* haploinsufficiency results in the erythroid-specific accumulation of the tumor suppressor protein p53, contributing to erythroid progenitor cell death and the development of anemia.¹⁶³ These data were corroborated in an *Rps14* haploinsufficient murine model of MDS, which additionally demonstrated that the danger associated molecular pattern (DAMP) proteins S100a8 and S100a9 were significantly up-regulated in haploinsufficient erythroid progenitors.¹⁶⁷ S100A9 is also increased intracellularly in BM-MNC and in the plasma of non-del(5q) MDS patients, which we demonstrated triggers

NLRP3 inflammasome activation, pyroptosis and nuclear localization of β -catenin.¹⁹⁹ Also, ribosomal stress not only activates p53 but also the NLRP3 inflammasome.³²³ Moreover, hypersensitivity to TLR4 signaling in del(5q) MDS results in aberrant activation of NF- κ B, which is known to drive transcriptional expression of NLRP3. In this way, loss of *mDia1* and *miR-146a*, which augment TLR4 signaling and responsiveness, would additionally increase NLRP3 expression. ROS generation resulting from genetic loss would serve as a secondary signal for NLRP3 activation, triggering aberrant inflammasome activation. Lastly, loss of casein kinase 1 alpha 1 (*CSNK1A1*), a model not studied in this manuscript, results in increased β -catenin activation in del(5q) MDS, as CK1 α is a central regulator of the β -catenin destruction complex and thereby of β -catenin nuclear translocation.¹⁶⁹ Here, we not only show that β -catenin activation is increased in murine models of del(5q) disease other than CK1 α haploinsufficiency, but also that activation occurs by an NOX-dependent mechanism. More specifically, induction of NOX-derived ROS additionally triggers β -catenin activation with concurrent activation of NLRP3. Together, biological events resulting from *Rps14*, *mDia1* and *miR-146a* haploinsufficiency can mechanistically be explained by NLRP3 inflammasome activation.

Finally, identification of the NLRP3 inflammasome complex as a driver of the del(5q) MDS phenotype allows for novel avenues for therapeutic intervention. This pathway is likely activated irrespective of the degree of genetic loss (size of the 5q chromosomal deletion), and therefore represents a very attractive therapeutic target with translational potential.

Methods

MDS patient specimens. MDS patients were consented on IRB approved protocols and recruited from the Eastern Cooperative Oncology Group (ECOG) E2905 trial (NCT00843882).

Mice. *Rps14* haploinsufficient and WT BM cells, and tibias and femurs from *mDia1/miR-146a* DWT and DKO mice were generously provided by Drs. Benjamin Ebert and Rebekka Kramann-Schneider and Dr. Peng Ji, respectively.

Reagents and cells. DPI was purchased from Sigma. ICTA was synthesized by the Chemical Biology Core Facility located at H. Lee Moffitt Cancer Center and Research Institute. Active caspase-1 and caspase-3/7 were detected using FAM-FLICA™ Caspase-1 (#98), FLICA-660 Caspase-1 (#9122), FLICA-660 Caspase-3 & 7 (#9125) and SR-FLICA™ Caspase-3 & 7 (#932) assay kits (ImmunoChemistry Technologies). NLRP3 antibodies were purchased from Abcam (ab4207) and β -catenin antibodies from BD Biosciences (610154).

Immunofluorescence confocal microscopy. Following isolation, BM cells were stained with 30x FAM-FLICA® Caspase-1 solution for 2 hr at 37°C at a ratio of 1:30, washed and cytospun at 450 rpm for 5 min. Slides were fixed using BD Cytofix Fixation Buffer (BD Biosciences) at 37°C for 10 min, and then washed with PBS. Cells were permeabilized with 0.1% Triton X-100/2% BSA in PBS for 15 min at room temperature, washed and then blocked using 2% BSA in PBS for 30 min at room temperature. Following washing, cells were incubated with the appropriate primary antibody overnight (1:400 for NLRP3, 1:20 for β -catenin) at 4°C. After 24 hr, cells were washed with PBS and incubated with the appropriate secondary antibodies (1:500) for 1 hr at room

temperature. Slides were washed and covered with ProLong Gold Antifade Reagent with DAPI and a coverslip (Life Technologies).

Cell death flow cytometry assay. *Rps14* haploinsufficient and WT BM cells were resuspended in 1x PBS and stained with 30x FAM-FLICA™ Caspase-1 and FLICA-660 Caspase-3 & 7 reagents at a 1:30 dilution for 30 min at 37°C. *mDia1/miR-146a* double KO and DWT cells were stained following a similar protocol, but rather with FLICA-660 Caspase-1 and SR-FLICA™ Caspase-3 & 7 reagents. Cells were washed with 1x PBS. For RI-RIV erythroid progenitor staining, cells were stained for surface receptors using CD71:BV510 (563112) and Ter119:BUV395 (563827) at a 1:20 dilution for 30 min at 4°C (BD Biosciences). For HSPC staining, cells were stained for surface receptors using lineage cocktail:V450 (561301), CD117:BUV395 (564011) and Ly-6A/E:BV786 (563991) under the same surface receptor staining protocol aforementioned (BD Biosciences). Following washing, cells were resuspended in 1x binding buffer. For *Rps14* and *mDia1/miR-146a* DKO experiments, cells were stained with annexin-V:PE (559763) and annexin-V:BV421 (563973), respectively, at a 1:20 dilution for 15 min at room temperature (BD Biosciences). The final volume was brought to 400 µL with 1x binding buffer. Sample acquisitions were made on a BD LSR II flow cytometer using FACSDiva software. To establish compensation settings, anti-Rat and Anti-Hamster Ig κ/Negative Control Compensation Particles Set was used (BD Biosciences). Data were analyzed using FlowJo 9.7.5 software (FlowJo, LLC).

ROS detection. ROS were detected using CellROX® Deep Red Reagent according to the manufacturer's protocol (Life Technologies).

ASC oligomerization. Cell pellets were permeabilized by resuspending in 1 mL of prewarmed BD Permeabilization Buffer III and incubating on ice for 30 min (BD Biosciences). Cells were washed twice with staining buffer, resuspended in 1x PBS and stained with rabbit anti-ASC primary antibodies at a 1:1500 dilution (Santa Cruz, sc-22514-R). Cells were incubated for 90 min at 37°C, and then washed. Cells were resuspended in staining buffer, stained for surface receptors and concurrently stained with secondary anti-rabbit antibodies at a 1:1500 dilution for 30 min at 4°C. Sample acquisitions were carried out using a BD LSR II flow cytometer and FACSDiva software.

Colony formation assays. 4 replicates of 3.5×10^5 BM cells/mL per mouse were plated in MethoCult methylcellulose medium with recombinant cytokines (Stemcell Technologies) supplemented with 1% v/v penicillin-streptomycin and increasing concentrations of ICTA, as indicated. Erythroid and CFU-GM colonies were manually scored fourteen days after plating using an inverted light microscope.

Statistical analyses. All data are reported as means \pm standard error. Microsoft Excel was used to carry out statistical analyses, specifically student's *t*-test. *P values <0.05, **p<0.01, and ***p<0.001 were considered to be statistically significant.

CHAPTER 4

NLRP3 Inflammasome-Derived ASC Specks are a Diagnostic Biomarker for Myelodysplastic Syndromes (MDS)

Introduction

Pyroptosis, or caspase-1-dependent cell death, is mediated by the formation of NLRP3 inflammasome complexes, which function as redox-sensitive, cytosolic sensors of danger signals.²²⁷ Upon stimulation, NLRP3 undergoes a conformational change fostering homotypic pyrin domain interaction with the adaptor protein ASC [apoptosis-associated speck-like protein containing a caspase activation and recruitment domain (CARD)], triggering ASC nucleation and polymerization to create large, cytoplasmic filaments.²³⁹ Exposure of the ASC^{CARD} on the filament surface serves as a docking platform for recruitment of pro-caspase-1 monomers that are activated by proximity-induced autocatalysis to initiate proteolytic processing of pro-caspase-1. The ASC speck formed by ASC filament clusters creates abundant caspase-1 activation sites, thereby acting as an inflammasome signal amplification mechanism.^{239,324}

ASC specks, or aggregated clusters of ASC filaments, are approximately one micron in diameter in size and are released into the extracellular milieu following cytolysis and execution of pyroptosis.²⁹⁸ Released ASC specks retain catalytic activity, whereby they continue to recruit and mature pro-caspase-1 and its substrate IL-1 β .²⁹⁸ Notably, neighboring cells may phagocytose released ASC specks, which subsequently function as a scaffold for ASC polymerization and nucleation in the recipient cell.²⁹⁸ In

this way, ASC specks function as danger signals which propagate inflammation not only in the extracellular space, but additionally in cells of the surrounding stroma.²⁹⁸

Myelodysplastic syndromes (MDS) are characterized by ineffective hematopoiesis resulting from caspase-1-dependent, pyroptotic cell death.¹⁹⁹ All too frequently, the pathologic diagnosis of MDS is not straightforward owing in part to the vast disease heterogeneity, quality of bone marrow aspirates for cytological examination and reliance on morphologic assessment, which is vulnerable to observer discrepancies.^{42,92,325} Additionally, a substantial number of hematologic conditions share features of MDS, particularly overlap syndromes like chronic myelomonocytic leukemia (CMML). As such, MDS is perceived to have a high diagnostic error rate, typically between 30-40%, highlighting the potential value and impact of an MDS-specific biomarker.

Importantly, co-localization of NLRP3 and active (a)-caspase-1 by confocal fluorescence microscopy confirmed selective activation of the NLRP3 inflammasome in MDS compared to other bone marrow malignancies.¹⁹⁹ As ASC specks are readily quantified by flow cytometry,²⁹⁸ we hypothesized that bone marrow (BM) or peripheral blood (PB) plasma-derived ASC specks may serve as a biologically rational biomarker for the diagnosis of MDS.

Results

ASC specks are significantly increased in MDS. For flow cytometric analyses, the gate for ASC specks was determined using the secondary only control (Figure 39A).

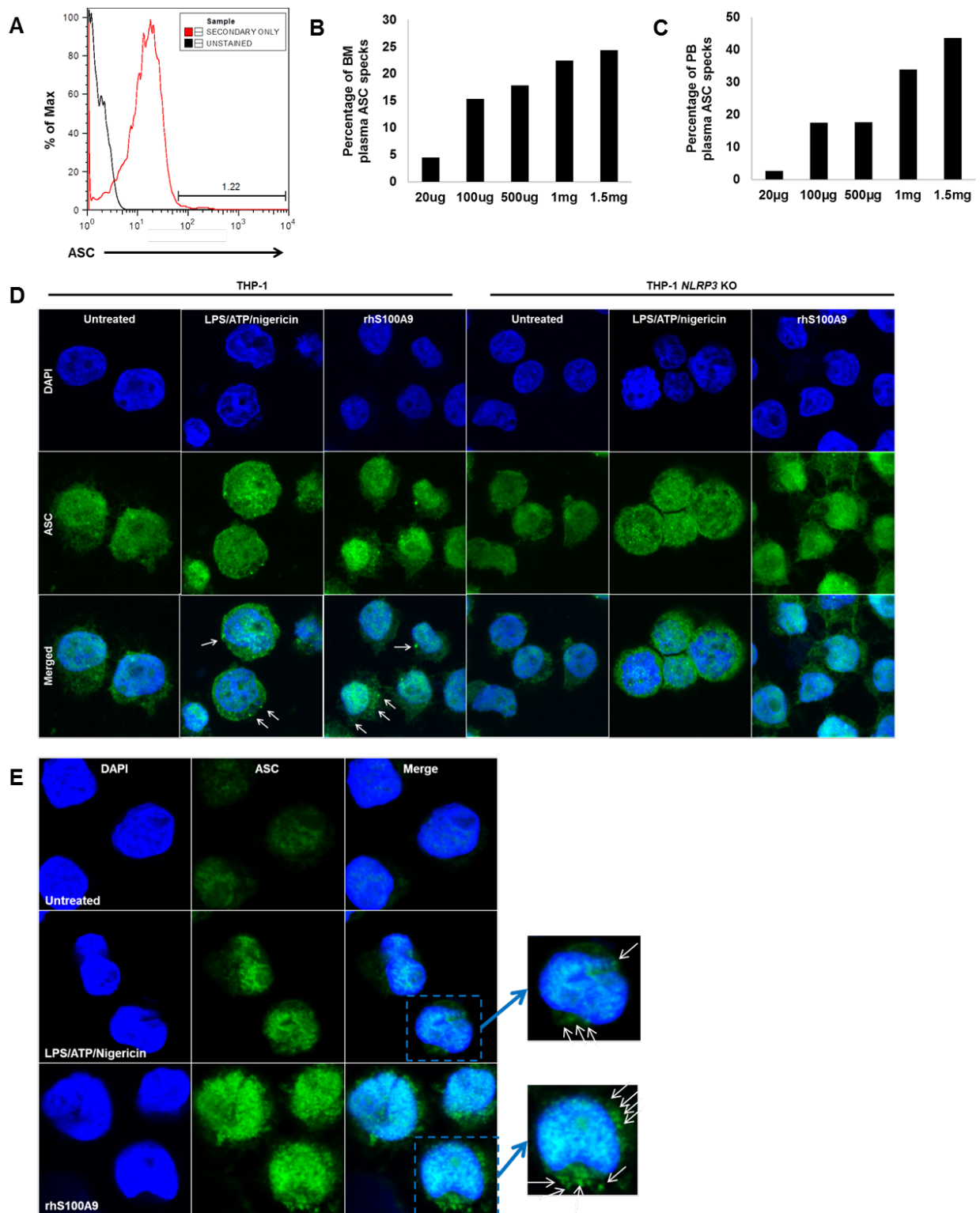


Figure 39. The percentage of plasma ASC specks increases with protein concentration. (A) Representative histogram of ASC speck staining, which is gated according to the secondary only antibody control. **(B-C)** Increasing BM and PB plasma protein concentrations were assessed for the mean percentage of **(B)** BM and **(C)** PB

plasma-derived ASC specks. **(D-E)** Representative confocal fluorescence micrograph (4725x and 4725x magnification, respectively) of ASC speck expression in **(D)** THP-1 and **(E)** U937 cells that were untreated, or treated with 100 ng/mL LPS, 5 mM ATP and 5 μ M nigericin or 5 μ g/mL rhS100A9 for 24 hours. DAPI (blue), ASC (green) and merged images show ASC specks.

The percentage of BM and PB plasma-derived ASC specks increased linearly with protein concentration, confirming assay specificity (Figure 39B and 39C). Next, the ability of the ASC antibody employed to detect ASC specks was further validated using confocal fluorescence microscopy in THP-1 parental, *NLRP3* knockout (KO) THP-1 and U937 cells. THP-1, *NLRP3* KO and U937 cells were treated with 100 ng/mL LPS, 5 mM ATP and 5 μ M nigericin or 5 μ g/mL recombinant human S100A9 (rhS100A9) for 24 hours, which is known to induce NLRP3 inflammasome activation.¹⁹⁹ In all three cell lines, LPS/ATP/nigericin and rhS100A9 treatment induced expression of ASC as a result of priming (Figure 39D and 39E). Whereas the formation of ASC specks, evidenced by the detection of punctate ASC staining, was induced in THP-1 parental and U937 cells, specks did not form in *NLRP3* KO cells, confirming NLRP3-dependence (Figure 39D and 39E).

To further assess ASC speck expression, we measured the percentage of ASC specks in a preliminary cohort of normal donors (n=3) and MDS patients (n=6). ASC specks were significantly increased ($p=0.015$) in MDS BM plasma compared to normal donors (Figure 40A), prompting validation of speck expression by confocal microscopy. Cellular expression of ASC specks in MDS compared to healthy donors confirmed that MDS BM-mononuclear cells (BM-MNC) display both increased ASC protein expression, consistent with inflammasome priming, and greater punctate staining, confirming ASC speck formation (Figure 40B). Furthermore, to assess ASC speck expression in MDS,

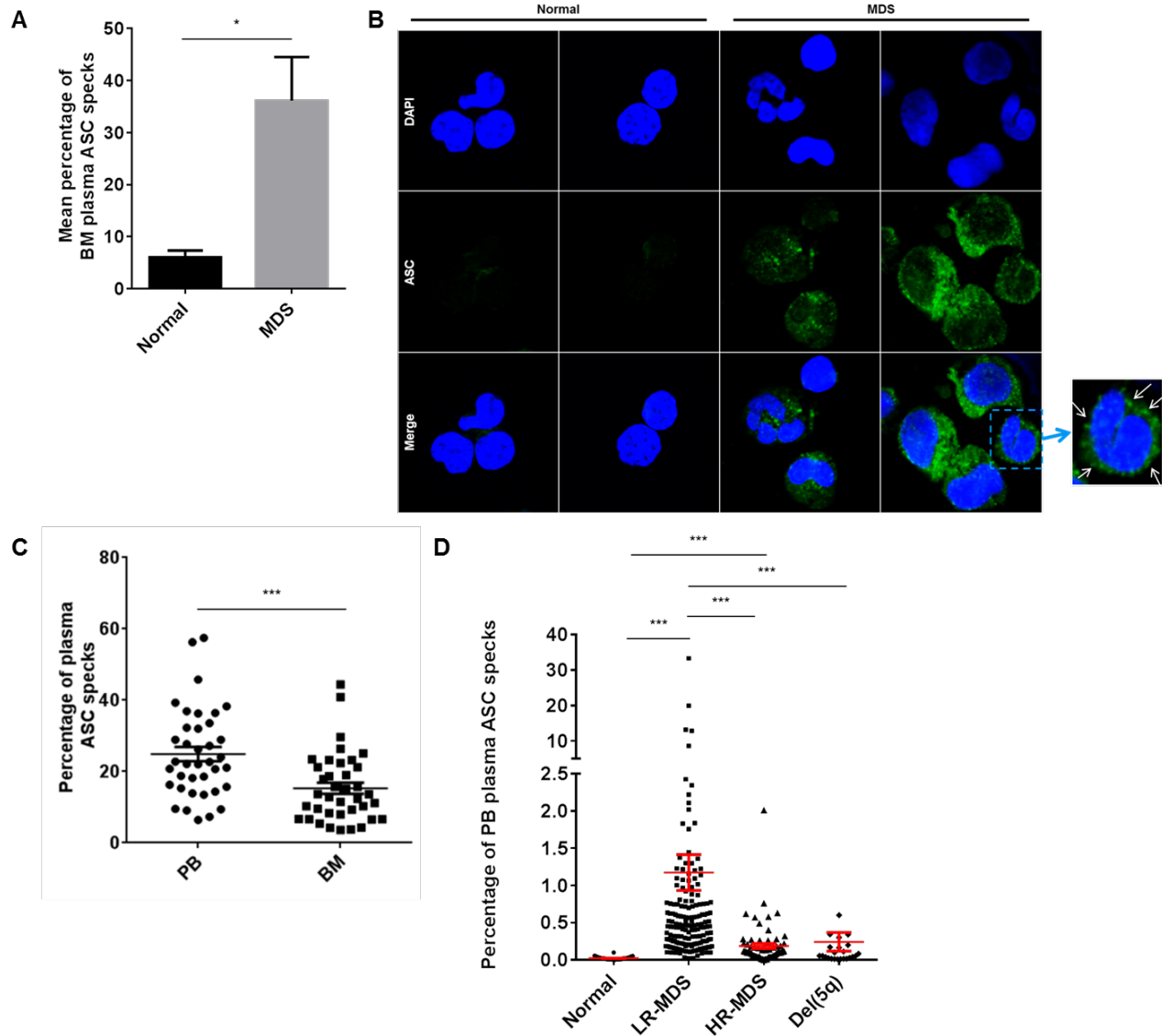


Figure 40. ASC specks are significantly increased in MDS and may have prognostic value. (A) The percentage of ASC specks in BM plasma samples is significantly greater in MDS specimens (n=6) than normal donors (n=3) (p=0.015). (B) Representative confocal fluorescence micrograph (2520x magnification) of ASC speck expression in BM-MNC from normal donors and lower-risk MDS patients. DAPI (blue), ASC (green), merged images and white arrows show and point to ASC specks, respectively. (C) The percentage of ASC specks in matched PB and BM plasma samples (n=38) is significantly greater in PB plasma (p=3.5x10⁻⁴). (D) The percentage of PB plasma-derived ASC specks was investigated in normal, healthy donors (n=40) and patients of lower-risk (n=180), higher-risk (n=69) and del(5q) (n=24) MDS. Error bars: SE, *p<0.05 and ***p<0.001.

we first measured the percentage of ASC specks in the BM of matched PB and BM plasma samples (n=38). The percentage of PB plasma-derived ASC specks in MDS significantly exceeded the percentage of BM plasma-derived specks ($p=3.5 \times 10^{-4}$) (Figure 40C). Given that PB samples are more readily accessible, and if sensitive and specific, could serve as a diagnostic screen determining the need for a BM aspirate and biopsy, further investigation of PB plasma was prioritized. The percentage of PB plasma-derived ASC specks was significantly increased in lower-risk (n=180) and higher-risk (n=69) MDS compared to normal, healthy donors (n=40, $p=2.8 \times 10^{-32}$ and 2.4×10^{-3} , respectively), whereas no significant difference was observed between normal donors and patients with deletion 5q [del(5q)] MDS (n=24) (Figure 40D). Given that del(5q) MDS is characterized by erythroid hypoplasia arising from p53 activation, these findings are not surprising, and perhaps suggest that molecular genetic testing on PB may be complimentary, and further enhance specificity. Importantly, the percentage of ASC specks was significantly increased in lower-risk compared to higher-risk MDS ($p=5.6 \times 10^{-14}$) (Figure 40D), which is consistent with our previous report illustrating that lower-risk MDS, but not higher-risk disease, is characterized by excessive NLRP3 inflammasome activation and pyroptotic cell death.¹⁹⁹ Together, these data suggest that PB plasma-derived ASC specks may have diagnostic utility and serve as a surrogate marker reflecting the extent of pyroptosis in hematopoietic cells and prognostic risk.

The percentage of PB plasma-derived ASC specks is a diagnostic biomarker for MDS. To determine the utility of PB plasma-derived ASC specks as a specific MDS diagnostic biomarker, ASC speck percentage was determined in plasma from patients with varied hematologic malignancies. As hyperglycemia stimulates

NLRP3 inflammasome assembly and activation, we measured plasma glucose levels by colorimetric assay to adjust for this potentially confounding variable and to optimize the assay. The data provided in Table 6 summarize the number and types of samples investigated, the mean percentage of ASC specks normalized to plasma glucose concentration and corrected for volume, and the statistical significance comparison of each respective sample group compared to normal, healthy donors (n=40) and MDS patients (n=294). The glucose-adjusted speck percentage in lower-risk MDS remained significantly elevated versus normal donors ($p=3.7 \times 10^{-6}$) (Figure 41). Although the corrected percentage of ASC specks was significantly greater in higher-risk MDS compared to normal donors ($p=6.7 \times 10^{-6}$), the glucose-adjusted speck percentage in lower-risk patients significantly exceeded the percentage in higher-risk samples ($p=7.6 \times 10^{-5}$). Compared to normal, healthy donors (n=40), ASC specks were significantly greater in patients with LR-MDS ($p=3.7 \times 10^{-6}$), HR-MDS ($p=6.7 \times 10^{-6}$), secondary acute myeloid leukemia (AML, $p=9.9 \times 10^{-3}$), essential thrombocythemia (ET, $p=0.04$), multiple myeloma (MM, $p=0.01$) and large granular lymphocytic leukemia (LGL, $p=0.02$) (Figure 41). Importantly, MDS samples displayed significantly greater corrected percentage of PB plasma-derived ASC specks compared to each hematologic malignancy investigated, including *de novo* AML ($p=6.5 \times 10^{-4}$), secondary AML ($p=4.3 \times 10^{-4}$), chronic myelomonocytic leukemia (CMML, $p=1.6 \times 10^{-6}$), chronic lymphocytic leukemia (CLL, $p=1.6 \times 10^{-6}$), chronic myeloid leukemia (CML, $p=2.1 \times 10^{-6}$), acute lymphoblastic leukemia (ALL, $p=2.1 \times 10^{-6}$), ET ($p=1.4 \times 10^{-4}$), polycythemia vera (PV, $p=7.9 \times 10^{-5}$), MM ($p=3.9 \times 10^{-5}$) and LGL ($p=5.1 \times 10^{-5}$) (Figure 41).

Table 6. Mean percentage of PB plasma-derived ASC speck values across sample cohorts. The mean percentage of ASC specks is normalized to plasma glucose concentration and corrected for volume. Statistical significance was determined by comparing normal, healthy donors (n=40) and MDS specimens (n=294) to each respective sample group. (ns, not significant)

	n	Mean ± SE	P-value compared to normal, healthy	P-value compared to MDS
Normal, healthy	40	0.02 ± 3.0x10 ⁻³	-----	1.3x10 ⁻⁶
LR-MDS	180	1.17 ± 0.24	3.7x10 ⁻⁶	-----
HR-MDS	69	0.19 ± 0.03	6.7x10 ⁻⁶	-----
MDS total	294	0.90 ± 0.18	1.2x10 ⁻⁶	-----
Del(5q) MDS	24	0.24 ± 0.13	ns	2.7x10 ⁻³
Acute myeloid leukemia (AML), <i>de novo</i>	16	0.25 ± 0.17	ns	6.5x10 ⁻⁴
Acute myeloid leukemia (AML), secondary	26	0.16 ± 0.05	9.9x10 ⁻³	4.3x10 ⁻⁴
Chronic myelomonocytic leukemia (CMML)	20	0.03 ± 0.01	ns	1.6x10 ⁻⁶
Chronic lymphocytic leukemia (CLL)	50	0.03 ± 4.4x10 ⁻³	ns	1.6x10 ⁻⁶
Chronic myeloid leukemia (CML)	52	0.04 ± 0.01	ns	2.1x10 ⁻⁶
Acute lymphoblastic leukemia (ALL)	7	0.15 ± 0.09	ns	2.1x10 ⁻⁴
Essential thrombocythemia (ET)	20	0.17 ± 0.07	0.04	1.4x10 ⁻⁴
Polycythemia vera (PV)	20	0.12 ± 0.06	ns	7.9x10 ⁻⁵
Multiple myeloma (MM)	20	0.14 ± 0.04	0.01	3.9x10 ⁻⁵
Large granular lymphocytic leukemia (LGL)	19	0.15 ± 0.05	0.02	5.1x10 ⁻⁵
Type 2 diabetes (T2D)	25	0.04 ± 0.01	ns	1.8x10 ⁻⁶

Notably, the NLRP3 inflammasome is activated in adipose-based macrophages in type 2 diabetes (T2D).³²⁶ In a cohort of T2D patients without cancer, the glucose-adjusted speck percentage was significantly lower than levels detected in MDS specimens ($p=1.8 \times 10^{-6}$) (Figure 41). Although ASC specks were about 2-fold greater in T2D patients compared to normal, healthy donors, the change was not significant. Therefore, although NLRP3 inflammasome assembly may not be MDS-specific, these data together indicate that NLRP3 inflammasome-driven pyroptosis and release of ASC

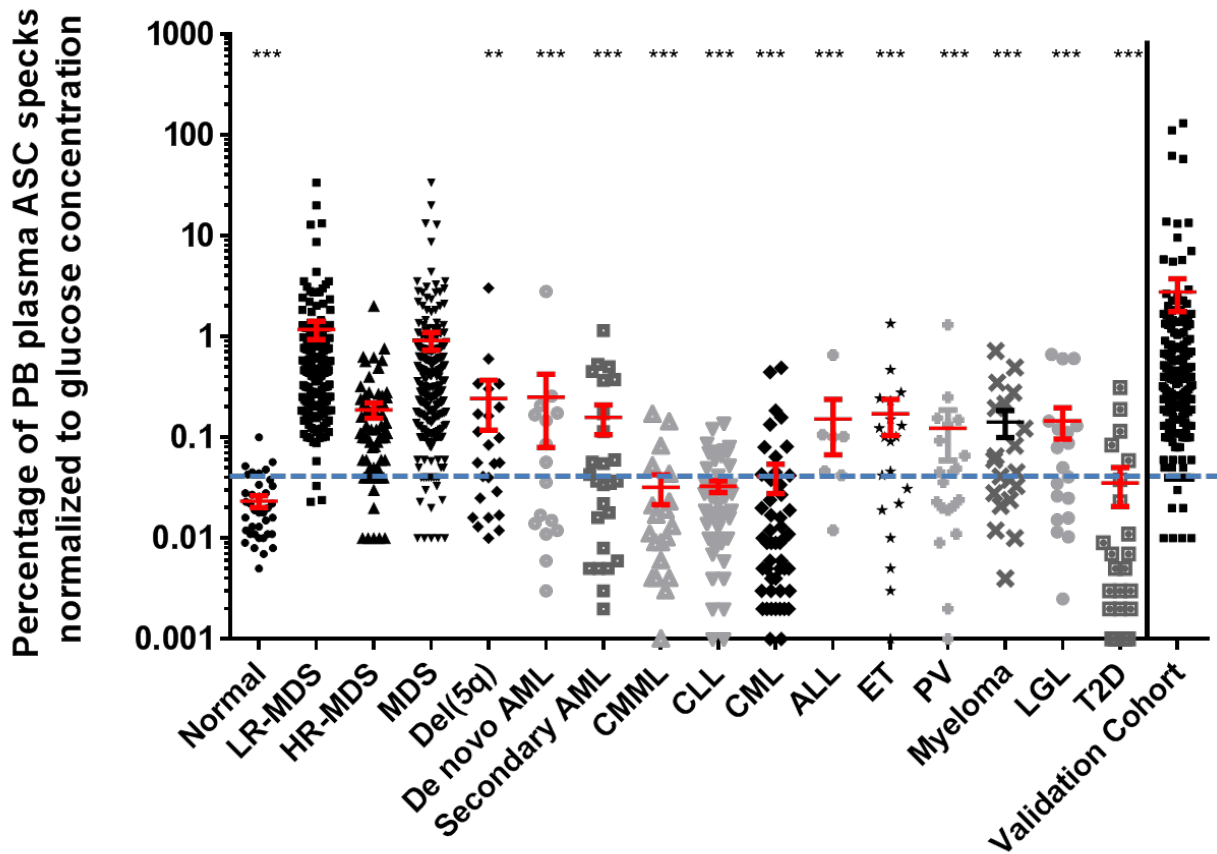


Figure 41. The percentage of glucose-adjusted, PB plasma-derived ASC specks is specific for MDS. Glucose-adjusted ASC speck percentage in normal donors (n=40), lower-risk MDS (n=180), higher-risk MDS (n=69), all MDS (n=249), del(5q) MDS (n=24), *de novo* acute myeloid leukemia (AML, n=16), secondary AML (n=26), chronic myelomonocytic leukemia (CMML, n=20), chronic lymphocytic leukemia (CLL, n=50), chronic myeloid leukemia (CML, n=52), acute lymphoblastic leukemia (ALL, n=7), essential thrombocythemia (ET, n=20), polycythemia vera (PV, n=20), multiple myeloma (myeloma, n=20), large granular lymphocytic leukemia (LGL, n=19) and type 2 diabetes (T2D, n=25). A cutoff of 0.039 was selected to minimize total misclassification error. At this cutoff point, the biomarker achieves 95% sensitivity and 82% specificity in classifying MDS from normal donors. In an external validation cohort (MDS, n=196), the biomarker achieved 96% sensitivity at the 0.039 cutoff point. Error bars: SE, **p<0.01 and ***p<0.001.

specks is specific for MDS in steady state, in the absence of infection. Moreover, these findings suggest that the corrected percentage of PB plasma-derived ASC specks may be a useful biomarker for the diagnosis of MDS.

Furthermore, statistical analyses were performed to determine a rational cutoff point for the diagnostic biomarker. Specifically, sensitivity, specificity, positive predictive value (PPV) and negative predictive value (NPV) were used to evaluate accuracy. A cutoff of 0.039 was selected to minimize total misclassification error, namely the sum of the false positive and false negative rate. With this cutoff, the PPV and NPV are 96%, and 76%, respectively, and the biomarker achieves 95% sensitivity and 82% specificity in classifying MDS from normal donors, other BM malignancies and T2D. These parameters were validated in an independent dataset (n=196) in which the biomarker achieved 96% sensitivity at the 0.039 cutoff point, confirming the high sensitivity of the biomarker (Figure 41).

Specks may serve as a biomarker index of ineffective hematopoiesis. We hypothesized that ASC specks reflect the magnitude of medullary pyroptosis and therefore may additionally serve as a PB biomarker of response to treatment in lower-risk MDS patients. To this end, we interrogated the glucose-adjusted percentage of ASC specks in the PB plasma of lenalidomide-treated, responding and non-responding patients at the time of screening and week 16. Among responders, 4 and 8 patients had del(5q) and non-del(5q) MDS, respectively. The corrected percentage of ASC specks decreased a mean of 63% (range 60-69%) at week 16 in the del(5q) patients, indicative of a significant reduction ($p=7.2 \times 10^{-5}$) (Figure 42A). Additionally, ASC specks decreased a mean of 21% (range 3-77%) at week 16 in the non-del(5q) responders (Figure 42B), findings that are consistent with prior clinical studies showing that suppression of the del(5q) clone with lenalidomide treatment more robustly restores effective erythropoiesis as measured by maximum rise in hemoglobin and response duration.^{61,159,327}

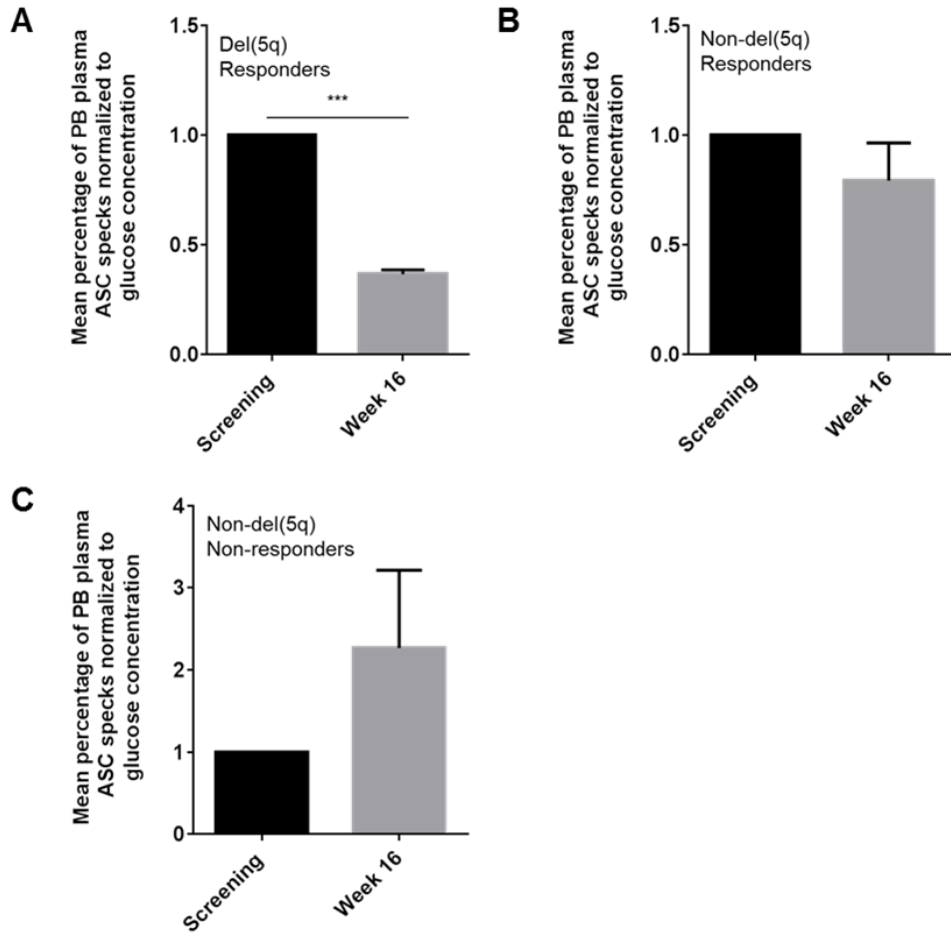


Figure 42. PB plasma-derived ASC specks are a response biomarker to lenalidomide treatment. (A-B) Mean corrected ASC speck percentage at the time of screening and week 16 in lenalidomide-treated, **(A)** del(5q) MDS (n=4) responding patients and **(B)** non-del(5q) MDS (n=8) responding patients. **(C)** Mean corrected ASC speck percentage at the time of screening and week 16 in lenalidomide-treated, non-del(5q) MDS (n=24) non-responding patients. Error bars: SE, ***p<0.01.

Conversely, the percentage of specks increased 2.4-fold at week 16 in non-responding patients (Figure 42C). Importantly, these findings were corroborated in two independent datasets of lenalidomide-treated, lower-risk MDS patients (Figure 43). Specifically, the corrected percentage of ASC specks decreased in responding patients and increased in non-responders over the course of treatment. The corrected percentage of ASC specks did not predict for treatment response to erythropoietin stimulating agents (ESAs) in LR-

MDS patients or to hypomethylating agents (HMAs) in HR-MDS patients (Figure 44). These data suggest that specks may serve as a biomarker index of ineffective hematopoiesis and perhaps of early response to immunomodulatory drug therapy.

Discussion

Recently, we reported that NLRP3 inflammasome-driven pyroptotic cell death is a hallmark of lower-risk MDS, driven by somatic gene mutations and danger associated molecular pattern (DAMP) signals, such as S100A9.¹⁹⁹ Pyroptosis culminates in cytolysis, with release of pro-inflammatory cytokines, DAMP signals and ASC specks, which together exacerbate inflammation in bystander cells. ASC specks, themselves an extracellular DAMP signal, are only one micron in diameter but retain catalytic activity, evidenced by their ability to catalyze maturation of pro-caspase-1 and pro-IL-1 β within the microenvironment.²⁹⁸ Since specks are only secreted upon cytolysis, they function as a surrogate marker of the magnitude of hematopoietic pyroptotic cell death. Given that pyroptosis is a hallmark of lower-risk MDS, we hypothesized that ASC specks may be a biologically rationale biomarker for the diagnosis of MDS.

To this end, we optimized a flow cytometry assay for the detection of extracellular ASC specks in BM and PB plasma. To start, the percentage of ASC specks increased linearly in both BM and PB plasma with increasing concentrations of protein. The ability of the primary ASC antibody employed to detect ASC specks was corroborated by confocal fluorescence microscopy, whereby expression of ASC and specks increased in THP-1 and U937 cells treated with either rhS100A9 or LPS/ATP/nigericin. Notably, the

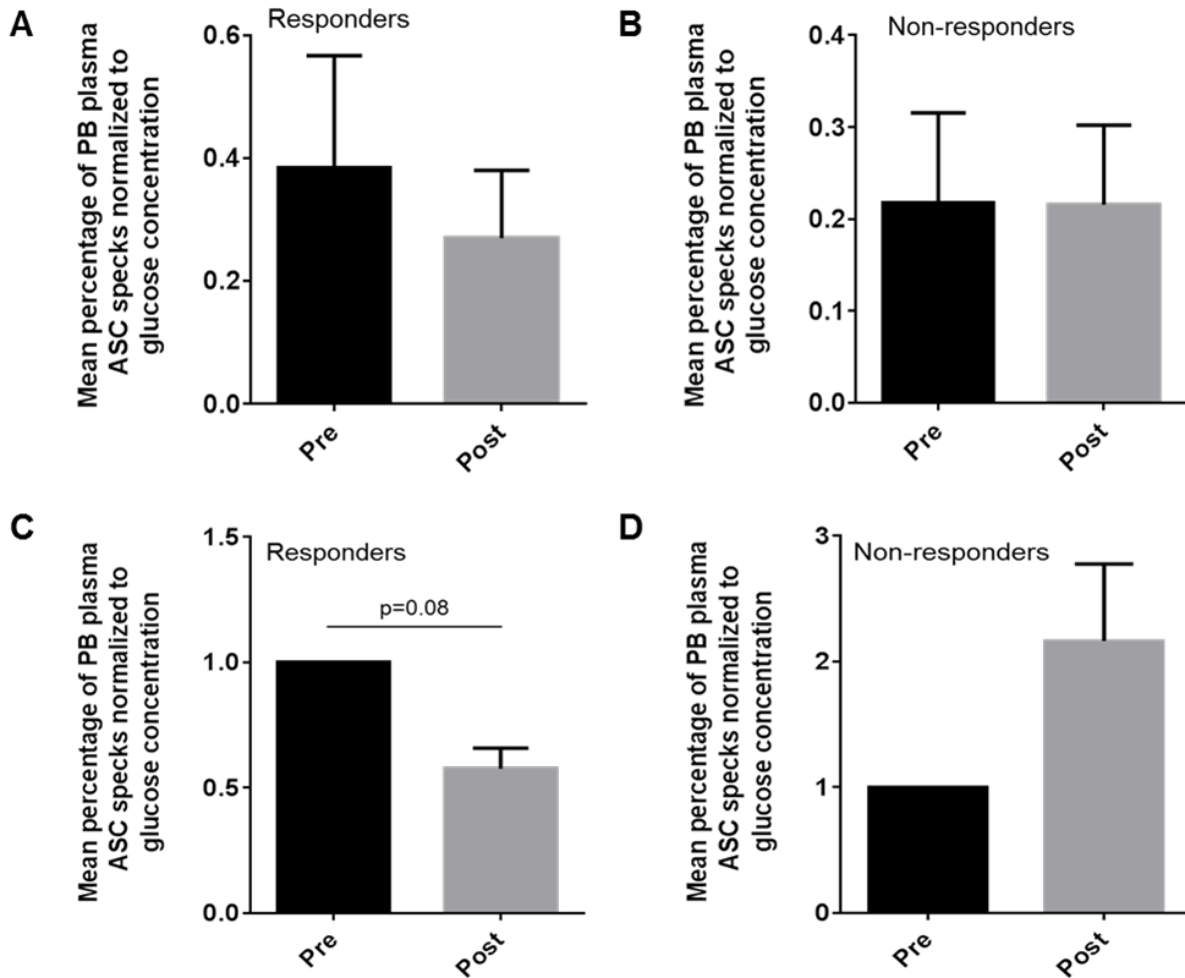


Figure 43. PB plasma-derived ASC specks are a response biomarker to lenalidomide treatment in two independent data sets. (A-B) Mean corrected ASC speck percentage pre- and post-lenalidomide treatment in MDS **(A)** responding (n=3) and **(B)** non-responding (n=7) patients from the University of Florence. **(C-D)** Mean corrected ASC speck percentage pre- and post-lenalidomide treatment in MDS **(C)** responding (n=28) and **(D)** non-responding (n=42) patients from the Groupe Francophone des Myélodysplasies (GFM) cooperative group.³²⁸ Error bars: SE.

formation of ASC specks is NLRP3-dependent, as specks failed to nucleate in the context of *NLRP3* deficiency.

Furthermore, comparison of matched PB and BM plasma samples from MDS patients illustrated that the percentage of ASC specks is significantly greater in the PB plasma. Notably, ASC specks have a prion-like phenotype, whereby they are resistant

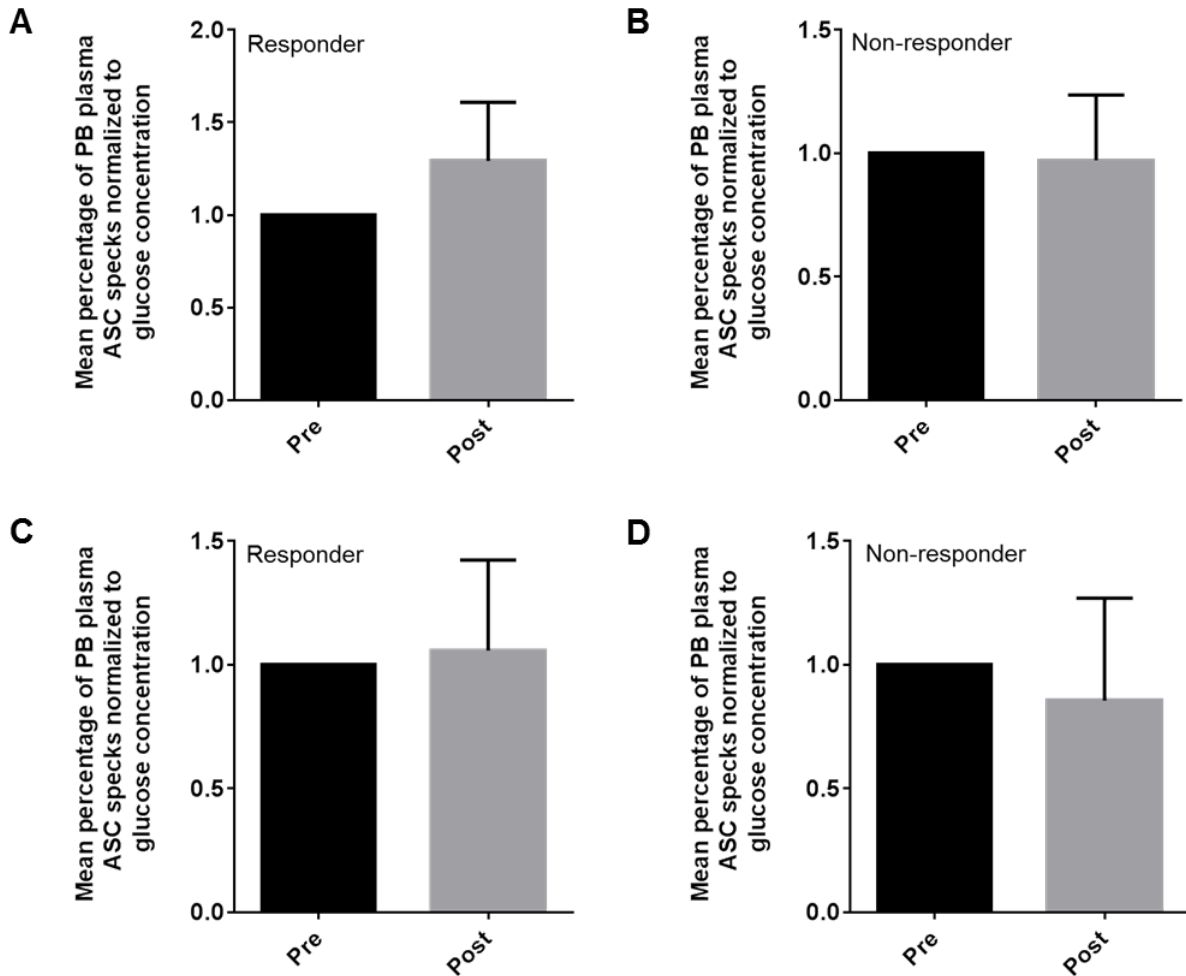


Figure 44. PB plasma-derived ASC specks remain unchanged after response to ESA or HMA therapy. (A-B) Mean corrected ASC speck percentage pre- and post-ESA treatment in LR-MDS **(A)** responding (n=10) and **(B)** non-responding (n=18) patients. **(C-D)** Mean corrected ASC speck percentage pre- and post-HMA treatment in HR-MDS **(C)** responding (n=15) and **(D)** non-responding (n=3) patients. Error bars: SE.

to proteolytic degradation and persist long after cell death.²⁹⁸ It is possible that while specks may be cleared quickly in the BM by resident macrophages, they persist within the PB because of poorer clearance and prion-like proteolytic resistance. Indeed, mouse models show that specks remain in tissues for up to 96 hours following injection, indicating that inflammasome-initiated pyroptosis may have prolonged effects on the microenvironment.²⁹⁸ This would reconcile the observation of greater expression of

specks within MDS PB plasma compared to BM plasma. In order to optimize the diagnostic assay, plasma glucose levels were measured by colorimetric assay to adjust for the confounding effects of hyperglycemia, which is a known stimulus of NLRP3 inflammasome activation. Consequently, the biomarker was defined as the percentage of ASC specks normalized to plasma glucose concentration corrected for volume. The glucose-adjusted speck percentage was significantly greater in both lower- and higher-risk MDS compared to normal donors. This increase in speck expression in MDS compared to normal donors was confirmed by confocal microscopy, whereby MDS BM-MNC demonstrated increased number of ASC specks. Importantly, speck expression was greater in lower-risk versus higher-risk MDS, suggesting possible utility for prognostic discrimination that might be enhanced when coupled with PB molecular genetic studies. Not surprisingly, expression of ASC specks did not differ between normal donors and patients with del(5q) MDS, which is characterized by erythroid hypoplasia (Chapter 3). As such, release of ASC specks would be expected to be lower in del(5q) MDS.

Moreover, investigation of ASC speck expression in a panel of other hematologic malignancies, including other myeloid and lymphoid leukemias, myeloproliferative neoplasms and overlap syndromes, like CMML, illustrated that specks are MDS-specific. Using statistical approaches, a cutoff point of 0.039 was identified to maximize sensitivity and specificity of the biomarker, which were 95% and 82%, respectively. Importantly, the biomarker achieved 96% sensitivity at the 0.039 cutoff point in an independent, external dataset, confirming high biomarker sensitivity. ASC specks additionally have utility as a measurement of the magnitude of pyroptotic cell death and

therefore response to treatment with lenalidomide. In responding patients, the glucose-corrected percentage of ASC specks was significantly reduced post-treatment whereas specks remained unchanged or even increased in non-responders. These findings were corroborated in two independent datasets. Changes in the corrected percentage of ASC specks, however, was not observed upon treatment response to ESA or HMA therapy in LR- and HR-MDS, respectively, suggesting utility as a response biomarker may be limited to immunomodulating agent therapy.

Lastly, ASC specks are readily quantified by flow cytometry. Using BM morphology alone, the error rate of MDS diagnosis is high, approximately 30-40%, which can be attributed to a number of confounding variables.^{325,329} Additionally, diagnoses rely heavily of morphological assessments of dysplasia, which are known to be vulnerable to observer error. The identification of a diagnostic assay that is independent of morphology is invaluable from a diagnostic perspective. Therefore, PB plasma-derived ASC specks represent the first diagnostic biomarker for MDS and may additionally be useful in monitoring incipient treatment responses in lower-risk patients.

Methods

Patient specimens. Normal plasma samples were obtained from peripheral blood samples purchased through Florida Blood Services. CMML plasma samples were generously provided by Dr. Eric Padron, and CML and CLL samples from Dr. Javier Pinilla-Ibarz. Plasma samples from other hematologic malignancies and type 2 diabetes patients were obtained from consented patients on a protocol approved by the

University of South Florida Institutional Review Board (Pro00026210). MDS patient plasma samples and BM-MNC were obtained from patients consented on the Eastern Cooperative Oncology Group (ECOG) E2905 trial (NCT00843882), and additionally provided by Drs. Valeria Santini and Erico Masala of University of Florence and Pierre Fenaux and Olivier Kosmider of the Groupe Francophone des Myélodysplasies (GFM) cooperative group. MDS patients were stratified according to the International Prognostic Scoring System (IPSS). Patients of low and intermediate-1 risk and intermediate-2 and high risk were considered to have lower-risk and higher-risk disease, respectively.

Reagents and cells. THP-1 and U937 cells were acquired from ATCC and maintained in RPMI-1640 supplemented with 10% FBS and 1% penicillin/streptomycin solution. Lipopolysaccharide (LPS), ATP and nigericin were purchased from Sigma-Aldrich. Normal BM cells were purchased from AllCells, LLC.

ASC speck staining. Plasma protein was quantified using BCA Protein Assay Kit (ThermoFisher Scientific). 300 µg of plasma from each donor was aliquoted into flow tubes and stained with anti-ASC primary antibodies (sc-22514-R, Santa Cruz) at a 1:1500 dilution for 1 hour at 37°C, followed by secondary antibody staining at a 1:1500 dilution for 30 minutes at 37°C. Samples were acquired using a BD FACSCalibur flow cytometer and threshold settings for forward scatter (FSC) and side scatter (SSC) were set to zero to allow for speck detection. Data were analyzed using FlowJo 9.7.5 software (FlowJo, LLC).

Immunofluorescence confocal microscopy. For cell line studies, THP-1 and U937 cells were plated and treated for 24 hours at 37°C concurrently with 100 ng/mL

LPS and 5 mM ATP or 5 µg/mL rhS100A9. After that, 5 µM nigericin was added to the LPS/ATP-treated cells for 1 hour at 37°C. Subsequently, cells were collected from all treatment groups and washed. Cytospins of cell lines and normal and MDS BM-MNC were generated by centrifugation for 5 min at 450 rpm, and fixed using BD Cytofix Fixation Buffer (BD Biosciences) for 10 min at 37°C. Slides were washed with 1x PBS, permeabilized with 0.1% Triton X-100/2% BSA in 1x PBS for 15 min at room temperature. Slides were washed again and blocked for 30 min at room temperature using 2% BSA in 1x PBS. After washing, slides were incubated with anti-ASC (sc-22514-R, Santa Cruz) primary antibodies at a 1:20 dilution at 4°C overnight. Slides were washed again in 1x PBS and incubated with goat anti-rabbit Alexa Fluor 488 secondary antibodies at a 1:250 dilution for 1 hour at room temperature. Slides were washed and ProLong Gold Antifade Reagent with DAPI (Life Technologies) and a coverslip were added. Images were taken using a Leica TCS SP8 AOBS Laser Scanning Confocal microscope (Leica Microsystems).

Enzyme-linked immunosorbent assays (ELISA). Plasma glucose concentration was measured using Glucose Colorimetric Assay Kit according to the manufacturer's protocol (#10009582, Cayman Chemical).

Statistical analyses. Data are expressed as means ± standard error. Measurements of statistical significance using student's t-test were made in Microsoft Excel. *P values <0.05, **p<0.01, and ***p<0.001 were considered to be statistically significant. Additional statistical analyses were carried out by the study statistician. The sample numbers used provided greater than 90% power to detect significant differences between diseases. The diagnostic biomarker was defined as the percentage of PB

plasma-derived ASC specks adjusted for glucose. Sensitivity, specificity, positive predictive value (PPV) and negative predictive value (NPV) were used to evaluate classification accuracy of the biomarker at varied cutoff points.

CHAPTER 5

Discussion

Implications

MDS-Specific Implications. Over the next few decades, the incidence of MDS and other age-related disorders is projected to dramatically increase, owing to the greying of populations in developed countries.⁴⁷ Irrespective of prognostic risk, the only curative treatment for MDS is allogeneic stem cell transplantation (alloSCT).^{48,49} Unfortunately, most patients are not eligible for alloSCT given their advanced age and the frequent presence of comorbid conditions. While three therapies have received FDA-approved designation for MDS, no novel therapies have been approved in over a decade. As patients become refractory to current treatment standards, care largely becomes empirical. For these reasons, there is a heightened necessity for novel therapeutic approaches that can directly and specifically target pathways central to disease pathobiology.

To date, despite the presence of vast genetic heterogeneity, lower-risk MDS pathobiology has been characterized by the proliferation of HSPC counter-balanced by programmed cell death mediated by pro-inflammatory cytokines.^{196,288} More specifically, cell death was attributed to apoptosis, a non-inflammatory mode of cell death. Despite this, the literature strongly supports the role of innate immune activation in the

pathobiology of MDS, evidenced by pro-inflammatory cytokine, chemokine and growth factor profiles, PRR expression and signaling, MDSC and the inflamed BM microenvironment.^{93,122,140} Indeed, a history of infection and autoimmune disease has been linked to MDS predisposition, suggesting that immune dysfunction precedes MDS development.²⁵ These findings support an apparent cell death paradox in MDS, whereby a non-inflammatory mechanism of cell death, namely apoptosis, has been implicated in the context of widespread inflammation. Notably, a pro-inflammatory cell death mechanism called pyroptosis, which is dependent on caspase-1 activation, was first characterized in microbial infection.²¹² Pyroptosis is mediated by the formation of inflammasome complexes, or cytosolic, heptameric oligomers of NOD-like receptors, or NLRs, that function to detect both host- and microorganism-derived danger signals. Among the five inflammasome-forming proteins, NLRP3 is the best characterized.

Here, we demonstrate that key hallmarks of MDS pathobiology can be attributed to aberrant activation of the NLRP3 inflammasome, which directs pyroptotic cell death, pro-inflammatory cytokine elaboration, cation influx and propagation of the MDS clone through β -catenin activation. Pyroptosis better accounts for characteristic features of MDS that have historically been ascribed to apoptosis, including inflammatory cell death in the context of HSPC proliferation. Importantly, NLRP3 inflammasome activation occurs irrespective of molecular phenotype, elucidating for the first time, a mechanism by which diverse genetic heterogeneity converges to yield a shared MDS phenotype. These data also provide a common circuit responsible for MDS pathobiology, as NLRP3 inflammasome-initiated pyroptosis and β -catenin activation are hallmarks of both non-del(5q) and del(5q) disease. As such, the causal role of NLRP3 inflammasome

activation in the pathobiology of MDS identifies biologically rational and novel avenues for therapeutic intervention, including neutralization of S100A9 and inhibition of the NLRP3 inflammasome. Given that these approaches directly target underlying aspects of disease biology, it is likely that they would have significant clinical benefit across MDS subtypes, and if applied early in the diagnosis of lower-risk MDS, could potentially be disease-modifying. In the context of del(5q) MDS, the therapeutic potential of NLRP3 inflammasome inhibition was demonstrated in this manuscript, and occurs by a mechanism distinct from that of lenalidomide, the standard of care for this disease subset. Accordingly, NLRP3 inflammasome inhibition may represent an innovative approach for treating del(5q) patients that have developed resistance to lenalidomide.

Furthermore, we have described the first diagnostic biomarker for MDS, namely the glucose-adjusted percentage of PB plasma-derived ASC specks. Given the magnitude of pyroptosis in lower-risk MDS, ASC specks provide an index of the extent of pyroptotic cell death and as such, serve as a biologically rational biomarker for the diagnosis of MDS. The biomarker is both sensitive and specific, and can accurately distinguish MDS from normal donors, various other BM malignancies and T2D. Since the biomarker is measured independent of cytological and morphological examination, it can be employed to complement current diagnostic methods and reduce diagnostic error, which is reported in approximately 30-40% of cases. The biomarker may also predict early treatment response to immunomodulatory drug therapy in lower-risk patients, illustrating additional potential clinical utility.

Implications Related to Other Inflammatory Conditions and Diseases of Major Health Concern. Activation of the NLRP3 inflammasome is tightly regulated,

evidenced by a two-step mechanism of activation and by the number of endogenous negative regulators that function to dampen inflammasome-driven responses. Deregulation of the inflammasome complex has been implicated in a vast number of diseases, including heritable and acquired inflammatory conditions and other autoimmune diseases that have an inflammatory pathobiology.^{330,331} Therefore, increased understanding of the nuances governing NLRP3 inflammasome signaling and regulation could lead to novel therapeutic agents that abrogate pathway activation. To this end, our findings with respect to the role of NLRP3 inflammasome activation in MDS pathobiology, as well as novel strategies aimed at inflammasome inhibition, can widely impact healthcare and effectively generate new treatment approaches for a number of malignancies, and metabolic and immune disorders. These conditions are generally summarized in Figure 45.

Inflammasomopathies. Appropriately named, inflammasomopathies represent the group of disorders resulting from autosomal dominant mutations in *NLRP3*, which render the inflammasome constitutively active.^{254,332} Of the 90 disease-associated mutations that have been reported, the majority reside within the nucleotide binding domain (NBD) of *NLRP3*. It has been hypothesized that these mutations disrupt binding ability of an unknown negative regulator or possibly the intrinsic ability of NLRP3 to self-regulate.²⁵⁴ Interestingly, while no mutations in *NLRP3* have been described in MDS to date, *NLRP3* single nucleotide polymorphisms (SNPs) are significantly enriched in patients with a history of autoimmune disorders.³³³ Further, prior to nomenclature changes, NLRP3 was previously referred to as cryopyrin. As such, these disorders are also referred to as cryopyrin-associated periodic syndromes (CAPS), or

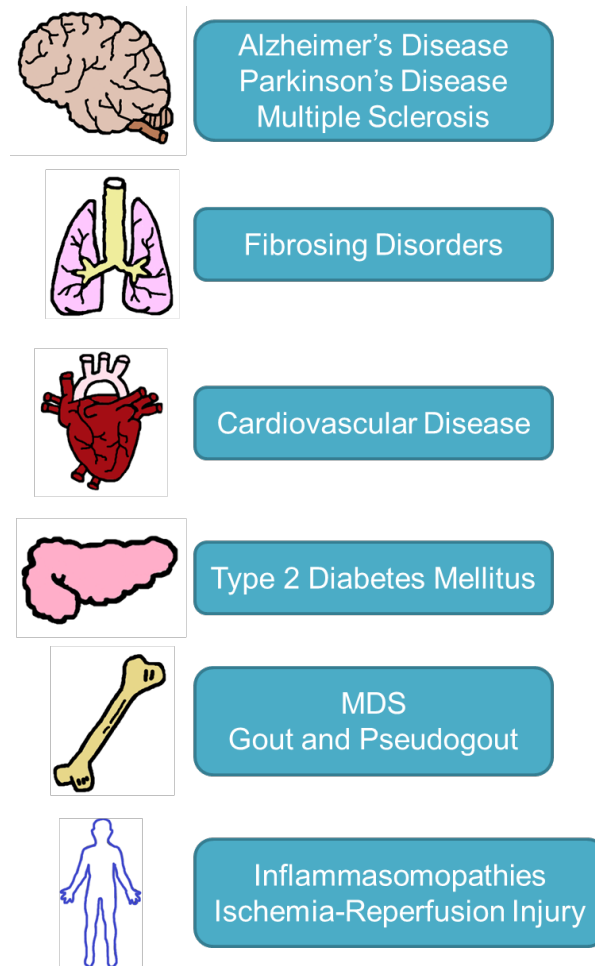


Figure 45. NLRP3 inflammasome activation is a pathobiological driver of many inflammatory conditions and diseases of major health concern. Aberrant activation of the NLRP3 inflammasome in the brain is a pathobiologic driver of Alzheimer's disease, Parkinson's disease and multiple sclerosis; in the lungs: fibrosing disorders; in the heart: cardiovascular disease; in the pancreas: type 2 diabetes mellitus; in the bone marrow and joints: MDS, gout and pseudogout, respectively. NLRP3 inflammasome activation also contributes pathobiologically to inflammasomopathies and ischemia-reperfusion injury.

cryopyrinopathies. The inflammasomopathies share a spectrum of clinical phenotypes, ranging from less to most severe, specifically familial cold autoinflammatory syndrome (FCAS), Muckle-Wells syndrome (MWS) and chronic infantile neurological cutaneous articular syndrome (CINCA), respectively.²⁵⁴

Notably, disease severity directly correlates with IL-1 β production, and as such, therapeutic interventions have been aimed at IL-1 receptor inhibition, IL-1 β neutralization and caspase-1 inhibition. For example, anakinra is an IL-1 receptor antagonist that significantly reduces both IL-1 β transcriptional priming and secretion of the mature cytokine.³³⁴ Although it is not FDA approved for the treatment of inflammasomopathies, anakinra is commonly used as an off-label treatment in these disorders.³³⁵ Because of its short half-life, patients require daily injections of anakinra which results in significant pain and discomfort. Of note, anakinra is FDA approved for the treatment of rheumatoid arthritis and is being investigated in other indications, including renal disease and dermatitis. Furthermore, neutralization of IL-1 β is achieved by riloncept, a chimeric protein generated by the fusion of the IL-1 receptor binding region to the Fc portion of human IgG₁.³³⁶ Riloncept received FDA approval in 2008 for inflammasomopathy treatment. The benefit of riloncept over anakinra therapy, namely weekly injections versus daily, is offset by the fact that riloncept is significantly greater in cost than anakinra.³³⁵ The last of the IL-1 β neutralization strategies is canakinumab, a human IL-1 β monoclonal antibody.³³⁵ With a significantly longer half-life, patients receive only one injection every eight weeks.³³⁵ Canakinumab received FDA approval for inflammasomopathies in 2009, and has since been explored in other indications, including rheumatoid arthritis, gout and type 2 diabetes mellitus. Finally, VX-765 is a selective inhibitor of caspase-1, which significantly reduces secretion of both IL-1 β and IL-18.³³⁷ Despite this, VX-765 has yet to be tested clinically for the treatment of inflammasomopathies. Taken together, while these therapies have had success, with some even gaining FDA approval, patients still acquire resistance, indicating the need

for novel, more effective treatment approaches. Such efforts have been aimed further upstream at the level of the NLRP3 inflammasome, as no NLRP3-specific inhibitors exist to date.

Type 2 diabetes mellitus. Type 2 diabetes mellitus (T2D) represents a major, global health concern and is generally characterized by peripheral insulin resistance arising from the impaired ability of pancreatic beta cells to produce and secrete insulin.³³² The literature strongly supports an aberrant role of innate immune activation in T2D. More specifically, IL-1 β and NLRP3 inflammasome activation have been identified as pathobiological drivers of the disease. Notably, the incidence of T2D is increased among patients with MDS,⁸ suggesting that increased understanding of NLRP3 inflammasome activation in MDS can increase understanding of T2D biology, and that novel therapeutic approaches can be utilized in both diseases.

To start, hyperglycemia induces innate immune signaling within pancreatic islets, up-regulating TLR2 and TLR4 gene and protein expression, NF- κ B activation, and both MyD88-dependent and -independent signaling pathways.³³⁸ This is accompanied by glucose-driven increases in IL-1 β transcriptional priming and secretion, caspase-1 activity and pancreatic beta cell death.^{339,340} Indeed, IL-1 β functions in a positive feedback loop, whereby hyperglycemia induces maturation of IL-1 β by beta cells, which upon secretion triggers cell death of islet cells and increased glucose concentrations.³³² These effects are mitigated by the *in vitro* treatment of islet cells with an IL-1 receptor antagonist.³⁴⁰ In a randomized clinical trial, IL-1 receptor antagonism significantly improved glycemic control and beta cell insulin secretory function, illustrating the importance of IL-1 β in disease pathobiology.³⁴¹ However, insulin sensitivity was not

changed among the control and treatment arms, indicating the need for more effective treatment approaches. Similar findings were observed in a murine model of T2D and in *I11b* knockout mice.^{342,343}

Importantly, increased NLRP3 inflammasome activation in pancreatic beta cells and fat-based macrophages, active caspase-1 and IL-1 β correlate not only with increased risk of developing diabetes, but also disease severity.³³¹ *Nlrp3* knockout mice display insulin sensitivity, enhanced insulin signaling and significant reductions in pro-inflammatory cytokines,³⁴⁴ implicating NLRP3 inflammasome activation in disease pathobiology. Pancreatic beta cells basally express NLRP3, ASC, caspase-1 and IL-1 β , but levels are profoundly increased upon high glucose exposure.²⁶¹ Notably, hyperglycemia also induces islet cell expression of thioredoxin-interacting protein (TXNIP),³³⁹ a redox protein known to directly bind to NLRP3, inducing a conformational change that results in inflammasome assembly and activation.²⁶¹ *Txnip*^{-/-} mice evidence reduced inflammasome activation, IL-1 β secretion and cell death.²⁶¹ Similarly, siRNA-directed silencing of *TXNIP* in human adipocytes significantly reduced levels of IL-1 β and mitigated the negative effects of hyperglycemia.³³⁹ Mechanistically, TXNIP directly and indirectly suppresses glucose uptake while additionally inducing NLRP3 inflammasome activation, leading to IL-1 β generation and cell death of insulin-producing beta cells.³³⁰ TXNIP serves as a key regulator of glucose homeostasis by directing degradation of the plasma membrane glucose transporter GLUT1 through internalization of clathrin-coated pits, whereas nuclear-localized TXNIP suppresses *GLUT1* gene transcription.³⁴⁵ As such, therapies aimed at NLRP3 inflammasome inhibition would likely impart significant clinical benefit to patients with T2D.

Cardiovascular disease. Cardiovascular disease is the leading cause of death worldwide. The literature strongly supports a causal role for inflammation, ROS and NLRP3 inflammasome activation in the pathobiology of various cardiovascular diseases, including hypertension and atherosclerosis. Intronic, tandem repeat polymorphisms in *NLRP3* are associated with increased systolic blood pressure and increased risk of developing hypertension compared to individuals with wild-type *NLRP3*.³⁴⁶ Interestingly, hypertension positively correlates with the development of T2D,²⁵⁴ implicating an aberrant role of NLRP3 in both diseases. In a rat model of hypertension, aortic cells from hypertensive animals significantly up-regulated NADPH oxidase (NOX) activity compared to littermate controls.³⁴⁷ NOX-derived ROS contribute to abnormal vascular structure and functionality, perpetuating disease severity.³⁴⁸

Nearly three decades ago, it was reported that inflammation is a central mediator of atherosclerosis, and today, inflammation is regarded as a causal factor in the formation and progression of atherosclerotic plaques.²⁵⁴ During atherosclerosis, cholesterol monohydrate crystals accumulate within lysosomes of macrophages following phagocytosis, as well as within lesions in the extracellular space.³⁴⁹ The accumulation of cholesterol crystals leads to hardening of the arterial walls as well as narrowing of arterial vessels, which together increase risk of heart attack and stroke.³³⁰ Until recently, the cause of chronic inflammation in the pathobiology of atherosclerosis was unknown but has since been attributed to the NLRP3 inflammasome. As plaques develop, monocytes are recruited to the site of the lesion whereby they differentiate into macrophages.³⁵⁰ The macrophages phagocytose the cholesterol crystals that are abundant in the lesions, resulting in lysosomal damage.^{350,351} Subsequently, through a

cathepsin B-dependent mechanism, the NLRP3 inflammasome becomes activated, generating and secreting mature IL-1 β in a caspase-1-dependent manner.^{350,351} In this way, the cholesterol crystals function as DAMPs triggering aberrant activation of the inflammasome complex. Notably, in a transplant model of disease, mice deficient in *Nlrp3* and *Il1* had reduced inflammation, smaller lesions and were more resistant to the development of atherosclerosis.³⁵¹ Similarly, siRNA-mediated silencing of *NLRP3* mitigated release of IL-1 β in response to cholesterol crystals.³⁵⁰ Perhaps not surprisingly, levels of IL-1 β correlate with disease severity.³⁵² These data together indicate a central role for inflammasome activation in disease pathobiology, and suggest that inflammasome inhibitors may have therapeutic efficacy in cardiovascular disease.

Multiple sclerosis. Although the pathobiology of multiple sclerosis (MS) is complex and still under investigation, the literature supports an aberrant role for NLRP3 inflammasome activation. Generally, MS is a devastating autoimmune disease characterized by demyelination resulting from myelin-specific CD4+ T cells that penetrate the central nervous system (CNS) to injure oligodendrocytes.³³⁰ Phenotypically, the CNS loses significant functionality, resulting in widespread challenges that are physical, mental and even psychiatric in nature.³³⁰ No cure for MS exists to date, illustrating the imperative need for new treatment approaches.

Experimental autoimmune encephalomyelitis (EAE) is a commonly used murine model of MS, whereby immunization of mice with myelin oligodendrocyte glycoprotein (MOG) results in the expansion of MOG-reactive T cells.³³⁰ An aberrant role of caspase-1 activation in MS pathobiology was described nearly a decade before NLRP3 was implicated. EAE induced transcriptional priming of caspase-1, expression of which

positively correlated with disease severity.³⁵³ Moreover, increased levels of active caspase-1 also correlated with circulating levels of pro-inflammatory cytokines, including IL-1 β ,³⁵³ suggesting that caspase-1 plays a central role in cytokine generation in MS. Finally, mice lacking caspase-1 had significant reductions in EAE severity, with marked loss of MOG-specific Th1 cells.³⁵³ Furthermore, a model of EAE in the context of *Nlrp3* loss elegantly supports these findings and the crucial role of the NLRP3 inflammasome/caspase-1 axis in MS. Loss of *Nlrp3* resulted in a significant reduction in disease severity and course, substantial reductions in inflammatory cell infiltration, reduced myelin destruction and diminished response capacity of Th1 and Th17 CD4+ cells.³⁵⁴ IFN- γ and IL-17 are pro-inflammatory cytokines secreted by Th1 and Th17 cells, respectively, and these CD4+ T cell populations have well-documented roles in the pathobiology of autoimmunity. Also, in a model of EAE in the context of *Il1* knockout, IFN- γ and IL-17 production were significantly reduced in the T cell compartment, which was associated with an improved phenotype.³⁵⁵ Interestingly, Th17 cells are profoundly increased in LR-MDS patients,⁹⁷ consistent with an autoimmune reaction. Taken together, these data suggest that akin to LR-MDS, therapies targeting the NLRP3 inflammasome may have clinical utility in treating MS.

Alzheimer's disease. Alzheimer's disease (AD) is a devastating neurodegenerative disease whereby progressive dementia occurs as a result of neuronal cell death, specifically of microglial cells.²⁷⁰ Mechanistically, the pathogenesis of AD has been linked to the accumulation of amyloid β , a fibrillar peptide, within senile plaques in the cerebrum.^{270,330} Nearly three decades ago, it was determined that expression of IL-1 β was significantly increased in senile plaques,³⁵⁶ and recent reports

have indicated that active caspase-1 expression is increased in patients with AD,³⁵⁷ suggesting a pathobiological role for NLRP3 inflammasome activation. Accordingly, microglial cells were shown to be recruited to senile plaques, whereby they become activated by and phagocytose amyloid β .³⁵⁸ Once phagocytosed, amyloid β damages lysosomes, resulting in release of cathepsin B,²⁷⁰ a known secondary trigger for NLRP3 inflammasome activation. Consequently, the NLRP3 inflammasome becomes activated, triggering autocatalytic cleavage of caspase-1 and subsequent generation and release of IL-1 β . Notably, genetic deletion of *Asc*, *Casp1* or *Il1b* prevented microglial activation, indicating the importance of the NLRP3 inflammasome axis in the pathobiology of AD.²⁷⁰ These findings were corroborated and strongly supported by experiments performed in *Nlrp3*^{-/-} mice crossed with APP/PS1 transgenic mice, a common model of AD characterized by amyloid β plaque deposition.³⁵⁷ In this context, deposition of amyloid β was significantly reduced, as was senile plaque size and activation of microglia.³⁵⁷ Together, these data suggest that inhibition of the NLRP3 inflammasome signaling pathway would likely afford therapeutic benefit in AD.

Parkinson's disease. Parkinson's disease (PD) is a neurodegenerative disease characterized by aberrant cell death of dopaminergic neurons within the substantia nigra of the midbrain, resulting in severe motor impairments.^{330,359} Within the dopaminergic neurons, Lewy bodies form, which are aggregated inclusions within the cell that contain significant amounts of the fibrillar protein alpha-synuclein (α -Syn).³⁵⁹ The α -Syn fibers that form in PD are similar to the amyloid β fibers that form in AD.³³⁰ Although unknown for a time, the marked inflammation characteristic of PD has since been attributed to an aberrant role of NLRP3 inflammasome activation. Mechanistically,

dopaminergic cells release α -Syn into the extracellular space, which is subsequently phagocytosed by microglial cells.³⁵⁹ Upon phagocytosis, and by a mechanism similar to amyloid β -induced NLRP3 inflammasome activation in AD, the α -Syn induces lysosomal damage, triggering the release of cathepsin B that serves as a secondary activation trigger for NLRP3 inflammasome complex assembly.³⁵⁹ Consequently, the inflammasome generates active caspase-1 and IL-1 β , which is secreted and propagates inflammation. Notably, the phagocytosis event also triggers activation of NOX, resulting in ROS generation that additionally may activate the inflammasome complex.³⁵⁹ Once released, inflammatory cytokines and ROS damage the surrounding dopaminergic cells, triggering cell death. The detrimental effects of NLRP3 inflammasome-driven IL-1 β production were demonstrated in a murine model, whereby mice were dosed daily with IL-1 β . Compared to controls, IL-1 β -treated mice phenocopied human PD just after three weeks of treatment, with significant cell death of dopaminergic neurons, increased microglial cell activation and inflammatory cell infiltrate, and severe akinesia.³⁶⁰ Finally, the aberrant role of NLRP3 inflammasome activation in PD was demonstrated in an alternative model. *Nlrp3*^{-/-} mice treated with the neurotoxin 1-methyl-4-phenyl-1,2,3,6-tetrahydropyridine (MPTP), a known inducer of the PD phenotype, were protected from overt development of PD compared to littermate controls.³⁶¹ These data indicate that abrogating NLRP3 inflammasome signaling or neutralization of IL-1 β may have clinical utility in PD.

Gout and pseudogout. Gout and pseudogout represent two common arthropathies, or rheumatic diseases, which are characterized by the abnormal deposition of crystals, specifically monosodium urate (MSU) and calcium pyrophosphate

dehydrate (CPPD), respectively, in the intra- and periarticular spaces within joints.³³² Phenotypically, these areas are acute and chronically inflamed, resulting in severe pain and swelling.^{331,332} Though MSU and CPPD have had a longstanding and well-described role in the pathobiology of gout and pseudogout, respectively, the precise mechanism underlying crystal-induced inflammation was just recently elucidated. Both MSU and CPPD induce NLRP3 inflammasome activation, triggering activation of caspase-1 and subsequent maturation and release of IL-1 β and IL-18.³⁶² Indeed, crystal-induced generation of IL-1 β is abrogated in macrophages that lack *ASC*, *CASP1* or *NLRP3*, indicating the importance of the NLRP3 inflammasome signaling cascade in the disease pathobiology. These data are supported by an *in vivo* model of disease, whereby mice deficient in *Nlrp3* had improved phenotypes and reduced infiltration of inflammatory cells, particularly neutrophils, which are associated with severe joint pain.³⁶² Finally, a small pilot study of anakinra, an IL-1 receptor antagonist, was performed in ten patients with gout refractory to standard anti-inflammatory therapies.³⁶³ Though responses varied among patients, 90% demonstrated resolution of arthritic symptoms in just three days after treatment was initiated, with no adverse effects reported among the cohort.³⁶³ While randomized trials would be required to confirm effectiveness, abrogation of the NLRP3 inflammasome axis is an attractive therapeutic approach in gout and pseudogout.

Fibrosing disorders. Prolonged exposure to environmental irritants is a known etiological factor of MDS, the pathobiology of which is intricately linked to NLRP3 inflammasome activation. Notably, fibrosing disorders represent a heterogeneous group of diseases that include idiopathic pulmonary fibrosis (IPF), silicosis and asbestosis.

These disorders are progressive and fatal, with no effective therapeutic strategies identified to date. However, they have been linked to aberrant inflammation, specifically resulting from NLRP3 inflammasome activation.

Silicosis and asbestosis develop after prolonged and chronic exposure to silica and asbestos, respectively, evidenced by increased production of pro-inflammatory cytokines, including IL-1 β , by alveolar macrophages isolated from individuals reporting greater than ten years of exposure, versus controls with less than ten years.²⁶⁹ Notably, in a British study, those harboring a polymorphism in the receptor *IL-1RA* were at 10.2-fold greater risk of developing a fibrosing disorder, implicating a role of aberrant IL-1 β production in these conditions.³⁶⁴ From a mechanistic standpoint, once inhaled, silica and asbestos deposit in the lung alveoli, whereby they undergo clearance by resident macrophages through phagocytosis.²⁶⁹ Subsequently, phagocytosis of these crystalline irritants results in NOX-dependent ROS generation and lysosomal destabilization, both of which trigger NLRP3 inflammasome activation.^{269,365,366} The inflammasome then activates caspase-1, triggering maturation and release of IL-1 β , which instigates inflammation and lung injury mediated by the activation of fibroblasts. The importance of the NOX/ROS/NLRP3 inflammasome-dependent pathway in pathobiology was confirmed by a number of *in vitro* and *in vivo* observations. For one, *Nlrp3*^{-/-} mice have reduced fibrosis, immune cell infiltrate and cytokine production when challenged by a model of asbestos inhalation.³⁶⁶ Also, shRNA-directed silencing of *p22phox*, a central subunit of the NOX complex, in the THP-1 monocytic cell line resulted in significant reductions in IL-1 β secretion.³⁶⁶ Finally, thioredoxin (TRX) is a key redox protein that regulates NLRP3 inflammasome activation by binding to TRX-interacting protein

(TXNIP) under basal conditions.²⁶⁰ In high ROS conditions, TRX undergoes oxidation, which liberates TXNIP and allows it to bind to NLRP3, leading to inflammasome assembly and activation.²⁶¹ Silencing of *TRX* in THP-1 cells resulted in a significant increase in mature IL-1 β production, implicating a redox-dependent mechanism of inflammasome activation.³⁶⁶

Lastly, IPF represents a particularly devastating condition whereby progressive lung injury, resulting in scarring and fibrosis, leads to respiratory failure and death. No effective therapies have been identified to date, indicating the need for increased understanding of disease pathobiology. Acute pulmonary injury is commonly investigated in a murine model whereby mice are treated with the cytotoxic agent bleomycin, which induces a phenotype akin to human IPF with increased inflammation, cytokine and chemokine production, and fibrosis.³⁶⁷ Notably, mice deficient in *Il1ra* were protected from bleomycin-induced lung injury, while those treated with recombinant murine IL-1 β were phenotypically similar to mice subjected to bleomycin treatment.³⁶⁷ Use of anakinra significantly decreased inflammation following bleomycin treatment,³⁶⁷ confirming the pathobiological role of IL-1 β generation in IPF. Importantly, IL-1 β production in response to bleomycin-induced injury required the NLRP3 inflammasome adaptor protein ASC, implicating a role for inflammasome activation.³⁶⁷ More than likely, unknown DAMP signals trigger NLRP3 inflammasome activation in IPF, resulting in caspase-1 activation and release of IL-1 β , leading to activation of fibroblasts that exacerbate lung injury. These data warrant investigation of inflammasome inhibitors in fibrosing disorders, which may represent the first effective, targeted therapeutic approach in these conditions.

Ischemia-reperfusion injury. Ischemia-reperfusion injury (IRI) describes the condition of tissue or organ damage resulting from loss of blood flow to the area, which culminates in significant injury and cell death that is exacerbated following the restoration of flow to the area, which increases immune cell infiltration, ROS and inflammation.³³¹ IRI is known to occur following a number of conditions, including serious trauma, stroke and transplantation surgery.³³¹ The inflammatory response generated as a consequence results in significant organ damage, morbidity and even mortality, as dysfunction in one organ can trigger a systemic immune reaction that damages other organs.³³¹ Presently, no therapies exist for the prevention or treatment of IRI, indicating a clear therapeutic need.

Renal, hepatic and myocardial IRI occur commonly, and the sterile inflammation resulting from each type of injury occurs as a consequence of NLRP3 inflammasome-driven inflammation. In murine models of renal IRI, loss of *Nlrp3* was associated with significant reduction in pro-inflammatory cytokine generation, specifically IL-1 β and IL-18, immune cell infiltration and preservation of renal function.³⁶⁸ Similarly, mice pre-treated with shRNAs targeting *Nlrp3* were protected from hepatic injury following ischemia induction.³⁶⁹ Active caspase-1, IL-1 β and IL-18 generation and NF- κ B activity were all significantly reduced with *Nlrp3* downregulation.³⁶⁹ Both pharmacologic inhibition of the IL-1 receptor as well as gene delivery of IL-1 receptor antagonist to the liver protected mice from IRI and increased survival following injury.^{370,371} Lastly, loss of *Casp1* and *Asc* protected mice from myocardial injury following IRI, with significant reductions in IL-1 β production, immune cell infiltration and fibrosis.³⁷² Neutralization of IL-18 or IL-1 β in murine models of myocardial IRI resulted in improved outcomes, with

reduced injury, inflammation and increased survival.³⁷³ In a small pilot study of 10 patients, treatment with the IL-1 receptor antagonist anakinra improved cardiac remodeling following IRI without adverse effects,³⁷⁴ warranting further investigation in randomized clinical trials.

From a generalized mechanistic overview, IRI results in the increased expression of ROS and DAMP signals, triggering NLRP3 inflammasome-dependent activation of caspase-1 and maturation of inflammatory cytokines IL-1 β and IL-18. The inflammatory response results in the recruitment of other immune cell infiltrate, which exacerbates inflammation, tissue damage and injury. Taken together, these data suggest that inhibition of the NLRP3 inflammasome may prevent IRI and adverse outcomes arising from organ injury.

Future Directions

NLRP1 Inflammasome Activation. Masters et al. reported the first evidence of pyroptosis in the hematopoietic system whereby infection-induced cytopenia occurred as a consequence of NLRP1 inflammasome activation.²³¹ Specifically, an activating point mutation in *Nlrp1a* (Q59P) results in aberrant Nlrp1 inflammasome-driven caspase-1 activation, leading to a lethal inflammatory phenotype characterized by severe cytopenia, abnormal myeloid lineage maturation and HSPC death.²³¹ These data suggest that ineffective hematopoiesis can be attributable to activation of the NLRP1 inflammasome in certain contexts. Given these findings, along with the casual role of

NLRP3 inflammasome activation in MDS pathobiology, we investigated the role of NLRP1 inflammasome activation in MDS.

We found that *NLRP1* transcript expression is significantly increased in BM-MNC from MDS patients (n=10) compared to normal donors (n=6), approximately 23.2-fold (Figure 46A). Formation of active NLRP1 inflammasome complexes was confirmed by confocal fluorescence microscopy (Figure 46B), whereby BM-MNC from LR- and HR-MDS specimens display significantly increased α -caspase-1 (MFI 21.1-fold increase in LR [$p=7.9 \times 10^{-4}$] and 23.8-fold in HR [$p=0.081$]) and co-localization with NLRP1 (MFI 34.3-fold increase in LR [$p=6.4 \times 10^{-3}$] and 23.2-fold in HR [$p=0.15$]) protein expression versus normal donors (Figure 46C). These findings indicate that NLRP1 inflammasome formation is significantly increased in MDS BM-MNC.

Moreover, given that S100A9 is a primary initiator of NLRP3 inflammasome activation and pyroptosis in LR-MDS, we investigated the ability of S100A9 to initiate assembly of NLRP1 inflammasome complexes. Treatment of the U937 monocytic cell line with 5 $\mu\text{g/mL}$ rhS100A9 (Figure 47A) resulted in a significant increase in NLRP1 inflammasome formation (1.2-fold, $p=1.1 \times 10^{-11}$), with corresponding increases in protein expression of α -caspase-1 (2.0-fold, $p=3.0 \times 10^{-5}$) and NLRP1 (1.2-fold, $p=1.6 \times 10^{-3}$) compared to untreated controls (Figure 47B). Importantly, treatment of normal BM-MNC with rhS100A9 significantly increased NLRP1 inflammasome formation and activation (5.6-fold, $p=3.9 \times 10^{-5}$), evidenced by co-localization of α -caspase-1 and NLRP1 (Figure 47C and 47D). While rhS100A9 treatment did induce protein expression of α -caspase-1 (1.4-fold, $p=0.02$) and NLRP1 (126.1-fold, $p=2.3 \times 10^{-3}$), as well as maturation of active

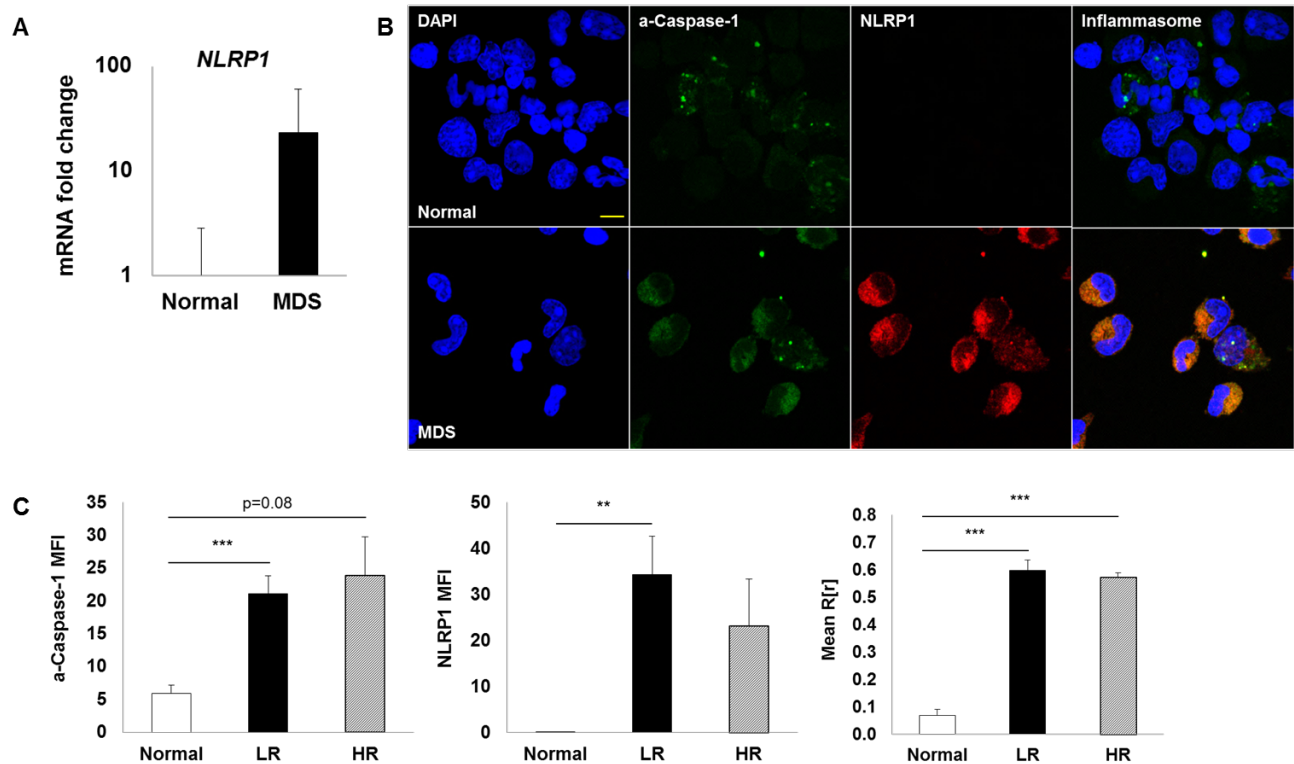


Figure 46. NLRP1 inflammasome formation and activation is significantly increased in MDS BM-MNC. (A) qPCR analysis of *NLRP1* gene expression in BM-MNC isolated from MDS patient specimens (n=10 total; n=5 lower-risk and n=5 higher-risk disease) compared to normal BM-MNC (n=6). (B) Representative confocal fluorescence micrograph (2520x magnification, 7.5 μm scale) of a-caspase-1 and NLRP1 expression in MDS versus normal BM-MNC. DAPI (blue), a-caspase-1 (green), NLRP1 (red); merged images show inflammasome formation. (C) Quantitative analysis of confocal images of BM-MNC isolated from MDS patients [LR (n=7), HR (n=3)] and normal donors (n=6). Error bars: SE, **p<0.01 and ***p<0.001.

NLRP1 inflammasome complexes, this occurred to a lesser extent than that observed in MDS specimens (Figure 47D). Together, these data indicate that S100A9 also initiates NLRP1 inflammasome activation in MDS.

Moving forward, it would be interesting and worthwhile to continue investigations into the role of NLRP1 inflammasome activation in MDS, given that both NLRP3 and NLRP1 inflammasomes are active. As activation of both complexes culminate in pyroptosis, it would be important to identify the contribution of NLRP1 inflammasome

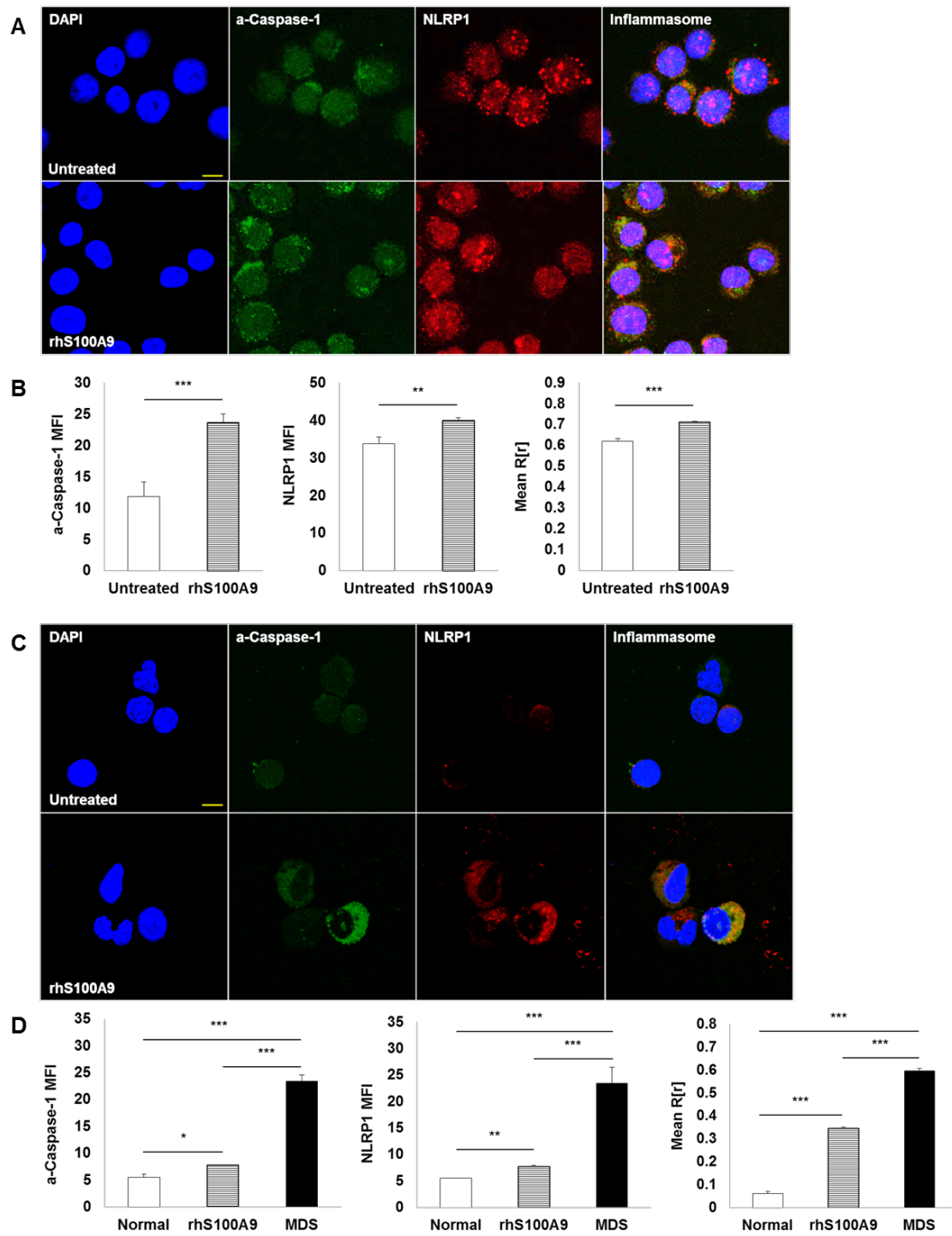


Figure 47. S100A9 induces NLRP1 inflammasome formation in U937 cells and normal BM-MNC. (A) Representative micrograph (2520x magnification, 7.5 μ m scale) depicting inflammasome formation in U937 cells untreated or treated with 5 μ g/mL rhS100A9 for 24 hours. DAPI (blue), a-caspase-1 (green), NLRP1 (red); merged images show inflammasome formation. **(B)** Quantitative analysis of confocal images from **(A)**. **(C)** Representative micrograph (2520x magnification, 7.5 μ m scale) depicting

inflammasome formation in normal, untreated BM-MNC or normal BM-MNC treated with 5 µg/mL rhS100A9 for 24 hours. DAPI (blue), a-caspase-1 (green), NLRP1 (red); merged images show inflammasome formation. **(D)** Quantitative analysis of confocal images of BM-MNC from normal donors (n=6), normal BM-MNC treated with rhS100A9 (n=2) and MDS patients (n=10). Error bars: SE, *p<0.05, **p<0.01 and ***p<0.001.

activation to MDS pathobiology. To start, preliminary investigations can be carried out in the THP-1 *NLRP3* knockout cell line, which would provide biological assessment of the contribution of NLRP1 inflammasome activation following inflammasome-specific stimuli. Following treatment of these cells with rhS100A9 or other stimuli, we can assess NLRP1 inflammasome formation, caspase-1 activation and generation of IL-1β. Moreover, as ICTA is an NLRP3 inflammasome inhibitor, it would be interesting to determine whether treatment of the NLRP3 KO cells additionally inhibits formation and activation of NLRP1 inflammasome complexes. Lastly, colony formation assays performed in THP-1 NLRP3 KO cells with and without CRISPR/Cas9-mediated deletion of *NLRP1* would confirm whether the NLRP1 inflammasome imparts negative effects on colony forming capacity.

To determine if NLRP1 inflammasome activation contributes to pyroptosis and ineffective hematopoiesis, colony formation assays can be performed on MDS BM-MNC following CRISPR/Cas9-mediated deletion of *NLRP1* and/or *NLRP3*. Genetic ablation of *NLRP3* would be expected to increase colony forming capacity, and deletion of *NLRP1* may also. It is likely that the combination would have additive effects on improving hematopoiesis. It would also be worthwhile to treat LR-MDS BM-MNC with ICTA as well as S100A9Tg BM cells, and assess changes in NLRP1 inflammasome activation. In the event that NLRP1 plays a non-redundant role in pathobiology, novel pharmacologic

inhibitors of inflammasome complexes would need to abrogate both NLRP1 and NLRP3 inflammasome formation to truly afford clinical benefit.

ER Stress/Inflammasome Signaling Axis. The function of the endoplasmic reticulum (ER) is intricately linked to cellular redox status. We reported a role for NADPH oxidase (NOX) 1/4-specific activation in LR-MDS, whereby somatic gene mutations and DAMP signals, particularly S100A9, activate these NOX-specific isoforms to generate ROS that initiate NLRP3 inflammasome and β -catenin activation.¹⁹⁹ Notably, NOX4 is associated both with the plasma membrane and is the only ER membrane resident NOX isoform. NOX4-dependent ROS production is a key upstream signal directing the ER stress response.³⁷⁵ Within the ER, three transmembrane proteins function as sensors of ER unfolded proteins, namely inositol-requiring enzyme 1 α (IRE1 α), protein kinase R (PKR)-like endoplasmic reticulum kinase (PERK) and activating transcription factor 6 (ATF6).³⁷⁶ Accumulation of unfolded proteins within the ER triggers activation of these sensors, resulting in downstream signaling aimed to restore cellular homeostasis or alternatively, in the absence of remediation, initiate cell death.³⁷⁶ Interestingly, TLR2 and TLR4 signaling activates IRE1 α , which augments innate immune signal response,³⁷⁷ which are significantly up-regulated and hyperactivated in LR-MDS. Furthermore, expression of the redox protein TXNIP is induced and stabilized upon IRE1 α activation, whereby IRE1 α marks a number of microRNAs (miRs) for degradation, including miR-17, which negatively regulates TXNIP activity.^{378,379} During basal conditions, TXNIP resides within the nucleus. However, during oxidative stress, it shuttles to the site of mitochondria whereby it directly binds mitochondrial-associated NLRP3,³⁸⁰ mediating NLRP3 activation. NLRP3 then activates

caspace-2 and Bid, which propagate mitochondrial damage, leading to the release of mitochondrial-derived ROS (mtROS) and mitochondrial DNA (mtDNA).^{381,382} Consequently, mtROS and mtDNA function as triggers of NLRP3 inflammasome assembly, resulting in inflammasome activation, maturation of caspase-1 and IL-1 β production.³⁷⁸ Pharmacologic inhibition of IRE1 α or TXNIP silencing were shown to block mature IL-1 β release,^{378,382} indicating the importance of ER stress-dependent activation of the NLRP3 inflammasome complex. The interaction between the ER, mitochondria and the NLRP3 inflammasome is outlined in Figure 48.

We have shown that MDS BM-MNC are under oxidative stress, that TXNIP gene and protein expressions are increased and others demonstrated that mitochondrial dysfunction is common.^{199,203} Therefore, it would be informative and worthwhile to investigate the ER stress/NLRP3 inflammasome axis in MDS. These investigations would further our understanding of the mechanisms governing NLRP3 inflammasome assembly, and may additionally identify novel therapeutic strategies. Finally, *NLRP1* is up-regulated during ER stress through an IRE1 α -dependent mechanism,³⁸³ which raises the notion that perhaps increased NLRP1 expression and activation in MDS is a consequence of ER stress. Elucidating the relationship between NLRP1 activation and the ER stress pathway, as well as potential interaction between NLRP1 and NLRP3 in MDS represents a promising line of investigation.

5' Adenosine Monophosphate (AMP)-Activated Protein Kinase. AMP-activated protein kinase (AMPK) is a central energy sensor and regulator of metabolism, with known anti-inflammatory actions.³⁴² Functional loss of AMPK activity has been associated with a growing number of inflammatory and metabolic conditions.³⁸⁴ AMPK

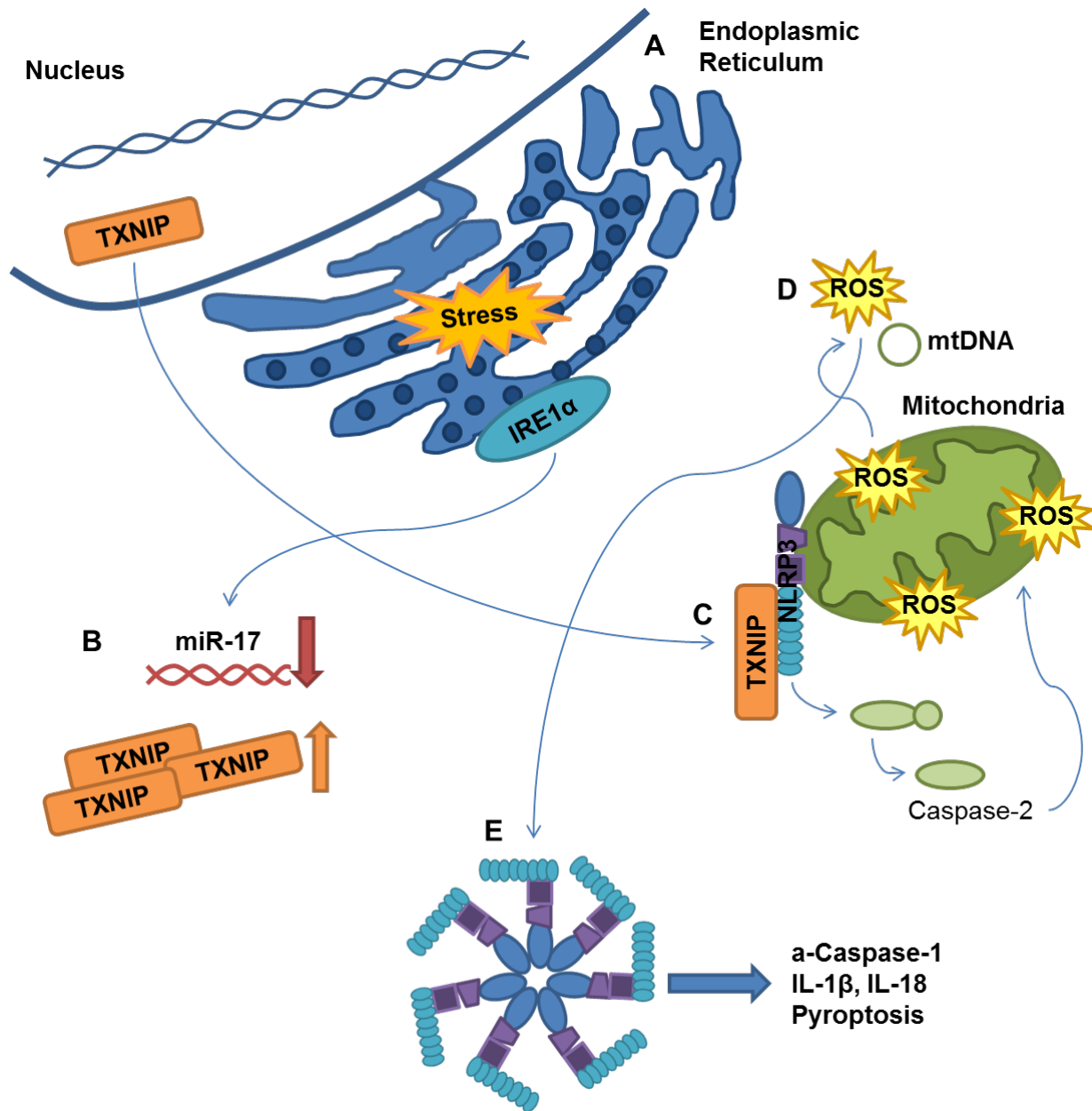


Figure 48. ER stress triggers NLRP3 activation, leading to mitochondrial dysfunction and activation of the NLRP3 inflammasome complex. (A) ER stress results in activation of one or more of the ER stress sensors, including IRE1 α . **(B)** Once active, IRE1 α triggers the degradation of miR-17, a negative regulator of the redox protein TXNIP, which increases TXNIP expression and function. **(C)** Under basal conditions, TXNIP resides within the nucleus but shuttles to mitochondria under conditions of oxidative stress. Here, it directly binds and activates NLRP3, which catalyzes maturation of caspase-2 to its proteolytically active form. **(D)** Active caspase-2 drives mitochondrial damage, which leads to the release of mitochondrial ROS (mtROS) and DNA (mtDNA) into the cytosol. **(E)** Both mtROS and mtDNA function as secondary signals for NLRP3 inflammasome activation, resulting in activation of caspase-1, release of IL-1 β and IL-18 and pyroptosis.

and NLRP3 inflammasome activation are negatively related, as loss of AMPK activity increases inflammasome-driven inflammation.³⁸⁴ More specifically, this occurs through a NOX-dependent mechanism. Wang et al. demonstrated that reduced AMPK activity increases expression of NOX1 and NOX4, including other key subunits required for NOX function.³⁸⁵ This was associated with reduced NOX-dependent ROS generation and NF- κ B activation, which was attenuated by pharmacological activation of AMPK or over-expression of a constitutively active form of AMPK, illustrating that AMPK negatively regulates NOX and ROS.³⁸⁵ Notably, metformin, a drug used in the treatment of type 2 diabetes mellitus, activates AMPK and reduces NLRP3 inflammasome activation, significantly reducing the release of both IL-1 β and IL-18.³⁸⁴ These findings are supported by AMPK-mediated phosphorylation of TXNIP during conditions of stress, which results in degradation of the redox protein.³⁴⁵

Given the pathobiological role of the NLRP3 inflammasome in MDS, it is highly plausible that AMPK activation is suppressed. As both NOX-derived ROS and TXNIP mediate NLRP3 inflammasome activation in LR-MDS, and AMPK negatively regulates the function of these proteins, activation of AMPK activity represents a worthwhile strategy for investigation in MDS. Moreover, reductions in AMPK activity result in mitochondrial dysfunction with augmented release of mtROS and mtDNA.³⁴² Evidence of aberrant mitophagy has been documented in LR-MDS,^{105,210} suggesting that reduced AMPK activity may be culpable. To start, AMPK activation could be assessed in LR-MDS BM-MNC specimens, S100A9Tg BM cells and in the mutant cell lines and models of gene mutation (Chapter 2). If AMPK activation were indeed reduced in MDS, then

identification of a potent and specific activator could inhibit NLRP3 inflammasome-driven signaling and pyroptosis.

Moreover, AMPK activation suppresses transcriptional reprogramming of somatic cells to a stem cell-like phenotype, characterized by increased expression of transcription factors like *Oct4*, *Sox2* and *c-Myc*.³⁸⁶ Interestingly, metformin treatment is capable of inhibiting somatic reprogramming, effectively creating a barrier to stemness.³⁸⁶ Given that MDS progression is associated with increased stem cell survival, self-renewal and propagation, it is likely that AMPK activation may prevent propagation of the MDS clone and disease progression to leukemia.

Conclusion

Identification of the NLRP3 inflammasome complex as a driver of the MDS phenotype, both in non-del(5q) and del(5q) disease, has the capacity to transform the present understanding of the pathobiology of MDS. More importantly, the findings described in this manuscript indicate that strategies intended to neutralize S100A9 or inhibit NLRP3 inflammasome assembly offer therapeutic potential in these disorders. In del(5q) MDS, our preliminary investigations indicate that NLRP3 inflammasome inhibition can promote effective erythropoiesis without selective clonal suppression. These data support the investigation of inflammasome inhibitors in patients that are refractory to lenalidomide, the current standard of care. Moreover, we have identified the first diagnostic biomarker of MDS, or the percentage of glucose-adjusted PB plasma-derived ASC specks. Specks are not only readily quantified by flow cytometry,

but also provide an independent parameter of morphology, which is invaluable from a diagnostic perspective. The implementation of speck quantitation at the time of diagnosis has the capacity to minimize diagnostic error. In implicating NLRP3 inflammasome activation in MDS pathobiology, we have opened new avenues for exploration. Specifically, pathways related to NLRP1 inflammasome activation, ER stress and AMPK activity have yet to be explored in MDS. Increased understanding of NLRP3 inflammasome signaling and regulation will surely lead to the identification of novel targets with potential clinical translation, not only in MDS but also diseases with aberrant inflammasome activation such as Alzheimer's disease, Parkinson's disease, type 2 diabetes mellitus, inflammatory bowel and rheumatologic disorders, among others.

REFERENCES

- 1 Raskind, W., Tirumali, N., Jacobson, R., J, S. & Fialkow, P. Evidence for a Multistep Pathogenesis of a Myelodysplastic Syndrome. *Blood* **63**, 1318-1323 (1984).
- 2 Tefferi, A., Thibodeau, S. & Solberg Jr, L. Clonal Studies in the Myelodysplastic Syndrome Using X-Linked Restriction Fragment Length Polymorphisms. *Blood* **75**, 1770-1773 (1990).
- 3 Janssen, J. W. *et al.* Clonal analysis of myelodysplastic syndromes: evidence of multipotent stem cell origin. *Blood* **73**, 248-254 (1989).
- 4 Chamseddine, A. N., Jabbour, E., Kantarjian, H. M., Bohannon, Z. S. & Garcia-Manero, G. Unraveling Myelodysplastic Syndromes: Current Knowledge and Future Directions. *Current oncology reports* **18**, 4, doi:10.1007/s11912-015-0489-2 (2016).
- 5 Garcia-Manero, G. Myelodysplastic syndromes: 2015 Update on diagnosis, risk-stratification and management. *American journal of hematology* **90**, 831-841, doi:10.1002/ajh.24102 (2015).
- 6 Rollison, D. E. *et al.* Epidemiology of myelodysplastic syndromes and chronic myeloproliferative disorders in the United States, 2001-2004, using data from the NAACCR and SEER programs. *Blood* **112**, 45-52, doi:10.1182/blood-2008-01-134858 (2008).
- 7 Cogle, C. R., Craig, B. M., Rollison, D. E. & List, A. F. Incidence of the myelodysplastic syndromes using a novel claims-based algorithm: high number of uncaptured cases by cancer registries. *Blood* **117**, 7121-7125, doi:10.1182/blood-2011-02-337964 (2011).
- 8 Goldberg, S. L. *et al.* Incidence and clinical complications of myelodysplastic syndromes among United States Medicare beneficiaries. *Journal of clinical oncology : official journal of the American Society of Clinical Oncology* **28**, 2847-2852, doi:10.1200/JCO.2009.25.2395 (2010).
- 9 Liew, E. & Owen, C. Familial myelodysplastic syndromes: a review of the literature. *Haematologica* **96**, 1536-1542, doi:10.3324/haematol.2011.043422 (2011).

- 10 Luddy, R., Champion, L. & Schwartz, A. A Fatal Myeloproliferative Syndrome in a Family with Thrombocytopenia and Platelet Dysfunction. *Cancer* **41**, 1959-1963 (1978).
- 11 Ho, C. Y. *et al.* Linkage of a familial platelet disorder with a propensity to develop myeloid malignancies to human chromosome 21q22.1-22.2. *Blood* **87**, 5218-5224 (1996).
- 12 Song, W. J. *et al.* Haploinsufficiency of CBFA2 causes familial thrombocytopenia with propensity to develop acute myelogenous leukaemia. *Nat Genet* **23**, 166-175, doi:10.1038/13793 (1999).
- 13 Lindstrand, A. *et al.* Detailed molecular and clinical characterization of three patients with 21q deletions. *Clinical genetics* **77**, 145-154, doi:10.1111/j.1399-0004.2009.01289.x (2010).
- 14 Gaitonde, S., Boumendjel, R., Angeles, R. & Rondelli, D. Familial childhood monosomy 7 and associated myelodysplasia. *Journal of pediatric hematology/oncology* **32**, e236-237, doi:10.1097/MPH.0b013e3181e75759 (2010).
- 15 Rau, A. T., Shreedhara, A. K. & Kumar, S. Myelodysplastic syndromes in children: where are we today? *The Ochsner journal* **12**, 216-220 (2012).
- 16 Hasle, H. & Niemeyer, C. M. Advances in the prognostication and management of advanced MDS in children. *British journal of haematology* **154**, 185-195, doi:10.1111/j.1365-2141.2011.08724.x (2011).
- 17 Gohring, G. *et al.* Complex karyotype newly defined: the strongest prognostic factor in advanced childhood myelodysplastic syndrome. *Blood* **116**, 3766-3769, doi:10.1182/blood-2010-04-280313 (2010).
- 18 Steensma, D. P. P39/Tsugane cells are a false cell line contaminated with HL-60 cells and are not suitable for mechanistic studies in myelodysplastic syndromes. *Haematologica* **95**, 1229-1230, doi:10.3324/haematol.2010.022988 (2010).
- 19 Wegrzyn, J., Lam, J. C. & Karsan, A. Mouse models of myelodysplastic syndromes. *Leukemia research* **35**, 853-862, doi:10.1016/j.leukres.2011.03.007 (2011).
- 20 Sekeres, M. A. The epidemiology of myelodysplastic syndromes. *Hematology/oncology clinics of North America* **24**, 287-294, doi:10.1016/j.hoc.2010.02.011 (2010).
- 21 Smit, C. G. & Meyler, L. Acute myeloid leukaemia after treatment with cytostatic agents. *Lancet* **2**, 671-672 (1970).

- 22 Allan, W. S. Acute myeloid leukaemia after treatment with cytostatic agents. *Lancet* **2**, 775 (1970).
- 23 Du, Y., Fryzek, J., Sekeres, M. A. & Taioli, E. Smoking and alcohol intake as risk factors for myelodysplastic syndromes (MDS). *Leukemia research* **34**, 1-5, doi:10.1016/j.leukres.2009.08.006 (2010).
- 24 Ma, X. *et al.* Obesity, lifestyle factors, and risk of myelodysplastic syndromes in a large US cohort. *American journal of epidemiology* **169**, 1492-1499, doi:10.1093/aje/kwp074 (2009).
- 25 Kristinsson, S. Y. *et al.* Chronic immune stimulation might act as a trigger for the development of acute myeloid leukemia or myelodysplastic syndromes. *Journal of clinical oncology : official journal of the American Society of Clinical Oncology* **29**, 2897-2903, doi:10.1200/JCO.2011.34.8540 (2011).
- 26 Cho, R. H., Sieburg, H. B. & Muller-Sieburg, C. E. A new mechanism for the aging of hematopoietic stem cells: aging changes the clonal composition of the stem cell compartment but not individual stem cells. *Blood* **111**, 5553-5561, doi:10.1182/blood-2007-11-123547 (2008).
- 27 Behrens, A., van Deursen, J. M., Rudolph, K. L. & Schumacher, B. Impact of genomic damage and ageing on stem cell function. *Nat Cell Biol* **16**, 201-207, doi:10.1038/ncb2928 (2014).
- 28 Dykstra, B., Olthof, S., Schreuder, J., Ritsema, M. & de Haan, G. Clonal analysis reveals multiple functional defects of aged murine hematopoietic stem cells. *The Journal of experimental medicine* **208**, 2691-2703, doi:10.1084/jem.20111490 (2011).
- 29 Rollison, D. E. *et al.* Telomere length in myelodysplastic syndromes. *Leukemia & lymphoma* **52**, 1528-1536, doi:10.3109/10428194.2011.568648 (2011).
- 30 Steensma, D. P. Historical perspectives on myelodysplastic syndromes. *Leukemia research* **36**, 1441-1452, doi:10.1016/j.leukres.2012.08.007 (2012).
- 31 Gilbert, H. S. A reappraisal of the "myeloproliferative disease" concept. *The Mount Sinai journal of medicine, New York* **37**, 426-435 (1970).
- 32 Bennett, J. M. *et al.* Proposals for the classification of the acute leukaemias. French-American-British (FAB) co-operative group. *British journal of haematology* **33**, 451-458 (1976).
- 33 Bennett, J. M. *et al.* Proposals for the classification of the myelodysplastic syndromes. *British journal of haematology* **51**, 189-199 (1982).

- 34 Vardiman, J. W., Harris, N. L. & Brunning, R. D. The World Health Organization (WHO) classification of the myeloid neoplasms. *Blood* **100**, 2292-2302, doi:10.1182/blood-2002-04-1199 (2002).
- 35 Van den Berghe, H. *et al.* Distinct haematological disorder with deletion of long arm of no. 5 chromosome. *Nature* **251**, 437-438 (1974).
- 36 Vardiman, J. W. *et al.* The 2008 revision of the World Health Organization (WHO) classification of myeloid neoplasms and acute leukemia: rationale and important changes. *Blood* **114**, 937-951, doi:10.1182/blood-2009-03-209262 (2009).
- 37 Arber, D. A. *et al.* The 2016 revision to the World Health Organization classification of myeloid neoplasms and acute leukemia. *Blood* **127**, 2391-2405, doi:10.1182/blood-2016-03-643544 (2016).
- 38 Greenberg, P. *et al.* International scoring system for evaluating prognosis in myelodysplastic syndromes. *Blood* **89**, 2079-2088 (1997).
- 39 Greenberg, P. L. *et al.* Revised international prognostic scoring system for myelodysplastic syndromes. *Blood* **120**, 2454-2465, doi:10.1182/blood-2012-03-420489 (2012).
- 40 Kantarjian, H. *et al.* Proposal for a new risk model in myelodysplastic syndrome that accounts for events not considered in the original International Prognostic Scoring System. *Cancer* **113**, 1351-1361, doi:10.1002/cncr.23697 (2008).
- 41 Extermann, M. Measurement and impact of comorbidity in older cancer patients. *Critical reviews in oncology/hematology* **35**, 181-200 (2000).
- 42 Naqvi, K. *et al.* Association of comorbidities with overall survival in myelodysplastic syndrome: development of a prognostic model. *Journal of clinical oncology : official journal of the American Society of Clinical Oncology* **29**, 2240-2246, doi:10.1200/JCO.2010.31.3353 (2011).
- 43 Daver, N. *et al.* Impact of comorbidities by ACE-27 in the revised-IPSS for patients with myelodysplastic syndromes. *American journal of hematology* **89**, 509-516, doi:10.1002/ajh.23675 (2014).
- 44 Kornblith, A. B. *et al.* Impact of azacytidine on the quality of life of patients with myelodysplastic syndrome treated in a randomized phase III trial: a Cancer and Leukemia Group B study. *Journal of clinical oncology : official journal of the American Society of Clinical Oncology* **20**, 2441-2452 (2002).
- 45 List, A. *et al.* Efficacy of lenalidomide in myelodysplastic syndromes. *The New England journal of medicine* **352**, 549-557, doi:10.1056/NEJMoa041668 (2005).

- 46 Kantarjian, H. *et al.* Decitabine improves patient outcomes in myelodysplastic syndromes: results of a phase III randomized study. *Cancer* **106**, 1794-1803, doi:10.1002/cncr.21792 (2006).
- 47 Aul, C., Germing, U., Gattermann, N. & Minning, H. Increasing incidence of myelodysplastic syndromes: real or fictitious? *Leukemia research* **22**, 93-100 (1998).
- 48 Koreth, J. *et al.* Role of reduced-intensity conditioning allogeneic hematopoietic stem-cell transplantation in older patients with de novo myelodysplastic syndromes: an international collaborative decision analysis. *Journal of clinical oncology : official journal of the American Society of Clinical Oncology* **31**, 2662-2670, doi:10.1200/JCO.2012.46.8652 (2013).
- 49 Cutler, C. S. *et al.* A decision analysis of allogeneic bone marrow transplantation for the myelodysplastic syndromes: delayed transplantation for low-risk myelodysplasia is associated with improved outcome. *Blood* **104**, 579-585, doi:10.1182/blood-2004-01-0338 (2004).
- 50 Chang, C. *et al.* Hematopoietic cell transplantation in patients with myelodysplastic syndrome or acute myeloid leukemia arising from myelodysplastic syndrome: similar outcomes in patients with de novo disease and disease following prior therapy or antecedent hematologic disorders. *Blood* **110**, 1379-1387, doi:10.1182/blood-2007-02-076307 (2007).
- 51 Shenoy, N., Vallumsetla, N., Rachmilewitz, E., Verma, A. & Ginzburg, Y. Impact of iron overload and potential benefit from iron chelation in low-risk myelodysplastic syndrome. *Blood* **124**, 873-881, doi:10.1182/blood-2014-03-563221 (2014).
- 52 Stein, R. S., Abels, R. I. & Krantz, S. B. Pharmacologic doses of recombinant human erythropoietin in the treatment of myelodysplastic syndromes. *Blood* **78**, 1658-1663 (1991).
- 53 Di Raimondo, F. *et al.* A good response rate to recombinant erythropoietin alone may be expected in selected myelodysplastic patients. A preliminary clinical study. *European journal of haematology* **56**, 7-11 (1996).
- 54 Terpos, E. *et al.* Prolonged administration of erythropoietin increases erythroid response rate in myelodysplastic syndromes: a phase II trial in 281 patients. *British journal of haematology* **118**, 174-180 (2002).
- 55 Moyo, V., Lefebvre, P., Duh, M. S., Yektashenas, B. & Mundle, S. Erythropoiesis-stimulating agents in the treatment of anemia in myelodysplastic syndromes: a meta-analysis. *Annals of hematology* **87**, 527-536, doi:10.1007/s00277-008-0450-7 (2008).

- 56 Steensma, D. P. Erythropoiesis-stimulating agents are effective in myelodysplastic syndromes, but are they safe? *American journal of hematology* **84**, 3-5, doi:10.1002/ajh.21323 (2009).
- 57 Jadersten, M., Montgomery, S. M., Dybedal, I., Porwit-MacDonald, A. & Hellstrom-Lindberg, E. Long-term outcome of treatment of anemia in MDS with erythropoietin and G-CSF. *Blood* **106**, 803-811, doi:10.1182/blood-2004-10-3872 (2005).
- 58 Mundle, S. *et al.* An assessment of erythroid response to epoetin alpha as a single agent versus in combination with granulocyte- or granulocyte-macrophage-colony-stimulating factor in myelodysplastic syndromes using a meta-analysis approach. *Cancer* **115**, 706-715, doi:10.1002/cncr.24090 (2009).
- 59 Jonasova, A. *et al.* Cyclosporin A therapy in hypoplastic MDS patients and certain refractory anaemias without hypoplastic bone marrow. *British journal of haematology* **100**, 304-309 (1998).
- 60 Lim, Z. Y. *et al.* Low IPSS score and bone marrow hypocellularity in MDS patients predict hematological responses to antithymocyte globulin. *Leukemia* **21**, 1436-1441, doi:10.1038/sj.leu.2404747 (2007).
- 61 Raza, A. *et al.* Phase 2 study of lenalidomide in transfusion-dependent, low-risk, and intermediate-1 risk myelodysplastic syndromes with karyotypes other than deletion 5q. *Blood* **111**, 86-93, doi:10.1182/blood-2007-01-068833 (2008).
- 62 Liu, X. *et al.* Selective inhibition of IDO1 effectively regulates mediators of antitumor immunity. *Blood* **115**, 3520-3530, doi:10.1182/blood-2009-09-246124 (2010).
- 63 Zhou, L. *et al.* Reduced SMAD7 leads to overactivation of TGF-beta signaling in MDS that can be reversed by a specific inhibitor of TGF-beta receptor I kinase. *Cancer research* **71**, 955-963, doi:10.1158/0008-5472.CAN-10-2933 (2011).
- 64 Suragani, R. N. *et al.* Transforming growth factor-beta superfamily ligand trap ACE-536 corrects anemia by promoting late-stage erythropoiesis. *Nature medicine* **20**, 408-414, doi:10.1038/nm.3512 (2014).
- 65 Attie, K. M. *et al.* A phase 1 study of ACE-536, a regulator of erythroid differentiation, in healthy volunteers. *American journal of hematology* **89**, 766-770, doi:10.1002/ajh.23732 (2014).
- 66 Reilly, M. *et al.* Randomized, double-blind, placebo-controlled, dose-escalating phase I, healthy subjects study of intravenous OPN-305, a humanized anti-TLR2 antibody. *Clinical pharmacology and therapeutics* **94**, 593-600, doi:10.1038/clpt.2013.150 (2013).

- 67 Wei, Y. *et al.* Toll-like receptor alterations in myelodysplastic syndrome. *Leukemia* **27**, 1832-1840, doi:10.1038/leu.2013.180 (2013).
- 68 Garcia-Manero, G. *et al.* A phase I study of oral ARRY-614, a p38 MAPK/Tie2 dual inhibitor, in patients with low or intermediate-1 risk myelodysplastic syndromes. *Clinical cancer research : an official journal of the American Association for Cancer Research* **21**, 985-994, doi:10.1158/1078-0432.CCR-14-1765 (2015).
- 69 Wattel, E. *et al.* Long-term follow-up of de novo myelodysplastic syndromes treated with intensive chemotherapy: incidence of long-term survivors and outcome of partial responders. *British journal of haematology* **98**, 983-991 (1997).
- 70 Beran, M. *et al.* High-dose chemotherapy in high-risk myelodysplastic syndrome: covariate-adjusted comparison of five regimens. *Cancer* **92**, 1999-2015 (2001).
- 71 Leone, G., Teofili, L., Voso, M. T. & Lubbert, M. DNA methylation and demethylating drugs in myelodysplastic syndromes and secondary leukemias. *Haematologica* **87**, 1324-1341 (2002).
- 72 Fenaux, P. *et al.* Efficacy of azacitidine compared with that of conventional care regimens in the treatment of higher-risk myelodysplastic syndromes: a randomised, open-label, phase III study. *The lancet oncology* **10**, 223-232, doi:10.1016/S1470-2045(09)70003-8 (2009).
- 73 Silverman, L. R. Randomized Controlled Trial of Azacitidine in Patients With the Myelodysplastic Syndrome: A Study of the Cancer and Leukemia Group B. *Journal of Clinical Oncology* **20**, 2429-2440, doi:10.1200/jco.2002.04.117 (2002).
- 74 Steensma, D. P. *et al.* Multicenter study of decitabine administered daily for 5 days every 4 weeks to adults with myelodysplastic syndromes: the alternative dosing for outpatient treatment (ADOPT) trial. *Journal of clinical oncology : official journal of the American Society of Clinical Oncology* **27**, 3842-3848, doi:10.1200/JCO.2008.19.6550 (2009).
- 75 Faderl, S. *et al.* Oral clofarabine in the treatment of patients with higher-risk myelodysplastic syndrome. *Journal of clinical oncology : official journal of the American Society of Clinical Oncology* **28**, 2755-2760, doi:10.1200/JCO.2009.26.3509 (2010).
- 76 Buckley, S. A. *et al.* A phase I/II study of oral clofarabine plus low-dose cytarabine in previously treated acute myeloid leukaemia and high-risk myelodysplastic syndrome patients at least 60 years of age. *British journal of haematology* **170**, 349-355, doi:10.1111/bjh.13437 (2015).

- 77 Kantarjian, H. *et al.* Phase I clinical and pharmacokinetic study of oral sapacitabine in patients with acute leukemia and myelodysplastic syndrome. *Journal of clinical oncology : official journal of the American Society of Clinical Oncology* **28**, 285-291, doi:10.1200/JCO.2009.25.0209 (2010).
- 78 Cashen, A. *et al.* Phase II study of the histone deacetylase inhibitor belinostat (PXD101) for the treatment of myelodysplastic syndrome (MDS). *Annals of hematology* **91**, 33-38, doi:10.1007/s00277-011-1240-1 (2012).
- 79 Kirschbaum, M. *et al.* A phase 1 clinical trial of vorinostat in combination with decitabine in patients with acute myeloid leukaemia or myelodysplastic syndrome. *British journal of haematology* **167**, 185-193, doi:10.1111/bjh.13016 (2014).
- 80 Tan, P. *et al.* Dual epigenetic targeting with panobinostat and azacitidine in acute myeloid leukemia and high-risk myelodysplastic syndrome. *Blood cancer journal* **4**, e170, doi:10.1038/bcj.2013.68 (2014).
- 81 Komrokji, R. S. *et al.* Phase I clinical trial of oral rigosertib in patients with myelodysplastic syndromes. *British journal of haematology*, doi:10.1111/bjh.12436 (2013).
- 82 Takahashi, K. *et al.* Dynamic acquisition of FLT3 or RAS alterations drive a subset of patients with lower risk MDS to secondary AML. *Leukemia* **27**, 2081-2083, doi:10.1038/leu.2013.165 (2013).
- 83 Yang, H. *et al.* Expression of PD-L1, PD-L2, PD-1 and CTLA4 in myelodysplastic syndromes is enhanced by treatment with hypomethylating agents. *Leukemia* **28**, 1280-1288, doi:10.1038/leu.2013.355 (2014).
- 84 Bejar, R., Levine, R. & Ebert, B. L. Unraveling the molecular pathophysiology of myelodysplastic syndromes. *Journal of clinical oncology : official journal of the American Society of Clinical Oncology* **29**, 504-515, doi:10.1200/JCO.2010.31.1175 (2011).
- 85 Haase, D. *et al.* New insights into the prognostic impact of the karyotype in MDS and correlation with subtypes: evidence from a core dataset of 2124 patients. *Blood* **110**, 4385-4395, doi:10.1182/blood-2007-03-082404 (2007).
- 86 Bejar, R. *et al.* Clinical effect of point mutations in myelodysplastic syndromes. *The New England journal of medicine* **364**, 2496-2506, doi:10.1056/NEJMoa1013343 (2011).
- 87 Papaemmanuil, E. *et al.* Clinical and biological implications of driver mutations in myelodysplastic syndromes. *Blood* **122**, 3616-3627; quiz 3699, doi:10.1182/blood-2013-08-518886 (2013).

- 88 Haferlach, T. *et al.* Landscape of genetic lesions in 944 patients with myelodysplastic syndromes. *Leukemia* **28**, 241-247, doi:10.1038/leu.2013.336 (2013).
- 89 Walter, M. J. *et al.* Clonal architecture of secondary acute myeloid leukemia. *The New England journal of medicine* **366**, 1090-1098, doi:10.1056/NEJMoa1106968 (2012).
- 90 Jaiswal, S. *et al.* Age-Related Clonal Hematopoiesis Associated with Adverse Outcomes. *New England Journal of Medicine* **371**, 2488-2498, doi:10.1056/NEJMoa1408617 (2014).
- 91 Steensma, D. P. *et al.* Clonal hematopoiesis of indeterminate potential and its distinction from myelodysplastic syndromes. *Blood* **126**, 9-16, doi:10.1182/blood-2015-03-631747 (2015).
- 92 Bejar, R. Myelodysplastic Syndromes Diagnosis: What Is the Role of Molecular Testing? *Current hematologic malignancy reports* **10**, 282-291, doi:10.1007/s11899-015-0270-5 (2015).
- 93 Ganan-Gomez, I. *et al.* Deregulation of innate immune and inflammatory signaling in myelodysplastic syndromes. *Leukemia* **29**, 1458-1469, doi:10.1038/leu.2015.69 (2015).
- 94 Anderson, L. A. *et al.* Risks of myeloid malignancies in patients with autoimmune conditions. *British journal of cancer* **100**, 822-828, doi:10.1038/sj.bjc.6604935 (2009).
- 95 de Hollanda, A. *et al.* Systemic and immune manifestations in myelodysplasia: a multicenter retrospective study. *Arthritis care & research* **63**, 1188-1194, doi:10.1002/acr.20504 (2011).
- 96 Mekinian, A. *et al.* Inflammatory arthritis in patients with myelodysplastic syndromes: a multicenter retrospective study and literature review of 68 cases. *Medicine* **93**, 1-10, doi:10.1097/MD.000000000000011 (2014).
- 97 Kordasti, S. Y. *et al.* IL-17-producing CD4(+) T cells, pro-inflammatory cytokines and apoptosis are increased in low risk myelodysplastic syndrome. *British journal of haematology* **145**, 64-72, doi:10.1111/j.1365-2141.2009.07593.x (2009).
- 98 Kitagawa, M. *et al.* Overexpression of tumor necrosis factor (TNF)-alpha and interferon (IFN)-gamma by bone marrow cells from patients with myelodysplastic syndromes. *Leukemia* **11**, 2049-2054 (1997).

- 99 Mundle, S. D. *et al.* Indication of an involvement of interleukin-1 beta converting enzyme-like protease in intramedullary apoptotic cell death in the bone marrow of patients with myelodysplastic syndromes. *Blood* **88**, 2640-2647 (1996).
- 100 Wetzler, M., Kurzrock, R., Estrov, Z., Estey, E. & Talpaz, M. Cytokine expression in adherent layers from patients with myelodysplastic syndrome and acute myelogenous leukemia. *Leukemia research* **19**, 23-34 (1995).
- 101 Brunner, B. *et al.* Blood levels of angiogenin and vascular endothelial growth factor are elevated in myelodysplastic syndromes and in acute myeloid leukemia. *Journal of hematology & stem cell research* **11**, 119-125, doi:10.1089/152581602753448586 (2002).
- 102 Tsimberidou, A. M. *et al.* The prognostic significance of cytokine levels in newly diagnosed acute myeloid leukemia and high-risk myelodysplastic syndromes. *Cancer* **113**, 1605-1613, doi:10.1002/cncr.23785 (2008).
- 103 Akiyama, T. *et al.* Involvement of transforming growth factor-beta and thrombopoietin in the pathogenesis of myelodysplastic syndrome with myelofibrosis. *Leukemia* **19**, 1558-1566, doi:10.1038/sj.leu.2403875 (2005).
- 104 Takeuchi, O. & Akira, S. Pattern recognition receptors and inflammation. *Cell* **140**, 805-820, doi:10.1016/j.cell.2010.01.022 (2010).
- 105 Sallman, D. A., Cluzeau, T., Basiorka, A. A. & List, A. Unraveling the Pathogenesis of MDS: The NLRP3 Inflammasome and Pyroptosis Drive the MDS Phenotype. *Front Oncol* **6**, 151, doi:10.3389/fonc.2016.00151 (2016).
- 106 Newton, K. & Dixit, V. M. Signaling in innate immunity and inflammation. *Cold Spring Harbor perspectives in biology* **4**, doi:10.1101/cshperspect.a006049 (2012).
- 107 Esplin, B. L. *et al.* Chronic exposure to a TLR ligand injures hematopoietic stem cells. *Journal of immunology* **186**, 5367-5375, doi:10.4049/jimmunol.1003438 (2011).
- 108 Holl, T. M. & Kelsoe, G. Outside influence: TLRs direct hematopoietic cell fates. *Immunity* **24**, 667-669, doi:10.1016/j.immuni.2006.06.007 (2006).
- 109 O'Hagan-Wong, K. *et al.* Increased IL-6 secretion by aged human mesenchymal stromal cells disrupts hematopoietic stem and progenitor cells' homeostasis. *Oncotarget* **7**, 13285-13296, doi:10.18632/oncotarget.7690 (2016).
- 110 Pietras, E. M. *et al.* Chronic interleukin-1 exposure drives haematopoietic stem cells towards precocious myeloid differentiation at the expense of self-renewal. *Nat Cell Biol* **18**, 607-618, doi:10.1038/ncb3346 (2016).

- 111 Sioud, M., Floisand, Y., Forfang, L. & Lund-Johansen, F. Signaling through toll-like receptor 7/8 induces the differentiation of human bone marrow CD34+ progenitor cells along the myeloid lineage. *Journal of molecular biology* **364**, 945-954, doi:10.1016/j.jmb.2006.09.054 (2006).
- 112 Maratheftis, C. I., Andreakos, E., Moutsopoulos, H. M. & Voulgarelis, M. Toll-like receptor-4 is up-regulated in hematopoietic progenitor cells and contributes to increased apoptosis in myelodysplastic syndromes. *Clinical cancer research : an official journal of the American Association for Cancer Research* **13**, 1154-1160, doi:10.1158/1078-0432.CCR-06-2108 (2007).
- 113 Velegraki, M. *et al.* Impaired clearance of apoptotic cells leads to HMGB1 release in the bone-marrow of MDS patients and induces TLR4-mediated cytokine production. *Haematologica*, doi:10.3324/haematol.2012.064642 (2013).
- 114 Dimicoli, S. *et al.* Overexpression of the toll-like receptor (TLR) signaling adaptor MYD88, but lack of genetic mutation, in myelodysplastic syndromes. *PloS one* **8**, e71120, doi:10.1371/journal.pone.0071120 (2013).
- 115 Starczynowski, D. T. *et al.* High-resolution whole genome tiling path array CGH analysis of CD34+ cells from patients with low-risk myelodysplastic syndromes reveals cryptic copy number alterations and predicts overall and leukemia-free survival. *Blood* **112**, 3412-3424, doi:10.1182/blood-2007-11-122028 (2008).
- 116 Rhyasen, G. W. *et al.* Targeting IRAK1 as a therapeutic approach for myelodysplastic syndrome. *Cancer cell* **24**, 90-104, doi:10.1016/j.ccr.2013.05.006 (2013).
- 117 Starczynowski, D. T. *et al.* Identification of miR-145 and miR-146a as mediators of the 5q- syndrome phenotype. *Nature medicine* **16**, 49-58, doi:10.1038/nm.2054 (2010).
- 118 Starczynowski, D. T. *et al.* MicroRNA-146a disrupts hematopoietic differentiation and survival. *Experimental hematology* **39**, 167-178 e164, doi:10.1016/j.exphem.2010.09.011 (2011).
- 119 Pittenger, M. F. *et al.* Multilineage potential of adult human mesenchymal stem cells. *Science* **284**, 143-147 (1999).
- 120 Medyouf, H. *et al.* Myelodysplastic cells in patients reprogram mesenchymal stromal cells to establish a transplantable stem cell niche disease unit. *Cell stem cell* **14**, 824-837, doi:10.1016/j.stem.2014.02.014 (2014).
- 121 Tauro, S., Hepburn, M. D., Peddie, C. M., Bowen, D. T. & Pippard, M. J. Functional disturbance of marrow stromal microenvironment in the

- myelodysplastic syndromes. *Leukemia* **16**, 785-790, doi:10.1038/sj.leu.2402440 (2002).
- 122 Raaijmakers, M. H. *et al.* Bone progenitor dysfunction induces myelodysplasia and secondary leukaemia. *Nature* **464**, 852-857, doi:10.1038/nature08851 (2010).
- 123 Balderman, S. R. *et al.* Targeting of the bone marrow microenvironment improves outcome in a murine model of myelodysplastic syndrome. *Blood* **127**, 616-625, doi:10.1182/blood-2015-06-653113 (2016).
- 124 Kouvidi, E. *et al.* Cytogenetic evaluation of mesenchymal stem/stromal cells from patients with myelodysplastic syndromes at different time-points during ex vivo expansion. *Leukemia research* **43**, 24-32, doi:10.1016/j.leukres.2016.02.007 (2016).
- 125 Lopez-Villar, O. *et al.* Both expanded and uncultured mesenchymal stem cells from MDS patients are genomically abnormal, showing a specific genetic profile for the 5q- syndrome. *Leukemia* **23**, 664-672, doi:10.1038/leu.2008.361 (2009).
- 126 Blau, O. *et al.* Mesenchymal stromal cells of myelodysplastic syndrome and acute myeloid leukemia patients have distinct genetic abnormalities compared with leukemic blasts. *Blood* **118**, 5583-5592, doi:10.1182/blood-2011-03-343467 (2011).
- 127 Orkin, S. H. & Zon, L. I. Hematopoiesis: an evolving paradigm for stem cell biology. *Cell* **132**, 631-644, doi:10.1016/j.cell.2008.01.025 (2008).
- 128 Orkin, S. H. Diversification of haematopoietic stem cells to specific lineages. *Nature reviews. Genetics* **1**, 57-64, doi:10.1038/35049577 (2000).
- 129 Kondo, M. Lymphoid and myeloid lineage commitment in multipotent hematopoietic progenitors. *Immunological reviews* **238**, 37-46, doi:10.1111/j.1600-065X.2010.00963.x (2010).
- 130 Epling-Burnette, P. K. *et al.* Reduced natural killer (NK) function associated with high-risk myelodysplastic syndrome (MDS) and reduced expression of activating NK receptors. *Blood* **109**, 4816-4824, doi:10.1182/blood-2006-07-035519 (2007).
- 131 Sternberg, A. *et al.* Evidence for reduced B-cell progenitors in early (low-risk) myelodysplastic syndrome. *Blood* **106**, 2982-2991, doi:10.1182/blood-2005-04-1543 (2005).
- 132 Kook, H. *et al.* Increased cytotoxic T cells with effector phenotype in aplastic anemia and myelodysplasia. *Experimental hematology* **29**, 1270-1277 (2001).

- 133 Zheng, Z. *et al.* In vitro deprivation of CD8(+)CD57(+)T cells promotes the malignant growth of bone marrow colony cells in patients with lower-risk myelodysplastic syndrome. *Experimental hematology* **38**, 677-684, doi:10.1016/j.exphem.2010.04.002 (2010).
- 134 Fozza, C. *et al.* Patients with myelodysplastic syndromes display several T-cell expansions, which are mostly polyclonal in the CD4(+) subset and oligoclonal in the CD8(+) subset. *Experimental hematology* **37**, 947-955, doi:10.1016/j.exphem.2009.04.009 (2009).
- 135 Kordasti, S. Y. *et al.* CD4+CD25high Foxp3+ regulatory T cells in myelodysplastic syndrome (MDS). *Blood* **110**, 847-850, doi:10.1182/blood-2007-01-067546 (2007).
- 136 Kotsianidis, I. *et al.* Kinetics, function and bone marrow trafficking of CD4+CD25+FOXP3+ regulatory T cells in myelodysplastic syndromes (MDS). *Leukemia* **23**, 510-518, doi:10.1038/leu.2008.333 (2009).
- 137 Mailloux, A. W. *et al.* Expansion of effector memory regulatory T cells represents a novel prognostic factor in lower risk myelodysplastic syndrome. *Journal of immunology* **189**, 3198-3208, doi:10.4049/jimmunol.1200602 (2012).
- 138 Gabrivovich, D. I. & Nagaraj, S. Myeloid-derived suppressor cells as regulators of the immune system. *Nature reviews. Immunology* **9**, 162-174, doi:10.1038/nri2506 (2009).
- 139 Huang, B. *et al.* Gr-1+CD115+ immature myeloid suppressor cells mediate the development of tumor-induced T regulatory cells and T-cell anergy in tumor-bearing host. *Cancer research* **66**, 1123-1131, doi:10.1158/0008-5472.CAN-05-1299 (2006).
- 140 Chen, X. *et al.* Induction of myelodysplasia by myeloid-derived suppressor cells. *The Journal of clinical investigation* **123**, 4595-4611, doi:10.1172/JCI67580 (2013).
- 141 Sinha, P. *et al.* Proinflammatory S100 proteins regulate the accumulation of myeloid-derived suppressor cells. *Journal of immunology* **181**, 4666-4675 (2008).
- 142 Chen, H., Xu, C., Jin, Q. & Liu, Z. S100 protein family in human cancer. *American journal of cancer research* **4**, 89-115 (2014).
- 143 Hessian, P. A., Edgeworth, J. & Hogg, N. MRP-8 and MRP-14, two abundant Ca(2+)-binding proteins of neutrophils and monocytes. *Journal of leukocyte biology* **53**, 197-204 (1993).

- 144 Vogl, T. *et al.* Mrp8 and Mrp14 are endogenous activators of Toll-like receptor 4, promoting lethal, endotoxin-induced shock. *Nature medicine* **13**, 1042-1049, doi:10.1038/nm1638 (2007).
- 145 Ghavami, S. *et al.* S100A8/A9 at low concentration promotes tumor cell growth via RAGE ligation and MAP kinase-dependent pathway. *Journal of leukocyte biology* **83**, 1484-1492, doi:10.1189/jlb.0607397 (2008).
- 146 Srikrishna, G. *et al.* Two Proteins Modulating Transendothelial Migration of Leukocytes Recognize Novel Carboxylated Glycans on Endothelial Cells. *The Journal of Immunology* **166**, 4678-4688, doi:10.4049/jimmunol.166.7.4678 (2001).
- 147 Riva, M. *et al.* Induction of nuclear factor-kappaB responses by the S100A9 protein is Toll-like receptor-4-dependent. *Immunology* **137**, 172-182, doi:10.1111/j.1365-2567.2012.03619.x (2012).
- 148 Song, X. *et al.* CD11b+/Gr-1+ Immature Myeloid Cells Mediate Suppression of T Cells in Mice Bearing Tumors of IL-1 -Secreting Cells. *The Journal of Immunology* **175**, 8200-8208, doi:10.4049/jimmunol.175.12.8200 (2005).
- 149 Verschoor, C. P. *et al.* Blood CD33(+)/HLA-DR(-) myeloid-derived suppressor cells are increased with age and a history of cancer. *Journal of leukocyte biology* **93**, 633-637, doi:10.1189/jlb.0912461 (2013).
- 150 Sokal, G. *et al.* A new hematologic syndrome with a distinct karyotype: the 5q-- chromosome. *Blood* **46**, 519-533 (1975).
- 151 Mathew, P. *et al.* The 5q- syndrome: a single-institution study of 43 consecutive patients. *Blood* **81**, 1040-1045 (1993).
- 152 Carbonell, F., Heimpel, H., Kubanek, B. & Fliedner, T. M. Growth and cytogenetic characteristics of bone marrow colonies from patients with 5q-syndrome. *Blood* **66**, 463-465 (1985).
- 153 Boulwood, J., Lewis, S. & Wainscoat, J. S. The 5q-syndrome. *Blood* **84**, 3253-3260 (1994).
- 154 Boulwood, J. *et al.* Narrowing and genomic annotation of the commonly deleted region of the 5q- syndrome. *Blood* **99**, 4638-4641 (2002).
- 155 Boulwood, J. *et al.* Gene expression profiling of CD34+ cells in patients with the 5q- syndrome. *British journal of haematology* **139**, 578-589, doi:10.1111/j.1365-2141.2007.06833.x (2007).

- 156 D'Amato, R. J., Loughnan, M. S., Flynn, E. & Folkman, J. Thalidomide is an inhibitor of angiogenesis. *Proceedings of the National Academy of Sciences of the United States of America* **91**, 4082-4085 (1994).
- 157 Corral, L. G. *et al.* Differential cytokine modulation and T cell activation by two distinct classes of thalidomide analogues that are potent inhibitors of TNF-alpha. *Journal of immunology* **163**, 380-386 (1999).
- 158 Raza, A. *et al.* Thalidomide produces transfusion independence in long-standing refractory anemias of patients with myelodysplastic syndromes. *Blood* **98**, 958-965 (2001).
- 159 List, A. *et al.* Lenalidomide in the myelodysplastic syndrome with chromosome 5q deletion. *The New England journal of medicine* **355**, 1456-1465, doi:10.1056/NEJMoa061292 (2006).
- 160 Ebert, B. L. *et al.* Identification of RPS14 as a 5q- syndrome gene by RNA interference screen. *Nature* **451**, 335-339, doi:10.1038/nature06494 (2008).
- 161 Ebert, B. L. *et al.* An erythroid differentiation signature predicts response to lenalidomide in myelodysplastic syndrome. *PLoS Biol* **5**, e35, doi:10.1371/journal (2008).
- 162 Barlow, J. L. *et al.* A p53-dependent mechanism underlies macrocytic anemia in a mouse model of human 5q- syndrome. *Nature medicine* **16**, 59-66, doi:10.1038/nm.2063 (2010).
- 163 Dutt, S. *et al.* Haploinsufficiency for ribosomal protein genes causes selective activation of p53 in human erythroid progenitor cells. *Blood* **117**, 2567-2576, doi:10.1182/blood-2010-07-295238 (2011).
- 164 Wei, S. *et al.* Lenalidomide promotes p53 degradation by inhibiting MDM2 auto-ubiquitination in myelodysplastic syndrome with chromosome 5q deletion. *Oncogene* **32**, 1110-1120, doi:10.1038/onc.2012.139 (2013).
- 165 Zhang, Y. & Lu, H. Signaling to p53: ribosomal proteins find their way. *Cancer cell* **16**, 369-377, doi:10.1016/j.ccr.2009.09.024 (2009).
- 166 Wu, L. *et al.* Low RPS14 expression in MDS without 5q - aberration confers higher apoptosis rate of nucleated erythrocytes and predicts prolonged survival and possible response to lenalidomide in lower risk non-5q- patients. *European journal of haematology* **90**, 486-493, doi:10.1111/ejh.12105 (2013).
- 167 Schneider, R. K. *et al.* Rps14 haploinsufficiency causes a block in erythroid differentiation mediated by S100A8 and S100A9. *Nature medicine* **22**, 288-297, doi:10.1038/nm.4047 (2016).

- 168 Li, C. *et al.* A novel p53 target gene, S100A9, induces p53-dependent cellular apoptosis and mediates the p53 apoptosis pathway. *The Biochemical journal* **422**, 363-372, doi:10.1042/BJ20090465 (2009).
- 169 Schneider, R. K. *et al.* Role of casein kinase 1A1 in the biology and targeted therapy of del(5q) MDS. *Cancer cell* **26**, 509-520, doi:10.1016/j.ccr.2014.08.001 (2014).
- 170 Winter, J., Jung, S., Keller, S., Gregory, R. I. & Diederichs, S. Many roads to maturity: microRNA biogenesis pathways and their regulation. *Nature Cell Biology* **11**, 228-234 (2009).
- 171 Varney, M. E. *et al.* Loss of Tifab, a del(5q) MDS gene, alters hematopoiesis through derepression of Toll-like receptor-TRAF6 signaling. *The Journal of experimental medicine* **212**, 1967-1985, doi:10.1084/jem.20141898 (2015).
- 172 Fang, J. *et al.* Myeloid malignancies with chromosome 5q deletions acquire a dependency on an intrachromosomal NF-kappaB gene network. *Cell reports* **8**, 1328-1338, doi:10.1016/j.celrep.2014.07.062 (2014).
- 173 Eisenmann, K. M. *et al.* 5q- myelodysplastic syndromes: chromosome 5q genes direct a tumor-suppression network sensing actin dynamics. *Oncogene* **28**, 3429-3441, doi:10.1038/onc.2009.207 (2009).
- 174 Keerthivasan, G. *et al.* Aberrant overexpression of CD14 on granulocytes sensitizes the innate immune response in mDia1 heterozygous del(5q) MDS. *Blood* **124**, 780-790, doi:10.1182/blood-2014-01-552463 (2014).
- 175 Shi, Y. *et al.* The mDial formin is required for neutrophil polarization, migration, and activation of the LARG/RhoA/ROCK signaling axis during chemotaxis. *Journal of immunology* **182**, 3837-3845, doi:10.4049/jimmunol.0803838 (2009).
- 176 Sakata, D. *et al.* Impaired T lymphocyte trafficking in mice deficient in an actin-nucleating protein, mDia1. *The Journal of experimental medicine* **204**, 2031-2038, doi:10.1084/jem.20062647 (2007).
- 177 Fuchs, Y. & Steller, H. Live to die another way: modes of programmed cell death and the signals emanating from dying cells. *Nature reviews. Molecular cell biology* **16**, 329-344, doi:10.1038/nrm3999 (2015).
- 178 Man, S. M. & Kanneganti, T. D. Converging roles of caspases in inflammasome activation, cell death and innate immunity. *Nature reviews. Immunology* **16**, 7-21, doi:10.1038/nri.2015.7 (2016).
- 179 Alnemri, E. S. *et al.* Human ICE/CED-3 protease nomenclature. *Cell* **87**, 171 (1996).

- 180 Stennicke, H. R. & Salvesen, G. S. Catalytic properties of the caspases. *Cell death and differentiation* **6**, 1054-1059, doi:10.1038/sj.cdd.4400599 (1999).
- 181 Lavrik, I. N., Golks, A. & Krammer, P. H. Caspases: pharmacological manipulation of cell death. *The Journal of clinical investigation* **115**, 2665-2672, doi:10.1172/JCI26252 (2005).
- 182 Saleh, M. *et al.* Differential modulation of endotoxin responsiveness by human caspase-12 polymorphisms. *Nature* **429**, 75-79, doi:10.1038/nature02451 (2004).
- 183 Van de Craen, M. *et al.* Identification of a new caspase homologue: caspase-14. *Cell death and differentiation* **5**, 838-846, doi:10.1038/sj.cdd.4400444 (1998).
- 184 Park, H. H. *et al.* The death domain superfamily in intracellular signaling of apoptosis and inflammation. *Annual review of immunology* **25**, 561-586, doi:10.1146/annurev.immunol.25.022106.141656 (2007).
- 185 Kiraz, Y., Adan, A., Kartal Yandim, M. & Baran, Y. Major apoptotic mechanisms and genes involved in apoptosis. *Tumor Biology*, doi:10.1007/s13277-016-5035-9 (2016).
- 186 Li, P. *et al.* Cytochrome c and dATP-dependent formation of Apaf-1/caspase-9 complex initiates an apoptotic protease cascade. *Cell* **91**, 479-489 (1997).
- 187 Schneider, P. & Tschopp, J. Apoptosis induced by death receptors. *Pharmaceutica acta Helvetiae* **74**, 281-286 (2000).
- 188 Ktistakis, N. T. & Tooze, S. A. Digesting the Expanding Mechanisms of Autophagy. *Trends in cell biology*, doi:10.1016/j.tcb.2016.03.006 (2016).
- 189 Youle, R. J. & Narendra, D. P. Mechanisms of mitophagy. *Nature reviews. Molecular cell biology* **12**, 9-14, doi:10.1038/nrm3028 (2011).
- 190 Cho, D. H. *et al.* Caspase-mediated cleavage of ATG6/Beclin-1 links apoptosis to autophagy in HeLa cells. *Cancer letters* **274**, 95-100, doi:10.1016/j.canlet.2008.09.004 (2009).
- 191 Wirawan, E. *et al.* Caspase-mediated cleavage of Beclin-1 inactivates Beclin-1-induced autophagy and enhances apoptosis by promoting the release of proapoptotic factors from mitochondria. *Cell death & disease* **1**, e18, doi:10.1038/cddis.2009.16 (2010).
- 192 Young, M. M. *et al.* Autophagosomal membrane serves as platform for intracellular death-inducing signaling complex (iDISC)-mediated caspase-8 activation and apoptosis. *The Journal of biological chemistry* **287**, 12455-12468, doi:10.1074/jbc.M111.309104 (2012).

- 193 Nakahira, K. *et al.* Autophagy proteins regulate innate immune responses by inhibiting the release of mitochondrial DNA mediated by the NALP3 inflammasome. *Nature immunology* **12**, 222-230, doi:10.1038/ni.1980 (2011).
- 194 Shi, C. S. *et al.* Activation of autophagy by inflammatory signals limits IL-1beta production by targeting ubiquitinated inflammasomes for destruction. *Nature immunology* **13**, 255-263, doi:10.1038/ni.2215 (2012).
- 195 Harris, J. *et al.* Autophagy controls IL-1beta secretion by targeting pro-IL-1beta for degradation. *The Journal of biological chemistry* **286**, 9587-9597, doi:10.1074/jbc.M110.202911 (2011).
- 196 Raza, A. *et al.* Apoptosis in bone marrow biopsy samples involving stromal and hematopoietic cells in 50 patients with myelodysplastic syndromes. *Blood* **86**, 268-276 (1995).
- 197 Parker, J. E. *et al.* The role of apoptosis, proliferation, and the Bcl-2-related proteins in the myelodysplastic syndromes and acute myeloid leukemia secondary to MDS. *Blood* **96**, 3932-3938 (2000).
- 198 Rajapaksa, R., Ginzton, N., Rott, L. S. & Greenberg, P. L. Altered oncoprotein expression and apoptosis in myelodysplastic syndrome marrow cells. *Blood* **88**, 4275-4287 (1996).
- 199 Basiorka, A. A. *et al.* The NLRP3 Inflammasome functions as a driver of the myelodysplastic syndrome phenotype. *Blood*, doi:10.1182/blood-2016-07-730556 (2016).
- 200 Kerbauy, D. M. *et al.* NF-kappaB and FLIP in arsenic trioxide (ATO)-induced apoptosis in myelodysplastic syndromes (MDSs). *Blood* **106**, 3917-3925, doi:10.1182/blood-2005-04-1424 (2005).
- 201 Claessens, Y. E. *et al.* In vitro proliferation and differentiation of erythroid progenitors from patients with myelodysplastic syndromes: evidence for Fas-dependent apoptosis. *Blood* **99**, 1594-1601 (2002).
- 202 Claessens, Y. E. *et al.* Rescue of early-stage myelodysplastic syndrome-deriving erythroid precursors by the ectopic expression of a dominant-negative form of FADD. *Blood* **105**, 4035-4042, doi:10.1182/blood-2004-08-3166 (2005).
- 203 Tehranchi, R. *et al.* Granulocyte colony-stimulating factor inhibits spontaneous cytochrome c release and mitochondria-dependent apoptosis of myelodysplastic syndrome hematopoietic progenitors. *Blood* **101**, 1080-1086, doi:10.1182/blood-2002-06-1774 (2003).

- 204 Boudard, D. *et al.* Expression and prognostic significance of Bcl-2 family proteins in myelodysplastic syndromes. *American journal of hematology* **70**, 115-125, doi:10.1002/ajh.10108 (2002).
- 205 Benesch, M., Platzbecker, U., Ward, J., Deeg, H. J. & Leisenring, W. Expression of FLIP(Long) and FLIP(Short) in bone marrow mononuclear and CD34+ cells in patients with myelodysplastic syndrome: correlation with apoptosis. *Leukemia* **17**, 2460-2466, doi:10.1038/sj.leu.2403180 (2003).
- 206 Komrokji, R. S. & List, A. F. Lenalidomide for treatment of myelodysplastic syndromes: current status and future directions. *Hematology/oncology clinics of North America* **24**, 377-388, doi:10.1016/j.hoc.2010.02.013 (2010).
- 207 Watson, A. S., Mortensen, M. & Simon, A. K. Autophagy in the pathogenesis of myelodysplastic syndrome and acute myeloid leukemia. *Cell Cycle* **10**, 1719-1725, doi:10.4161/cc.10.11.15673 (2014).
- 208 Gattermann, N. *et al.* Heteroplasmic point mutations of mitochondrial DNA affecting subunit I of cytochrome c oxidase in two patients with acquired idiopathic sideroblastic anemia. *Blood* **90**, 4961-4972 (1997).
- 209 van de Loosdrecht, A. A. *et al.* Mitochondrial disruption and limited apoptosis of erythroblasts are associated with high risk myelodysplasia. An ultrastructural analysis. *Leukemia research* **25**, 385-393 (2001).
- 210 Houwerzijl, E. J. *et al.* Erythroid precursors from patients with low-risk myelodysplasia demonstrate ultrastructural features of enhanced autophagy of mitochondria. *Leukemia* **23**, 886-891, doi:10.1038/leu.2008.389 (2009).
- 211 Brennan, M. A. & Cookson, B. T. Salmonella induces macrophage death by caspase-1-dependent necrosis. *Molecular microbiology* **38**, 31-40 (2000).
- 212 Cookson, B. T. & Brennan, M. A. Pro-inflammatory programmed cell death. *Trends in microbiology* **9**, 113-114 (2001).
- 213 LaRock, C. N. & Cookson, B. T. Burning down the house: cellular actions during pyroptosis. *PLoS pathogens* **9**, e1003793, doi:10.1371/journal.ppat.1003793 (2013).
- 214 Fink, S. L. & Cookson, B. T. Caspase-1-dependent pore formation during pyroptosis leads to osmotic lysis of infected host macrophages. *Cellular microbiology* **8**, 1812-1825, doi:10.1111/j.1462-5822.2006.00751.x (2006).
- 215 Erener, S. *et al.* Inflammasome-activated caspase 7 cleaves PARP1 to enhance the expression of a subset of NF-kappaB target genes. *Mol Cell* **46**, 200-211, doi:10.1016/j.molcel.2012.02.016 (2012).

- 216 Watson, P. R. *et al.* Salmonella enterica serovars Typhimurium and Dublin can lyse macrophages by a mechanism distinct from apoptosis. *Infection and immunity* **68**, 3744-3747 (2000).
- 217 Zhong, Z. *et al.* TRPM2 links oxidative stress to NLRP3 inflammasome activation. *Nature communications* **4**, 1611, doi:10.1038/ncomms2608 (2013).
- 218 Zhang, W. *et al.* TRPM2 is an ion channel that modulates hematopoietic cell death through activation of caspases and PARP cleavage. *American journal of physiology. Cell physiology* **290**, C1146-1159, doi:10.1152/ajpcell.00205.2005 (2006).
- 219 Black, R. A., Kronheim, S. R., Merriam, J. E., March, C. J. & Hopp, T. P. A pre-aspartate-specific protease from human leukocytes that cleaves pro-interleukin-1 beta. *The Journal of biological chemistry* **264**, 5323-5326 (1989).
- 220 Kostura, M. J. *et al.* Identification of a monocyte specific pre-interleukin 1 beta convertase activity. *Proceedings of the National Academy of Sciences of the United States of America* **86**, 5227-5231 (1989).
- 221 Fantuzzi, G. & Dinarello, C. A. Interleukin-18 and interleukin-1 beta: two cytokine substrates for ICE (caspase-1). *Journal of clinical immunology* **19**, 1-11 (1999).
- 222 Winkler, S. & Rosen-Wolff, A. Caspase-1: an integral regulator of innate immunity. *Seminars in immunopathology*, doi:10.1007/s00281-015-0494-4 (2015).
- 223 Keller, M., Ruegg, A., Werner, S. & Beer, H. D. Active caspase-1 is a regulator of unconventional protein secretion. *Cell* **132**, 818-831, doi:10.1016/j.cell.2007.12.040 (2008).
- 224 Ting, J. P. *et al.* The NLR gene family: a standard nomenclature. *Immunity* **28**, 285-287, doi:10.1016/j.immuni.2008.02.005 (2008).
- 225 Martinon, F. & Tschopp, J. Inflammatory caspases and inflammasomes: master switches of inflammation. *Cell death and differentiation* **14**, 10-22, doi:10.1038/sj.cdd.4402038 (2007).
- 226 Chen, G., Shaw, M. H., Kim, Y. G. & Nunez, G. NOD-like receptors: role in innate immunity and inflammatory disease. *Annual review of pathology* **4**, 365-398, doi:10.1146/annurev.pathol.4.110807.092239 (2009).
- 227 Broz, P. & Dixit, V. M. Inflammasomes: mechanism of assembly, regulation and signalling. *Nature reviews. Immunology* **16**, 407-420, doi:10.1038/nri.2016.58 (2016).

- 228 Martinon, F., Burns, K. & Tschopp, J. The inflammasome: a molecular platform triggering activation of inflammatory caspases and processing of proIL-beta. *Mol Cell* **10**, 417-426 (2002).
- 229 Chavarria-Smith, J. & Vance, R. E. The NLRP1 inflammasomes. *Immunological reviews* **265**, 22-34, doi:10.1111/imr.12283 (2015).
- 230 Kummer, J. A. *et al.* Inflammasome components NALP 1 and 3 show distinct but separate expression profiles in human tissues suggesting a site-specific role in the inflammatory response. *The journal of histochemistry and cytochemistry : official journal of the Histochemistry Society* **55**, 443-452, doi:10.1369/jhc.6A7101.2006 (2007).
- 231 Masters, S. L. *et al.* NLRP1 inflammasome activation induces pyroptosis of hematopoietic progenitor cells. *Immunity* **37**, 1009-1023, doi:10.1016/j.immuni.2012.08.027 (2012).
- 232 Fernandes-Alnemri, T., Yu, J. W., Datta, P., Wu, J. & Alnemri, E. S. AIM2 activates the inflammasome and cell death in response to cytoplasmic DNA. *Nature* **458**, 509-513, doi:10.1038/nature07710 (2009).
- 233 Hornung, V. *et al.* AIM2 recognizes cytosolic dsDNA and forms a caspase-1-activating inflammasome with ASC. *Nature* **458**, 514-518, doi:10.1038/nature07725 (2009).
- 234 Zhao, Y. *et al.* The NLRC4 inflammasome receptors for bacterial flagellin and type III secretion apparatus. *Nature* **477**, 596-600, doi:10.1038/nature10510 (2011).
- 235 Xu, H. *et al.* Innate immune sensing of bacterial modifications of Rho GTPases by the Pyrin inflammasome. *Nature* **513**, 237-241, doi:10.1038/nature13449 (2014).
- 236 Kimura, T. *et al.* TRIM-mediated precision autophagy targets cytoplasmic regulators of innate immunity. *The Journal of cell biology* **210**, 973-989, doi:10.1083/jcb.201503023 (2015).
- 237 de Vasconcelos, N. M., Van Opdenbosch, N. & Lamkanfi, M. Inflammasomes as polyvalent cell death platforms. *Cellular and molecular life sciences : CMLS* **73**, 2335-2347, doi:10.1007/s00018-016-2204-3 (2016).
- 238 Srinivasula, S. M. *et al.* The PYRIN-CARD protein ASC is an activating adaptor for caspase-1. *The Journal of biological chemistry* **277**, 21119-21122, doi:10.1074/jbc.C200179200 (2002).

- 239 Lu, A. *et al.* Unified polymerization mechanism for the assembly of ASC-dependent inflammasomes. *Cell* **156**, 1193-1206, doi:10.1016/j.cell.2014.02.008 (2014).
- 240 Yamamoto, M. *et al.* ASC is essential for LPS-induced activation of procaspase-1 independently of TLR-associated signal adaptor molecules. *Genes to cells : devoted to molecular & cellular mechanisms* **9**, 1055-1067, doi:10.1111/j.1365-2443.2004.00789.x (2004).
- 241 Sborgi, L. *et al.* Structure and assembly of the mouse ASC inflammasome by combined NMR spectroscopy and cryo-electron microscopy. *Proceedings of the National Academy of Sciences of the United States of America* **112**, 13237-13242, doi:10.1073/pnas.1507579112 (2015).
- 242 Kayagaki, N. *et al.* Non-canonical inflammasome activation targets caspase-11. *Nature* **479**, 117-121, doi:10.1038/nature10558 (2011).
- 243 Shi, J. *et al.* Inflammatory caspases are innate immune receptors for intracellular LPS. *Nature* **514**, 187-192, doi:10.1038/nature13683 (2014).
- 244 Kayagaki, N. *et al.* Caspase-11 cleaves gasdermin D for non-canonical inflammasome signalling. *Nature* **526**, 666-671, doi:10.1038/nature15541 (2015).
- 245 Baker, P. J. *et al.* NLRP3 inflammasome activation downstream of cytoplasmic LPS recognition by both caspase-4 and caspase-5. *European journal of immunology*, doi:10.1002/eji.201545655 (2015).
- 246 Schmid-Burgk, J. L. *et al.* Caspase-4 mediates non-canonical activation of the NLRP3 inflammasome in human myeloid cells. *European journal of immunology*, doi:10.1002/eji.201545523 (2015).
- 247 Ruhl, S. & Broz, P. Caspase-11 activates a canonical NLRP3 inflammasome by promoting K(+) efflux. *European journal of immunology* **45**, 2927-2936, doi:10.1002/eji.201545772 (2015).
- 248 Shi, J. *et al.* Cleavage of GSDMD by inflammatory caspases determines pyroptotic cell death. *Nature* **526**, 660-665, doi:10.1038/nature15514 (2015).
- 249 Aglietti, R. A. *et al.* GsdmD p30 elicited by caspase-11 during pyroptosis forms pores in membranes. *Proceedings of the National Academy of Sciences of the United States of America* **113**, 7858-7863, doi:10.1073/pnas.1607769113 (2016).
- 250 Ding, J. *et al.* Pore-forming activity and structural autoinhibition of the gasdermin family. *Nature* **535**, 111-116, doi:10.1038/nature18590 (2016).

- 251 Sborgi, L. *et al.* GSDMD membrane pore formation constitutes the mechanism of pyroptotic cell death. *The EMBO journal* **35**, 1766-1778, doi:10.15252/embj.201694696 (2016).
- 252 Liu, X. *et al.* Inflammasome-activated gasdermin D causes pyroptosis by forming membrane pores. *Nature* **535**, 153-158, doi:10.1038/nature18629 (2016).
- 253 Sutterwala, F. S. *et al.* Critical role for NALP3/CIAS1/Cryopyrin in innate and adaptive immunity through its regulation of caspase-1. *Immunity* **24**, 317-327, doi:10.1016/j.immuni.2006.02.004 (2006).
- 254 Abderrazak, A. *et al.* NLRP3 inflammasome: From a danger signal sensor to a regulatory node of oxidative stress and inflammatory diseases. *Redox biology* **4C**, 296-307, doi:10.1016/j.redox.2015.01.008 (2015).
- 255 Sutterwala, F. S., Haasken, S. & Cassel, S. L. Mechanism of NLRP3 inflammasome activation. *Annals of the New York Academy of Sciences* **1319**, 82-95, doi:10.1111/nyas.12458 (2014).
- 256 Bauernfeind, F. G. *et al.* Cutting edge: NF-kappaB activating pattern recognition and cytokine receptors license NLRP3 inflammasome activation by regulating NLRP3 expression. *Journal of immunology* **183**, 787-791, doi:10.4049/jimmunol.0901363 (2009).
- 257 Py, B. F., Kim, M. S., Vakifahmetoglu-Norberg, H. & Yuan, J. Deubiquitination of NLRP3 by BRCC3 Critically Regulates Inflammasome Activity. *Mol Cell* **49**, 331-338, doi:10.1016/j.molcel.2012.11.009 (2013).
- 258 Liao, P. C. *et al.* Lipopolysaccharide/adenosine triphosphate-mediated signal transduction in the regulation of NLRP3 protein expression and caspase-1-mediated interleukin-1beta secretion. *Inflammation research : official journal of the European Histamine Research Society ... [et al.]* **62**, 89-96, doi:10.1007/s00011-012-0555-2 (2013).
- 259 Bedard, K. & Krause, K. H. The NOX family of ROS-generating NADPH oxidases: physiology and pathophysiology. *Physiological reviews* **87**, 245-313, doi:10.1152/physrev.00044.2005 (2007).
- 260 Nishiyama, A. *et al.* Identification of thioredoxin-binding protein-2/vitamin D(3) up-regulated protein 1 as a negative regulator of thioredoxin function and expression. *The Journal of biological chemistry* **274**, 21645-21650 (1999).
- 261 Zhou, R., Tardivel, A., Thorens, B., Choi, I. & Tschopp, J. Thioredoxin-interacting protein links oxidative stress to inflammasome activation. *Nature immunology* **11**, 136-140, doi:10.1038/ni.1831 (2010).

- 262 Masters, S. L. *et al.* Activation of the NLRP3 inflammasome by islet amyloid polypeptide provides a mechanism for enhanced IL-1beta in type 2 diabetes. *Nature immunology* **11**, 897-904, doi:10.1038/ni.1935 (2010).
- 263 Rassool, F. V. *et al.* Reactive oxygen species, DNA damage, and error-prone repair: a model for genomic instability with progression in myeloid leukemia? *Cancer research* **67**, 8762-8771, doi:10.1158/0008-5472.CAN-06-4807 (2007).
- 264 Doussiere, J., Bouzidi, F. & Vignais, P. V. The S100A8/A9 protein as a partner for the cytosolic factors of NADPH oxidase activation in neutrophils. *European Journal of Biochemistry* **269**, 3246-3255, doi:10.1046/j.1432-1033.2002.03002.x (2002).
- 265 Kerkhoff, C. *et al.* The arachidonic acid-binding protein S100A8/A9 promotes NADPH oxidase activation by interaction with p67phox and Rac-2. *FASEB journal : official publication of the Federation of American Societies for Experimental Biology* **19**, 467-469, doi:10.1096/fj.04-2377fje (2005).
- 266 Simard, J. C. *et al.* S100A8 and S100A9 induce cytokine expression and regulate the NLRP3 inflammasome via ROS-dependent activation of NF-kappaB(1.). *PloS one* **8**, e72138, doi:10.1371/journal.pone.0072138 (2013).
- 267 Heid, M. E. *et al.* Mitochondrial reactive oxygen species induces NLRP3-dependent lysosomal damage and inflammasome activation. *Journal of immunology* **191**, 5230-5238, doi:10.4049/jimmunol.1301490 (2013).
- 268 Zhou, R., Yazdi, A. S., Menu, P. & Tschopp, J. A role for mitochondria in NLRP3 inflammasome activation. *Nature* **469**, 221-225, doi:10.1038/nature09663 (2011).
- 269 Hornung, V. *et al.* Silica crystals and aluminum salts activate the NALP3 inflammasome through phagosomal destabilization. *Nature immunology* **9**, 847-856, doi:10.1038/ni.1631 (2008).
- 270 Halle, A. *et al.* The NALP3 inflammasome is involved in the innate immune response to amyloid-beta. *Nature immunology* **9**, 857-865, doi:10.1038/ni.1636 (2008).
- 271 Munoz-Planillo, R. *et al.* K(+) efflux is the common trigger of NLRP3 inflammasome activation by bacterial toxins and particulate matter. *Immunity* **38**, 1142-1153, doi:10.1016/j.immuni.2013.05.016 (2013).
- 272 Murakami, T. *et al.* Critical role for calcium mobilization in activation of the NLRP3 inflammasome. *Proceedings of the National Academy of Sciences of the United States of America* **109**, 11282-11287, doi:10.1073/pnas.1117765109 (2012).

- 273 Humke, E. W., Shriver, S. K., Starovasnik, M. A., Fairbrother, W. J. & Dixit, V. M. ICEBERG: a novel inhibitor of interleukin-1beta generation. *Cell* **103**, 99-111 (2000).
- 274 Lee, S. H., Stehlik, C. & Reed, J. C. Cop, a caspase recruitment domain-containing protein and inhibitor of caspase-1 activation processing. *The Journal of biological chemistry* **276**, 34495-34500, doi:10.1074/jbc.M101415200 (2001).
- 275 Lamkanfi, M. *et al.* INCA, a novel human caspase recruitment domain protein that inhibits interleukin-1beta generation. *The Journal of biological chemistry* **279**, 51729-51738, doi:10.1074/jbc.M407891200 (2004).
- 276 Stehlik, C. *et al.* The PAAD/PYRIN-only protein POP1/ASC2 is a modulator of ASC-mediated nuclear-factor-kappa B and pro-caspase-1 regulation. *The Biochemical journal* **373**, 101-113, doi:10.1042/BJ20030304 (2003).
- 277 de Almeida, L. *et al.* The PYRIN Domain-only Protein POP1 Inhibits Inflammasome Assembly and Ameliorates Inflammatory Disease. *Immunity* **43**, 264-276, doi:10.1016/j.immuni.2015.07.018 (2015).
- 278 Ali, A. *et al.* Sequential activation of caspase-1 and caspase-3-like proteases during apoptosis in myelodysplastic syndromes. *Journal of hematology & stem cell research* **8**, 343-356 (1999).
- 279 Chung, H. *et al.* NLRP3 regulates a non-canonical platform for caspase-8 activation during epithelial cell apoptosis. *Cell death and differentiation*, doi:10.1038/cdd.2016.14 (2016).
- 280 Deretic, V. Autophagy as an innate immunity paradigm: expanding the scope and repertoire of pattern recognition receptors. *Current opinion in immunology* **24**, 21-31, doi:10.1016/j.coi.2011.10.006 (2012).
- 281 Dupont, N. *et al.* Autophagy-based unconventional secretory pathway for extracellular delivery of IL-1beta. *The EMBO journal* **30**, 4701-4711, doi:10.1038/emboj.2011.398 (2011).
- 282 Sun, Q. *et al.* Caspase 1 activation is protective against hepatocyte cell death by up-regulating beclin 1 protein and mitochondrial autophagy in the setting of redox stress. *The Journal of biological chemistry* **288**, 15947-15958, doi:10.1074/jbc.M112.426791 (2013).
- 283 Guo, L. *et al.* [Autophagy level of bone marrow mononuclear cells in patients with myelodysplastic syndromes]. *Zhonghua xue ye xue za zhi = Zhonghua xueyexue zazhi* **36**, 1016-1019, doi:10.3760/cma.j.issn.0253-2727.2015.12.008 (2015).

- 284 Clevers, H. & Nusse, R. Wnt/beta-catenin signaling and disease. *Cell* **149**, 1192-1205, doi:10.1016/j.cell.2012.05.012 (2012).
- 285 Wu, X. *et al.* Rac1 activation controls nuclear localization of beta-catenin during canonical Wnt signaling. *Cell* **133**, 340-353, doi:10.1016/j.cell.2008.01.052 (2008).
- 286 Coant, N. *et al.* NADPH oxidase 1 modulates WNT and NOTCH1 signaling to control the fate of proliferative progenitor cells in the colon. *Molecular and cellular biology* **30**, 2636-2650, doi:10.1128/MCB.01194-09 (2010).
- 287 Funato, Y., Michiue, T., Asashima, M. & Miki, H. The thioredoxin-related redox-regulating protein nucleoredoxin inhibits Wnt-beta-catenin signalling through dishevelled. *Nat Cell Biol* **8**, 501-508, doi:10.1038/ncb1405 (2006).
- 288 Span, L. F. *et al.* Bone marrow mononuclear cells of MDS patients are characterized by in vitro proliferation and increased apoptosis independently of stromal interactions. *Leukemia research* **31**, 1659-1667, doi:10.1016/j.leukres.2007.06.013 (2007).
- 289 Garcia-Manero, G. Myelodysplastic syndromes: 2014 update on diagnosis, risk-stratification, and management. *American journal of hematology* **89**, 97-108, doi:10.1002/ajh.23642 (2014).
- 290 Yoshida, K. *et al.* Frequent pathway mutations of splicing machinery in myelodysplasia. *Nature* **478**, 64-69, doi:10.1038/nature10496 (2011).
- 291 Takizawa, H., Boettcher, S. & Manz, M. G. Demand-adapted regulation of early hematopoiesis in infection and inflammation. *Blood* **119**, 2991-3002, doi:10.1182/blood-2011-12-380113 (2012).
- 292 Ehrchen, J. M., Sunderkotter, C., Foell, D., Vogl, T. & Roth, J. The endogenous Toll-like receptor 4 agonist S100A8/S100A9 (calprotectin) as innate amplifier of infection, autoimmunity, and cancer. *Journal of leukocyte biology* **86**, 557-566, doi:10.1189/jlb.1008647 (2009).
- 293 Hofmann, W. K. *et al.* Characterization of gene expression of CD34+ cells from normal and myelodysplastic bone marrow. *Blood* **100**, 3553-3560, doi:10.1182/blood.V100.10.3553 (2002).
- 294 Bergsbaken, T., Fink, S. L. & Cookson, B. T. Pyroptosis: host cell death and inflammation. *Nature reviews. Microbiology* **7**, 99-109, doi:10.1038/nrmicro2070 (2009).

- 295 Kessel, C., Holzinger, D. & Foell, D. Phagocyte-derived S100 proteins in autoinflammation: putative role in pathogenesis and usefulness as biomarkers. *Clinical immunology* **147**, 229-241, doi:10.1016/j.clim.2012.11.008 (2013).
- 296 Lim, S. Y., Raftery, M. J., Goyette, J., Hsu, K. & Geczy, C. L. Oxidative modifications of S100 proteins: functional regulation by redox. *Journal of leukocyte biology* **86**, 577-587, doi:10.1189/jlb.1008608 (2009).
- 297 Sester, D. P. *et al.* A novel flow cytometric method to assess inflammasome formation. *Journal of immunology* **194**, 455-462, doi:10.4049/jimmunol.1401110 (2015).
- 298 Franklin, B. S. *et al.* The adaptor ASC has extracellular and 'prionoid' activities that propagate inflammation. *Nature immunology* **15**, 727-737, doi:10.1038/ni.2913 (2014).
- 299 Chirico, V. *et al.* High-mobility group box 1 (HMGB1) in childhood: from bench to bedside. *European journal of pediatrics* **173**, 1123-1136, doi:10.1007/s00431-014-2327-1 (2014).
- 300 Tzur, A., Moore, J. K., Jorgensen, P., Shapiro, H. M. & Kirschner, M. W. Optimizing optical flow cytometry for cell volume-based sorting and analysis. *PloS one* **6**, e16053, doi:10.1371/journal.pone.0016053 (2011).
- 301 Coll, R. C. *et al.* A small-molecule inhibitor of the NLRP3 inflammasome for the treatment of inflammatory diseases. *Nature medicine* **21**, 248-255, doi:10.1038/nm.3806 (2015).
- 302 Rharass, T. *et al.* Ca²⁺-mediated mitochondrial reactive oxygen species metabolism augments Wnt/beta-catenin pathway activation to facilitate cell differentiation. *The Journal of biological chemistry* **289**, 27937-27951, doi:10.1074/jbc.M114.573519 (2014).
- 303 Kajla, S. *et al.* A crucial role for Nox 1 in redox-dependent regulation of Wnt-beta-catenin signaling. *FASEB journal : official publication of the Federation of American Societies for Experimental Biology* **26**, 2049-2059, doi:10.1096/fj.11-196360 (2012).
- 304 Xu, J. *et al.* Clinical significance of nuclear non-phosphorylated beta-catenin in acute myeloid leukaemia and myelodysplastic syndrome. *British journal of haematology* **140**, 394-401, doi:10.1111/j.1365-2141.2007.06914.x (2008).
- 305 Masala, E. *et al.* Hypermethylation of Wnt antagonist gene promoters and activation of Wnt pathway in myelodysplastic marrow cells. *Leukemia research* **36**, 1290-1295, doi:10.1016/j.leukres.2012.05.023 (2012).

- 306 Bello, E. *et al.* CSNK1A1 mutations and gene expression analysis in myelodysplastic syndromes with del(5q). *British journal of haematology*, doi:10.1111/bjh.13563 (2015).
- 307 Obeng, E. A. *et al.* Mutant Splicing Factor 3b Subunit 1 (SF3B1) Causes Dysregulated Erythropoiesis and a Stell Cell Disadvantage. *Blood* **124**, 828 (2014).
- 308 Abdel-Wahab, O. *et al.* Deletion of Asxl1 results in myelodysplasia and severe developmental defects in vivo. *The Journal of experimental medicine* **210**, 2641-2659, doi:10.1084/jem.20131141 (2013).
- 309 Moran-Crusio, K. *et al.* Tet2 loss leads to increased hematopoietic stem cell self-renewal and myeloid transformation. *Cancer cell* **20**, 11-24, doi:10.1016/j.ccr.2011.06.001 (2011).
- 310 Shirai, C. L. *et al.* Mutant U2AF1 Expression Alters Hematopoiesis and Pre-mRNA Splicing In Vivo. *Cancer cell* **27**, 631-643, doi:10.1016/j.ccell.2015.04.008 (2015).
- 311 Kim, E. *et al.* SRSF2 Mutations Contribute to Myelodysplasia by Mutant-Specific Effects on Exon Recognition. *Cancer cell* **27**, 617-630, doi:10.1016/j.ccell.2015.04.006 (2015).
- 312 Graubert, T. A. *et al.* Recurrent mutations in the U2AF1 splicing factor in myelodysplastic syndromes. *Nat Genet* **44**, 53-57, doi:10.1038/ng.1031 (2012).
- 313 Pellagatti, A. *et al.* Deregulated gene expression pathways in myelodysplastic syndrome hematopoietic stem cells. *Leukemia* **24**, 756-764, doi:10.1038/leu.2010.31 (2010).
- 314 Bauernfeind, F. *et al.* Cutting edge: reactive oxygen species inhibitors block priming, but not activation, of the NLRP3 inflammasome. *Journal of immunology* **187**, 613-617, doi:10.4049/jimmunol.1100613 (2011).
- 315 Lee, S. C. *et al.* Modulation of splicing catalysis for therapeutic targeting of leukemia with mutations in genes encoding spliceosomal proteins. *Nature medicine* **22**, 672-678, doi:10.1038/nm.4097 (2016).
- 316 Yang, Y., Akada, H., Nath, D., Hutchison, R. E. & Mohi, G. Loss of Ezh2 cooperates with Jak2V617F in the development of myelofibrosis in a mouse model of myeloproliferative neoplasm. *Blood* **127**, 3410-3423, doi:10.1182/blood-2015-11-679431 (2016).

- 317 Baroja-Mazo, A. *et al.* The NLRP3 inflammasome is released as a particulate danger signal that amplifies the inflammatory response. *Nature immunology* **15**, 738-748, doi:10.1038/ni.2919 (2014).
- 318 Kashio, M. *et al.* Redox signal-mediated sensitization of transient receptor potential melastatin 2 (TRPM2) to temperature affects macrophage functions. *Proceedings of the National Academy of Sciences of the United States of America* **109**, 6745-6750, doi:10.1073/pnas.1114193109 (2012).
- 319 Yamamoto, S. *et al.* TRPM2-mediated Ca²⁺influx induces chemokine production in monocytes that aggravates inflammatory neutrophil infiltration. *Nature medicine* **14**, 738-747, doi:10.1038/nm1758 (2008).
- 320 Kuhn, F. J., Heiner, I. & Luckhoff, A. TRPM2: a calcium influx pathway regulated by oxidative stress and the novel second messenger ADP-ribose. *Pflugers Archiv : European journal of physiology* **451**, 212-219, doi:10.1007/s00424-005-1446-y (2005).
- 321 Sallmyr, A., Fan, J. & Rassool, F. V. Genomic instability in myeloid malignancies: increased reactive oxygen species (ROS), DNA double strand breaks (DSBs) and error-prone repair. *Cancer letters* **270**, 1-9, doi:10.1016/j.canlet.2008.03.036 (2008).
- 322 Martinez-Hoyer, S. *et al.* Mechanisms of Resistance to Lenalidomide in Del(5q) Myelodysplastic Syndrome Patients. *Blood* **126**, 5228 (2015).
- 323 Vyleta, M. L., Wong, J. & Magun, B. E. Suppression of ribosomal function triggers innate immune signaling through activation of the NLRP3 inflammasome. *PloS one* **7**, e36044, doi:10.1371/journal.pone.0036044 (2012).
- 324 Dick, M. S., Sborgi, L., Ruhl, S., Hiller, S. & Broz, P. ASC filament formation serves as a signal amplification mechanism for inflammasomes. *Nature communications* **7**, 11929, doi:10.1038/ncomms11929 (2016).
- 325 Font, P. *et al.* Interobserver variance in myelodysplastic syndromes with less than 5 % bone marrow blasts: unilineage vs. multilineage dysplasia and reproducibility of the threshold of 2 % blasts. *Annals of hematology* **94**, 565-573, doi:10.1007/s00277-014-2252-4 (2015).
- 326 Lee, H. M. *et al.* Upregulated NLRP3 inflammasome activation in patients with type 2 diabetes. *Diabetes* **62**, 194-204, doi:10.2337/db12-0420 (2013).
- 327 Santini, V. *et al.* Randomized Phase III Study of Lenalidomide Versus Placebo in RBC Transfusion-Dependent Patients With Lower-Risk Non-del(5q) Myelodysplastic Syndromes and Ineligible for or Refractory to Erythropoiesis-Stimulating Agents. *Journal of clinical oncology : official journal of the American*

- Society of Clinical Oncology* **34**, 2988-2996, doi:10.1200/JCO.2015.66.0118 (2016).
- 328 Toma, A. *et al.* Lenalidomide with or without erythropoietin in transfusion-dependent erythropoiesis-stimulating agent-refractory lower-risk MDS without 5q deletion. *Leukemia* **30**, 897-905, doi:10.1038/leu.2015.296 (2016).
- 329 Naqvi, K. *et al.* Implications of discrepancy in morphologic diagnosis of myelodysplastic syndrome between referral and tertiary care centers. *Blood* **118**, 4690-4693, doi:10.1182/blood-2011-03-342642 (2011).
- 330 Guo, H., Callaway, J. B. & Ting, J. P. Inflammasomes: mechanism of action, role in disease, and therapeutics. *Nature medicine* **21**, 677-687, doi:10.1038/nm.3893 (2015).
- 331 Leemans, J. C., Cassel, S. L. & Sutterwala, F. S. Sensing damage by the NLRP3 inflammasome. *Immunological reviews* **243**, 152-162, doi:10.1111/j.1600-065X.2011.01043.x (2011).
- 332 Masters, S. L., Simon, A., Aksentijevich, I. & Kastner, D. L. Horror autoinflammaticus: the molecular pathophysiology of autoinflammatory disease (*). *Annual review of immunology* **27**, 621-668, doi:10.1146/annurev.immunol.25.022106.141627 (2009).
- 333 Mian, S. *et al.* NLRP3 Inflammasome Polymorphisms Are Enriched in Myelodysplastic Syndrome Patients with Autoimmune Disorders. *Blood* **126**, 1659 (2015).
- 334 Leslie, K. S. *et al.* Phenotype, genotype, and sustained response to anakinra in 22 patients with autoinflammatory disease associated with CIAS-1/NALP3 mutations. *Archives of dermatology* **142**, 1591-1597, doi:10.1001/archderm.142.12.1591 (2006).
- 335 Yu, J. R. & Leslie, K. S. Cryopyrin-associated periodic syndrome: an update on diagnosis and treatment response. *Current allergy and asthma reports* **11**, 12-20, doi:10.1007/s11882-010-0160-9 (2011).
- 336 Stahl, N., Radin, A. & Mellis, S. Riloncept--CAPS and beyond. *Annals of the New York Academy of Sciences* **1182**, 124-134, doi:10.1111/j.1749-6632.2009.05074.x (2009).
- 337 Wannamaker, W. *et al.* (S)-1-((S)-2-[[1-(4-amino-3-chloro-phenyl)-methanoyl]-amino]-3,3-dimethyl-butanoyl)-pyrrolidine-2-carboxylic acid ((2R,3S)-2-ethoxy-5-oxo-tetrahydro-furan-3-yl)-amide (VX-765), an orally available selective interleukin (IL)-converting enzyme/caspase-1 inhibitor, exhibits potent anti-inflammatory activities by inhibiting the release of IL-1beta and IL-18. *The*

- Journal of pharmacology and experimental therapeutics* **321**, 509-516, doi:10.1124/jpet.106.111344 (2007).
- 338 Rajamani, U. & Jialal, I. Hyperglycemia induces Toll-like receptor-2 and -4 expression and activity in human microvascular retinal endothelial cells: implications for diabetic retinopathy. *Journal of diabetes research* **2014**, 790902, doi:10.1155/2014/790902 (2014).
- 339 Koenen, T. B. *et al.* Hyperglycemia activates caspase-1 and TXNIP-mediated IL-1beta transcription in human adipose tissue. *Diabetes* **60**, 517-524, doi:10.2337/db10-0266 (2011).
- 340 Maedler, K. *et al.* Glucose-induced β cell production of IL-1 β contributes to glucotoxicity in human pancreatic islets. *Journal of Clinical Investigation* **110**, 851-860, doi:10.1172/jci200215318 (2002).
- 341 Larsen, C. M. *et al.* Interleukin-1-receptor antagonist in type 2 diabetes mellitus. *The New England journal of medicine* **356**, 1517-1526, doi:10.1056/NEJMoa065213 (2007).
- 342 Wen, H. *et al.* Fatty acid-induced NLRP3-ASC inflammasome activation interferes with insulin signaling. *Nature immunology* **12**, 408-415, doi:10.1038/ni.2022 (2011).
- 343 Sauter, N. S., Schulthess, F. T., Galasso, R., Castellani, L. W. & Maedler, K. The antiinflammatory cytokine interleukin-1 receptor antagonist protects from high-fat diet-induced hyperglycemia. *Endocrinology* **149**, 2208-2218, doi:10.1210/en.2007-1059 (2008).
- 344 Vandanmagsar, B. *et al.* The NLRP3 inflammasome instigates obesity-induced inflammation and insulin resistance. *Nature medicine* **17**, 179-188, doi:10.1038/nm.2279 (2011).
- 345 Wu, N. *et al.* AMPK-dependent degradation of TXNIP upon energy stress leads to enhanced glucose uptake via GLUT1. *Mol Cell* **49**, 1167-1175, doi:10.1016/j.molcel.2013.01.035 (2013).
- 346 Omi, T. *et al.* An intronic variable number of tandem repeat polymorphisms of the cold-induced autoinflammatory syndrome 1 (CIAS1) gene modifies gene expression and is associated with essential hypertension. *European journal of human genetics : EJHG* **14**, 1295-1305, doi:10.1038/sj.ejhg.5201698 (2006).
- 347 Fukui, T. *et al.* p22phox mRNA expression and NADPH oxidase activity are increased in aortas from hypertensive rats. *Circulation research* **80**, 45-51 (1997).

- 348 Touyz, R. M. Oxidative stress and vascular damage in hypertension. *Current hypertension reports* **2**, 98-105 (2000).
- 349 Tangirala, R. K. *et al.* Formation of cholesterol monohydrate crystals in macrophage-derived foam cells. *Journal of lipid research* **35**, 93-104 (1994).
- 350 Rajamaki, K. *et al.* Cholesterol crystals activate the NLRP3 inflammasome in human macrophages: a novel link between cholesterol metabolism and inflammation. *PloS one* **5**, e11765, doi:10.1371/journal.pone.0011765 (2010).
- 351 Duewell, P. *et al.* NLRP3 inflammasomes are required for atherogenesis and activated by cholesterol crystals. *Nature* **464**, 1357-1361, doi:10.1038/nature08938 (2010).
- 352 Galea, J. *et al.* Interleukin-1 beta in coronary arteries of patients with ischemic heart disease. *Arteriosclerosis, thrombosis, and vascular biology* **16**, 1000-1006 (1996).
- 353 Furlan, R. *et al.* Caspase-1 regulates the inflammatory process leading to autoimmune demyelination. *Journal of immunology* **163**, 2403-2409 (1999).
- 354 Gris, D. *et al.* NLRP3 plays a critical role in the development of experimental autoimmune encephalomyelitis by mediating Th1 and Th17 responses. *Journal of immunology* **185**, 974-981, doi:10.4049/jimmunol.0904145 (2010).
- 355 Matsuki, T., Nakae, S., Sudo, K., Horai, R. & Iwakura, Y. Abnormal T cell activation caused by the imbalance of the IL-1/IL-1R antagonist system is responsible for the development of experimental autoimmune encephalomyelitis. *International immunology* **18**, 399-407, doi:10.1093/intimm/dxh379 (2006).
- 356 Griffin, W. S. *et al.* Brain interleukin 1 and S-100 immunoreactivity are elevated in Down syndrome and Alzheimer disease. *Proceedings of the National Academy of Sciences of the United States of America* **86**, 7611-7615 (1989).
- 357 Heneka, M. T. *et al.* NLRP3 is activated in Alzheimer's disease and contributes to pathology in APP/PS1 mice. *Nature* **493**, 674-678, doi:10.1038/nature11729 (2013).
- 358 Simard, A. R., Soulet, D., Gowing, G., Julien, J. P. & Rivest, S. Bone marrow-derived microglia play a critical role in restricting senile plaque formation in Alzheimer's disease. *Neuron* **49**, 489-502, doi:10.1016/j.neuron.2006.01.022 (2006).
- 359 Codolo, G. *et al.* Triggering of inflammasome by aggregated alpha-synuclein, an inflammatory response in synucleinopathies. *PloS one* **8**, e55375, doi:10.1371/journal.pone.0055375 (2013).

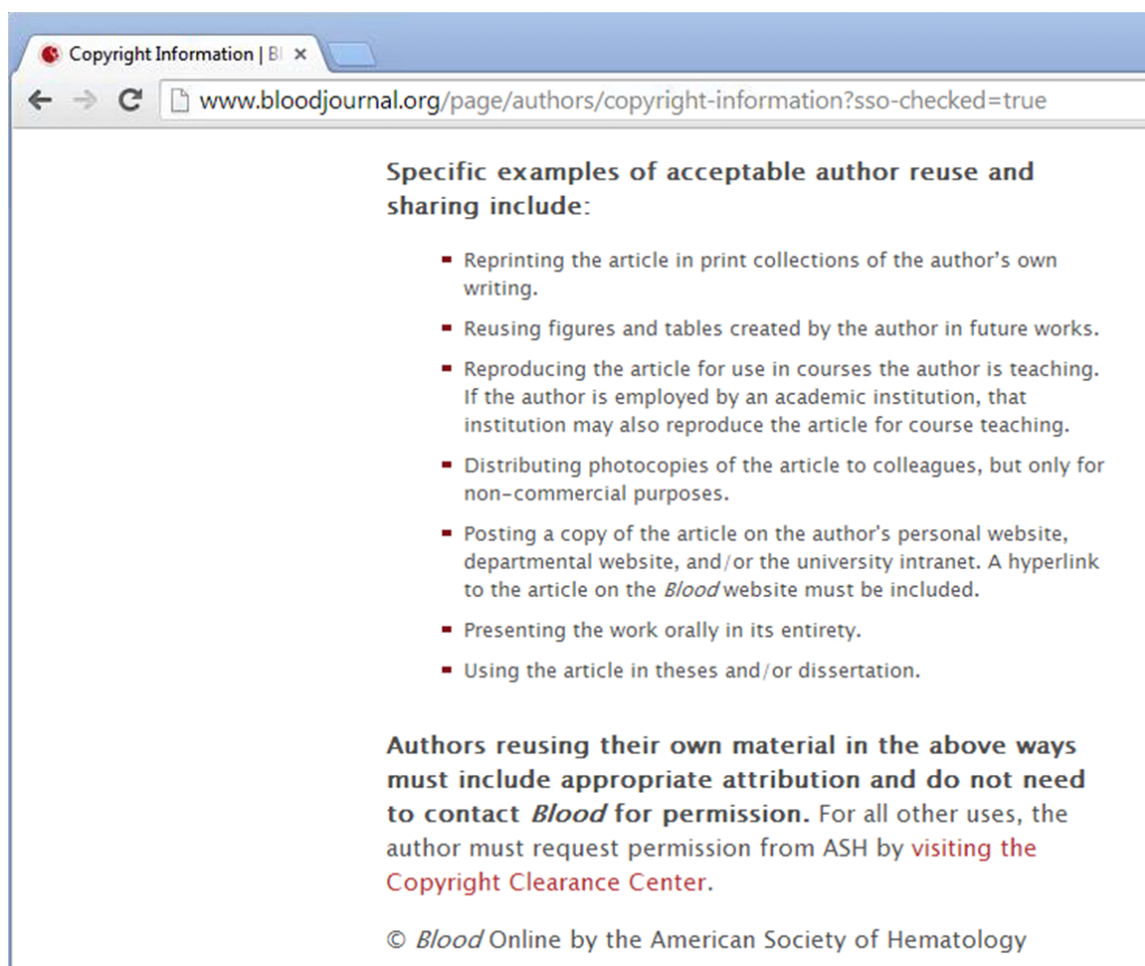
- 360 Ferrari, C. C. *et al.* Progressive neurodegeneration and motor disabilities induced by chronic expression of IL-1beta in the substantia nigra. *Neurobiology of disease* **24**, 183-193, doi:10.1016/j.nbd.2006.06.013 (2006).
- 361 Yan, Y. *et al.* Dopamine controls systemic inflammation through inhibition of NLRP3 inflammasome. *Cell* **160**, 62-73, doi:10.1016/j.cell.2014.11.047 (2015).
- 362 Martinon, F., Petrilli, V., Mayor, A., Tardivel, A. & Tschopp, J. Gout-associated uric acid crystals activate the NALP3 inflammasome. *Nature* **440**, 237-241, doi:10.1038/nature04516 (2006).
- 363 So, A., De Smedt, T., Revaz, S. & Tschopp, J. A pilot study of IL-1 inhibition by anakinra in acute gout. *Arthritis research & therapy* **9**, R28, doi:10.1186/ar2143 (2007).
- 364 Whyte, M. *et al.* Increased risk of fibrosing alveolitis associated with interleukin-1 receptor antagonist and tumor necrosis factor-alpha gene polymorphisms. *American journal of respiratory and critical care medicine* **162**, 755-758, doi:10.1164/ajrccm.162.2.9909053 (2000).
- 365 Cassel, S. L. *et al.* The Nalp3 inflammasome is essential for the development of silicosis. *Proceedings of the National Academy of Sciences of the United States of America* **105**, 9035-9040, doi:10.1073/pnas.0803933105 (2008).
- 366 Dostert, C. *et al.* Innate immune activation through Nalp3 inflammasome sensing of asbestos and silica. *Science* **320**, 674-677, doi:10.1126/science.1156995 (2008).
- 367 Gasse, P. *et al.* IL-1R1/MyD88 signaling and the inflammasome are essential in pulmonary inflammation and fibrosis in mice. *The Journal of clinical investigation* **117**, 3786-3799, doi:10.1172/JCI32285 (2007).
- 368 Shigeoka, A. A. *et al.* An inflammasome-independent role for epithelial-expressed Nlrp3 in renal ischemia-reperfusion injury. *Journal of immunology* **185**, 6277-6285, doi:10.4049/jimmunol.1002330 (2010).
- 369 Zhu, P. *et al.* Gene silencing of NALP3 protects against liver ischemia-reperfusion injury in mice. *Human gene therapy* **22**, 853-864, doi:10.1089/hum.2010.145 (2011).
- 370 Harada, H. *et al.* Transfer of the interleukin-1 receptor antagonist gene into rat liver abrogates hepatic ischemia-reperfusion injury. *Transplantation* **74**, 1434-1441, doi:10.1097/01.TP.0000034711.92003.EC (2002).

- 371 Shito, M. *et al.* Interleukin 1 receptor blockade reduces tumor necrosis factor production, tissue injury, and mortality after hepatic ischemia-reperfusion in the rat. *Transplantation* **63**, 143-148 (1997).
- 372 Kawaguchi, M. *et al.* Inflammasome activation of cardiac fibroblasts is essential for myocardial ischemia/reperfusion injury. *Circulation* **123**, 594-604, doi:10.1161/CIRCULATIONAHA.110.982777 (2011).
- 373 Pomerantz, B. J., Reznikov, L. L., Harken, A. H. & Dinarello, C. A. Inhibition of caspase 1 reduces human myocardial ischemic dysfunction via inhibition of IL-18 and IL-1beta. *Proceedings of the National Academy of Sciences of the United States of America* **98**, 2871-2876, doi:10.1073/pnas.041611398 (2001).
- 374 Abbate, A. *et al.* Interleukin-1 blockade with anakinra to prevent adverse cardiac remodeling after acute myocardial infarction (Virginia Commonwealth University Anakinra Remodeling Trial [VCU-ART] Pilot study). *The American journal of cardiology* **105**, 1371-1377 e1371, doi:10.1016/j.amjcard.2009.12.059 (2010).
- 375 Zeeshan, H. M., Lee, G. H., Kim, H. R. & Chae, H. J. Endoplasmic Reticulum Stress and Associated ROS. *International journal of molecular sciences* **17**, 327, doi:10.3390/ijms17030327 (2016).
- 376 Shin, S. & Argon, Y. Stressed-Out Endoplasmic Reticulum Inflames the Mitochondria. *Immunity* **43**, 409-411, doi:10.1016/j.immuni.2015.08.027 (2015).
- 377 Martinon, F., Chen, X., Lee, A. H. & Glimcher, L. H. TLR activation of the transcription factor XBP1 regulates innate immune responses in macrophages. *Nature immunology* **11**, 411-418, doi:10.1038/ni.1857 (2010).
- 378 Lerner, A. G. *et al.* IRE1alpha induces thioredoxin-interacting protein to activate the NLRP3 inflammasome and promote programmed cell death under irremediable ER stress. *Cell metabolism* **16**, 250-264, doi:10.1016/j.cmet.2012.07.007 (2012).
- 379 Upton, J. P. *et al.* IRE1alpha cleaves select microRNAs during ER stress to derepress translation of proapoptotic Caspase-2. *Science* **338**, 818-822, doi:10.1126/science.1226191 (2012).
- 380 Saxena, G., Chen, J. & Shalev, A. Intracellular shuttling and mitochondrial function of thioredoxin-interacting protein. *The Journal of biological chemistry* **285**, 3997-4005, doi:10.1074/jbc.M109.034421 (2010).
- 381 Bronner, D. N., O'Riordan, M. X. & He, Y. Caspase-2 mediates a *Brucella abortus* RB51-induced hybrid cell death having features of apoptosis and pyroptosis. *Frontiers in cellular and infection microbiology* **3**, 83, doi:10.3389/fcimb.2013.00083 (2013).

- 382 Robertson, J. D., Enoksson, M., Suomela, M., Zhivotovsky, B. & Orrenius, S. Caspase-2 acts upstream of mitochondria to promote cytochrome c release during etoposide-induced apoptosis. *The Journal of biological chemistry* **277**, 29803-29809, doi:10.1074/jbc.M204185200 (2002).
- 383 D'Oswaldo, A. *et al.* Transcription Factor ATF4 Induces NLRP1 Inflammasome Expression during Endoplasmic Reticulum Stress. *PloS one* **10**, e0130635, doi:10.1371/journal.pone.0130635 (2015).
- 384 Bullon, P. *et al.* AMPK Phosphorylation Modulates Pain by Activation of NLRP3 Inflammasome. *Antioxidants & redox signaling* **24**, 157-170, doi:10.1089/ars.2014.6120 (2016).
- 385 Wang, S. *et al.* AMPKalpha2 deletion causes aberrant expression and activation of NAD(P)H oxidase and consequent endothelial dysfunction in vivo: role of 26S proteasomes. *Circulation research* **106**, 1117-1128, doi:10.1161/CIRCRESAHA.109.212530 (2010).
- 386 Vazquez-Martin, A. *et al.* Activation of AMP-activated protein kinase (AMPK) provides a metabolic barrier to reprogramming somatic cells into stem cells. *Cell Cycle* **11**, 974-989, doi:10.4161/cc.11.5.19450 (2012).

APPENDIX 1

Copyright Permission



Copyright Information | Blood Online

www.bloodjournal.org/page/authors/copyright-information?sso-checked=true

Specific examples of acceptable author reuse and sharing include:

- Reprinting the article in print collections of the author's own writing.
- Reusing figures and tables created by the author in future works.
- Reproducing the article for use in courses the author is teaching. If the author is employed by an academic institution, that institution may also reproduce the article for course teaching.
- Distributing photocopies of the article to colleagues, but only for non-commercial purposes.
- Posting a copy of the article on the author's personal website, departmental website, and/or the university intranet. A hyperlink to the article on the *Blood* website must be included.
- Presenting the work orally in its entirety.
- Using the article in theses and/or dissertation.

Authors reusing their own material in the above ways must include appropriate attribution and do not need to contact *Blood* for permission. For all other uses, the author must request permission from ASH by [visiting the Copyright Clearance Center](#).

© *Blood* Online by the American Society of Hematology